UNIVERSITY OF CALIFORNIA, MERCED

Climatic Controls on Critical Zone Nutrient Biogeochemistry in Semiarid and Mediterranean Ecosystems

A dissertation submitted in partial satisfaction of the requirements
for the degree Doctor of Philosophy

in

Environmental Systems

by

Morgan E. Barnes

Committee in charge:

Dr. Stephen C Hart, Co-Chair
Dr. Asmeret Asefaw Berhe, Co-Chair
Dr. Peggy O'Day
Dr. Robert Young

2020

The Dissertation of Morgan E. Barnes is approved, and it is acceptable in quality and form for publication on microfilm and electronically:

_____
Peggy O'Day

_____
Robert Young

_____
Asmeret Asefaw Berhe, Co-Chair

_____
Stephen C. Hart, Co-Chair

University of California, Merced
2020

Table of Contents

List of Tables

List of Figures

Acknowledgements

This dissertation would not have been possible without the help and support of numerous people. I am incredibly lucky to have amassed mentors, colleagues, and friends while at UC Merced. I will always cherish these relationships.

I'd like to start by thanking my co-advisors, Stephen C. Hart and Asmeret Asefaw Berhe. From the very beginning, they both encouraged me to research what I was most interested in and then guided me along the way, and for that I am incredibly lucky and very grateful. Steve's enthusiasm towards learning new concepts, trying new techniques, and asking novel questions was infectious. Asmeret taught me to think about the big picture of not only why my research matters and how to take advantage of fellowship and grant opportunities, but also how to create a safe space for all. The two of them were pivotal in helping me become the scientist I am today by providing me with a solid foundation to build from. With their help, I was able to answer original research questions at the molecular to ecosystem scale in my dissertation and also cultivate multiple successful outside collaborations. One could argue that my dissertation got a little too big, but I still wouldn't change that. I love my dissertation research and I could not have done it without both of them.

I was fortunate to have many collaborators with different areas of expertise to help my dissertation improve even more. I'd like to thank Dr. Peggy O'Day for introducing me to the wild synchrotron world. I had no idea what running "just a few samples" would turn into. Robert Young used his NMR knowledge to run experiments on soil phosphorus. It was such a cool learning experience to work together figuring out the best way to run my soil samples. Robert Graham established the White Mountain Elevational Transect that allowed for an excellent climate comparison to the Mediterranean Southern Sierra Critical Zone Observatory. He also graciously went on a multi-day field exhibition to show me the sites and share his pedology insight. I'd like to thank Dale Johnson for establishing the resin plots I used to characterize soil nutrient hot spots and hot moments, Mike Zhu who provided insightful conversations about phosphorus biogeochemistry and analyses, and Nancy Washton for serving as my Pacific Northwest National Lab host so that I could experience research outside of an academic setting.

I am incredibly appreciative for Kimber Moreland and Nicholas Dove. We were fortunate to start this journey together and to each take a separate piece of the Critical Zone to answer with our dissertations. Not only were both of them pivotal in collaborating on sample collection, conducting laboratory analyses, and learning statistical tests, but they showed me how graduate school is more than just science, it's also about the friends we make along the way. Having their support and friendship through each step was critical to my success.

I would also like to thank many undergraduate students including Madeline Castro, Oscar Elias, Susan Glasser, Veronika Ullman, Paige Klotz, Florence Lucy, Susana Canela, and Mai Yee Vang. Not only did they help with field collection and laboratory analyses, but they allowed me to learn that mentoring students is just as

fulfilling as teaching in a classroom. Paul Aronstein, Ben Lash, Alex Leven, and Godwin Nwosu helped me learn about XANES and assisted with data collection and processing. I could not have collected the quantity or quality of data without their help. Erin Stacy and Mike McDonald, the ferocious tree climbers, helped to collect most of the tree foliage samples used in my third chapter. Rebecca Abney was my wise older graduate student who always had words of advice and was more than willing to share resources. Yang Yang really helped in my final year by providing detailed comments on drafts of my dissertation and helping with statistical analyses. Russel Callahan taught me the geologist perspective on how to properly collect rock outcrop samples. And lastly, Liying Zhao used her instrument expertise and taught me how to independently run samples. All of these folks helped with a piece of the puzzle to make this research possible.

Finally, I'd like to thank my family and friends. Your continued support, even when what I was doing really didn't make much sense to you, meant so much. In particular, I'd like to thank my Mom and Dad for the check-ins to make sure I was doing well, my brother Andy and cousin Alexa for cheering me on from a distance, and my Grandma Dar for sending me pictures of her flowers. My friends, Danaan DeNeve Weeks, Dasha Taraban, and Michelle Gilmore are also greatly appreciated. Danaan was my adventure buddy that helped me explore beautiful California, Dasha was always there for me with funny texts and a place to visit, and Michelle helped keep me sane with neighborhood walks. All of the big and small things they have done for me helped keep me motivated during the process of getting my PhD.

My research would also not have been possible without many funding sources. This includes awards and fellowships that finically supported me from the University of California Graduate Division, Environmental Systems Graduate Group, Department of Energy, and the Institute for the Study of Ecological Effects of Climate Impacts. My research was supported by the National Science Foundation (Southern Sierra Critical Zone Observatory, EAR-1331939), Department of Energy, the Institute for the Study of Ecological Effects of Climate Impacts, and grants through the University of California.

Curriculum Vitae

mbarnes7@ucmerced.edu
(831) 920-8509
5200 N. Lake Rd. Merced, CA 95343
Personal Website: mebarn4.wixsite.com/website
Linked In: linkedin.com/in/morgan-barnes-56b587121/
ORCID: 0000-0001-8722-6552

Education

University of California, Merced, Merced, CA
Ph.D., Environmental Systems — Aug 2014-Dec 2020

University of Kentucky, Lexington, Kentucky
B.S. in Natural Resource Conservation and Management, Minor in Plant and Soil Science — Aug 2008-May 2020

Publications

Yang, Y., Hart, S.C., Berhe, A.A., McCorkle, E., **Barnes, M.E.**, Stacy, E., Hunsaker, C., & Bales, R., 2020. Stream water chemistry in mixed-conifer headwater basins: role of water sources, watershed characteristics, and disturbances. Ecosystems. Under Review.

Varga, T, A.H. Ahkami, K.K. Hixson, R.K. Chu, L.R. Reno, A.K. Battu, C.D. Nicora, T.E. Winkler, **M.E. Barnes**, S.C. Fakra, D.Y. Parkinson, O. Antipova, J.R. Hall, A.W. Sher, and S.L. Doty. 2020. Endophyte-promoted phosphorus solubilization in Populus. Frontiers in Plant Science 11:1-16.

O'Day, P.A. Nwosu, U.G., **Barnes, M.E.**, Hart, S.C., Berhe, A.A., Christensen, J.N., Williams, K.H. 2020. Phosphorus Speciation in Atmospherically Deposited Particulate Matter and Implications for Terrestrial Ecosystem Productivity. Environmental Science and Technology 54(8): 4984-4994.

Aciego, S., Clakowski, M., Dove, N., Hart, S.C., Arvin, L., Riebe, C., Maltz, M., Aronson, E., **Barnes, M.E.**, Botthoff, J., Koornneef, J., Johnson, K. 2019. Competing droughts affect dust delivery to Sierra Nevada. Aeolian Research 41: 100545

Santos, F., Abney, R., **Barnes, M.E.**, Jin, L., Moreland, K., Bogie, N., Sulman, B., Ghezzehei, T. A., Berhe, A.A. 2018. The role of soil physical properties for determining biogeochemical responses to soil warming. Ecosystem Consequences of Soil Warming: Microbes, Vegetation, Fauna and Soil Biogeochemistry. Editor: Jacqueline Mohan

Research Experience

Instrumental

Lachat Quickchem Flow Injection Analysis System
ICP-OES, X-ray Absorption Near Edge Structure
Nuclear Magnetic Resonance
Elemental Analysis and Mass Spectroscopy
Fourier-Transform Ion Cyclotron Resonance Mass Spectrometry -

Field & Laboratory

Plant, soil, and aeolian particulate matter field collection
Soil and plant digestions for elemental analyses
KCl extractions for soil elemental analyses
Chloroform fumigation for microbial biomass stoichiometry
Lithium metaborate fusion for elemental analyses

Research Funding

Research Support

DOE Pacific Northwest Lab User Proposal ($55,000)	Oct 2018
Using UC Reserves to Detect and Forecast Climate Impacts ($9,000)	May 2018
ISEECI ($10,000)	May 2018
Mildred E. Mathias Graduate Research Grant ($3,000)	Aug 2017
Faculty Senate Grant (lead author; $10,000)	Aug 2017

Fellowships

Dean's Dissertation Year Fellowship ($18,500)	Aug 2020
DOE Office of Science Graduate Student Research Program ($18,000)	Jan 2019
Environmental Systems ($18,000)	May 2015, 2016, 2017, 2019
ISEECI ($44,000)	2015 and 2017

Travel Awards

Graduate Student Association ($400)	Dec 2018
ES Professional Development Fellowship ($6,000)	2017, 2018, 2019

Presentations

Oral Presentations

Berhe, A.A., Zhu, M., O'Day, P.A., **Barnes, M.E.**, & S.C. Hart. Phosphorus dynamics in soil and dust: a XANES application. The Third African Synchrotron Light Source Conference. Virtual. November 18, 2020.

Barnes, M.E. & P. O'Day. Using XAS and complementary methods to probe the speciation of phosphorus and iron in environmental samples. Advanced Light Source. Virtual. August 28, 2020.

Barnes, M.E., P. O'Day, R. Young, & S.C. Hart, A.A. Berhe. Aeolian particulate matter as a source of bioavailable phosphorus to Sierra Nevada soil. American Geophysical Union Annual Meeting. San Francisco, CA. December 9, 2019.

Barnes, M.E., A.A. Berhe, P. O'Day, R. Young, & S.C. Hart. Using advanced techniques to understand phosphorus biogeochemistry in a changing climate. Enviro-lunch Seminar Series. Merced, CA. October 10, 2019.

Barnes, M.E., A.A. Berhe, P. O'Day, R.Young, & S.C. Hart. Soil phosphorus speciation changes with climate. Climate Change and the Ecology of the Sierra Nevada Forests Symposium. Merced, CA. September 21, 2019.

Barnes, M.E., A.A. Berhe, P. O'Day, & S.C. Hart. Soil phosphorus stock and speciation in a changing climate. Soil Science Society of America International Soils Meeting. San Diego, CA. January 7, 2019.

Hart, S.C., S. Aarons, S. Aciego, E.L. Aronson, L.J. Arvin, **M.E. Barnes**, M. Blakowski, C.J. Carey, J.N. Christensen, A.A. Coble, N.C. Dove, C. Gu, M.R. Maltz, G. Nqosu, P. O'Day, C. Riebe, & M. Zhu. Ashes to ashes, dust to dust: the significance of aeolian particulate inputs to temperate ecosystems. Ecological Society of America. New Orleans, LA. August 10, 2018.

Nwosu, U.G., **M.E. Barnes**, S.C. Hart, A.A. Berhe, J.N. Christensen, K.H. Williams, & P.A. O'Day. Phosphorus speciation in atmospherically deposited particulate matter and potential impact on terrestrial soil nutrient cycling and ecosystem productivity. Annual Department of Energy Environmental System Science Principal Investigator Meeting. Potomac, MD. May 1, 2018.

Nwosu, U.G., B. Lash, **M.E. Barnes**, S.C. Hart, A.A. Berhe, & P.A. O'Day. Phosphorus speciation in atmospherically deposited air particulates from high and low elevation sites of California and Colorado. American Chemical Society. New Orleans, LA. Mar 18-22, 2018.

Hart, S, **M.E. Barnes**, D. Johnson, &M. Meadows. 2015. The median isn't the message: elucidating nutrient hot spots and hot moments in a Sierra Nevada forest soil. American Geophysical Union. San Francisco, CA. December 15, 2015.

Poster Presentations

Barnes, M.E., P. O'Day, R. Young, S.C. Hart, & A.A. Berhe. Soil phosphorus stock and speciation with regolith development: does the Walker and Syers model apply to a climatic weathering gradient? American Geophysical Union Annual Meeting. Virtual. December 7, 2020.

Varga, T, A.H. Ahkami, K.K. Hixson, R.K. Chu, L.R. Reno, A.K. Battu, C.D. Nicora, T.E. Winkler, **M.E. Barnes**, S.C. Fakra, D.Y. Parkinson, O. Antipova, J.R. Hall, A.W. Sher, & S.L. Doty. 2020. Endophyte-promoted phosphorus solubilization in Populus. American Geophysical Union Annual Meeting. Virtual. December 7, 2020.

Susan M. Glasser, **M.E. Barnes**, N.C. Dove, A.A. Berge, & S.C. Hart. Climatic impacts on soil microbial biomass and potential enzyme activity. UC Merced Research Week. Merced, CA. March 5, 2020.

Yang, Y, S.C. Hart, A. Kelly, Z. Tian, K. Moreland, **M.E. Barnes**, R. Bales, C. Hunsaker, D. Johnson, M. Goulden, & A.A. Berhe. Biogeochemistry of carbon, nitrogen and phosphorus along an elevation gradient at Southern Sierra Critical Zone Observatory in California. American Geophysical Union Annual Meeting. San Francisco, CA. December 9, 2019.

Varga, T, R.K. Kukkadapu, A. Dohnalkova, L. Kovarik, M. Marcus, A.H. Ahkami, R.K. Chu, K. Hixson, C. Nicora, T.E. Winkler, L.R. Reno, A.K. Battu, **M.E. Barnes**, O. Antipova, S.C. Fakra, D. Parkinson, & S.L. Doty. Studies of soil mineral organic matter associations and plant nutrient fixation using synchrotron x-ray methods. American Geophysical Union Annual Meeting. San Francisco, CA. December 9, 2019.

Barnes, M.E., S.C. Hart, R.Y. Young, P.A. O'Day, & A.A. Berhe. Organic and inorganic phosphorus speciation changes along a Sierra Nevada elevational gradient. Southern Sierra Critical Zone Observatory Annual Meeting. Merced, CA. August 22, 2019.

Barnes, M.E., S.C. Hart, & A.A. Berhe. Temperature and precipitation alters soil phosphorus stock and plant nutrient stoichiometry. Southern Sierra Critical Zone Observatory Annual Meeting. Berkeley, CA. October 17, 2018.

Nwosu, U.G., **M.E. Barnes**, B. Lash, S.C. Hart, & P. O'Day. Phosphorus speciation in atmospherically deposited air particulates from high and low elevation sites of California and Colorado. Stanford Synchrotron Radiation Lightsource User Meeting. Stanford, CA. Sep 27, 2017.

Barnes, M.E., S.C. Hart, & A.A. Berhe. Climatic controls on soil phosphorus pools and implications for vegetation. Southern Sierra Critical Zone Observatory Annual Meeting. Merced, CA. August 2, 2017.

Barnes, M.E., S.C. Hart, & A.A. Berhe. Climatic controls on the biogeochemical cycling of phosphorus in the critical zone. Institute for the Study of Ecological and Evolutionary Climate Impacts Meeting. Santa Barbara, CA. May 6, 2017.

Barnes, M.E., S.C. Hart, & A.A. Berhe. Soil phosphorus biogeochemistry in the critical zone. Southern Sierra Critical Zone Observatory Annual Meeting, Merced, CA. August 3, 2016.

Barnes, M.E., C. Matocha, & M. Coyne. Long-term effects of nitrogen fertilization on the phenol oxidase enzyme. Kentucky Water Resources Symposium. Lexington, KY. March 15, 2012.

Professional Experience

Graduate Student Researcher
University of California, Merced — May 2015 - Aug 2019, Jan 2020-Present

Mentor and Trainer to Undergraduate Lab Assistants
University of California, Merced May — 2015 - 2019
• 11 students

Guest Lecture
University of California, Merced
Introduction to Soil Science — March 2017, Feb 2020
Critical Zone Science — Oct 2018
Terrestrial Ecosystem Ecology — April 2018

Teaching Assistant
University of California, Merced

Contemporary Biology	Aug-May 2016, Aug 2019-Dec 2019
Fundamentals of Soil Science	Jan-May 2016

Committees, Workshops, & Service

Reviewer for Geoderma Journal	Feb 2020
Discipline Based Education Research Journal Club	Aug 2018- May 2019
Lawrence Berkeley National Lab Watershed Science Meeting	Nov 2017
Stanford Synchrotron Radiation Light Source Workshop	June 2017
Graduate Student Association Delegate Assembly Member	May 2017- Aug 2018
Leadership Award Reviewer	April 2017
CA Naturalist Training Volunteer	March 2017
Outreach Activities with the SSCZO	April 2016-Aug 2019
Reviewer for Global Biogeochemical Cycles Journal	March 2016
Environmental Systems Coursework Committee	Feb 2016-Dec 2017
Questx Nonprofit Organization	Jan 2016-Aug 2018
Women in STEM Mentoring Group	Oct 2015-Aug 2018
Graduate Pedagogy Association Founding Officer & President	Sept 2015-May 2019
Environmental Systems, Ecology, and Evolution	Aug 2015-Present
Environmental Systems Student Representative	Aug 2015-Aug 2020
Critical Zone Observatory Graduate Research Group Member	Aug 2015-Aug 2019

Professional Affiliations

Soil Science Society of America
American Geophysical Union

Abstract of the Dissertation

Climatic Controls on Critical Zone Nutrient Biogeochemistry in Semiarid and Mediterranean Ecosystems

by

Morgan E. Barnes

Doctor of Philosophy, Environmental Systems
University of California, Merced 2020
Drs. Stephen C. Hart & Asmeret Asefaw Berhe, Co-Chairs

Global climate models demonstrate that temperate ecosystems are likely to serve as carbon (C) sinks in the coming decades, however any realized increase in C storage on land will also require increases in the availabilities of plant essential nutrients such as nitrogen (N) and phosphorus (P). Additionally, nutrient limitation to plant productivity remains one of the most uncertain factors to global climate projections. Our understanding of how nutrient biogeochemistry is altered under different climatic conditions is unclear. Using a combination of field, laboratory, and advanced analytical techniques, I show P biogeochemistry is intrinsically related to soil development in a semiarid (White Mountains Elevational Transect) to Mediterranean (Southern Sierra Nevada Critical Zone Observatory) climatic gradient. Specifically, P stock increases, inorganic P transitions from calcium to iron and aluminum association, and organic P proportionally decreases with increasing climate-driven weathering. With increasing precipitation, soil and aboveground foliage became progressively more P-limited, whereas the microbial biomass and fine roots are more N-limited and enzyme activity is largely unaffected. Overall, the transition from a semiarid to Mediterranean climate creates more chemically weathered soil that is able to retain P that may not be readily bioavailable. These relatively more weathered soils appear to be relying on faster cycling organic P species to support ecosystem development. Furthermore, using three-dimensional resin capsule pots in a Mediterranean forest site, I characterized how nutrient fluxes under more biological (PO_4^{3-}, NH_4^+, NO_3^-) or geochemical (Ca^{2+}, Mg^{2+}, and Na^+) control are impacted by water year, seasonality, and depth to form hot spots (HS) or hot moments (HM). A multi-year drought occurred during the study, causing geochemically controlled nutrient fluxes to be transient over time and characterizing them as HM.

Alternatively, biologically controlled outliers formed HS and HM. Macronutrient HS and HM are found at higher concentrations relative to the surrounding soil matrix, and co-occur in discrete spatial locations where belowground biomass can detect, proliferate, and exploit these resources. Overall, water flux controls nutrient biogeochemical cycles in these drylands. Therefore, nutrient HS and HM will likely play a disproportionate role in supporting ecosystem development in these temperature drylands under a changing climate.

1 Introduction

All life on Earth is supported by the interactions of biological, geological, and chemical processes that occur in the Critical Zone (CZ), or the area from groundwater through vegetation (Brantly et al. 2007). Soils are an important component of the CZ as they provide nutrients to microbes and vegetation, sequester carbon (C), and store water (Binkley and Fisher 2012). Understanding nutrient limitation is imperative to better predict how terrestrial ecosystems will respond to a changing climate. Nutrient availability drives net ecosystem production and also promotes greater carbon use efficiency. This results in more C stored in biomass and soil than is lost through respiration (Fernández-Martínez et al. 2014). Even though nutrient limitation constrains net primary production by up to 25%, it remains one of the most uncertain factors to global climate model projections (Hungate et al. 2003; Wieder et al. 2015). Nutrient cycles may be disrupted by global climate change which has important implications for ecosystem processes and C sequestration.

Dryland ecosystems comprise over 40% of the Earth's land surface and are particularly vulnerable to a changing climate (Reynolds et al. 2007; Schimel 2010). Climate change in dryland ecosystems has been shown to disrupt ecosystem functions, including soil weathering, organic matter turnover, and desorption and dissolution reactions (Austin et al. 2004; Delgado-Baquerizo et al. 2013), which impacts soil C storage, plant productivity, and species biodiversity (Maestre et al. 2012). Climate models project dryland ecosystem temperatures will increase by 4 °C at the end of the 21st century (Solomon et al. 2007), which enhances potential evapotranspiration and will likely lead to concurrent increases in drought (Dai 2012). Specifically, in California, the occurrence of drought has increased in the past two decades compared to the last century and anthropogenic warming increases the probability that future dry conditions will co-occur with warm periods, making future droughts more probable (Diffenbaugh et al. 2015). As the amount of land area classified as drylands is expected to increase up to 23% by 2100 (Feng and Fu 2013; Huang et al. 2016), it is imperative that we gain a better understanding of how nutrient biogeochemistry in arid and Mediterranean ecosystems is altered by climate.

Primary production is commonly constrained by nitrogen (N) and phosphorus (P) availability in ecosystems globally (Elser et al. 2007). However, some terrestrial ecosystems are expected to shift from N limitation to P limitation due to high N input from anthropogenic activities (Perring et al. 2008) or changes in climate and CO_2 concentrations (Menge and Field, 2007; Matear et al. 2010). A recent meta-analysis found global P limitation to be more widespread than previously considered (Hou et al. 2020). Phosphorus has been described as the ultimately limiting nutrient in terrestrial C storage because P inputs are unlikely to meet nutrient demand (Walker and Syers 1976; Yang and Post 2011).

Phosphorus biogeochemistry is intrinsically related to soil development as stock, chemical speciation, and bioavailability are altered by pedogenesis and ecosystem succession (Walker and Syers 1976; Crews et al. 1995; Turner et al. 2007). Our current

understanding of phosphorus biogeochemistry with pedogenesis is heavily based on surficial soil chronosequence observations (e.g., McGroddy et al. 2008; Turner and Laliberte 2015; Selmants and Hart 2010) rather than climate gradients. In addition, P studies commonly use sequential fractionation techniques to assign P into operationally defined pools, thereby not taking into account the differing bioavailability of the wide range of organic and inorganic chemical species (Dick and Tabatabai 1978; Condron et al. 2005; Darch et al. 2014). Recently, molecular-level spectroscopic techniques such as x-ray absorption near edge structure (XANES) and ^{31}P nuclear magnetic resonance (NMR) have shown to be powerful tools for quantifying P chemical speciation in environmental samples (Kizewski et al. 2011). In Chapter 2, I investigated how climate-induced soil weathering is altered along elevational gradients in temperate water-limited semiarid- and Mediterranean- type ecosystems. I then tested if the Walker and Syers (1976) conceptual model applies to this climatic weathering gradient and the implications for soil P concentration, stock, and chemical speciation within and among master soil horizons.

Nitrogen and P biogeochemistry are under dissimilar controls, therefore they may respond in contrasting ways to increasing atmospheric CO_2 and global change (Vitousek et al. 2008, 2010; Yuan and Chen 2015). Stoichiometry, or the relative quantities of chemical elements, is a powerful tool to investigate how C, N, and P in living organisms relates to the surrounding environment (Redfield 1958). Stochiometric ratios impact ecological processes including biological N_2 fixation (Dynarski and Houlton 2018), litter decomposition (Güsewell and Gessner 2009), soil enzyme production (Sinsabaugh et al. 2008), microbial immobilization (Manzoni et al. 2010), and ecosystem composition and diversity (Roem and Berendse 2000; Güsewell et al. 2005). Therefore, stoichiometric ratios can be an indicator of ecosystem function and serve as a proxy for limiting nutrient(s) (Koerselman and Meuleman 1996; Güsewell et al. 2003). Previous studies investigating ecosystem stoichiometry have focused on aboveground vegetation or microbial biomass rather than measuring nutrient dynamics in multiple ecosystem compartments. This may omit important feedbacks and interactions that can help elucidate nutrient partitioning and competitive dynamics between above- and belowground processes (but see Dijkstra et al. 2012; Delgado-Baquerizo et al. 2018). Therefore, the objective of Chapter 3 was to use a space for time substitution approach along elevational gradients to determine how climate and depth into the soil profile impacts soil, microbial biomass, enzyme activity, fine root, and foliar C:N:P stoichiometry in temperate drylands. Using the same semiarid and Mediterranean elevational gradients as Chapter 2, it allowed me to evaluate a large climate gradient to aid in our understanding of nutrient cycling and limitation in terrestrial ecosystems (Sterner and Elser 2002).

It is well known that soil nutrient distribution is heterogeneous in space and time, impacting competition between plant species (Hodge et al. 1999; Robinson et al. 1999; Wang et al. 2018) and microorganisms (Kaye and Hart 1997; Schimel and Bennet 2004; Hodge et al. 2000). Soil nutrient hot spots (HS), or patches with elevated biogeochemical activity, have been recognized for a long time (Parkin 1987; Hill et al. 2000; McClain et al. 2003; Vidon et al. 2010), whereas hot moments (HM; McClain et al. 2003; Vidon et al. 2010), or areas with a high rate of biogeochemical activity occurring for a short period

of time, have received less attention. In addition, many investigations of HS-HM exam the dynamics of only one or two nutrients (Bernhardt et al. 2017) over a relatively short timeframe (Gibson 1986; Kleb and Wilson 1997; Johnson et al. 2014; Barcellos et al. 2018), and often use destructive sampling techniques when conducted in the field (i.e., Charley and West 1977; Kleb and Wilson 1997; Bruckner et al. 1999; Farley and Fitter 2001; Washburn and Arthur 2003; Harms and Grimm 2008; Mueller et al. 2008). This makes repeated sampling of the same location impossible, and therefore an inability to quantitatively differentiate HS from HM when they are at the same spatial scale. Therefore, the overall objective of Chapter 4 was to investigate the long-term spatial and temporal patterns in nutrient fluxes in a Mediterranean mixed-conifer forest using ion exchange resin capsules to characterize the magnitude and spatial distribution of nutrient fluxes (PO_4^{3-}, NH_4^+, NO_3^-, Na^+, Ca^{2+}, and Mg^{2+}). By sampling the soil solution at the same spatial locations (horizontally and vertically) repeatedly over time, I operationally separated the occurrence of nutrient HS from HM for nutrients primarily under biological or geochemical controls. Because this study co-occurred during a multi-year drought, I also elucidated how HS-HM formation may be altered in a changing climate. Hot spots and HM may be formed via dissimilar mechanisms and they likely play different roles in supporting short- versus long-term vegetation and microorganism nutrient acquisition; therefore, separating this terminology is critical for the advancement of ecology.

The overall goal of my dissertation was to investigate climatic effects on nutrient biogeochemistry in semiarid and Mediterranean ecosystems. Using climatic gradients of temperature and precipitation moving from semiarid to Mediterranean sites, I quantified P stock and chemical speciation in Chapter 2 and then determined the relative concentrations of C, N, and P in multiple ecosystem compartments in Chapter 3. In Chapter 4, I used a site from the Mediterranean gradient as an exemplar to understand how nutrient fluxes under biological or geochemical control are impacted by depth, season, and water year (including over drought) to form HS or HM. Taken together, these findings help broaden our understanding of how nutrient biogeochemical cycling in soil, microbes, and vegetation are altered by climate, and increases our understanding of how dryland ecosystems may respond to a changing climate.

1.1 References

Austin AT, Yahdjian L, Stark JM, et al. (2004) Water pulses and biogeochemical cycles in arid and semiarid ecosystems. Oecologia 141:221-235.

Barcellos D, O'Connell C, Silver W, Meile C, Thompson A (2018) Hot spots and hot moments of soil moisture explain fluctuations in iron and carbon cycling in a humid topical forest soil. Soil Systems 2:1-22.

Bernhardt ES, Blaszczak JR, Ficken CD, Fork ML, Kaiser KE, Seybold EC (2017) Control Points in Ecosystems: Moving Beyond the Hot Spot Hot Moment Concept. Ecosystems 20:665-682.

Binkley D, Fisher R (2012) Ecology and Management of Forest Soils. John Wiley & Sons, New Jersey.

Brantley SL, Goldhaber MB, Ragnarsdottir KV (2007) Crossing disciplines and scales to understand the critical zone. Elements 3:307-314.

Bruckner A, Kandeler E, Kampichler C (1999) Plot-scale spatial patterns of soil water content, pH, substrate-induced respiration and N mineralization in a temperate coniferous forest. Geoderma 93:207-223.

Charley JL, West NE (1977) Micro-patterns of nitrogen mineralization activity in soils of some shrub-dominated semi-desert ecosystems of Utah. Soil Biology and Biochemistry 9:357-365.

Condron LM, Turner BL, Cade-Menun BJ (2005) Chemistry and dynamics of soil organic phosphorus. In: Sims JT, Sharpley AN (eds) Phosphorus: Agriculture and the Environment. American Society of Agronomy, Crop Science Society of America, Soil Science Society of America, Inc., Madison, WI pp. 87-121.

Crews TE, Kitayama K, Fownes JH, et al. (1995) Changes in Soil Phosphorus Fractions and Ecosystem Dynamics across a Long Chronosequence in Hawaii. Ecology 76:1407-1424.

Dai A (2012) Increasing drought under global warming in observations and models. Nature Climate Change 3:52-58.

Darch T, Blackwell MSA, Hawkins JMB, et al. (2014) A Meta-Analysis of Organic and Inorganic Phosphorus in Organic Fertilizers, Soils, and Water: Implications for Water Quality. Critical Reviews in Environmental Science and Technology 44:2172-2202.

Delgado-Baquerizo M, Eldridge DJ, Maestre FT et al. (2018) Aridity Decouples C:N:P Stoichiometry Across Multiple Trophic Levels in Terrestrial Ecosystems. Ecosystems 21:459-468.

Delgado-Baquerizo M, Maestre FT, Gallardo A, et al. (2013) Decoupling of soil nutrient cycles as a function of aridity in global drylands. Nature 502:672-676.

Dick WA, Tabatabai MA (1978) Hydrolysis of organic and inorganic phosphorus compounds added to soils. Geoderma 21:175-182.

Diffenbaugh NS, Swain DL, Touma D (2015) Anthropogenic warming has increased drought risk in California. Proceedings of the National Academy of Sciences 112:3931-3936.

Dynarski KA, Houlton BZ (2018) Nutrient limitation of terrestrial free-living nitrogen fixation. New Phytologist 217:1050-1061.

Elser JJ, Bracken MES, Cleland EE, et al. (2007) Global analysis of nitrogen and phosphorus limitation of primary producers in freshwater, marine and terrestrial ecosystems. Ecology Letters 10:1135-1142.

Farley RA, Fitter AH (2001) Temporal and spatial variation in soil resources in a deciduous woodland. Journal of Ecology 87:688-96.

Feng S, Fu Q (2013) Expansion of global drylands under a warming climate. Atmospheric Chemistry and Physics Discussions 13:14637-14665.

Fernández-Martínez M, Vicca S, Janssens IA, et al. (2014) Nutrient availability as the key regulator of global forest carbon balance. Nature Climate Change 4:471-476.

Gibson DJ (1986) Spatial and temporal heterogeneity in soil nutrient supply measured using in situ ion-exchange resin bags. Plant and Soil 96:445-450.

Güsewell S, Bailey KM, Roem WJ, Bedford BL (2005) Nutrient limitation and botanical diversity in wetlands: can fertilisation raise species richness? Oikos 109:71-80.

Güsewell S, Koerselman W, Verhoeven JTA (2003) Biomass N:P ratios as indicators of nutrient limitation for plant populations in wetlands. Ecological Applications 13:372-384.

Harms TK, Grimm NB (2008) Hot spots and hot moments of carbon and nitrogen dynamics in a semiarid riparian zone. Journal of Geophysical Research: Biogeosciences 113:1-14.

Hill AR, Devito KJ, Campagnolo S, Sanmugadas K (2000) Sub-surface denitrification in a forest riparian zone. Biogeochemistry 51:193-223.

Hodge A, Robinson D, Griffiths BS, Fitter AH (1999) Why plants bother: root proliferation results in increased nitrogen capture from an organic patch when two grasses compete. Plant, Cell & Environment 22:811-820.

Hodge A, Stewart J, Robinson D, Griffiths BS, Fitter AH (2000) Competition between roots and soil micro-organisms for nutrients from nitrogen-rich patches of varying complexity. Journal of Ecology 88:150-64.

Hou E, Luo Y, Kuang Y, et al. (2020) Global meta-analysis shows pervasive phosphorus limitation of aboveground plant production in natural terrestrial ecosystems. Nature Communications 11:1-9.

Huang J, Yu H, Guan X, Wang G, Guo R (2016) Accelerated dryland expansion under climate change. Nature Climate Change 6:166-171.

Hungate BA, Dukes JS, Shaw R, et al. (2003) Nitrogen and climate change. Science 302:1512-1513.

Johnson DW, Woodward C, Meadows MW (2014) A Three-Dimensional View of Nutrient Hotspots in a Sierra Nevada Forest Soil. Soil Science Society of America Journal 78:225-236.

Kaye JP, Hart SC (1997) Competition for nitrogen between plants and soil microorganisms. Trends in Ecology & Evolution 12:139-43.

Kizewski F, Liu YT, Morris A, Hesterberg D (2011) Spectroscopic Approaches for Phosphorus Speciation in Soils and Other Environmental Systems. Journal of Environmental Quality 40:751-766.

Kleb HR, Wilson SD (1997) Vegetation Effects on Soil Resource Heterogeneity in Prairie And Forest. The American Naturalist 150:283-298.

Koerselman W, Meuleman AFM (1996) The Vegetation N:P Ratio: a New Tool to Detect the Nature of Nutrient Limitation. The Journal of Applied Ecology 33:1441-1450.

Maestre FT, Quero JL, Gotelli NJ, et al. (2012) Plant species richness and ecosystem multifunctionality in global drylands. Science 335: 214-218.

Manzoni S, Trofymow JA, Jackson RB, Porporato A (2010) Stoichiometric controls on carbon, nitrogen, and phosphorus dynamics in decomposing litter. Ecological Monographs 80:89-106.

Matear RJ, Wang YP, Lenton A (2010) Land and ocean nutrient and carbon cycle interactions. Current Opinion in Environmental Sustainability 2:258-263

McClain ME, Boyer EW, Dent CL, et al. (2003) Biogeochemical Hot Spots and Hot Moments at the Interface of Terrestrial and Aquatic Ecosystems. Ecosystems 6:301-312.

McGroddy ME, Silver WL, de Oliveira RC, et al. (2008) Retention of phosphorus in highly weathered soils under a lowland Amazonian forest ecosystem. Journal of Geophysical Research Biogeosciences 113:1-11.

Menge DNL, Field CB (2007) Simulated global changes alter phosphorus demand in annual grassland. Global Change Biology 13:2582-2591

Mueller EN, Wainwright J, Parsons AJ. (2008) Spatial variability of soil and nutrient characteristics of semi-arid grasslands and shrublands, Jornada Basin, New Mexico. Ecohydrology 1:3-12.

Parkin TB (1987) Soil Microsites as a Source of Denitrification Variability. Soil Science Society of America Journal 51:1194-1199.

Perring MP, Hedin LO, Levin SA, et al. (2008) Increased plant growth from nitrogen addition should conserve phosphorus in terrestrial ecosystems. Proceedings of the National Academy of Sciences 105:1971-1976.

Redfield A (1958) The biological control of chemical factors in the environment. American Scientist 46:205-221

Roem WJ, Berendse F (2000) Soil acidity and nutrient supply ratio as possible factors determining changes in plant species diversity in grassland and heathland communities. Biological Conservation 92:151-161.

Reynolds JF, Smith DMS, Lambin EF, et al. (2007) Global desertification: building a science for dryland development. Science 316:847-851.

Robinson D, Hodge A, Griffiths BS, Fitter AH (1999) Plant root proliferation in nitrogen rich patches confers competitive advantage. Proceedings of the Royal Society of London Series B: Biological Sciences 266:431-435.

Selmants PC, Hart SC (2010) Phosphorus and soil development: Does the Walker and Syers model apply to semiarid ecosystems? Ecology 91:474-484.

Schimel DS (2010) Drylands in the Earth System. Science 327:418-419.

Schimel JP, Bennett J. (2004) Nitrogen mineralization: challenges of a changing paradigm. Ecology 85:591-602.

Sinsabaugh RL, Lauber CL, Weintraub MN, et al. (2008) Stoichiometry of soil enzyme activity at global scale. Ecology Letters 11:1252-1264.

Solomon S, Manning M, Marquis M, Qin D (2007) Climate change 2007-the physical science basis: Working group I contribution to the fourth assessment report of the IPCC. Cambridge University Press, United Kingdom and New York.

Sterner RW Elser JJ (2002) Ecological Stoichiometry: The Biology of Elements from Molecules to the Biosphere. Princeton University Press, New Jersey.

Turner BL, Condron LM, Richardson SJ, et al. (2007) Soil organic phosphorus transformations during pedogenesis. Ecosystems 10:1166-1181.

Turner B, Laliberte E (2015) Soil development and nutrient availability along a 2 million-year costal dune chronosequence under species-rich Mediterranean shrubland in southwestern Australia. Ecosystems 18:287-309.

Vidon P, Allan C, Burns D, et al. (2010) Hot spots and hot moments in riparian zones: potential for improved water quality management. Journal of the American Water Resources Association 46:278-298.

Vitousek PM, Aber JD, Howarth RW, et al. (2008) Human alteration of the global nitrogen cycle: sources and consequences. Ecological Applications 7:737-750.

Vitousek PM, Porder S, Houlton BZ, Chadwick OA (2010) Terrestrial phosphorus limitation: mechanisms, implications, and nitrogen–phosphorus interactions. Ecological Applications 20:5-15.

Walker TW, Syers JK (1976) The fate of phosphorus during pedogenesis. Geoderma 15:1-19.

Wang P, Shu M, Mou P, Weiner J (2018) Fine root responses to temporal nutrient heterogeneity and competition in seedlings of two tree species with different rooting strategies. Ecology and Evolution 8:3367–3375.

Washburn CS, Arthur MA (2003) Spatial variability in soil nutrient availability in an oak-pine forest: potential effects of tree species. Canadian Journal of Forest Research 33:2321-30.

Wieder WR, Cleveland CC, Smith WK, Todd-Brown K (2015) Future productivity and carbon storage limited by terrestrial nutrient availability. Nature Geoscience 8:441-444.

Yang X, Post WM (2011) Phosphorus transformations as a function of pedogenesis: A synthesis of soil phosphorus data using Hedley fractionation method. Biogeosciences 8:2907-2916.

Yuan ZY, Chen HYH (2015) Decoupling of nitrogen and phosphorus in terrestrial plants associated with global changes. Nature Publishing Group 5:465-469.

2 Soil Phosphorus Stock and Speciation with Regolith Development: Does the Walker and Syers Model Apply to Dryland Climatic Gradients?

2.1 Abstract

Global environmental change models state that temperate ecosystems will serve as a carbon (C) sink, however any realized increase in C storage will also require increases in the availabilities of key nutrients. Phosphorus (P) has been described as the ultimately limiting nutrient to terrestrial ecosystem productivity because new inputs may not be able to meet nutrient demands. The conceptual model of Walker and Syers (W&S) describes the evolution of soil P with ecosystem development, where primary mineral (i.e., Ca-bound) P is increasingly incorporated into bioavailable, organic, and occluded pools. During late stages of pedogenesis, total P declines and the remaining P is tightly cycled between the vegetation and soil principally through the organic, and to a lesser degree the occluded pools. The W&S model is widely supported along soil chronosequences. Our understanding of P transformations in soil, especially with ecosystem development and global climate change, is complicated due to the complexity of P species within each of the W&S pools and their range in bioavailability. We used a space-for-time substitution approach along Mediterranean and semiarid elevational gradients to study how soil P biogeochemistry is altered by changes in climate. Although weathering intensity increases with changes in climate from semiarid to Mediterranean sites, the total P stock also increased and therefore inconsistent with the W&S model. Alternatively, chemical speciation as identified by X-ray absorption near edge structure (XANES) spectroscopy of bulk soil identified inorganic P (Pi) transitions from proportionally more Ca-Pi to more Al- and Fe-Pi with increases in weathering, supporting the W&S model. ^{31}P nuclear magnetic resonance spectroscopy (NMR) indicated the relative percent of extractable organic P (Po) monoesters and diesters decreased with weathering. Ultimately, changes in temperature and precipitation, along with a transition in dominate vegetation species (pinyon pine and shrubland at the semiarid sites to mixed conifer forests at the Mediterranean ecosystem), creates more chemically weathered soil that is able to retain P at a greater rate than what is lost from leaching. These relatively more weathered sites may be relying on faster cycling organic species rather than primary mineral, precipitated secondary minerals, and sorbed species to support ecosystem development.

2.2 Introduction

Phosphorus (P) availability often limits terrestrial ecosystem productivity (Elser 2007; Vitousek et al. 2010) by controlling carbon (C) and nitrogen (N) mineralization rates (Munevar and Wollum 1977), nitrogen fixation (Griffith 1978;Cole and Heil 1981), and driving ecosystem retrogression (Peltzer et al. 2010). Phosphorus is an essential element to all life on Earth due to its involvement with energy transport (ATP), cell wall structural support (phospholipids), and genetic material (DNA and RNA; Smil 2000). A recent meta-analysis found global P limitation to be more widespread than previously considered (Hou et al. 2020). Phosphorus has been described as the ultimately limiting nutrient in terrestrial C storage because new inputs are likely insufficient to meet nutrient demand in a changing climate (Walker and Syers 1976; Yang and Post 2011; Wieder et al. 2015). Global climate models show the amount of C sequestered as net primary production in a changing climate is limited by key nutrients (N and P), but nutrient limitation is one of the most uncertain factors to model projections (Goll et al. 2012; Wieder et al. 2015).

Phosphorus biogeochemistry is intrinsically related to soil development, as stock, chemical speciation, and bioavailability are altered by pedogenesis and ecosystem succession (e.g., Walker and Syers 1976; Crews et al. 1995; Turner et al. 2007). Walker and Syers (W&S; 1976) developed a conceptual model describing the evolution of P transformation with pedogenesis and ecosystem development based on four New Zealand soil chronosequences. The W&S model has been validated for a wide range of chronosequences, or substrate age gradients, especially for surficial soils developed from parent materials with relatively high P concentrations. Previous studies that support the W&S conceptual model include sedimentary tropical forests (McGroddy et al. 2008), Mediterranean coastal dune shrublands (Turner and Laliberte 2015), volcanic arid woodlands (Selmants and Hart 2010), metamorphic temperate rain-forests (Richardson et al. 2004), tropical forests formed on volcanic ash (Schlesinger et al. 1998), subtropical coastal dunes (Chen et al. 2015), humid montane forest on basalt (Crews et al. 1995), and Mediterranean forests on marine sedimentary soils (Izquierdo et al. 2013). Therefore, the W&S model provides a framework to understand how P biogeochemistry is altered by soil development and weathering intensity.

In the early stages of soil development, apatite minerals in the parent material are converted into labile (i.e., plant available) P forms via weathering and acidification. Labile P is increasingly incorporated into live plant, soil organic matter, sorbed or precipitated with secondary compounds (Ca, Fe, or Al), and occluded (within the mineral matrix, associated with distinct mineral phases) P pools over time (Walker and Syers, 1976). The total ecosystem P stock decreases with time due to its loss from the soil system by leaching and surface erosion (e.g., Lajtha and Schlesinger 1988; Hedin et al. 2003). In the late stages of ecosystem development, the system is thought to experience limitation where P remaining in the soil is held in forms inaccessible to plants including stable organic species and crystalline Al and Fe oxyhydroxides (Cross and Schlesinger 2001). Therefore, highly weathered soils are thought to be reliant on the internal

recycling of organic P (Po; e.g., Wardle et al. 2004) and exogeneous dust fluxes (e.g., Gu et al. 2019).

Although previous research has focused on validating the W&S conceptual model on soils forming over time, the rate of soil development and P cycling are controlled by other state factors as well (climate, organisms, relief, and parent material; Jenny 1941; Deiss et al. 2018; Letkeman et al. 1996; Wilson 2019). In particular, the W&S model can be tested along climate gradients because pedogenesis is principally driven by the volume of water leached through the soil regardless if this occurs from increased soil age or from changes in climate (Walker and Syers 1976). Although there have been many studies conducted on chronosequences, P biogeochemistry along climatic gradients has only recently received increased attention (e.g., Emadi et al. 2012; Ippolito et al. 2010; Zhou et al. 2016; Feng et al. 2016; Helfenstein et al. 2018; Mou et al. 2020). A recent meta-analysis on soil age gradients even found total and available P is controlled more by climate, vegetation, and parent material rather than the age of the soil (Delgado-Baquerizo et al. 2020).

Previous P biogeochemistry studies across climate gradients have found changes to stock, concentration, and composition. Along an elevational gradient, total P stock was greater in subalpine elevations where temperature is colder and mean annual precipitation (MAP) is high, but surficial soil P concentration had a quadratic relationship with elevation (Zhou et al. 2016). Similarly, total P concentration has been found to have a parabolic relationship with aridity (Feng et al. 2016) and altitude (He et al. 2016), but warming alone can cause total P concentration to decrease in the top 30 cm of soil (Sardans et al. 2006). The Pi pool is higher in arid locations and decreases with increased precipitation (Emadi et al. 2012). In contrast, the Po pool is greater in colder and wetter sites (Mou et al. 2020). Within the Po pool, diesters have been found to increase with precipitation, causing the monoester:diester ratio to increase with MAP in topsoil (Sumann et al. 1998; Mage and Porder 2012; Feng et al. 2016). Increasing MAP has also resulted in a decrease of Ca-P and increase in occluded forms in the central Great Plains, USA (dry ecosystem; Ippolito et al. 2010), on a sequence of moisture regimes in northern Iran (Emadi et al. 2012), and on a Hawaiian precipitation gradient (Helfenstein et al. 2018). Increasing humidity in arid and semiarid grassland topsoils caused Ca-P to decline and occluded P to increase (Feng et al. 2016). Overall, increases in elevation, precipitation, or humidity have been found to influence P amount and chemical speciation, where Ca-P transitions to organic and occluded Fe- and Al-P.

Soil P is found in a wide range of organic and inorganic (Pi) species that vary in their bioavailability, or the rate at which they can supply orthophosphate to the soil solution, based on molecular composition and interactions with soil constituents (Dick and Tabatabai 1978; Condron et al. 2005; Darch et al. 2014). Within Po species, diesters have a lower charge density (phosphate is bound to C by two ester linkages) making them less able to interact compared to monoesters (one covalent bond to C; McDowell and Stewart 2006). This allows monoesters, particularly phytate, to be protected by sorption to soil organic matter, clays, sesquioxides, or cations in the soil solution; diesters are more prone to microbial or enzymatic attack, and are therefore considered relatively more bioavailable (Anderson 1980; Tate 1984; Stewart and Tiessen 1987). The W&S model

provides insight into how P pools change with pedogensis, however the contribution of Po as a source of bioavailable P is less understood because all species are grouped together.

Recently, molecular-level spectroscopic techniques have shown to be powerful tools for quantifying P speciation in environmental samples (Kizewski et al. 2011). X-ray absorption near edge structure (XANES) is element specific and the experiment can be conducted on the intact soil sample (e.g., Beauchemin et al. 2003; Sato et al. 2005; Kruse and Leinweber 2008; Prietzel et al. 2010, 2013, 2016; Kizewski et al. 2011; Giguet-Covex et al. 2013; Eriksson et al. 2016; Werner et al. 2017; Hesterberg et al. 2017; Stahr et al. 2017; Gu et al. 2019). This technique provides information on the molecular environment of the main species present and can distinguish P bound by metal oxides or hydroxides (Prietzel et al. 2013). Quantification of species present in XANES spectra is done through linear combination fitting, which limits the number of possible species that can be identified to 3 or 4. Identifying and quantifying Pi speciation is preferable with XANES than other methods currently available (Kruse et al. 2015). Previous studies have noted that differentiating reference compound spectra in XANES can be challenging, particularly among Po species (Kruse and Leinweber 2008; Hurtarte et al. 2020), in these complex matrices.

A complementary technique to overcome limitations with XANES Po characterization is solution-state ^{31}P NMR (Liu et al. 2013; Kruse et al. 2015), which is performed on alkaline soil extracts. The distinct resonances produced by Po functional groups provide greater identification and quantification of subtle components of organic species compared to XANES. Nuclear magnetic resonance (^{31}P NMR) detects P species in liquid extracts by identifying chemical forms of the nuclei in the sample and can differentiate the number of ester linkages or species with a direct C-P bond (Doolette et al. 2011). Therefore, ^{31}P NMR has been extensively used to identify and quantify extractable monoesters, diesters, phosphonates, pyrophosphate, polyphosphate, and orthophosphate (e.g. Turrión et al. 2001; Turner et al. 2003; McDowell et al. 2007; Cade-Menun 2015).

In order to adequately forecast the response of terrestrial ecosystems to global change, it is imperative that we obtain a more comprehensive understanding of how P biogeochemistry is altered with changes in climate using molecular characterization techniques and in locations that are understudied (low P-containing parent material and drylands). Our current understanding of P biogeochemistry with pedogenesis is heavily based on soil chronosequence studies that commonly use sequential fractionation techniques to assign P into operationally defined pools. The most commonly used Hedley fractionation technique, and subsequent modifications, cannot differentiate between Fe and Al bound P as they are extracted within the same step (Hedley et al. 1982; Tiessen and Moir 1993). Additionally, fractionation techniques do not correspond to chemical specificity which may lead to erroneous conclusions about the actual chemical speciation within an extract (Kar et al. 2011). This can lead to overestimation of Ca-P and underestimation of Fe- and Al-P (Hunger et al. 2005; Helfenstein et al. 2018; Gu et al. 2020), ultimately hindering the ability to accurately quantify and model how these important forms of P are transformed along environmental gradients.

Critical knowledge gaps remain on how P dynamics are regulated by climate, particularly in low P containing parent material. Additionally, only a small number of studies have examined P content within drylands (e.g., Lajtha and Schlesinger 1988; Sumann et al. 1998; Selmants and Hart 2010; Mage and Porder 2012; Feng et al. 2016) even though drylands are the largest biome and encompass ~45% percent of terrestrial ecosystems types (Schimel 2010). Therefore, the overall objective of this study was to evaluate how soil weathering is altered along elevational gradients in temperate water-limited ecosystems (semiarid- and Mediterranean- type climates) and the implications for P concentration, stock, and chemical speciation within and among master soil horizons. We hypothesized that: (H1) chemical weathering will increase as temperature and precipitation becoming overall less limiting to ecosystem development when transitioning from semiarid to Mediterranean locations. This will cause (H2) P concentration and stock to decrease and a shift from proportionally more Ca bound P to Fe, Al, and organic species (decrease in Pi:Po), similar to the W&S model. Within the Po pool, we anticipate (H3) monoesters will preferentially accumulate relative to diesters (increase in monoester:diester) due to preferential sorption to soil constituents.

2.3 Methods

2.3.1 Study Sites

Two complimentary elevational gradients within California were selected for this study. The White Mountain Elevational Transect (WM) is along the west side of the White-Inyo Range and is a semiarid climate. The Southern Sierra Critical Zone Observatory (CZO; Table 2-1) traverses the west side of the Sierra Nevada and experiences a Mediterranean-type climate. The White-Inyo Range is located east of the Sierra Nevada and is within the rain shadow. Elevational gradients (i.e., bioclimatic sequences) allow research on soils forming under different climates because temperature and precipitation vary with elevation. Bioclimatic sequences have also been used as space for time substitutions to research climate change effects as different elevations may represent future climatic conditions (Tate 1992; Egli et al. 2003; Hart 2006). In the current study, the space-for-time substitution allows investigation on how pedogenesis is altered under different mean annual air temperatures (MAT) and MAP to influence P distribution. Previous relevant studies conducted in the CZO and WM have established a link between bedrock mineralogy and vegetation (Hahm et al. 2014) along with climate and soil physio-chemical conditions (Frisbie 2014; Jenny et al. 1949; Dahlgren et al. 1997; Dixon et al. 2009; Moreland 2020) setting a perfect stage for climate change research on P dynamics in these natural laboratories.

Both elevational gradients are formed from granitic parent material of similar age. The CZO formed 104 to 115 Ma (Bateman and Busacca 1982; Lockwood and Bateman 1976; Bateman and Wones 1972), with the exception of SH (highest elevation site) that was glaciated during the last glacial maximum (Clark and Gillespie 1997). The WM began forming ~163 Ma with an intrusion forming ~70 million years later (Ernst and Rumble 2003; Ferre et al. 2012).

2.3.2 Climate Parameters

Climate data was obtained from PRISM for calendar years 1981 through 2018 based on the latitude and longitude of each site, with a resolution of ~4 km (Daly et al. 2000). Monthly total precipitation (mm) and mean air temperature (C) was downloaded and aggregated to determine mean annual precipitation (MAP) and mean annual air temperature (MAT) over this period (PRISM Climate Group, Oregon State University, http://prism.oregonstate.edu, created 4 Feb 2004; accessed May 2020).

Effective energy and mass transfer (EEMT) is an integrative climate value that represents the input of mass and energy into the system that regulates pedogenesis (Rasmussen et al. 2005; Rasmussen and Tabor 2007). This variable is particularly valuable because it integrates energy and mass from components that correlate along elevational gradients, including temperature, precipitation, and vegetation. Mass and energy from solar radiation, carbon input from primary production, and actual water flux derived from precipitation, evapotranspiration, and surface runoff, are all incorporated into a single value for EEMT (Rasmussen and Tabor 2007). Effective energy mass transfer was calculated with the following equation:

$$EEMT\ (MJ\ m^{-2}y^{-1}) = 1000\ \times\ 347{,}134exp\left\{-0.5\left[\left(\frac{MAT-21.5}{-10.1}\right)^2+\left(\frac{MAP-4412}{1704}\right)^2\right]\right\}$$

2.3.3 Field Collection

The locations of four soil pits at each site were determined to be representative of the major topographic features of the landscape, and therefore were not selected randomly. Samples were collected based on master and subordinate genetic horizons. To capture the entire regolith, additional geoprobe samples were collected at both SPR and PR (CZO). Geoprobe samples were collected using a hydraulic coring device to collect soil samples until refusal (model DT22; outside diameter 5.72 cm). The five deepest geoprobe samples collected by Tian (2018) were chosen and added to soil pits for the current study.

Between three to five rock outcrops were sampled from all sites except SH to use as a proxy for parent material chemical composition. The SH site was excluded from this because no outcrops are located near the site and also because this site was glaciated (Clark and Gillespie 1997). The elemental composition of the outcrops sampled from site GR5 at the WM was significantly different from the other sites along this gradient, including P concentration, as assessed by analysis of variance (ANOVA) of individual elements and principle components analysis (PCA) of all elements (Figure 2-S1). Comparison of outcrop values to soil C_r horizons was used to determine if this difference was observed in the soil or if it is an artifact of outcrop chemistry. Site GR5 C_r soil horizons had similar elemental composition to the soil of other sites in the gradient and therefore these outcrops were considered outliers and not representative of the WM parent material composition. Consequently, outcrop chemical composition from GR5 was removed prior to averaging parent material elemental concentrations at the gradient level.

Soil bulk density measurements were collected by volumetric cores at the SSCZO (Dane et al. 2002) and obtained by the plaster cast method from a previous study at the WMC (Frisbie 2014). Bulk density was determined after removal of coarse fragments (> 2 mm fraction) and visible roots. Samples were oven dried at 105 °C and reported as the weight of the fine fraction (<2 mm) divided by the volume of the fine fraction. The volume percent of gravel in soil pits was estimated by dividing the weight of the coarse fraction by 2.65 Mg m^{-3}, dividing by the total volume of >2 mm plus <2 mm material, and multiplying by 100. Geoprobe bulk density and gravel percent was obtained by Tian (2018).

2.3.4 Laboratory Analyses

Soil samples were air dried and sieved to separate the <2 mm from the >2 mm gravel fraction and visible roots were removed. Soil pH was measured in a 1:2 suspension:solution slurry in deionized water and 0.01M $CaCl_2$ (Accumet Basic, Model AB15, Fisher Scientific with an Ag/AgCl electrode; Sparks et al. 1996). Elemental results are reported on an oven-dry basis using gravimetric water content (oven dried at 105 °C until constant mass). Textural Class was determined using the hydrometer method (Gee and Bauder 1986).

Lithium metaborate fusion was used to identify total elemental concentrations (P, Ca, Na, K, Fe, Al, Mg, Si) for soil samples and rock outcrops (Robertson et al. 1999). Concentration was determined by inductively-coupled plasma optical-emission spectrometry (ICP-OES; Perkin-Elmer Optima 5300 DV; Environmental Analytical Laboratory at the University of California, Merced).

Organic C and total N were measured on ground samples (CZO were ball milled for 3.5 minutes and WM samples were crushed using an agate mortar and pestle). Carbon and N were obtained for the CZO sites from Moreland (2020). Carbonates from WM sites were removed by hydrochloric acid fumigation prior to measurements (Harris et al., 2001). No free carbonates were present at the CZO sites based on no effervescence after addition of 1 M HCl to soil samples. Organic C and total N were measured on an elemental analyzer (Costech Analytical ECS 4010 Elemental Analyzer, Costech Analytical Technologies, Inc., Valencia, CA; Stable Isotope Laboratory at the University of California, Merced).

2.3.5 Chemical Index of Weathering

The chemical index of weathering (CIW; Harnois 1988) was used to determine the degree of soil chemical weathering at the sampling locations. Weathering indices reflect the transformation of primary mineral feldspars into secondary clay minerals (Nesbitt and Young 1982) as Ca and Na are leached while Al accumulates. Total element concentrations from the lithium metaborate fusion were converted into the molecular proportion of the oxide form. Calcium oxide was corrected for carbonate and apatite content by using the mole value of Na_2O when CaO was greater than Na_2O, as recommended for the chemical index of alteration (Nesbitt and Young 1982; McLennan 1993). The chemical index of alteration, another commonly used weathering index, was

not used because parent material at the WM contained a significantly higher concentration of K compared to the CZO. There were no significant differences between Al, Ca, or Na between gradients as assessed by a one-way ANOVA (data not shown). Mineral soil sample CIW versus CIA is reported in Figure 2-S3.

$$CIW = \left[\frac{Al_2O_3}{(Al_2O_3 + CaO + Na_2O)}\right] \times 100$$

A single value for each master horizon elemental concentration, pH, and CIW within a soil pit was calculated by weighting subordinate horizon values by bulk density, thickness, and removing gravel (>2 mm) content. Geoprobe samples were included in elemental concentration and CIW calculations. Due to the uncertainty with horizon designation in geoprobe samples, only Cr horizon material was used. The contribution of geoprobe samples was determined by weighting elemental concentrations by gravel corrected bulk density and thickness in each geoprobe sample (n = 10). Horizon thickness was determined by the lower boundary of each pit to the bottom of the individual geoprobe sample. Then a weighted average of all five geoprobe samples was determined for each pit. All soil pits were excavated to C_r material at PR, however only two pits at SPR were able to reach this material. In one SPR pit, C material was reached and the other extended to the bottom of the B horizon. The lower boundary of this B horizon is past the average B to C transition depth of the other pits. We assumed the boundary of Cr horizons began after each of these. Standard error (δ) was propagated for soil C horizons (δ_C) at SPR and PR sites when including both soil and geoprobe samples using the following:

$$\delta_C = \sqrt{(\delta_{soil})^2 + (\delta_{geoprobe})^2}$$

2.3.6 Phosphorus Stock

Phosphorus stock was calculated using fusion P concentrations, bulk density, horizon thickness, and gravel content. Stock from subordinate horizons, including geoprobe C_r material at PR and SPR, were summed to obtain a single value per master horizon at each pit.

$$Stock\ \left(\frac{kg}{m^2}\right) = \frac{P_{soil}\ (\frac{g}{kg})}{P_{PM}(\frac{g}{kg})}\ \times\ bulk\ density\ \left(\frac{kg}{m^3}\right) \times\ depth(m)\ \times \left(1 - \frac{rock\ fraction\ (\%)}{100}\right)$$

Stock values were normalized by parent material P concentration (P_{PM}; g kg^{-1}) to account for the higher concentration of parent material at the WM sites. Globally, granite rocks have a mean P concentration of 0.57 g kg^{-1} and granodiorite is 0.81 g kg^{-1} (Porder and Ramachandran 2013). Granite parent material P concentrations were determined by lithium metaborate fusion for the CZO and WM and found a mean and standard error of 0.74 ± 0.05 and 1.5 ± 0.05 g kg^{-1}, respectively.

2.3.7 Phosphorus Speciation

X-ray absorption near edge structure (XANES) and nuclear magnetic resonance (NMR) spectroscopy were used to quantify P chemical speciation. At least three field replicate A horizons were run for XANES and NMR at each site. One depth profile per site was collected for NMR, and most sites had at least one subsurface horizon run for XANES. Data were collected on the uppermost subordinate horizon when multiple subordinate horizons were present.

2.3.7.1 XANES

Bulk XANES spectra were collected at beamline 14-3 at the Stanford Synchrotron Radiation Lightsource (SSRL, Stanford, CA) and at the soft X-ray microcharacterization beamline (SXRMB) at the Canadian Light Source (CLS, Saskatoon, Canada). Sample and reference compound material were transferred to carbon tape and were in a He gas environment or a vacuum at room temperature during collection (due to different beamline configurations). X-ray absorption near edge structure was collected for 37 soil samples. A reference compound library (n = 35) was compiled using compounds that were either purchased from a manufacturer (reagent grade or better), or synthesized in the laboratory. Methods for synthesized compounds are described in the Supplementary Information (SI). A total of 35 organic and inorganic reference compounds were used to build a library for identifying P chemical species that are commonly found in soil (Table 2-S2). Comparisons between reference compounds are discussed in the SI.

Spectra were imported to Sam's Interface XAS Package (SIXPACK; Web 2005) for averaging and then into the ATHENA software package (Demeter 0.9.20; Ravel and Newville 2005) for calibration, baseline correction, normalization, and linear combination fitting. Energy was calibrated at the P K-edge with sodium phosphate (NaH_2PO_4) at 2152.6 eV, or tetraphenylphosphonium bromide (PPh_4Br) with the first peak at 2146.96 eV. Baseline correction and edge-step normalization parameters were varied for individual samples and reference compounds to reduce error (Werner and Prietzel 2015). Linear combination fitting (LCF) was used to determine the main species present within the unknown samples. The fits were conducted with up to four reference compounds and the sum was not forced to unity. The final fit was chosen based on that which had the lowest R-factor and number of reference compounds, and only best fits within 2.5% of 100% were accepted. The R-factor of all sample LCF were <0.05 indicating a good quality of fit (Kelly et al. 2008). Previous research investigating uncertainty of LCF accuracy of phase determination have found an overall error estimated to be between 1~15% (Beauchemin et al. 2003; Ajiboye et al. 2007; Werner and Prietzel 2015); therefore, reference compounds that fit below 5% were removed and the remaining compounds were refit as recommended by Werner and Prietzel (2015). The relative error of LCF has been found to be less when the proportion of Ca-P in the mixture increased (Ajiboye et al. 2007). Mean and standard error of field replicates are reported, which reflects the larger variability among samples within a site than error from precision of the LCF and likely from the uncertainty of accurate phase identification (Ajiboye et al. 2007).

Previous studies have noted that differentiating reference compound spectra can be challenging, particularly among Po species (Kruse and Leinweber 2008; Hurtarte et al. 2020), in these complex matrices. However, lack of inclusion of multiple Pi and Po compounds of a given metal within the reference compound library can result in erroneous fits and underestimation of the contributions from metal and Po species (Prietzel and Klysubun 2018). Recent studies using P K-edge XANES are more commonly using larger reference compound libraries (e.g. Giguet-Covex et al. 2013; Hashimoto et al. 2014; Hashimoto and Watanabe 2014; Prietzel et al. 2016; Werner et al. 2017; Hesterberg et al. 2017; Schmieder et al. 2018; O'Day et al. 2020) because it is critical for the reference compounds used in LCF to contain representative species found within the environmental sample. Hence, the current study collected a large reference library of Pi and Po species associated with Ca, Al, Fe, and Na and then individual reference compounds were classified into groups based on the associated metal prior to statistical analyses (Table 2-S2).

2.3.7.2 ^{31}P NMR

Solution state ^{31}P NMR was conducted on 39 soil samples to characterize chemical speciation, particularly for Po compounds that are found in low concentrations. Three grams of finely ground <2 mm soil samples were extracted for four hours at ambient temperature with 30 mL of 0.25 M NaOH and 0.05 M EDTA (Turner et al., 2008; Cade-Menun and Liu 2014). Following this, samples were centrifuged at 10,000 g for 30 minutes and the supernatant was filtered through a 0.45 μm nylon membrane using a syringe. A 5 mL aliquot was removed from the filtered extract and frozen for elemental determination (P and others) using an ICP-OES. The remaining extract was frozen with liquid N_2 and lyophilized. Just prior to the NMR experiment, 1.08 mL of a 1.0 M NaOH and 0.05 M EDTA solution plus 0.12 mL of deuterium oxide (D_2O) were added to the lyophilized powders and thoroughly mixed by vortex until all solids dissolved. Finally, samples were centrifuged with 0.22 μm nylon spin filters for 10 min at 13k rpm. The pH of each filtrate was recorded and all samples were above 14. Approximately 550 μL of the reconstituted sample was spiked with 5 μL of 61 mM methylene diphosphonic acid (MDP; included to allow comparison to prior studies that used this for calibration) and transferred to a 5 mm NMR tube. The remaining sample was transferred to a separate NMR tube and spiked, if necessary (details provided in SI), with 1 M $Na_3PO4_3^-$ for pulse-width calibration and determination of relaxation times. Solution state ^{31}P 1D NMR experiments were acquired on a Bruker Advance III spectrometer equipped with a Bruker 5mm BBO direct detect probe. Additional experiment details including the pulse program, T_1 measurements, and experiment length, are described in the Supplementary Information.

Post-acquisition processing included zero-filling to 128k total points, exponential multiplication (1 – 10 Hz line-broadening), and automated baseline correction with a 5th order polynomial using TopSpin 4.0.7 (Bruker, Germany). Quantification of individual peak areas were conducted by spectral deconvolution and integration using MestReNova 14.0 software (Mestrelab Research, Spain). Peaks were "picked" automatically by the software using the Global Spectral Deconvolution method and then clearly visible peaks

that were missed by the software were manually selected. Previous work has suggested that error for solution ^{31}P NMR spectroscopy of soil extracts is approximately 3% for total Po, 6% for monoesters, and 10% for DNA based on three replicate extracts (Turner 2008), however uncertainty is specific to each spectrum based on the signal-to-noise ratio. The estimation of error from Turner (2008) would encompass variability within the extraction, NMR experiment, and spectral processing. Error for the current study was estimated using four NMR experiments collected on a single extract. Using one sample (SH Pit 1 A horizon) as an example, mean and standard error was 80 ± 0.7% for orthophosphate, 0.3 ± 0.0% for pyrophosphate, 3 ± 1.0% for monoesters, 7 ± 0.6% for diesters, and 3 ± 0.1% for DNA. Monoester and diester regions were corrected for degradation of α-glycerophosphate, but β-glycerophosphate concentration was too low to be detected with deconvolution (low signal to noise in these four hour experiments). Because variability of the NMR experiment and spectral deconvolution was lower than field replication, we are reporting mean and standard error of the field replicates (A horizons only; lack of instrument time prevented replication in subsurface horizons). Other studies have recognized that the largest source of error is inadequately identifying chemical shifts (Kizewski et al. 2011).

Initial chemical shift referencing was established using an external orthophosphoric acid standard (85%), which placed the orthophosphate peak in samples between 5.8 and 6.2 ppm. The orthophosphate peak was then set to $\delta = 6.0$ ppm in all spectra for alignment and comparison to literature values. Chemical shifts of P species were compared to published literature for identification and, ultimately, assignments were confirmed via spiking experiments (Cade-Menun 2015; Schneider et al. 2016; Recena et al. 2018). Spiking experiments were conducted by sequentially adding solutions containing known compounds from commercial sources, including DL-α-glycerophosphate, β-glycerophosphate, RNA, myo-IHP, glucose-6-phosphate, and glucose-1-phosphate. These known P compounds were dissolved in the reconstitution buffer at concentrations of approximately 60 mM and added in 5 – 10 μL amounts to samples after initial sample NMR measurements (Figure 2-S6).

Degradation of RNA and phospholipids (diesters) to monoesters occurs in the highly alkaline extraction and reconstitution solutions and, depending on the length of time between mixing and acquisition, continues during the duration of the NMR experiment (Turner et al. 2003; Doolette et al. 2009; Vincent et al. 2013). As a result, a degradation correction is commonly applied during data processing (e.g., Young et al. 2013; Schneider et al. 2016; Recena et al. 2018). Degradation of phospholipids were corrected for by shifting the integrated areas of α and β-glycerophosphate peaks from the monoester to diester region. In instances where the β-glycerophosphate signal overlapped with phytate, two times the first phytate peak was subtracted from the β-glycerophosphate peak area (Smernik and Dougherty 2007). Overlap with other peaks in the monoester region prevented unequivocal identification of RNA degradation products in all samples; therefore, RNA degradation could not be corrected.

2.3.8 Statistical Analyses

All statistical tests were conducted using R (version 3.4.2; R Development Core Team, 2013). Mixed effect models were used to test the relationships between chemical weathering (i.e., CIA and pH) with climate (i.e., EEMT), master soil horizon, and their interaction (Hypothesis 1). Least squares linear regression was used to investigate how climate (i.e., EEMT) impacts soil P stock (calculated to 43 cm; Hypothesis 2). Mixed effect models were also ran to examine how climate (i.e., EEMT), master soil horizon, and their interaction impacts soil P concentration, stock, and speciation (Hypotheses 2 and 3). Mixed effect models were fit by restricted maximum likelihood and a random effect of pit was included to account for lack of spatial independence when sampling. Mixed effect models were performed with the lme4 package (Bates et al. 2015). Marginal (only fixed effects considered) and conditional (both fixed and random effects considered) adjusted R^2 values were calculated following Nakagawa et al. (2013) using the MuMIn package (Barton and Barton 2019). Speciation concentrations were log (value + 1) transformed to meet model assumptions. Additional linear models were ran as a post hoc test of individual horizons with EEMT when this interaction was significant in the original mixed effect model. A linear model was also ran on the Pi:Po ratio (identified by XANES) in A horizons only because the low sample size with depth prevented investigation between horizons. Relationships are considered significant when $p < 0.05$. All data is presented with mean ± standard error of field replicates unless otherwise stated.

We used redundancy analysis (RDA) to understand how changes in climate and soil properties influence speciation. We investigated the relationship of climate (MAP and MAT) and soil (pH in $CaCl_2$, and Fe, Ca, Al, C, and P concentrations) properties with the relative percent of NMR and XANES P speciation. This multivariate analysis uses multiple predictor and response variables (an extension of multiple linear regression), which are ordinated in three-dimensional space (Legendre and Legendre 2012). Although similar to principal components analysis (PCA), ordination is constrained for RDA, while ordination is unconstrained for PCA (Zurr et al. 2007). Linear combinations of predictor and response variables are scored to determine which predictor variables explain most of the variance. The RDA was calculated using the rda function in the vegan package (Oksanen et al. 2018). Response variables were centered to a mean of zero and standardized to a deviation of one. Separate RDA were conducted for NMR (n = 39) and XANES (n = 37) speciation and are presented as triplots (coordinate system defined by two RDA axes with vectors included for predictor and response variables). Type 2 scaling was used that allows angles to be interpreted as correlations (each eigenvector is scaled to the square root of its eigenvalue). Response variables are included as points where the location indicates the degree of association with the RDA axes, with maximum positive at 0 degrees, maximum negative at 180 degrees, and minimum at 90 or 270 degrees. Predictor vector length and direction provides insight to the relative contribution to the RDA axes. Significance of the entire model, axis, and predictor variables was assessed by permutation. A variance inflation factor (VIF) was calculated with the car package for explanatory variables to ensure multicollinearity assumptions were not violated. All VIFs were below 8.

2.4 Results

2.4.1 Changes in Weathering Intensity with Climate and Depth

The chemical index of weathering (CIW) was positively related to EEMT in all mineral horizons (marginal $R^2 = 0.41$, $p < 0.05$, n = 87) suggesting that soil weathering intensity increases with EEMT (Figure 2-1). Effective energy and mass transfer increased from the semiarid WM (5.41 ± 2.22 MJ m^{-2} yr^{-1}; n = 4) to the Mediterranean CZO (21.59 ± 6.67 MJ m^{-2} yr^{-1}; n = 4) elevational transect, with BAR (WM high-elevation) as the least weathered site and SPR (CZO mid-elevation) as the most weathered (Table 2-S1). The CIW was comparatively lower in all mineral horizons at the WM than at the CZO, with an average of 45.5 ± 0.49 (n = 42) and 56.5 ± 1.3 (n = 45), respectively (Table 2-S1). Although EEMT at the WM ranged from 2.78 to 7.64 MJ m^{-2} y^{-1}, there was little variation in CIW values suggesting that there is little influence of climate driving their formation within the elevational transect (Figure 2-1a). On the other hand, the CZO CIW values expressed higher variability among sites and encompassed a greater range of EEMT values from 12.87 to 29.10 MJ m^{-2} y^{-1} (n = 45). Although SJER had a relatively high EEMT (22.30 MJ m^{-2} y^{-1}), the CIW values did not reflect this. This discrepancy may be due to differences in parent material Al, Ca, and Na concentrations at that site. Rock outcrop CIW values were not significantly different at the gradient scale (WM 46.43 ± 0.68, n = 15;and CZO 45.87 ± 1.2, n = 13) using a one-way ANOVA ($p = 0.67$, n = 28; Table 2-S1)

Within a gradient, EEMT was positively correlated to elevation at the WM and was negatively correlated with precipitation ($r^2 = 0.99$, $p < 0.05$, n = 4) and positively correlated with temperature ($r^2 = 1.00$, $p < 0.05$, n = 4). Although the least weathered site at the CZO was also at the highest elevation (SH; 2700 m), the most weathered site was at mid-elevation (SPR 1160 m). Mean annual precipitation ($r^2 = -0.27$, $p = 0.61$, n = 4) and MAT ($r^2 = 0.32$, $p = 0.26$, n = 4) were not significantly correlated with EEMT at the CZO. When considering all eight sampling locations across both elevational gradients, EEMT was significantly related to MAT ($r^2 = 0.63$, $p < 0.05$) but not to MAP ($r^2 = 0.23$, $p = 0.13$).

The impact of climate and depth was also investigated for pH (Figure 2-1b). Mixed effect models found pH measured in both $CaCl_2$ (marginal $R^2 = 0.24$, conditional $R^2 = 0.92$) and DI water (marginal $R^2 = 0.44$, conditional $R^2 = 0.95$; data not shown) significantly decreased with EEMT across all sites ($p < 0.05$, n = 87). There were no significant differences among horizons and no significant interactions between horizon and EEMT occurred.

2.4.2 Changes in P Concentration and Stock with Climate and Depth

Phosphorus stock increased with EEMT when considering a consistent depth across all sites and when investigating trends in all master soil horizons (Figures 2-2a and 2-2b). Phosphorus stock in the top 43 cm of mineral soil that was normalized to parent material concentration had a positive relationship with EEMT ($r^2 = 0.51$, $p < 0.05$, n = 33;

Fig 2a). The main effect of EEMT and A and B interaction terms were not significant, indicating that O, A, and B horizon stock is largely unaffected by EEMT ($p > 0.05$; n = 119). However, P stock in C horizons were significantly different from O horizons ($\beta = 0.109$) and had a more positive slope ($\beta = 134$) indicating a greater rate of change in C horizons with increasing EEMT. Linear regression was used to determine the relationship of only C horizons with EEMT; this analysis found stock significantly increased with EEMT ($r^2 = 0.38$, $p < 0.05$, $\beta = 135$, n = 26).

Phosphorus concentration significantly increased with EEMT in O horizons ($p < 0.05$, $\beta = 0.02$, n = 21) and A horizons ($p = 0.50$, n = 32; Fig 2c). On the other hand, B ($p < 0.05$, $\beta = 0.002$, n = 29) and C ($p < 0.05$, $\beta = -0.02$, n = 26) horizons have a significantly different relationship with EEMT than O horizons. Post-hoc linear models found B horizons were unchanged ($r^2 = -0.03$, $p = 0.72$, $\beta = -0.004$, n = 29) and C ($r^2 = 0.10$, $p = 0.08$, $\beta = -0.02$, n = 26) horizons had a negative relationship, although this was not significant at $p < 0.05$.

There was little difference in P concentration and stock with depth into the soil (Fig 2). Results from mixed effect model did not show any significant difference in P stock between A, B, or C horizons and O horizons. However, P concentration in the C horizon was significantly lower than O horizons ($p < 0.05$) but A and B horizons were not significantly different.

2.4.3 XANES P Speciation

Phosphorus K-edge XANES samples contained different spectral features based on site and horizon (Figure 2-3). Apatite and other Ca-Pi species comprised the greatest relative percent of all species at the WM (Figures 2-3 and 2-5a, Table 2-S3). Calcium- Pi in A, B, and C horizons at the WM contained an average of 50 ± 7% (n = 12), 55 ± 11% (n = 5), and 97 ± 4% (n = 3), respectively. Calcium-Pi was often identified as primary mineral apatite at WM sites with an average of 44 ± 7% (n = 20) across all samples. In contrast, Fe- and Al-Pi dominated the CZO sites. The CZO averaged 27 ± 7% (n = 13), 28 ± 7% (n = 2), and 11 ± 11% (n = 2) Fe-Pi in A, B, and C horizons, respectively. Aluminum bound Pi averaged 55 ± 5% (n = 13), 71 ± 7% (n = 2), and 59 ± 10% (n = 2) in A, B, and C horizons, respectively. Aluminum- and Fe-Pi was primarily fit as P sorbed onto the surface of minerals at both gradients.

The percentage of total Po relative to total P and the composition of the pool varied between sites. The greatest percent of Po was found in WM A horizons with an average of 29 ± 6 (n = 12)%. In comparison, the CZO had only an average of 11 ± 3% (n = 13) Po in A horizons. Organic P species were fit as both monoesters and diesters, with Na, Ca, Fe, or Al as the counter-cation. Organic P species were commonly identified as sorbed species on minerals rather than as precipitated forms, and were more readily associated with Fe or Al than Ca. Diesters sorbed on Al were fit at both gradients in A horizons, but were a greater fraction of the total P in WM sites. Total Al-Po in A, B, and C horizons averaged 12 ± 5% (n = 12), 5 ± 5% (n = 5), and 0.0 ± 0.0% (n = 3) in the WM and 2 ± 2% (n = 13), 0.0 ± 0.0% (n = 2), and 6 ± 6% (n = 2) at the CZO. Organic P was identified as diesters sorbed on Fe at the CZO, largely due to SJER (400 m site). Iron

bound Po was not found in B or C horizons at the CZO. Calcium-Po was only identified at the WM.

2.4.4 ^{31}P NMR Speciation

Sodium hydroxide-EDTA soil extracts from the WM and CZO elevational transects contained a variety of Pi and Po species as detected by ^{31}P NMR (Figures 2-4 and 2-5b). Inorganic P compounds comprised the greatest proportion of extractable P in most samples. Sites at the WM contained an average Pi of 61 ± 6 (n = 12), 61 ± 13 (n = 4), 85 ± 3% (n = 4) and CZO sites averaged 83 ± 4 (n = 12), 90 ± 4% (n = 3), 94 ± 1% (n = 4) in A, B, and C horizons, respectively (Figure 2-5b and Table 2-S4). Inorganic P species identified include orthophosphate (6 ppm) and pyrophosphate (~-3.5 ppm), with proportionally more orthophosphate. Pyrophosphate only made up 0.7 ± 0.1% (n = 19) of total P at the WM and 1.0 ± 0.2% (n = 20) of total P at the CZO.

The relative proportion of Po was greater at the WM in A, B, and C horizons with 39 ± 6% (n = 12), 39 ± 13% (n = 4), 15 ± 3% (n = 4) compared to 17 ± 4% (n = 12), 10 ± 4% (n = 3), and 6 ± 1% (n = 4) at the CZO (Figure 2-5b and Table 2-S4). The observed high Po at the WM was largely due to the least weathered site (BAR) having 66 ± 4% in A horizons (n=3) and 78% (n=1) in the B horizons The majority of Po species identified at both gradients were monoesters and diesters, with phosphonates (18.5 to 20.1 ppm) only identified at BAR, GR3, PR, and SH. Phosphonates comprised < ~1% in all samples (n = 39) of total P (Table 2-S4). Across all samples, peaks in the monoester region indicated the presence of *myo*- (~5.3, ~4.3, ~4.0, ~3.9 ppm) and *scyllo*-IHP (~3.5 ppm; i.e., phytate), glucose-6-phosphate (~5.2 ppm), α- and β-glycerophosphate (~4.7 ppm, ~4.3 ppm; phospholipid degradation), mononucleotides (~4.2; RNA degradation), choline phosphate, and some unknown monoesters. The diester region (2.3 to -3.2 ppm) was largely composed of DNA (~-1.0 ppm), with evidence of phospholipids (2.3 to -0.5 ppm) and an unknown diester (di 2, ~-2.8 ppm).

Quantification of individual monoester species was not possible in all samples with the exception of α- and β-glycerophosphate due to signal overlap. Therefore, only phospholipid degradation was corrected and the remaining species are reported as monoesters (5.7 to 2.3 ppm; Figure 2-4). Correcting for degradation shifted monoesters at the WM from 30 ± 4% to 12 ± 2% (n = 20) and from 12 ± 2% to 4.8 ± 0.7% (n = 19) at the CZO across all horizons and sites. Diesters increased from 2.4 ± 0.5% to 23 ± 3% (n = 20) and 2.2 ± 0.4% to 9 ± 2% (n = 19) at the WM and CZO, respectively. On average, diesters were more common than monoesters across both elevational gradients, with the exception of CZO C horizons.

Concentrations of NaOH-EDTA extractable total P increased with EEMT (p < 0.05), with higher values at the CZO in A and C horizons compared to the WM. There was also a greater extraction efficiency at the CZO in all horizons. The percent of total P extracted by NaOH-EDTA ranged from 13.4 - 79.1% (n = 19) at the CZO and 0.7 - 36.5% (n = 20) at the WM, with extraction efficiency decreasing with depth into the soil (Table 2-S5).

2.4.5 Changes in P Speciation with Climate

Chemical speciation examined by phosphorus K edge XANES and ^{31}P NMR found notable changes with EEMT (Figures 2-6 and 2-7). The relative percent of total and extractable Pi, identified by XANES and NMR, respectively, had a positive relationship with EEMT in A and B horizons ($p < 0.05$). Although total Pi in C horizons had a negative relationship with EEMT, it was not significantly different from A horizons, likely due to the lower sample size (A: n = 25; B: n = 7; C n = 5). Total Po measured by XANES and extractable Po measured by NMR followed each other. As EEMT increased, Po decreased in A horizons ($p < 0.05$) and the relationship of B horizons with EEMT were not significantly different (XANES: $p = 0.37$; NMR $p = 0.30$). Although Po in C horizons had a significantly different relationship when identified by XANES, a post hoc test found Po was unchanged by EEMT in this horizon ($p = 0.29$). The ratio of Pi:Po increased with EEMT in A horizons for XANES data ($p < 0.05$; B and C horizons were not included in the model). Extractable Pi:Po was also positively related to EEMT. Specifically, Pi:Po in A horizons increased ($p < 0.05$) and the relationship was similar among deeper horizons (B: p=0.29, C: P=0.51). Overall, increases in climate-induced weathering increased Pi and decreased Po, leading to increased Pi:Po across master soil horizons in bulk and extractable measurements.

With increasing EEMT, Pi species shifted from predominately Ca to Fe and Al associated in all horizons (Figure 2-6). Calcium bound Pi decreased with EEMT in A horizons ($p<0.05$), and this relationship was similar in B ($p = 0.32$) and C ($p = 0.42$) horizons. On the other hand, Fe- and Al-Pi increased in A horizons ($p < 0.05$) and the interaction terms for B (Fe: $p = 0.08$, Al: $p = 0.31$) and C (Fe: $p = 0.43$, Al: $p = 0.05$) horizons were not significantly different.

Extractable Pi and Po species demonstrated opposite trends with climate-induced weathering (Figure 2-7). Extractable orthophosphate increased with EEMT ($p < 0.05$) across all horizons (B: $p = 0.60$, C: $p = 0.13$). Although pyrophosphate was unaffected by EEMT in A ($p = 0.55$) and C ($p = 0.89$) horizons, it significantly increased in B horizons ($p < 0.05$). Both monoesters (A: $p < 0.05$, B: $p = 0.59$, C: $p = 0.34$) and diesters (A: $p < 0.05$, B: $p = 0.15$, C: $p = 0.92$) had a negative relationship with EEMT across all horizons. The monoester:diester ratio did not significantly change with EEMT in any horizons (A: $p = 0.43$, B: $p = 0.10$, C: $p = 0.12$).

2.4.6 Changes in P Speciation with Depth

Total and extractable Pi and Po species differed by depth into the soil profile. Total and extractable Pi percent was higher in C horizons compared to A horizons, as measured by XANES and NMR, respectively ($p < 0.05$; Figures 2-6 and 2-7). Although extractable pyrophosphate decreased in B horizons compared to A, orthophosphate increased to a greater degree resulting in extractable total Pi to increase with depth. Aluminum bound Pi also decreased in C horizons compared to the surficial soil ($p < 0.05$). In contrast to Pi, total and extractable Po decreased with depth. The extractable Po pool was largely driven by decreasing diesters in C horizons compared to both A and B

horizons ($p < 0.05$), resulting in the extractable Pi:Po ratio increasing with depth ($p < 0.05$).

2.4.7 Changes in P Speciation with Climate and Soil Properties

Redundancy analysis was used to investigate the multivariate relationship between climate (MAP and MAT) and soil (pH in CaCl2, and Fe, Ca, Al, C, P, and N concentrations) properties with P speciation identified by XANES or NMR (Figure 2-8). A permutation test found the independent variables included in both RDAs to be overall significant predictors of P speciation ($p < 0.05$). Sites tended to cluster together in both RDAs within their respective elevational gradient.

P species identified by XANES were significantly predicted by climate and soil properties ($p < 0.05$, adjusted $R^2 = 0.23$). The first RDA axis was strongly associated with clay, MAP, pH, Al, MAT, and C, and explained 57.7% of the constrained variation. The second RDA axis was mostly associated with Fe and P, and explained an additional 14.2% of the variation. Calcium-Pi was positively correlated with clay, pH, and Ca. Alternatively, Al- and Fe- Pi were positively related to MAP, MAT, and Al and C concentrations. Organic species, regardless of metal association, were negatively correlated with P and Fe concentrations.

P species identified by NMR were also significantly explained by climate and soil properties ($p < 0.05$; $R^2 = 0.30$). The first axis was mainly composed of pH, MAP, MAT, and P and Fe concentrations, which explained 78% of the constrained variation. The second axis explained 14% of the variation and was strongly associated with Ca and C concentrations. Organic species including diesters, monoesters and RNA, and phosphonates were positively correlated with pH. Pyrophosphate was positively correlated to C and P concentrations and MAP. Orthophosphate was most closely related to MAT and Fe.

2.5 Discussion

2.5.1 Climate-Driven Soil Weathering Intensity

To test the validity of the W&S (1976) conceptual model to climatic weathering gradients, we quantified soil P stock, concentration, and chemical speciation using advanced analytical techniques between and among master soil horizons. We found important implications for P concentration and stock and the occurrence, transformation, and persistence of chemical species. A transition from semiarid to Mediterranean-type climate resulted in soil with more chemical weathering that supported greater P stock, redistribution of P concentration with depth, a shift from Pi associated with Ca to more Fe and Al species, and a proportional decrease of Po. Overall, climate-induced increases in weathering intensity in these dryland ecosystems resemble Pi transformations that occur along chronosequences. However, total P stock accumulated and the Po pool did not proportionally increase as we hypothesized. This indicates there may a greater amount of P for vegetation and microorganisms to utilize at relatively more weathered

sites, and biota are likely exploiting turnover of organic species as a source of bioavailable P.

Climate positively impacts the degree of soil weathering across semiarid and Mediterranean regions, which can impact a suite of soil chemical and physical characteristics. Soil weathering increased with EEMT, an integrative climate variable. A global analysis of EEMT values established a threshold of 70 MJ m^2 y^{-1} to indicate the transition from water to energy limited ecosystems (Rasmussen et al. 2010b). Values ranged from to 2.8 to 29 MJ m^2 y^{-1} in the current study, indicating ecosystem development (chemical weathering reactions and primary production) at these sites is overall moisture limited. Previous work has established a relationship between EEMT and soil weathering intensity, with significant relationships between EEMT and pedon depth, clay content, subsurface CIW, and the ratio of free Fe oxides to total Fe (Rasmussen and Tabor 2007). Other studies have demonstrated increased weathering along chronosequences (Zhou et al. 2013; Gu et al. 2019) and climosequences (Rasmussen et al. 2010a; Sheldon et al. 2015) using a chemical weathering index (chemical index of alteration or chemical index of weathering). We found that increasing EEMT resulted in higher soil CIW and decreased pH in all mineral horizons, suggesting that chemical weathering increases with climate-induced pedogenesis (Figure 2-1).

As expected, the CIW across all sites demonstrate these soils are not highly weathered. With an average of 45.9 ± 1 in the parent material at the WM and 46.4 ± 0.7 at the CZO, mobile ions in soil were largely not depleted with values of 45.5 ± 0.5 and 56.5 ± 1, respectively. In comparison, highly weathered locations in humid tropical regions have demonstrated CIW values above 90 (Zhang et al. 2007). At the CZO gradient, the mid elevation sites tended to have higher chemical weathering, as assessed by the CIW, likely due to water limitation at low elevation and temperature limitation upslope (Rasmussen et al. 2010a; Goulden and Bales 2014; Kelly and Goulden 2016; Figure2-1 and Table 2-S1). Others have reported a shift from highly developed to weakly weathered soils at elevations encompassing the shift from rain to snow dominated climate in basalt and granite soils (Dahlgren et al. 1997; Rasmussen and Tabor 2007; Dixon et al. 2009; Rasmussen et al. 2010a). A previous study conducted at the same CZO mid-elevation sites also found SPR, where precipitation is rain-dominated, exhibited a greater degree of pedogenesis (Tian 2018). This was supported by an increase in clay and extractable Fe content compared to the snow-dominated PR site, even though regolith is thicker (due to weathered saprock) and and NPP is greater at the PR site (Tian 2018). Interestingly, the WM did not follow the same weathering trend with elevation as CIW was relatively unchanged across the gradient (Table 2-S1). This may be because soil development is exceptionally water limited, causing evapotranspiration to exceed precipitation at all elevations, and therefore preventing leaching of mobile cations (Peltzer et al. 2010).

2.5.2 Walker and Syers Model Comparison

2.5.2.1 P Concentration and Stock Changes with Climate

Transitioning from semiarid to Mediterranean- type climates altered the rate of pedogenesis to influence P concentration and stock (Figures 2-2 and 2-9). According to the W&S model, P stock is anticipated to decrease over long-term soil development due to leaching and erosion loss. Numerous studies have also reported P concentration decreases over time (e.g., Lajtha and Schlesinger 1988; Prietzel et al. 2013; Wu et al. 2014). This characteristic feature of P concentration or stock declining has been supported in a number of different soil and ecosystem types along chronosequences (i.e., Wardle et al. 2004; Turner et al. 2012, 2018; Chen et al. 2015), with few exceptions (Crews et al. 1995; Schlesinger et al. 1998; Vincent et al. 2013). Although there are relatively few P biogeochemistry studies conducted along climate gradients, those conducted to date have reported total P concentration or stock has a non-linear relationship with increasing precipitation (Miller et al. 2001; Helfenstein et al. 2018), elevation (He et al. 2016; Zhou et al. 2016), aridity (Feng et al. 2016), or temperature (Mou et al. 2020), while others have found the predicable linear decrease in total P (Turner et al. 2018). A non-linear relationship between P concentration and precipitation has been attributed to decreasing total P with initial increases in precipitation, but an accumulation of Po from lower mineralization rates in anaerobic conditions at humid sites (Miller et al. 2001) or because increased plant productivity concentrates P in surficial horizons (Feng et al. 2016). A peak in total P at subhumid sites has also been attributed to biological uplift and dust deposition that is retained by soils with high sorption capacity until leaching exceeds P input in wetter sites (Helfenstein et al. 2018). Therefore, P concentration and stock with increased soil weathering along climate gradients appear to frequently be inconsistent with the W&S model.

We found P stock increased with climate-induced weathering at a consistent depth across the gradient (Figure 2-2a), contradicting the W&S model. Further examination of individual horizons in the entire regolith found only C horizon stock significantly increased, although all horizons had a positive relationship with EEMT (Figure 2-2b). Additional investigation of P concentration with EEMT demonstrated opposing relationships in master soil horizons. Organic and A horizon concentrations increased with EEMT, B were relatively unchanged, and C horizons decreased. Therefore, our hypothesis of decreasing concentration and stock was only supported with C horizon concentration. The increase in stock was largely due to an accumulation of P in O and A horizons along with deep regolith from weathered saprock at sites with the greatest degree of soil development (CZO PR and SPR). The observed increase of P stock is unexpected, particularly because precipitation exceeds evapotranspiration at the CZO, which should drive nutrient depletion compared to the less weathered WM sites (Porder and Chadwick 2009). However, P stock appears to be accumulating in these slightly to intermediately weathered dryland sites because exogeneous P inputs and internal cycling allows for more P retention than is lost via leaching and erosion.

The increase of P stock is likely driven by the interaction of vegetation composition and input of aeolian dust. The transition from pinyon pine and shrubland at

the semiarid WM to mixed conifer forest at the Mediterranean CZO sites brings a larger input of soil organic matter. This is supported by the presence of thicker organic horizons in the more weathered mixed conifer sites, increased C concentration in O horizons, and increased A horizon C stock with EEMT (data not shown). The increased input of SOM likely caused both Pi and Po concentration, and subsequently P stock, to increase in surficial soil because both of these chemical species are found within plant material (Noack et al. 2012). Additionally, because P concentration increased with depth at WM sites but decreased with depth at the CZO, vegetation at the CZO sites may be mining P from deeper soil layers and redistributing it back to the soil surface through litterfall and subsequent mineralization to cause the depletion of P concentration with depth (Smeck 1973; Jobbágy and Jackson 2001; Ippolito et al. 2010). Phosphorus redistribution has been previously suggested at the sites (Wilson 2020). Deep rooting tree species are also more likely to contribute to nutrient redistribution compared to shallow rooted grass and shrubs (Zhou et al. 2016). The presence of deep roots in the weathered saprock at the forested CZO has been observed (Stone and Kalisz 1991; Graham et al. 2010) and, although the presence of deep roots is largely driven by water exploitation from the saprock, they may also be accessing primary mineral P and causing P concentration to decrease with depth at these sites (Graham et al. 2010; but see Newman et al. 2020). Fine roots tend to occur at greater depths in water limited ecosystems (Schenk and Jackson, 2002), but water and nutrient demand can both contribute to increased root activity with depth (McCulley et al. 2004; Newman et al. 2020). Therefore, we speculate deep rooting tree species are mining Pi from C horizons and redistributing it to surficial soil, contributing to the observed increases of P stock in more chemically weathered soil.

Although wetter locations tend to lose P at a greater rate than drier sites from increased weathering and leaching loss, this may be mitigated by the increased plant biomass found at wetter sites (Porder and Chadwick 2009; Turner et al. 2018). Porder and Chadwick (2009) demonstrated an enrichment of P in upper soil horizons at intermediate precipitation compared to drier sites because increased plant cover, along with a negative water balance (potential evapotranspiration > precipitation), allows P to accumulate. The authors identify a threshold where plants can no longer offset nutrient leaching losses at high rainfall (potential evapotranspiration < precipitation) and older, more weathered soil. Although potential evapotranspiration exceeds precipitation at the Mediterranean CZO, these sites have likely not passed a threshold where plants play only a minor role in retaining soil P due to the young chronological and pedogenic age compared to wet tropical sites (Porder and Chadwick 2009). The Mediterranean-type climate may also prevent this threshold from being exceeded, especially in the snow-dominated high elevations where leaching is confined to short periods right after snowmelt, thus preventing year-round nutrient loss (Homyak et al. 2014). We provide evidence that the comparatively more weathered Mediterranean CZO sites that support deep rooted tree species are retaining more P than is lost through leaching and erosion, allowing P to accumulate with increased climate-induced weathering.

Increasing stock may also be driven by greater P inputs from aeolian dust at the Mediterranean CZO compared to the semiarid WM (Aciego et al. 2017, O'Day et al. 2020). Total mass input of aeolian particulate matter at the semiarid WM has been

estimated to be between 1.4 to 20.3 g m^{-2} y^{-1} (Marchand 1970), whereas fluxes at the Mediterranean CZO range from 3 to 36 g m^{-2} y^{-1} (Aciego et al. 2017). However, we would like to note that regionally sourced dust that is high in soluble salts can constitute up to 50% of the silt fraction of soil in the WM (Matchand 1970, Reheis 1997). Aeolian particulate matter fluxes also form vesicular horizons at some sites (i.e., GR2 and GR3; Turk and Graham 2011), therefore, fluxes are not negligible at the WM sites and suggests relatively high aeolian dust inputs. Aeolian particulate matter provides an important flux of P at the CZO. In particular, the low bedrock nutrient concentration and slow weathering rates lead to the total P flux from dust to be higher than long-term input from bare rock (Aciego et al. 2017). Exogeneous dust fluxes are a source of P into the soil system, possibly contributing to the observed increase in P stock.

2.5.2.2 P Speciation Changes with Climate

Following the Walker and Syers (1976) model, P speciation distribution generally appeared pedogenically older with increasing climate-induced weathering intensity (Figure 2-9). Specifically, there was a shift from Ca to Fe and Al associated Pi, but Po species did not accumulate as hypothesized (Figures 2-6 and 2-7). Apatite minerals were identified in all pedogenically immature semiarid WM sites across all master soil horizons, and many sites also fit as secondary Ca-Pi. In addition, Po species were commonly associated with Ca at the WM. As weathering intensity progressed at the Mediterranean CZO, apatite was lost from the soil (with the exception of SJER C horizon and a deep C horizon at PR site; data not shown), few Ca-Pi species persisted, and no Po species were identified as associated with Ca. The observed decrease in Ca-P with soil weathering intensity follows the W&S model, and is consistent with other studies on weathering gradients (Yang and Post 2011; Emadi et al. 2012; Prietzel et al. 2013; Wu et al. 2014; Feng et al. 2016; Helfenstein et al. 2018; Bernhard et al. 2018). However, Ca-P, especially as primary mineral apatite, persisted across the semiarid WM sites, similar to other arid studies (Lajtha and Schlesinger 1988; Selmants and Hart 2010) and also persisted with depth parallel to other arid studies (Emadi et al. 2012).

Iron and Al associated P both increased with weathering (Figure 2-6), following the traditional understanding of P biogeochemistry using fractionation schemes conducted along chronosequences. Multiple studies using XANES across soil chronosequences have also reported an increase of Fe-P with weathering, however Al-P tends to decrease (Prietzel et al. 2013; Wu et al. 2014). Alternatively, in a climate gradient study, humid sites were shown to have increased Al-P relative to arid locations due to greater weathering from increased precipitation, allowing apatite dissolution and transformation of P to amorphous Al-oxides (Baumann et al. 2018). Similar results were found in Helfenstein et al. (2018) along a precipitation gradient where Ca-P (HCl extractable) decreased and Fe- and Al- Pi and Po (NaOH extractable) increased with increasing MAP. This was corroborated with XANES where apatite was identified in drier locations and Fe- and Al-P species were found in wetter locations (Helfenstein et al. 2018). Therefore, climate-induced weathering intensity can result in shifts of Pi speciation, similar to the W&S model using chronosequences.

Another component of the W&S conceptual model is a proportional increase of Po compounds relative to Pi. The proportion of Po to total P typically increases with soil development along chronosequences and along precipitation gradients (Walker and Syers 1976; Turner et al. 2018). Therefore, we anticipated increasing climate-induced weathering would result in lower Pi:Po, however XANES and NMR both rejected this hypothesis (Table 2-S4, Figures 2-5, 2-6, and 2-7). The proportional decrease of Po relative to Pi was likely due to climate impacts to mineralization rates, changes in vegetation that regulated the input of Po to the soil, and from bioavailability differences of other chemical species.

Organic P did not accumulate in more chemically weathered soil, as hypothesized. Instead, both total and extractable proportions of Po were greatest in the colder and drier WM sites overall. This is likely because these conditions reduced the rate of P mineralization, promoting accumulation of organic species. This has also been observed in a study by Baumann et al. (2018) where Po was greatest in the arid site because microbial activity was water-limited, preventing mineralization and enzymatic hydrolysis. Higher temperatures and wetter conditions in the Mediterranean CZO likely created a positive feedback to promote mineralization of labile Po compounds (Makarov et al. 2002). The percentage of Po was also higher in the current study at the semiarid sites compared to other studies. For example, Lajtha and Schlesinger (1988) found Po was undetectable across the entire profile, Selmants and Hart (2010) found <8% in surficial soils, and a review by Yang and Post (2011) found Aridisols have an average ~25% in surficial soils. This compares to the current study that found 23% Po in all horizons by XANES and 34% by NMR at the WM sites. Therefore, along climate gradients, Po accumulation may be regulated by the interaction of temperature and precipitation that dictates if mineralization exceeds biological input.

It is also possible the changes in dominant vegetation regulated the input of Po into the soil and use the Po pool as a source of bioavailable P. The highest Po was found in grassland sites (BAR high elevation at WM, SJER low elevation at CZO) and this pattern did not follow C concentrations. Senesced-leaf P concentrations in grasslands has been shown to be higher than Mediterranean forests (Yuan and Chen 2009), which may explain why both grassland ecosystems had greater Po than shrub and mixed conifer forest sites. Additionally, organic species tended to accumulate when Ca-P was not exhausted. Walker and Syers (1976) suggested that when the dissolution of apatite cannot offset P loss from leaching or conversion to occluded forms, organic matter values will decline. Our findings support this hypothesis where observed Po proportionally accumulated at the semiarid WM when Ca-P was not exhausted, and Po declined in the Mediterranean CZO sites where Ca-P was largely depleted (Figure 2-5). This phenomena has also been observed in a humid soil chronosequence (Crews et al. 1995). Therefore, mixed conifer forests that are supported in the Ca-P depleted CZO, are likely relying on turnover of the Po as a source of bioavailable P. Turnover of the Po pool (accessible through synthesis of phosphatase enzymes, secretion of organic acids, and root association with mycorrhizal fungi; Attiwill and Adams 1993) is a key component of labile P especially in the late stages of soil development (Cross and Schlesinger 1995; Turner et al. 2007; Stutter et al. 2012). This suggests these sites may be more P-limited and utilizing both diester and relatively less bioavailable monoester species (Turner et al.

2014) because both monoester and diester species decreased with EEMT (Figure 2-7). We provide evidence that Po turnover is likely an important source of bioavailable P in moderately weathered soils.

The shift in vegetation to species with ectomycorrhizae may have contributed to the decline in Po in the more weathered locations (Chen et al., 2004). Pyrophosphate increased with EEMT likely due to shifts in vegetation that support ectomycorrhizal fungi. The two sites containing the most pyrophosphate identified by XANES and NMR are SPR and PR (Figure 2-5). Polyphosphates, including pyrophosphate, originates mainly from soil fungal tissue (Makarov et al. 2005). Overall, as soil weathering increased and vegetation transitioned from pinyon pine and shrubland to mixed conifer forests, soil acidification occurred increasing apatite dissolution along with potentially more organic acid production by microbes, mycorrhizae, and roots. This likely shifted the P acquisition strategy of microorganisms and plants from apatite dissolution to organic matter mineralization (Lang et al. 2016). The transition in P species from semiarid to Mediterranean sites is likely driving changes in P acquisition strategies. Phosphorus acquisition is likely decoupled from C and N in semiarid WM sites, where the primary mechanism for P is apatite dissolution (Delgado-Baquerizo et al. 2013). In the Mediterranean CZO, primary mineral apatite has largely been depleted, therefore biota rely on P desorption from secondary Fe and Al compounds, Po mineralization, or deep roots scavenging Ca-Pi. However, most Pi at the CZO sites is Al-Pi which may not be readily bioavailable in the pH range of the sites (Penn and Camberato 2019), leading organisms to preferentially utilize organic sources of P.

2.5.3 P Speciation Changes with MAP, MAT, and Soil Properties

Inorganic and organic P compounds were impacted by soil and climatic properties that control physio-chemical and biological reactions within the soil (Turner et al. 2002; Deiss et al. 2018). Variation in temperature and precipitation can alter soil physio-chemical properties from changing vegetation composition and microbial dynamics, weathering rates (creating more secondary minerals or modify the synthesis of minerals), pH, and the turnover of organic matter (Miller et al. 2001; Davidson and Janssens 2006; Sardans et al. 2006; Zhou et al. 2016; Bojko and Kabala 2017; Mou et al. 2020). Multi-dimensional analysis of XANES and NMR P species suggested potential mechanisms of how P speciation is altered by changing temperature, precipitation, pH, and elemental concentrations (Figure 2-8). Calcium bound Pi and Po species were greatest under more alkaline conditions at the semiarid WM, but as pH declines with increasing MAP and MAT at the Mediterranean CZO sites, Fe and Al-Pi accumulates. These are similar findings to a precipitation gradient where apatite was identified in drier locations and Fe- and Al- Pi species were found in wetter locations (Helfenstein et al. 2018). Therefore, greater precipitation at the CZO accelerated soil acidification, likely increasing P fluxes into the soil from residual parent material weathering (Parfitt 1989). Calcium species were also higher in sites with greater clay. However, the percentage of clay across the sites was likely driven by differences in parent material composition or atmospheric input of dust, rather than a reflection of weathering intensity (Matchand 1970, Reheis 1997; Turk and Graham 2011; Aciego et al. 2017). Overall, clay was higher at the WM sites

where the parent material may have had smaller clay-sized particles within its matrix including potassium feldspars. This is supported by significantly greater K when comparing parent material concentrations across gradients. Aluminum and Ca bound species were regulated by increased metal concentrations, but Fe-P and most organic species were more dependent on environmental factors.

Extractable Pi and Po species were largely regulated by climatic factors. Monoesters (including RNA), diesters, and phosphonates were greater in more alkaline conditions and where clay was higher. Organic P typically increases with precipitation (Tate and Newman 1982; Sumann et al. 1998; Turrión et al. 2001) but this was not reflected in the current study. On the other hand, extractable Pi increased with increasing MAT, MAP, P and Fe. Therefore, as soil development increased from semiarid to Mediterranean sites and pH declined, apatite mineral dissolution likely increased and released soluble P into the soil solution where it was then taken up by organisms and redistributed as Po, interacted with soil constituents by precipitating with or sorbing to the surface of Ca in less weathered soils, or associated with Fe and Al in more weathered locations.

2.5.4 Implications for Ecosystem Productivity in a Changing Climate

Many precipitation events are predicted to become more variable with a greater interval between events and increase of intensity (Brinkman 1990; Easterling et al. 2000). Specifically in California, the occurrence of drought has increased in the past two decades compared to the last century and anthropogenic warming increases the probability that future dry conditions will co-occur with warm periods, making future droughts more probable (Diffenbaugh et al. 2015). A relatively low threshold has been identified where only minor climatic changes in temperature and precipitation are needed to shift Mediterranean ecosystems to semiarid and arid areas, especially as they are often adjacent to each other (Lavee et al. 1998). This has important implications for P biogeochemistry in temperate drylands as increased potential evapotranspiration will enhance aridity and may disrupt key processes that control bioavailable P (Austin et al. 2004; Delgado-Baquerizo et al. 2013; Feng and Fu 2013; Huang et al. 2016).

The semiarid WM and Mediterranean CZO are already water limited, which likely will be exacerbated by climate change. Decreasing soil moisture slows important biogeochemical processes including soil weathering, organic matter turnover, and desorption and dissolution reactions (Austin et al. 2004; Delgado-Baquerizo et al. 2013). In semiarid locations, this will likely decrease bioavailable P, which is currently largely being supported by weathering of primary mineral apatite along with dissolution and desorption of secondary Ca-P. Therefore, Po mineralization, which is likely the primary source of bioavailable P in the Mediterranean CZO sites, will likely be dampened. Drought can reduce phosphatase activity, leading to an accumulation of Po (Sardans and Peñuelas 2008). This will likely impact plant productivity, especially at the Mediterranean CZO sites that appear to be relying on turnover of organic species for ecosystem development. A six-year drought manipulation experiment in a Mediterranean forest decreased soil moisture by an average of 15% and resulted in approximately 33% less P in aboveground biomass (Sardans and Peñuelas 2007). Although total soil P may

accumulate from drought due to reduced dissolution and desorption reactions, increased water limitation would likely result in reduced nutrient uptake and movement of P from roots to shoots (Bradford and Hsiao 1982; Sardans and Peñuelas 2007). Therefore, the Mediterranean sites that are largely relying on microbial processes for bioavailable P, would likely shift from biological to geochemical control, causing P to become decoupled from C and N (Delgado-Baquerizo et al. 2013; Feng et al. 2016). Overall, P acquisition at the Mediterranean CZO sites may resemble the geochemically controlled semiarid WM sites with global climate change (Delgado-Baquerizo et al. 2013; Feng et al. 2016).

Our study demonstrates the sensitivity of P biogeochemistry to alterations in water content triggered by a changing climate. Increasing temperature with climate change can increase NPP and organic matter cycling rates, potentially alter the availability of the current speciation, and likely impact the amount of energy and mass entering the system. These alterations will impact short-term bioavailable P and the rate of soil development, and therefore has long-term implications for P speciation. Availability of nutrients may even constrain vegetation shifts to higher elevations in these montane ecosystems (Hagedorn et al. 2019) because they are more susceptible to warming than lower elevations (Pepin et al. 2015). In the long-term, increased drought may cause bioavailable P to decrease, however fluxes of P from exogenous dust may provide a critical source of bioavailable P input. Fluxes of exogenous particulate matter P at the CZO exceeds the rate of P from primary mineral weathering (Aciego et al. 2017) and is found in readily bioavailable Po forms, especially at high elevations (O'Day et al. 2020). Additionally, plants have been found to utilize P from aeolian particulate matter as a significant source of P (Arvin et al. 2017). Ultimately, ecosystem development in a changing climate is going to depend on how bioavailability of the current P chemical speciation responds and the degree of continued input of atmospheric particulate matter in bioavailable forms.

2.6 Summary

Changes in temperature, precipitation, and vegetation along semiarid and Mediterranean elevational gradients influenced P concentration, stock, and chemical speciation. The shift from pinyon pine and shrubs at the semiarid WM to mixed conifer forest at the Mediterranean CZO likely caused greater soil organic matter input, accelerated soil acidification, and promoted apatite dissolution from primary minerals. This supported increased P stock, higher P concentration in O and A horizons, shifted species from Ca-Pi to Fe- and Al-Pi, increased pyrophosphate concentrations, and proportionally increased Pi than Po. This likely shifted the P acquisition strategy of fungi, microbes, and plants from apatite dissolution to Po mineralization. Although these sites are comparatively pedogenically immature due to time since development and the volume of water leaching through the system compared to humid environments, changes in climate caused a redistribution of Pi species similar to the W&S model. In contrast to the W&S model, total P stock increased and organic species proportionally decreased. This indicates moderately weathered soils in Mediterranean climates are able to retain

more P via sorption to Fe and Al than what is lost from leaching and erosion, and turnover of the organic pool likely serves as a main source of bioavailable P.

2.7 References

Aciego SM, Riebe CS, Hart SC, et al. (2017) Dust outpaces bedrock in nutrient supply to montane forest ecosystems. Nature Communications 8:1-10.

Ajiboye B, Akinremi OO, Jürgensen A (2007) Experimental Validation of Quantitative XANES Analysis for Phosphorus Speciation. Soil Science Society of America Journal 71:1288-1291.

Anderson G (1980) Assessing Organic Phosphorus in Soils. In: Khasawneh FE, Sample EC, Kamprath EJ (eds) The Role of Phosphorus in Agriculture. American Society of Agronomy, Madison, WI pp. 411-431.

Arvin LJ, Riebe CS, Aciego SM, Blakowski MA (2017) Global patterns of dust and bedrock nutrient supply to montane ecosystems. Science Advances 3:1-10.

Attiwill PM, Adams MA (1993) Nutrient cycling in forests. New Phytologist 124:561-582.

Austin AT, Yahdjian L, Stark JM, et al. (2004) Water pulses and biogeochemical cycles in arid and semiarid ecosystems. Oecologia 141:221-235.

Barton K, Barton MK (2019) Package 'MuMIn'. R package version, 1:6.

Bateman CP, Wones RD (1972) Geologic Map of the Huntington Lake Quadrangle, Central Sierra Nevada, California. United States Geological Survey.

Bateman P and Busacca A (1982) Geologic Map of the Millerton Lake Quadrangle, West-Central Sierra Nevada, California. United States Geological Survey.

Bates D, Maechler M, Bolker B, Walker S (2015) Fitting Linear Mixed-Effects Models Using lme4. Journal of Statistical Software 67:1-48.

Baumann K, Jung P, Samolov E, et al. (2018) Biological soil crusts along a climatic gradient in Chile: Richness and imprints of phototrophic microorganisms in phosphorus biogeochemical cycling. Soil Biology and Biochemistry 127:286–300.

Beauchemin S, Hesterberg D, Chou J, et al. (2003) Speciation of Phosphorus in Phosphorus-Enriched Agricultural Soils Using X-Ray Absorption Near-Edge Structure Spectroscopy and Chemical Fractionation. Journal of Environment Quality 32:1809-1819.

Bernhard N, Moskwa L-M, Schmidt K, et al (2018) Pedogenic and microbial interrelations to regional climate and local topography: New insights from a climate gradient (arid to humid) along the Coastal Cordillera of Chile. Catena 170:335-355.

Bojko O, Kabala C (2017) Organic carbon pools in mountain soils - Sources of variability and predicted changes in relation to climate and land use changes. Catena 149:209–220.

Bradford KJ, Hsiao TC (1982) Physiological responses to moderate water stress. In: Physiological Plant Ecology II. Lange OL, Nobel PS, Osmond CB, and Ziegler H (eds). Springer, Berlin pp. 246-324.

Brinkman R (1990) Resilience against climate change. In: Sharpenseel HW, Shoemaker M, Ayoub A (eds) Soils on a Warmer Earth. Elsevier, Amsterdam pp. 51–60.

Cade-Menun BJ (2015) Improved peak identification in 31P-NMR spectra of environmental samples with a standardized method and peak library. Geoderma 257–258:102–114.

Cade-Menun B, Liu CW (2014) Solution Phosphorus-31 Nuclear Magnetic Resonance Spectroscopy of Soils from 2005 to 2013: A Review of Sample Preparation and Experimental Parameters. Soil Science Society of America Journal 78:19-37.

Chen CR, Condron LM, Turner BL, Mahieu N, Davis MR, Xu ZH, Sherlock RR (2004) Mineralization of soil orthophosphate monoesters under pine seedlings and ryegrass. Australian Journal of Soil Research 42:189-196.

Chen CR, Hou EQ, Condron LM, et al (2015) Soil phosphorus fractionation and nutrient dynamics along the Cooloola coastal dune chronosequence, southern Queensland, Australia. Geoderma 257:4-13.

Clark DH, Gillespie AR (1997) Timing and significance of Late-glacial and Holocene cirque glaciation in the Sierra Nevada, California. Quaternary Science 38:21-38.

Cole CV, Heil RD (1981) Phosphorus effects on terrestrial nitrogen cycling. Ecological Bulletins 33:363-374.

Condron LM, Turner BL, Cade-Menun BJ (2005) Chemistry and dynamics of soil organic phosphorus. In: Sims JT, Sharpley AN (eds) Phosphorus: Agriculture and the Environment. American Society of Agronomy, Crop Science Society of America, Soil Science Society of America, Inc., Madison, WI pp. 87-121.

Crews TE, Kitayama K, Fownes JH, et al. (1995) Changes in Soil Phosphorus Fractions and Ecosystem Dynamics across a Long Chronosequence in Hawaii. Ecology 76:1407-1424.

Cross AF, Schlesinger WH (2001) Biological and geochemical controls on phosphorus fractions in semiarid soils. Biogeochemistry 52:155–172.

Cross AF, Schlesinger WH (1995) A literature review and evaluation of the Hedley fractionation: Applications to the biogeochemical cycle of soil phosphorus in natural ecosystems. Geoderma 64:197-214.

Dahlgren RA, Boettinger JL, Huntington GL, Amundson RG (1997) Soil development along an elevational transect in the western Sierra Nevada, California. Geoderma 78:207-236.

Daly C, Taylor G, Gibson W, et al. (2000) High-quality spatial climate data sets for the united states and beyond. American Society of Agricultural Engineers 43:1957-1962

Dane JH, Topp GC, Campbell GS, et al. (2002) Methods of Soil Analysis Part 4-Physical Methods. Soil Science Society of America, Madison, WI.

Darch T, Blackwell MSA, Hawkins JMB, et al. (2014) A Meta-Analysis of Organic and Inorganic Phosphorus in Organic Fertilizers, Soils, and Water: Implications for Water Quality. Critical Reviews in Environmental Science and Technology 44:2172-2202.

Davidson EA, Janssens IA (2006) Temperature sensitivity of soil carbon decomposition and feedbacks to climate change. Nature 440:165-173.

Deiss L, de Moraes A, Maire V (2018) Environmental drivers of soil phosphorus composition in natural ecosystems. Biogeosciences 15:4575-4592.

Delgado-Baquerizo M, Maestre FT, Gallardo A, et al. (2013) Decoupling of soil nutrient cycles as a function of aridity in global drylands. Nature 502:672-676.

Delgado-Baquerizo M, Reich PB, Bardgett RD, et al. (2020) The influence of soil age on ecosystem structure and function across biomes. Nature Communications 11:1-14.

Dick WA, Tabatabai MA (1978) Hydrolysis of organic and inorganic phosphorus compounds added to soils. Geoderma 21:175-182.

Diffenbaugh NS, Swain DL, Touma D (2015) Anthropogenic warming has increased drought risk in California. Proceedings of the National Academy of Sciences 112:3931-3936.

Dixon JL, Heimsath AM, Amundson R (2009) The critical role of climate and saprolite weathering in landscape evolution. Earth Surface Processes and Landforms 34:1507-1521.

Doolette AL, Smernik RJ, Dougherty WJ (2009) Spiking Improved Solution Phosphorus-31 Nuclear Magnetic Resonance Identification of Soil Phosphorus Compounds. Soil Science Society of America Journal 73:919-9.

Doolette AL, Smernik RJ, Dougherty WJ (2011) Overestimation of the importance of phytate in NaOH–EDTA soil extracts as assessed by 31P NMR analyses. Organic Geochemistry 42:955-964.

Easterling DR, Meehl GA, Parmesan C, et al (2000) Climate Extremes: Observations, Modeling, and Impacts. Science 289:2068-2074.

Egli M, Mirabella A, Sartori G, Fitze P (2003) Weathering rates as a function of climate: results from a climosequence of the Val Genova (Trentino, Italian Alps). Geoderma 111:99-121.

Elser JJ, Bracken MES, Cleland EE, et al. (2007) Global analysis of nitrogen and phosphorus limitation of primary producers in freshwater, marine and terrestrial ecosystems. Ecology Letters 10:1135-1142.

Emadi M, Baghernejad M, Bahmanyar MA, Morovvat A (2012) Changes in soil inorganic phosphorous pools along a precipitation gradient in northern Iran. International Journal of Forest, Soil and Erosion 2:143-147.

Eriksson AK, Hillier S, Hesterberg D, et al. (2016) Evolution of phosphorus speciation with depth in an agricultural soil profile. Geoderma 280:29-37.

Ernst WG, Rumble D (2003) Oxygen isotopic study of Late Mesozoic cooling of the Mount Barcroft area, central White Mountains, eastern California. Contributions to Mineralogy and Petrology 144:639-651.

Feng S, Fu Q (2013) Expansion of global drylands under a warming climate. Atmospheric Chemistry and Physics 13:14637-14665.

Feng J, Turner BL, Lü X, et al. (2016) Phosphorus transformations along a large-scale climosequence in arid and semiarid grasslands of northern China. Global Biogeochemical Cycles 30:1264-1275.

Ferre EC, Michelsen KJ, Ernst WG, et al. (2012) Vertical zonation of the Barcroft granodiorite, White Mountains, California: Implications for magmatic processes. American Mineralogist 97:1049-1059.

Frisbie JA (2014) Soil organic carbon storage and aggregate stability in an Arid Mountain Range, White Mountains, CA. Dissertation, University of California.

Gee GW, Bauder JM, Klute A (1986) Methods of Soil Analysis Part 1-Physical and Mineralogical Methods. Soil Science Society of America, Madison, WI. pp. 383-411.

Giguet-Covex C, Poulenard J, Chalmin E, et al. (2013) XANES spectroscopy as a tool to trace phosphorus transformation during soil genesis and mountain ecosystem development from lake sediments. Geochimica et Cosmochimica Acta 118:129-147.

Goll DS, Brovkin V, Parida BR, et al. (2012) Nutrient limitation reduces land carbon uptake in simulations with a model of combined carbon, nitrogen and phosphorus cycling. Biogeosciences 9:3547-3569.

Goulden ML, Bales RC (2014) Mountain runoff vulnerability to increased evapotranspiration with vegetation expansion. Proceedings of the National Academy of Sciences of the United States of America 111:14071-14075.

Graham R, Rossi A, Hubbert R (2010) Rock to regolith conversion: Producing hospitable substrates for terrestrial ecosystems. GSA Today 20:4-9.

Griffith WK (1978). Effects of phosphorus and potassium on nitrogen fixation. In: Phosphorus for Agriculture: A Situation Analysis. Potash/Phosphate Institute, Atlanta pp. 80-94.

Gu C, Hart SC, Turner BL, et al. (2019) Aeolian dust deposition and the perturbation of phosphorus transformations during long-term ecosystem development in a cool, semi-arid environment. Geochimica et Cosmochimica Acta 246:498-514.

Gu C, Dam T, Hart SC, Turner BL, Chadwick OA, Berhe AA, Hu Y, Zhu M (2020) Quantifying uncertainties in sequential chemical extraction of soil phosphorus using XANES spectroscopy. Environmental Science & Technology 54:2257-2267.

Hagedorn F, Gavazov K, Alexander JM (2019) Above- and belowground linkages shape responses of mountain vegetation to climate change. Science 365:1119-1123.

Hahm WJ, Riebe CS, Lukens CE, Araki S (2014) Bedrock composition regulates mountain ecosystems and landscape evolution. Proceedings of the National Academy of Sciences of the United States of America 111:3338–3343.

Harnois L (1988) The CIW index: A new chemical index of weathering. Sedimentary Geology 55:319-322.

Harris D, Horwáth WR, Van Kessel C (2001) Acid fumigation of soils to remove carbonates prior to total organic carbon or carbon-13 isotopic analysis. Soil Science Society of America Journal 65:1853-1856.

Hart SC (2006) Potential impacts of climate change on nitrogen transformations and greenhouse gas fluxes in forests: a soil transfer study. Global Change Biology 12:1032-1046.

Hashimoto Y, Takamoto A, Kikkawa R, et al. (2014) Formations of Hydroxyapatite and Inositol Hexakisphosphate in Poultry Litter during the Composting Period: Sequential Fractionation, P K-edge XANES and Solution 31P NMR Investigations. Environmental Science & Technology 48:5486-5492.

Hashimoto Y, Watanabe Y (2014) Combined applications of chemical fractionation, solution 31P-NMR and P K-edge XANES to determine phosphorus speciation in soils formed on serpentine landscapes. Geoderma 230:143-150.

He X, Hou E, Liu Y, Wen D (2016) Altitudinal patterns and controls of plant and soil nutrient concentrations and stoichiometry in subtropical China. Scientific Reports 6:1-9.

Hedin LO, Vitousek PM, Matson PA (2003) Nutrient losses over four million years of tropical forest development. Ecology 84:2231-2255.

Hedley MJ, Stewart JWB, Chauhan B (1982) Changes in inorganic and organic soil phosphorus fractions induced by cultivation practices and by laboratory incubations. Soil Science Society of America Journal 46:970-976.

Helfenstein J, Tamburini F, Sperber C von, et al. (2018) Combining spectroscopic and isotopic techniques gives a dynamic view of phosphorus cycling in soil. Nature Communications 9:1-9.

Hesterberg D, McNulty I, Thieme J (2017) Speciation of Soil Phosphorus Assessed by XANES Spectroscopy at Different Spatial Scales. Journal of Environmental Quality 46:1190-1197.

Homyak PM, Sickman JO, Melack JM (2014) Pools, transformations, and sources of P in high-elevation soils: Implications for nutrient transfer to Sierra Nevada lakes. Geoderma 217:65-73.

Hou E, Luo Y, Kuang Y, et al. (2020) Global meta-analysis shows pervasive phosphorus limitation of aboveground plant production in natural terrestrial ecosystems. Nature Communications 11:1-9.

Hunger S, Sims JT, Sparks DL (2005) How Accurate Is the Assessment of Phosphorus Pools in Poultry Litter by Sequential Extraction? Journal of Environmental Quality 34:382-389.

Hurtarte LCC, Amorim HCS, Kruse J, et al. (2020) A Novel Approach for the Quantification of Different Inorganic and Organic Phosphorus Compounds in Environmental Samples by P L 2,3-Edge X-ray Absorption Near-Edge Structure (XANES) Spectroscopy. Environmental Science & Technology 54:2812-2820.

Ippolito JA, Blecker SW, Freeman CL, et al. (2010) Phosphorus biogeochemistry across a precipitation gradient in grasslands of central North America. Journal of Arid Environments 74:954-961.

Izquierdo JE, Houlton BZ, van Huysen TL (2013) Evidence for progressive phosphorus limitation over long-term ecosystem development: Examination of a biogeochemical paradigm. Plant and Soil 367:135-147.

Jenny H (1941) Factors of soil formation; a system of quantitative pedology. McGraw-Hill, New York.

Jenny H, Gessel SP, Bingham FT (1949) Comparative study of decomposition rates of organic matter in temperate and tropical regions. Soil Science 68:419-432.

Jobbagy, EG, Jackson, RB (2001) The distribution of soil nutrients with depth: global patterns and the imprint of plants. Biogeochemistry 53:51-77.

Kar G, Hundal LS, Schoenau JJ, Peak D (2011) Direct Chemical Speciation of P in Sequential Chemical Extraction Residues Using P K-Edge X-Ray Absorption Near-Edge Structure Spectroscopy. Soil Science 176:589-595.

Kelly AE, Goulden ML (2016) A montane Mediterranean climate supports year-round photosynthesis and high forest biomass. Tree Physiology 36:459-468.

Kelly SD, Hesterberg D, Ravel B (2008) Methods of Soil Analysis Part 5-Mineralogical Methods. Soil Science Society of America, Madison, WI. pp. 387-463.

Kizewski F, Liu Y-T, Morris A, Hesterberg D (2011) Spectroscopic Approaches for Phosphorus Speciation in Soils and Other Environmental Systems. Journal of Environmental Quality 40:751-766.

Kruse J, Abraham M, Amelung W, et al. (2015) Innovative methods in soil phosphorus research: A review. Journal of Plant Nutrition and Soil Science 178:43-88.

Kruse J, Leinweber P (2008) Phosphorus in sequentially extracted fen peat soils: A K-edge X-ray absorption near-edge structure (XANES) spectroscopy study. Journal of Plant Nutrition and Soil Science 171:613–620.

Lajtha K, Schlesinger WH (1988) The Biogeochemistry of Phosphorus Cycling and Phosphorus Availability Along a Desert Soil Chronosequence. Ecology 69:24-39.

Lang F, Bauhus J, Frossard E, et al. (2016) Phosphorus in forest ecosystems: New insights from an ecosystem nutrition perspective. Journal of Plant Nutrition and Soil Science 179:129-135.

Lavee H, Imeson AC, Sarah P (1998) The impact of climate change on geomorphology and desertification along a Mediterranean-arid transect. Land Degradation and Development 9:407-422.

Legendre P, Legendre L (2012) Numerical ecology. Elsevier, Amsterdam.

Letkeman LP, Tiessen H, Campbell CA (1996) Phosphorus transformations and redistribution during pedogenesis of western Canadian soils. Geoderma 71:201-218.

Liu J, Yang J, Cade-Menun BJ, et al (2013) Complementary Phosphorus Speciation in Agricultural Soils by Sequential Fractionation, Solution 31 P Nuclear Magnetic Resonance, and Phosphorus K-edge X-ray Absorption Near-Edge Structure Spectroscopy. Journal of Environmental Quality 42:1763-1770.

Lockwood PJ, Bateman CP (1976) Geologic Map of the Shaver Lake Quadrangle, Central Sierra Nevada, California. United States Geological Survey.

Marchand DE (1970) Soil contamination in the White Mountains, eastern California. Geological Society of America Bulletin 81:2497-2506.

Mage SM, Porder S (2012) Parent Material and Topography Determine Soil Phosphorus Status in the Luquillo Mountains of Puerto Rico. Ecosystems 16:284-294.

Makarov MI, Haumaier L, Zech W (2002) Nature of soil organic phosphorus: an assessment of peak assignments in the diester region of 31P NMR spectra. Soil Biology and Biochemistry 34:1467-1477.

Makarov MI, Haumaier L, Zech W, et al. (2005) Can 31P NMR spectroscopy be used to indicate the origins of soil organic phosphates? Soil Biology and Biochemistry 37:15-25.

McCulley RL, Jobbagy EG, Pockman WT, Jackson RB (2004) Nutrient uptake as a contributing explanation for deep rooting in arid and semi-arid ecosystems. Oecologia 141:620-628.

McDowell RW, Menun BC, Stewart I (2007) Organic phosphorus speciation and pedogenesis: analysis by solution 31P nuclear magnetic resonance spectroscopy. European Journal of Soil Science 58:1348-1357.

McDowell RW, Stewart I (2006) The phosphorus composition of contrasting soils in pastoral, native and forest management in Otago, New Zealand: Sequential extraction and 31P NMR. Geoderma 130:176-189.

McGroddy ME, Silver WL, Oliveira RC de, et al. (2008) Retention of phosphorus in highly weathered soils under a lowland Amazonian forest ecosystem. Journal of Geophysical Research Biogeosciences 113:1-11

McLennan SM (1993) Weathering and Global Denudation. Journal of Geology 101:295-303.

Miller AJ, Schuur EAG, Chadwick OA (2001) Redox control of phosphorus pools in Hawaiian montane forest soils. Geoderma 102:219-237.

Mou XM, Wu Y, Niu Z, et al. (2020) Soil phosphorus accumulation changes with decreasing temperature along a 2300 m altitude gradient. Agriculture, Ecosystems and Environment 301.

Moreland KM (2020) Climatic controls on deep soil carbon and nitrogen dynamics. University of California, Merced, Merced, CA.

Munevar F, Wollum AG (1977) Effects of the Addition of Phosphorus and Inorganic Nitrogen on Carbon and Nitrogen Mineralization in Andepts From Colombia. Soil Science Society of America Journal 41:540-545.

Nakagawa S, Schielzeth H (2013) A general and simple method for obtaining R^2 from generalized linear mixed-effects models. Methods in Ecology and Evolution. 4:133-142.

Nesbitt H, Young GM (1982) Early Proterozoic Climates and Plate Motions Inferred from Major Element Chemistry of Lutites. Nature 299:715-717.

Newman GS, Coble AA, Haskins KE, Kowler AL, Hart SC (2020) The expanding role of deep roots during long-term terrestrial ecosystem development. Journal of Ecology 108:2256-2269.

Noack SR, McLaughlin MJ, Smernik RJ, et al (2012) Crop residue phosphorus: speciation and potential bio-availability. Plant and Soil 359:375-385.

O'Day PA, Nwosu UG, Barnes ME, et al. (2020) Phosphorus Speciation in Atmospherically Deposited Particulate Matter and Implications for Terrestrial Ecosystem Productivity. Environmental Science & Technology 54:4984-4994.

Oksanen J, Kindt R, Legendre P, O'Hara B, Stevens MHH, et al. (2007) Vegan: Community Ecology Package. R package version 1.17-10.

Parfitt RL (1989) Phosphate reactions with natural allophane, ferrihydrite and goethite. Journal of Soil Science 40:359-369.

Peltzer DA, Wardle DA, Allison VJ, et al. (2010) Understanding ecosystem retrogression. Ecological Monographs 80:509-529.

Penn CJ, Camberato JJ (2019) A Critical Review on Soil Chemical Processes that Control How Soil pH Affects Phosphorus Availability to Plants. Agriculture 9:1-18.

Pepin N, Bradley RS, Diaz HF, et al (2015) Elevation-dependent warming in mountain regions of the world. Nature Climate Change 5:424-430.

Porder S, Chadwick OA (2009) Climate and soil-age constraints on nutrient uplift and retention by plants. Ecology 90:623-636.

Porder S, Ramachandran S (2013) The phosphorus concentration of common rocks—a potential driver of ecosystem P status. Plant and Soil 367:41-55.

Prietzel J, Dümig A, Wu Y, et al. (2013) Synchrotron-based P K-edge XANES spectroscopy reveals rapid changes of phosphorus speciation in the topsoil of two glacier foreland chronosequences. Geochimica et Cosmochimica Acta 108:154-171.

Prietzel J, Klysubun W (2018) Phosphorus K-edge XANES spectroscopy has probably often underestimated iron oxyhydroxide-bound P in soils. Journal of Synchrotron Radiation 25:1736-1744.

Prietzel J, Klysubun W, Werner F (2016) Speciation of phosphorus in temperate zone forest soils as assessed by combined wet-chemical fractionation and XANES spectroscopy. Journal of Plant Nutrition and Soil Science 179:168-185.

Prietzel J, Thieme J, Paterson D (2010) Phosphorus speciation of forest-soil organic surface layers using P K-edge XANES spectroscopy. Journal of Plant Nutrition and Soil Science 173:805-807.

Rasmussen C, Dahlgren RA, Southard RJ (2010a) Basalt weathering and pedogenesis across an environmental gradient in the southern Cascade Range, California, USA. Geoderma 154:473-485.

Rasmussen C, Southard RJ, Horwath WR (2005) Modeling Energy Inputs to Predict Pedogenic Environments Using Regional Environmental Databases. Soil Science Society of America Journal 69:1266-1274.

Rasmussen C, Tabor NJ (2007) Applying a Quantitative Pedogenic Energy Model across a Range of Environmental Gradients. Soil Science Society of America Journal 71:1719-1729.

Rasmussen C, Troch PA, Chorover J, et al. (2010b) An open system framework for integrating critical zone structure and function. Biogeochemistry 102:15-29.

Ravel B, Newville M (2005) ATHENA, ARTEMIS, HEPHAESTUS: Data analysis for X-ray absorption spectroscopy using IFEFFIT. Journal of Synchrotron Radiation 12:537-541.

Recena R, Cade-Menun BJ, Delgado A (2018) Organic phosphorus forms in agricultural soils under Mediterranean climate. Soil Science Society of America 82:783-795.

Reheis MC (1997) Dust deposition downwind of Owens (dry) Lake, 1991–1994: Preliminary findings. Journal of Geophysical Research: Atmospheres 102:25999-26008.

Richardson SJ, Peltzer DA, Allen RB, et al. (2004) Rapid development of phosphorus limitation in temperate rainforest along the Franz Josef soil chronosequence. Plant Ecology 139:267-276.

Robertson GP, Coleman DC, Sollins P, Bledsoe CS (1999) Standard Soil Methods For Long-term Ecological Research. Oxford University Press, New York.

Sardans J, Peñuelas J (2007) Drought changes phosphorus and potassium accumulation patterns in an evergreen Mediterranean forest. Functional Ecology 21:191-201.

Sardans J, Peñuelas J, Estiarte M (2006) Warming and drought alter soil phosphatase activity and soil P availability in a Mediterranean shrubland. Plant and Soil 289:227-238.

Sardans J, Peñuelas J, Ogaya R (2008) Experimental drought reduced acid and alkaline phosphatase activity and increased organic extractable P in soil in a *Quercus ilex* Mediterranean forest. European Journal of Soil Biology 44:509-520.

Sato S, Solomon D, Hyland C, et al (2005) Phosphorus Speciation in Manure and Manure-Amended Soils Using XANES Spectroscopy. Environmental Science & Technology 39:7485-7491.

Schimel DS (2010) Drylands in the Earth System. Science 327:418–419.

Schlesinger WH, Bruijnzeel LA, Bush MB, et al. (1998) The biogeochemistry of phosphorus after the first century of soil development on Rakata Island, Krakatau, Indonesia. Biogeochemistry 40:37-55.

Schmieder F, Bergström L, Riddle M, et al (2018) Phosphorus speciation in a long-term manure-amended soil profile – Evidence from wet chemical extraction, 31P-NMR and P K-edge XANES spectroscopy. Geoderma 322:19-27.

Schenk HJ, Jackson RB (2002b) Rooting depths, lateral root spreads and below-ground/above-ground allometries of plants in water-limited ecosystems. Journal of Ecology 90:480-494.

Schneider KD, Cade-Menun BJ, Lynch DH, Voroney RP (2016) Soil Phosphorus Forms from Organic and Conventional Forage Fields. Soil Science Society of America Journal 80:328-340.

Selmants PC, Hart SC (2010) Phosphorus and soil development: Does the Walker and Syers model apply to semiarid ecosystems? Ecology 91:474-484.

Sheldon ND, Retallack GJ, Tanaka S (2015) Geochemical Climofunctions from North American Soils and Application to Paleosols across the Eocene-Oligocene Boundary in Oregon. The Journal of Geology 110:687-696.

Smeck NE (1973) Phosphorus: An indicator of pedogenetic weathering processes. Soil Science 115:199-206.

Smil V (2000) Phosphorus in the Environment: Natural Flows and Human Interferences. Annual Review of Energy and the Environment 25:53-88.

Stahr S, Graf-Rosenfellner M, Klysubun W, et al. (2017) Phosphorus speciation and C:N:P stoichiometry of functional organic matter fractions in temperate forest soils. Plant and Soil 427:53-69.

Stewart JWB, Tiessen H (1987) Dynamics of soil organic phosphorus. Biogeochemistry 4:41-60.

Stone EL, Kalisz PJ (1991) On the maximum extent of tree roots. Forest Ecology and Management 46:59-102.

Stutter MI, Shand CA, George TS, et al. (2012) Recovering Phosphorus from Soil: A Root Solution? Environmental Science & Technology 46:1977-1978.

Sumann M, Amelung W, Haumaier L, Zech W (1998) Climatic Effects on Soil Organic Phosphorus in the North American Great Plains Identified by Phosphorus-31 Nuclear Magnetic Resonance. Soil Science Society of America Journal 62:1580-1586.

Tate KR (1984) The biological transformation of P in soil. Plant and Soil 76:245-256.

Tate KR (1992) Assessment, based on a climosequence of soils in tussock grasslands, of soil carbon storage and release in response to global warming. Journal of Soil Science 43:697-707.

Tate KR, Newman RH (1982) Phosphorus fractions of a climosequence of soils in New Zealand tussock grassland. Soil Biology and Biochemistry 14:191-196.

Tian, Z (2018) Soil and weathered bedrock evolution along an elevation gradient in the Southern Sierra Nevada, California. University of California, Davis, Davis, CA.

Tiessen HJ, Moir JO (1993) Characterization of available P by sequential extraction. In: MR Carter (ed) Soil sampling and methods of analysis Lewis Publishers, Ann Arbor pp. 75-86.

Turk JK, Graham RC (2011) Distribution and properties of vesicular horizons in the western United States. Soil Science Society of America Journal 75:1449-1461.

Turner BL (2008) Soil organic phosphorus in tropical forests: an assessment of the NaOH–EDTA extraction procedure for quantitative analysis by solution ^{31}P NMR spectroscopy. European Journal of Soil Science 59:453-466.

Turner B, Laliberte E (2015) Soil development and nutrient availability along a 2 million-year costal dune chronosequence under species-rich Mediterranean shrubland in southwestern Australia. Ecosystems 18:287-309.

Turner BL, Condron LM, Richardson SJ, et al. (2007) Soil organic phosphorus transformations during pedogenesis. Ecosystems 10:1166-1181.

Turner BL, Condron LM, Wells A, Andersen KM (2012) Soil nutrient dynamics during podzol development under lowland temperate rain forest in New Zealand. Catena 97:50-62.

Turner BL, Hayes PE, Laliberté E (2018) A climosequence of chronosequences in southwestern Australia. European Journal of Soil Science 69:69–85.

Turner BL, Mahieu N, Condron LM (2003) Phosphorus-31 Nuclear Magnetic Resonance Spectral Assignments of Phosphorus Compounds in Soil NaOH–EDTA Extracts. Soil Science Society of America Journal 67:497-510.

Turner BL, Papházy MJ, Haygarth PM, Mckelvie ID (2002) Inositol phosphates in the environment. Philosophical Transactions of the Royal Society B: Biological Sciences 357:449-469.

Turner BL, Wells A, Condron LM (2014) Soil organic phosphorus transformations along a coastal dune chronosequence under New Zealand temperate rain forest. Biogeochemistry 121:595-611.

Turrión MB, Gallardo JF, Haumaier L, et al. (2001) ^{31}P-NMR characterization of phosphorus fractions in natural and fertilized forest soils. Annals of Forest Science 58:89-98.

Vincent AG, Vestergren J, Gröbner G, et al (2013) Soil organic phosphorus transformations in a boreal forest chronosequence. Plant and Soil 367:149-162.

Vitousek PM, Porder S, Houlton BZ, Chadwick OA (2010) Terrestrial phosphorus limitation: Mechanisms, implications, and nitrogen–phosphorus interactions. Ecological Applications 20:5-15.

Walker TW, Syers JK (1976) The fate of phosphorus during pedogenesis. Geoderma 15:1-19.

Wardle DA, Walker LR, Bardgett RD (2004) Ecosystem Properties and Forest Decline in Contrasting Long-Term Chronosequences. Science 305:509-513.

Webb SM (2005) SIXpack: a graphical user interface for XAS analysis using IFEFFIT. Physica Scripta 115:1011-1014.

Werner F, Mueller CW, Thieme J, et al. (2017) Micro-scale heterogeneity of soil phosphorus depends on soil substrate and depth. Scientific Reports 7:1-9.

Werner F, Prietzel J (2015) Standard Protocol and Quality Assessment of Soil Phosphorus Speciation by P K-Edge XANES Spectroscopy. Environmental Science & Technology 49:10521-10528.

Wieder WR, Cleveland CC, Smith WK, Todd-Brown K (2015) Future productivity and carbon storage limited by terrestrial nutrient availability. Nature Geoscience 8:441-444.

Wilson, SG (2019) Phosphorus in California: sustainable management, predictive soil mapping and pedogenesis. University of California, Davis, Davis, CA.

Wu Y, Prietzel J, Zhou J, et al. (2014) Soil phosphorus bioavailability assessed by XANES and Hedley sequential fractionation technique in a glacier foreland chronosequence in Gongga Mountain, Southwestern China. Science China Earth Sciences 57:1860-1868.

Yang X, Post WM (2011) Phosphorus transformations as a function of pedogenesis: A synthesis of soil phosphorus data using Hedley fractionation method. Biogeosciences 8:2907-2916.

Young EO, Ross DS, Cade-Menun BJ, Liu CW (2013) Phosphorus Speciation in Riparian Soils: A Phosphorus-31 Nuclear Magnetic Resonance Spectroscopy and Enzyme Hydrolysis Study. Soil Science Society of America Journal 77:1636–1647.

Yuan Z, Chen HYH (2009) Global trends in senesced-leaf nitrogen and phosphorus. Global Ecology and Biogeography 18:532-542.

Zhang GL, Pan JH, Huang CM, Gong ZT (2007) Geochemical features of a soil chronosequence developed on basalt in Hainan Island, China. Mexican Journal of Geophysical Sciences 24:261–269.

Zhou J, Wu Y, Bing H, et al. (2016) Variations in soil phosphorus biogeochemistry across six vegetation types along an altitudinal gradient in SW China. Catena 142:102-111.

Zhou J, Wu Y, Prietzel J, et al. (2013) Changes of soil phosphorus speciation along a 120-year soil chronosequence in the Hailuogou Glacier retreat area (Gongga Mountain, SW China). Geoderma 195:251-259.

Zurr AF, Ieno EN, Smith GM (2007) Principal component analysis and redundancy analysis. In: Analysing Ecological Data. Statistics for Biology and Health. (eds) Gail M, Krickeberg K, Tsiatis, Wong W. Springer, New York. pp. 193-224.

2.8 Tables

Table 2-1. Sites at the White Mountain (WM) and Southern Sierra Critical Zone Observatory (CZO) elevational transects with the corresponding elevation, mean annual precipitation (MAP; mm y^{-1}), mean annual temperature (MAT; °C), effective energy and mass transfer (EEMT; MJ m^{-2} y^{-1}), soil moisture regime (SMR), soil temperature regime (STR), and dominate vegetation. Site abbreviations represent Granite 2 (GR2), Granite 3 (GR3), Granite 5 (GR5), Barcroft (BAR), San Joaquin Experimental Range (SJER), Soaproot (SPR), Providence (PR) and Short Hair (SH).

Gradient	Site	Elevation (m)	MAP (mm y^{-1})	MAT (C)	EEMT ($MJ/m^2/y$)	SMR	STR	Vegetation
WM	GR2	2220	247	8.5	7.64	Aridic	Mesic	Pinyon-Juniper Woodland
WM	GR3	2480	277	7.3	6.80	Aridic	Frigid	Pinyon-Juniper Woodland
WM	GR5	3070	421	3.3	3.07	Aridic	Cryic	Subalpine Woody Shrubland
WM	BAR	3870	538	0.1	2.78	Aridic	Cryic	Alpine Desert Grassland
CZO	SJER	400	502	16.7	22.3	Xeric	Thermic	Oak Savannah
CZO	SPR	1160	860	13.6	29.1	Xeric	Mesic	Pine/Oak Forest
CZO	PR	2020	994	9.2	22.1	Xeric	Frigid	Mixed Conifer Forest
CZO	SH	2700	1066	4.8	12.9	Xeric	Cryic	Subalpine Forest

2.9 Figures

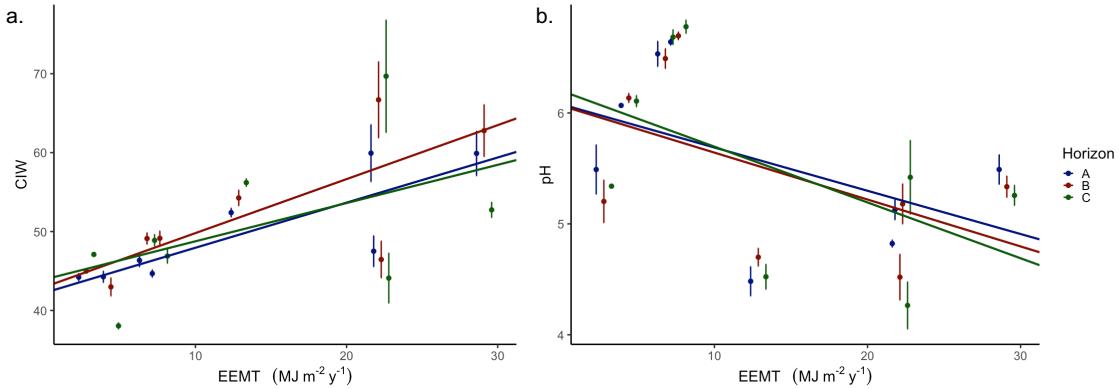

Figure 2-1. Relationship between effective energy and mass transfer (EEMT) and a.) chemical index of weathering (CIW; marginal $R^2 = 0.41$, conditional $R^2 = 0.81$, n = 87) and b.) pH in $CaCl_2$ (marginal $R^2 = 0.24$, conditional $R^2 = 0.92$, n = 87) for all mineral master soil horizons. The CIW and pH are presented as the mean and standard error for each master soil horizon after subordinate horizons were weighted to obtain a single value. Best-fit regression was determined by restricted maximum likelihood with a mixed effects model where EEMT, horizon, and their interaction were included as fixed effects and the vertical spatial dependency of horizons collected from within the same pit was accounted for as a random effect. EEMT was the only significant fixed effect for both variables ($p < 0.05$).

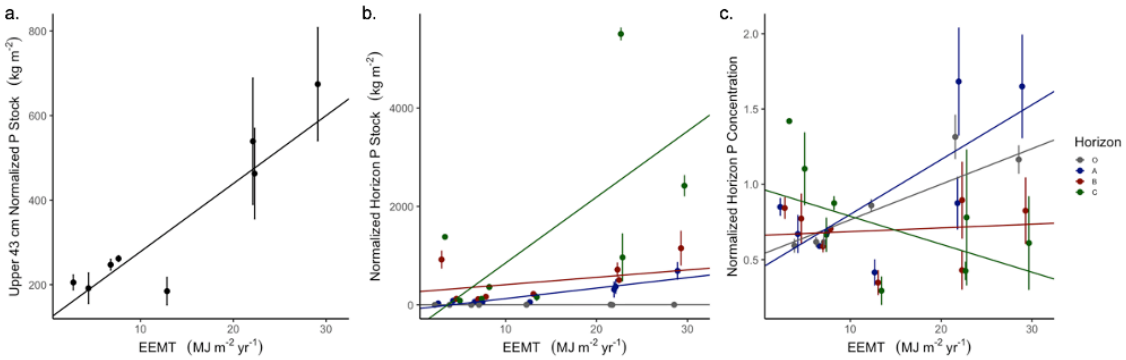

Figure 2-2. Relationships between EEMT with parent material normalized (a) mineral soil pit P stock to 43 cm (n = 33), (b) horizon P stock within master soil horizons (n = 119), and (c) horizon P concentration of master soil horizons (unitless ratio; n = 108). Least squares linear regression was used to determine the relationship in plot a and mixed effect model results are presented for b and c. Best-fit regression for the mixed effect models were determined by restricted maximum likelihood where EEMT, horizon, and their interaction were included as fixed effects and the vertical spatial dependency of horizons collected from within the same pit was accounted for as a random effect.

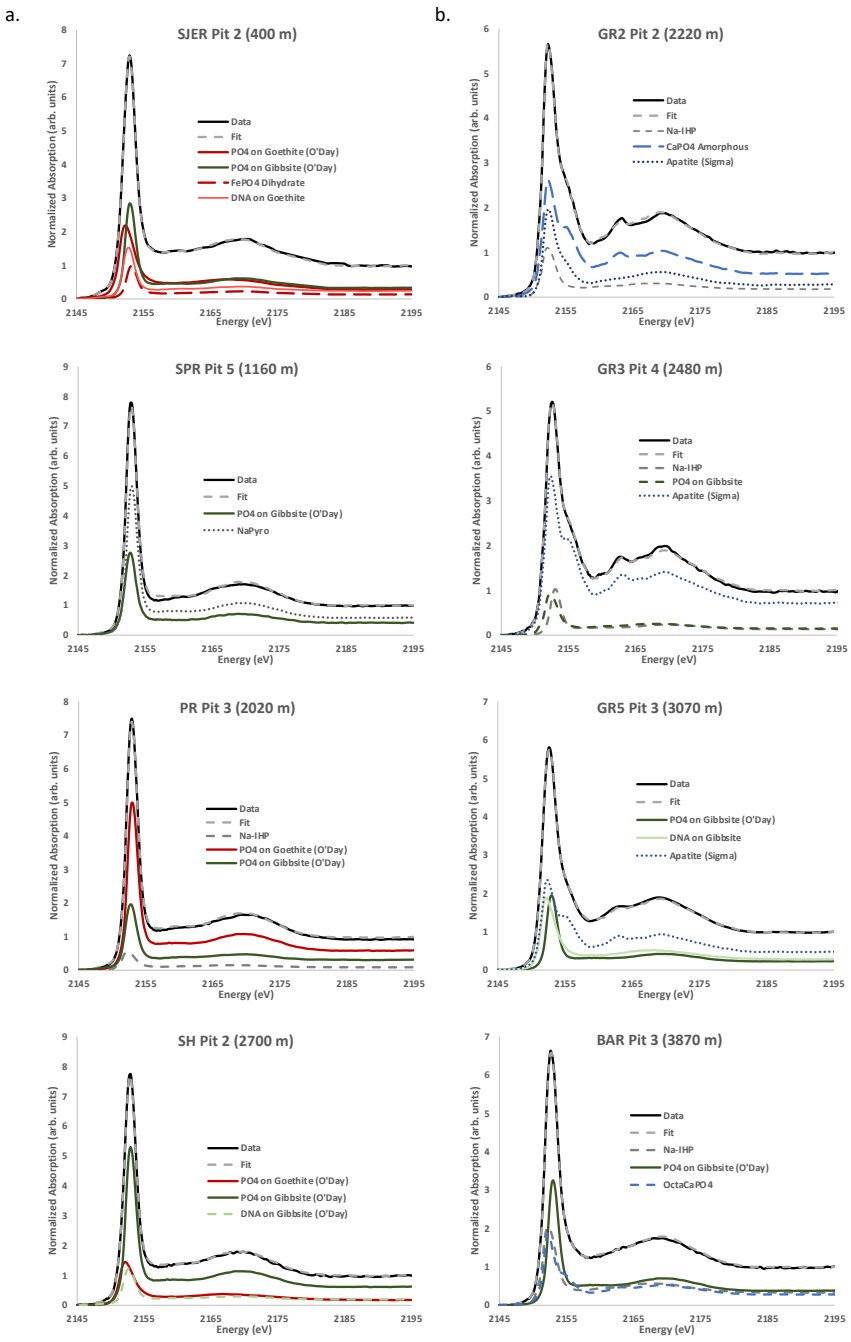

Figure 2-3. Phosphorus K edge XANES for bulk soil samples in representative A horizons at the Southern Sierra Critical Zone Observatory (CZO; a) and White Mountain (WM; b) elevational transects. Site descriptions are included in Table 1. Data (black line), linear combination best fit (dashed gray line), and spectral deconvolutions of the reference compounds (colored lines) are presented. Reference compounds include adsorbed and precipitated organic and inorganic species with a complete list included in Figure S2.

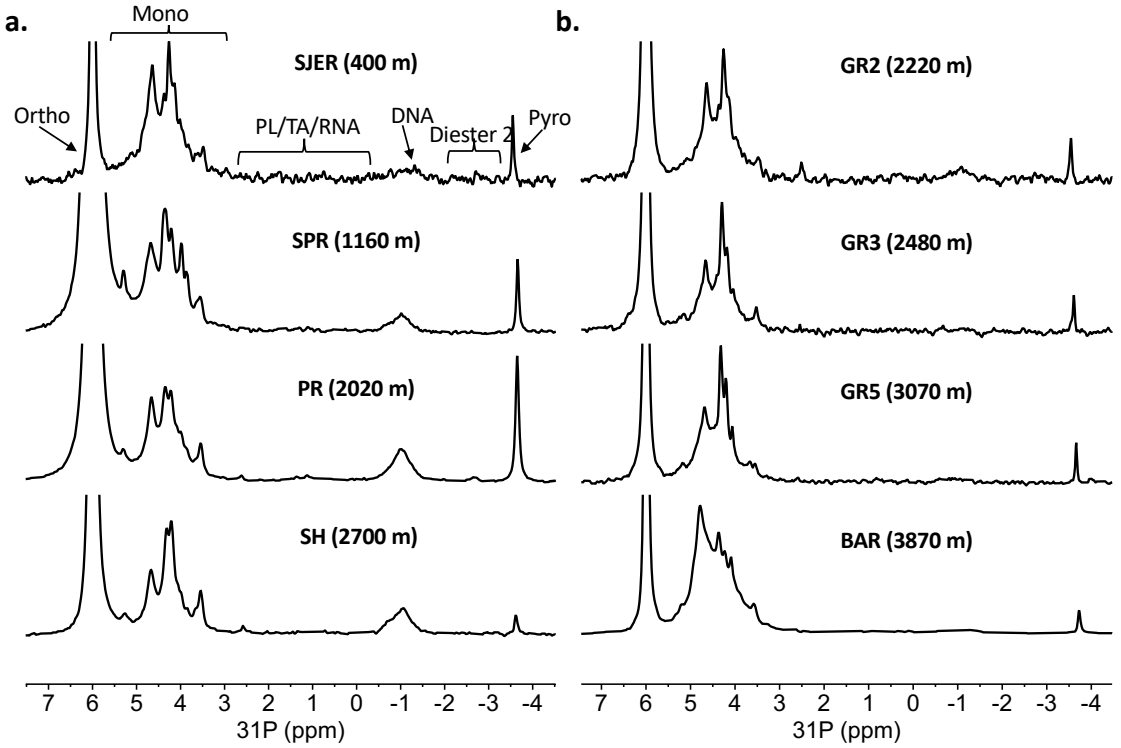

Figure 2-4. ^{31}P solution NMR spectra (shown with 10 Hz line broadening) of extracted soil from a representative A horizon at the Southern Sierra Critical Zone Observatory (CZO; a) and arid White Mountain (WM; b) elevational transects. Site information is describe in Table 1. The number of scans collected for each sample varied based on relaxation time and therefore direct comparisons of peak intensities can only be made within a spectrum not necessarily between spectra. Chemical shifts were assigned as orthophosphate (ortho), monoesters (mono), phospholipids (PL), lipoteichoic acids (TA), ribonucleic acid (RNA), deoxyribonucleic acid (DNA), unknown diesters (diester 2), and pyrophosphate (pyro).

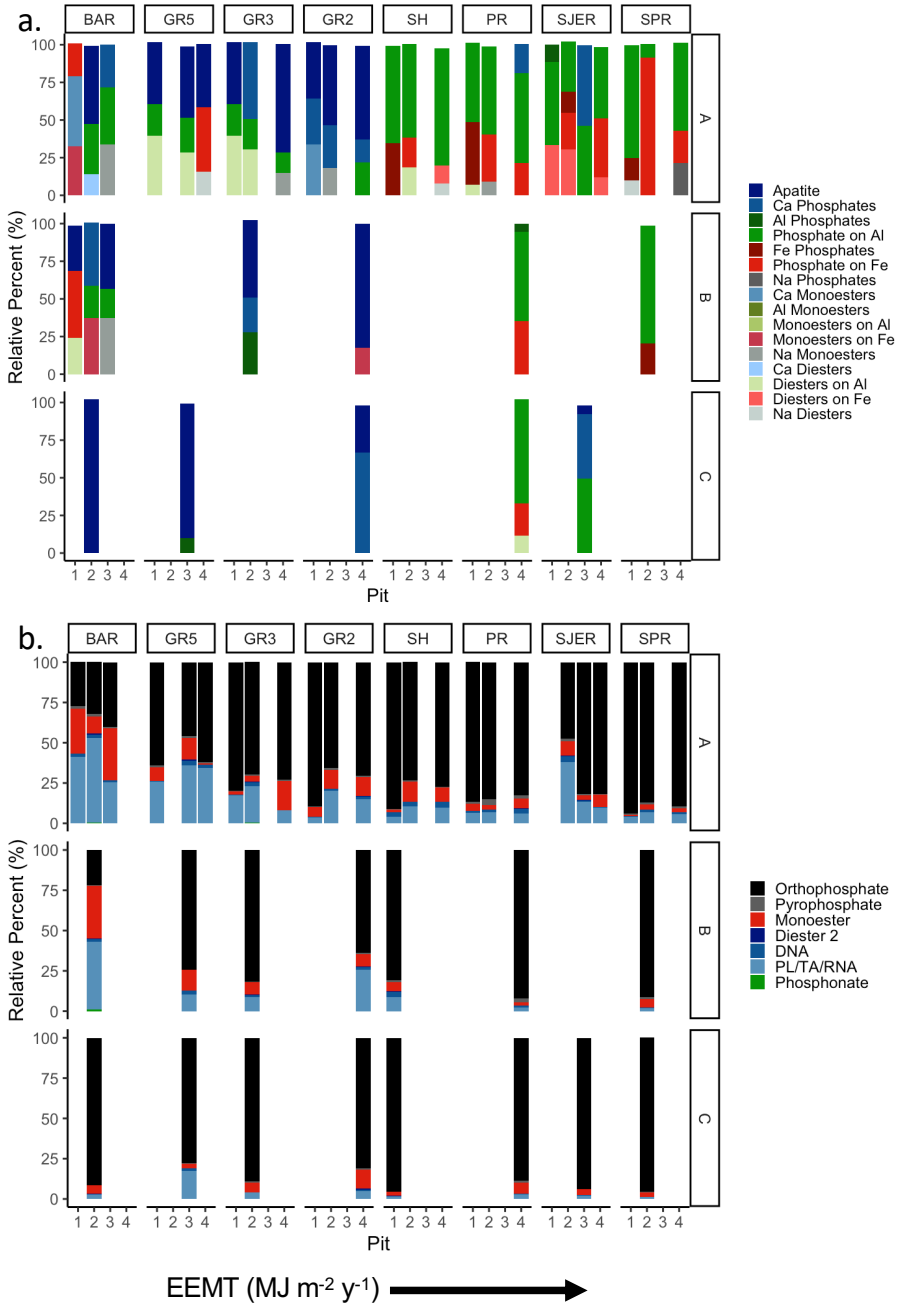

Figure 2-5. a.) Summary of linear combination fits of phosphorus K edge XANES spectra for A, B, and C master soil horizons with increasing effective energy and mass transfer (EEMT). Numerical fits are reported in SI. b.) Summary of ^{31}P solution NMR spectra of extracted soil for A, B, and C master soil horizons with increasing EEMT. Chemical shifts were assigned as orthophosphate, pyrophosphate, monoesters, unknown diesters (diester 2), deoxyribonucleic acid (DNA), phospholipids (PL)/lipoteichoic acids (TA)/ribonucleic acid (RNA), and phosphonates. Missing bars represent field replicates where data were not collected for XANES or NMR.

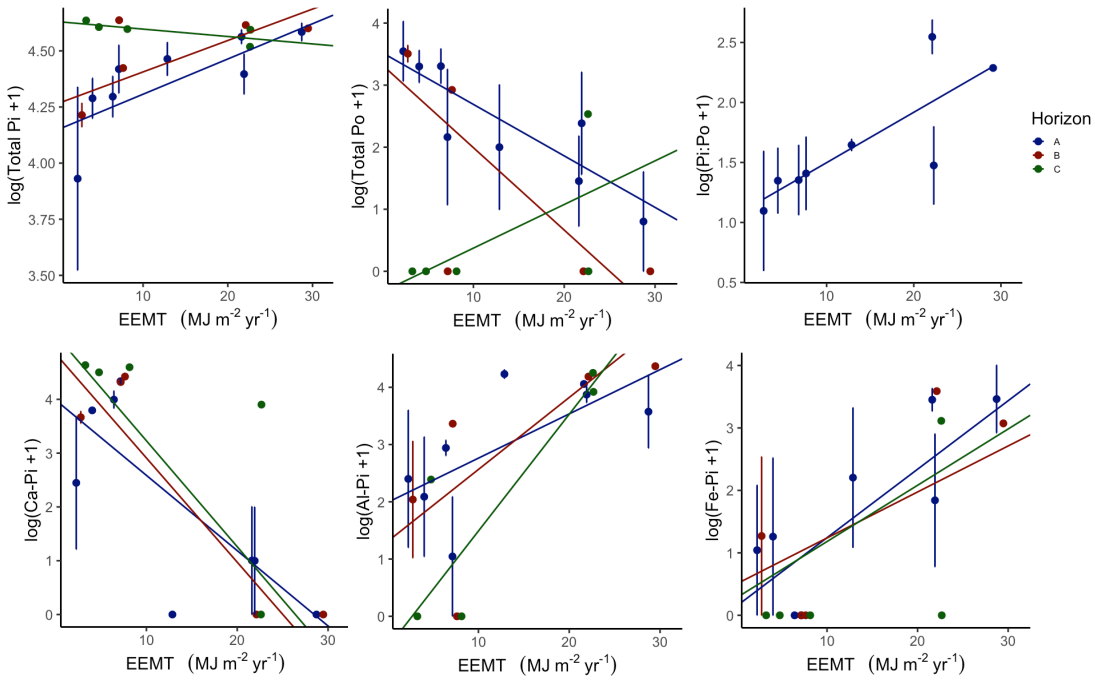

Figure 2-6. Mixed effect regression model results of phosphorus K edge XANES chemical speciation relative percent as a function of effective energy and mass transfer (EEMT) by master soil horizon (n = 37 with 25 A, 7 B, and 5 C horizons). A random effect was included to account for spatial dependence when sampling within a soil pit.

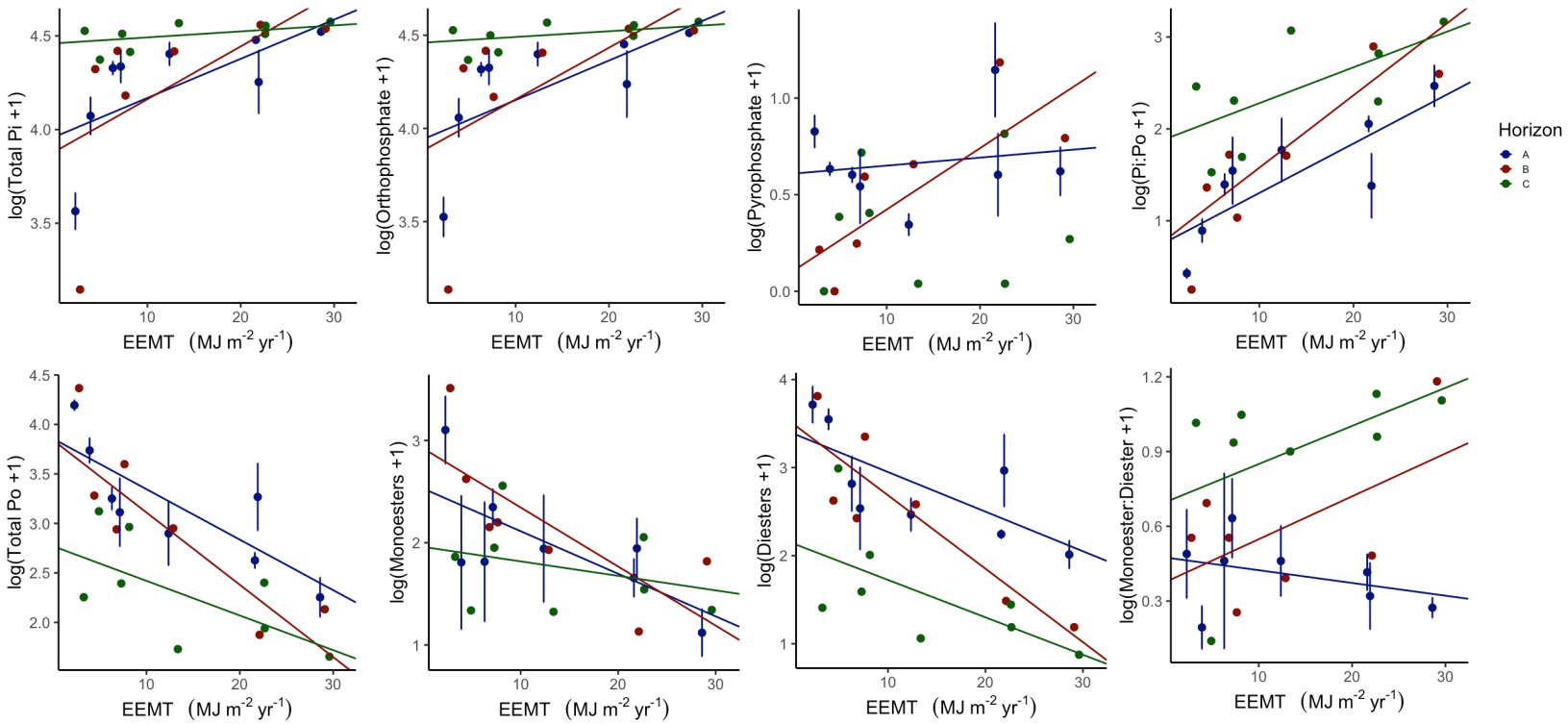

Figure 2-7. Mixed effect regression model results of ^{31}P solution NMR chemical speciation relative percent as a function of effective energy and mass transfer (EEMT) by master soil horizon (n = 39 with 24 A, 7 B, and 8 C horizons). A random effect was included to account for spatial dependence when sampling within a soil pit.

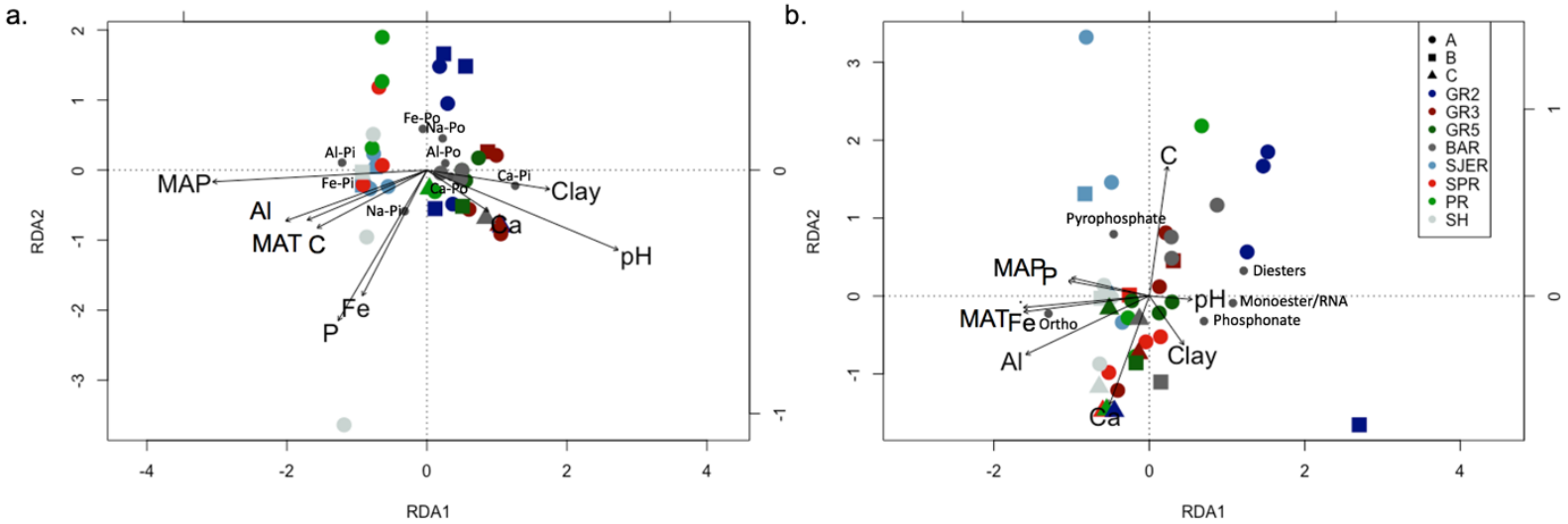

Figure 2-8. Redundancy analysis of the multi-dimensional relationship between a.) XANES and b.) ^{31}P solution NMR chemical species (small gray circles) with climate (mean annual precipitation, MAP; mean annual temperature, MAT) and soil (pH, clay, and P, C, N, Al, Fe, and Ca concentrations) properties (arrows). Samples are colored based on sites at the arid White Mountain (GR2, GR3, GR5, and BAR) and Mediterranean Critical Zone Observatory (SJER, SPR, PR, and SH) elevational gradients and master soil horizons are denoted by different shapes. Additional site details are described in Table 1.

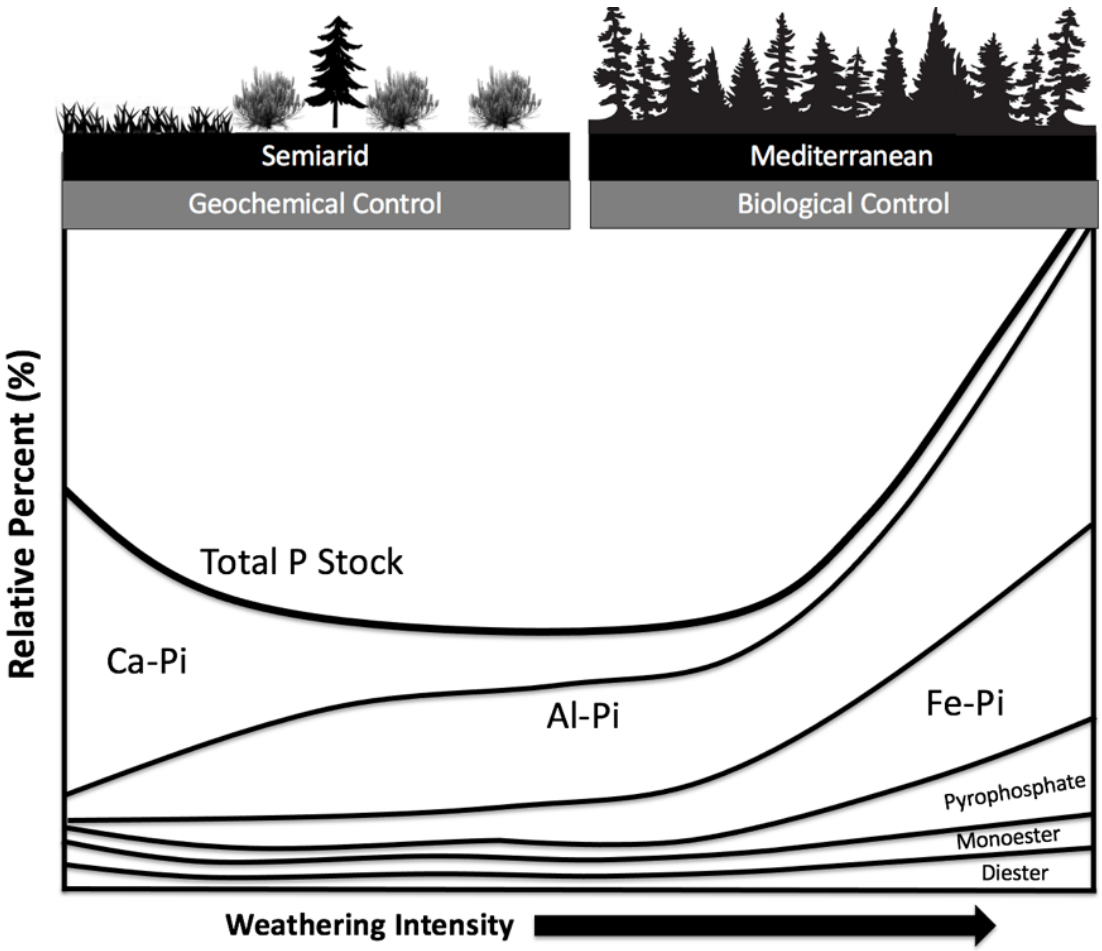

Figure 2-9. New conceptual model for the total stock and relative percent of phosphorus chemical speciation in bulk soil as a function of climate-induced weathering intensity.

2.10 Supplementary Information

2.10.1 XANES

Some synthesized compound spectra were used from O'Day et al. (2020) including Ca-, Ca-, and Fe-phytate, PO_4^{3-} and IHP adsorbed to ferrihydrite and goethite, and DNA adsorbed to gibbsite. Additional sorbed and precipitated compounds were prepared for the current study. Ferrihydrite (amorphous $Fe(OH)_3$) and goethite (FeOOH) minerals were prepared following published methods (Schwertmann, 2000) and gibbsite ($Al(OH)_3$) was purchased from Huber Engineered Materials (Micral 916). Briefly, 600 mg of $Fe(OH)_3$, 300 mg of FeOOH, or 600 mg of $Al(OH)_3$ were added to 50 mL of a 0.1 M NaCl solution containing NaH_2PO_4, phytic acid sodium salt (IHP), or DNA (pH=6), shaken for 18 h in the dark, filtered through a 0.45 μm membrane, and air dried (Prietzel et al. 2016). Phosphorus concentrations were varied based on anticipated loadings with 1 mM of NaH_2PO_4, 1 mM IHP, or 0.05 g DNA for ferrihydrite, 0.05 mM NaH_2PO_4, 0.05 mM IHP, or 0.3 g DNA for goethite, or 0.5 mM NaH_2PO_4, 0.5 mM IHP or 0.1 g DNA for gibbsite. Iron-, Al-, and Ca-PO_4 precipitates were also synthesized. Iron and Al phosphate were synthesized by mixing 250 mL of 0.2 M $FeCl_3$ or 0.3 M $AlCl_3$ with 250 mL of 0.3 M NaH_2PO_4, pH was adjusted to 3, centrifuged at 3000 rpm for 45 minutes, washed with DI water 2 times, and air dried (Hsu 1975; Enyard et al. 1992; Schwertmann 2000). Calcium PO_4 was prepared by mixing 400 mL of 0.2 M K_2HPO_4 with 400 mL of 0.02M $CaCl_2$, adjusted to pH 6.5, centrifuged for 40 minutes at 10,000 rpm, rinsed 2 times with DI water, and air dried (Hsu 1975). Inositol hexakisphosphate bound to gibbsite was not used in the final reference compound library due to the lack of distinct spectral features compared to Pi sorbed to gibbsite.

2.10.2 ^{31}P NMR

Solution state ^{31}P 1D NMR experiments were acquired on a Bruker Advance III spectrometer operating at a field-strength of 17.6 T (750.2 MHz, ^{1}H and 303.7 MHz, ^{31}P) equipped with a Bruker 5mm BBO direct detect probe. The sample temperature was regulated at 20 °C. 1D experiments were performed with Bruker's "zg" standard 1D pulse program using 90° pulses calibrated on the ortho-phosphate signal in each sample or an ortho-phosphate (1 M $Na_3PO_4^{3-}$) spiked duplicate sample in cases where the intrinsic orthophosphate signal intensity was too low to perform this task in a timely manner. T_1 measurements were performed on each sample, or its spiked duplicate, using the inversion-recovery pulse sequence (Bruker 't1ir' pulse program) to ensure that the recycle delay between pulses (acquisition time + relaxation delay) was at least 5 × the T_1 of orthophosphate (delays ranged between 1.5 – 23.8 s). The spectral width was 100 ppm and 49,378 total points were acquired in 0.8 s. Each 1D spectrum was measured for approximately 16 hours in experiment blocks of four hours. The total number of transients co-added for each spectrum ranged from 3,072 to 24,576 depending on a particular sample's recycle delay. Post-acquisition processing included zero-filling to 128k total points, exponential multiplication (1 – 10 Hz line-broadening), and automated

baseline correction with a 5th order polynomial. Spectral deconvolutions were fit using Lorentzian-Gaussian shaped curves.

2.10.3 XANES Reference Compounds

Distinct P K-edge spectra were produced by differences in the local molecular bonding environment of known reference compounds, particularly from influence of the counter cations (Kizewski et al. 2011). Diverse spectral features were found for Pi and Po species associated with Ca, Al, and Fe including differences in the energy, intensity, and broadening of the white line along with pre- and post-edge features (Figures 2-S4 and 2-S5). These findings are similar to previous studies (e.g., Ingall et al. 2010). For example, the energy of the white line shifted ~ 0.8 eV for inorganic species and ~0.3 eV for organic species when comparing these metals (Table 2-S2). Precipitated Pi species shifted from 2153.12 eV for $AlPO_4$ and 2153.07 eV for $FePO_4$ to 2152.3 eV for $CaPO_4$. Precipitated Po species (as IHP) with metals also resulted in different white line energies, although this was less pronounced. Aluminum-IHP had a white line of 2152.71 eV which was similar to Fe-IHP at 2152.86 eV but also differed from Ca-IHP at 2152.49 eV. Iron and Al associated P overall had lower white line energies for organic species than inorganic species (Fe-Pi: 2152.96 ± 0.17, Fe-Po: 2152.51 ± 0.26, Al-Pi: 2153.09 ± 0.08, Al-Po: 2152.36 ± 0.30), but Ca-P compounds were similar (Ca-Pi: 2152.32 ± 0.06, Ca-Po: 2152.35 ± 0.21). Calcium bound P had a broadening of the white line with a post edge composed of two features that is more pronounced in less soluble species (e.g. apatite; Kizewski et al. 2011). Iron bound P demonstrated a pre-edge feature that is proportional to the number of PO_4-Fe(III) bonds (Kizewski et al. 2011). Aluminum-P had a post edge feature that are more subtle than found in Ca species. Pre- and post-edge features were more pronounced for precipitated than sorbed species helping to differentiate between these species (Beauchemin et al. 2003, Sato et al. 2005). Overall, Po species pre- and post-edge features were less pronounced than the Pi species, but demonstrated a broadening of the white line (e.g., Hesterberg et al. 2017) and exhibited differences in features (e.g., He et al. 2007; O'Day et al. 2020) similar to previous studies (Figures 2-S4 and 2-S5).

2.10.4 Supplementary Tables

Table 2-S1. Soil and rock outcrop properties including elemental concentrations (g kg^{-1}) of P, C, N, Fe, Ca and Al, chemical index of weathering (CIW), pH in DI, pH in $CaCl_2$, and percent clay. Mean and standard error (field replicates) are reported across all master soil horizons within a site and calculated after each subordinate horizon was weighted by bulk density, thickness, and gravel to obtain a single value for each master soil horizon per soil pit. When no data were collected, it is indicated by nd. When standard error could not be calculated (n=1) it is denoted by na.

Site (Elevation; m)	Soil Horizon	n Conc./ Clay & pH	P (g kg^{-1})	C (g kg^{-1})	N (g kg^{-1})	Fe (g kg^{-1})	Ca (g kg^{-1})	Al (g kg^{-1})	CIW	Clay (%)	pH ($CaCl_2$)	pH (DI)
GR2 (2220)	O	3/0	0.923 (0.056)	155 (28)	5.82 (0.98)	23.9 (1.1)	17.8 (0.39)	55.1 (2.5)	nd	nd	nd	nd
	A	4/4	1.02 (0.044)	13.0 (2.8)	0.692 (0.10)	38.0 (1.3)	20.5 (0.99)	75.6 (1.6)	44.7 (0.46)	7.8 (0.45)	6.6 (0.03)	7.1 (0.04)
	B	2/2	1.06 (0.010)	6.72 (0.094)	0.533 (0.086)	48.3 (6.5)	27.1 (4.0)	77.3 (2.4)	49.2 (91)	12.8 (1.1)	6.7 (0.04)	7.3 (0.11)
	C	4/4	1.31 (0.068)	3.54 (1.9)	0.258 (0.076)	46.0 (1.7)	30.8 (3.5)	76.4 (3.3)	46.9 (0.91)	6.7 (2.3)	6.8 (0.06)	7.4 (0.10)
	Outcrop	5/0	1.36 (0.065)	nd	nd	36.6 (0.78)	27.2 (0.45)	93.0 (1.6)	45.9 (1.2)	nd	nd	nd
GR3 (2480)	O	4/0	0.920 (0.048)	68.8 (16)	3.68 (0.46)	19.6 (6.6)	13.3 (4.5)	49.4 (14)	nd	nd	nd	nd
	A	4/4	0.884 (0.020)	14.6 (3.9)	0.747 (0.073)	36.7 (1.7)	18.0 (0.57)	78.6 (0.7)	46.3 (0.81)	15.1 (3.6)	6.5 (0.11)	7.3 (0.17)
	B	4/4	0.876 (0.056)	6.36 (1.7)	0.380 (0.029)	43.9 (2.8)	20.5 (0.93)	86.5 (2.0)	49.1 (0.72)	25.6 (1.2)	6.5 (0.09)	7.3 (0.25)
	C	4/4	0.993 (0.168)	2.94 (0.84)	0.208 (0.065)	45.7 (1.4)	22.4 (1.8)	83.9 (2.5)	48.9 (0.73)	19.6 (3.7)	6.7 (0.07)	7.3 (0.23)
	Outcrop	5/0	1.48 (0.075)	nd	nd	38.6 (1.4)	26.4 (3.4)	90.5 (1.2)	46.5 (1.5)	nd	nd	nd
GR5 (3070)	O	4/4	0.888 (0.067)	110 (36)	4.32 (1.1)	21.7 (1.8)	13.7 (0.96)	62.9 (3.2)	nd	nd	nd	nd
	A	4/4	1.00 (0.19)	14.5 (1.5)	1.17 (0.070)	30.9 (3.3)	16.9 (1.1)	79.1 (1.7)	44.3 (0.71)	6.5 (0.56)	6.1 (0.01)	6.8 (0.08)
	B	4/4	1.16 (0.24)	6.05 (1.5)	0.582 (0.16)	40.8 (4.3)	20.5 (3.5)	82.9 (3.6)	43.0 (1.1)	10.1 (0.8)	6.1 (0.04)	6.9 (0.04)
	C	3/3	1.65 (0.37)	2.76 (1.1)	0.237 (0.092)	43.6 (6.9)	25.7 (7.0)	86.2 (3.6)	38.0 (0.39)	9.2 (2.5)	6.1 (0.05)	6.9 (0.03)
	Outcrop	4/4	0.400 (0.082)	nd	nd	14.0 (2.3)	6.75 (2.7)	86.7 (1.2)	50.7 (0.63)	nd	nd	nd
BAR (3870)	O	0/0	nd	nd	nd	nd	nd	nd	nd	nd	nd	nd
	A	4/4	1.27 (0.088)	34.0 (2.3)	3.06 (0.24)	26.5 (2.2)	19.5 (1.6)	74.4 (2.6)	44.2 (0.46)	6.4 (0.37)	5.5 (0.22)	6.0 (0.13)
	B	4/4	1.26 (0.10)	2.48 (0.61)	0.239 (0.080)	41.9 (2.9)	29.9 (0.59)	85.8 (0.4)	45.0 (0.8)	5.9 (040)	5.20 (0.2)	6.2 (0.11)
	C	1/1	2.12 (na)	0.533 (na)	0.00 (na)	56.1 (na)	39.0 (na)	88.7 (na)	47.1 (na)	4.4 (na)	5.34 (na)	6.3 (na)
	Outcrop	5/0	1.65 (0.085)	nd	nd	47.0 (1.3)	38.2 (1.1)	93.7 (2.0)	46.9 (0.91)	nd	nd	nd

SJER (400)	O	nd	nd	nd	nd	nd	nd	nd	nd	nd	nd
	A	0.649 (0.13)	6.84 (0.86)	0.657 (0.067)	31.8 (7.5)	24.5 (4.6)	92.7 (5.3)	47.5 (1.9)	9.8 (0.35)	5.1 (0.18)	5.6 (0.32)
	B	0.319 (0.094)	1.52 (0.26)	0.178 (0.037)	23.7 (9.1)	20.9 (3.9)	88.4 (7.2)	46.5 (2.3)	3.6 (2.5)	5.2 (0.31)	5.5 (0.44)
	C	0.580 (0.33)	0.805 (0.32)	0.0929 (0.04)	27.8 (16)	26.5 (7.4)	88.6 (9.4)	44.1 (3.2)	3.6 (1.1)	5.4 (0.58)	5.5 (0.49)
	Outcrop	0.65 (0.072)	nd	nd	15.2 (1.3)	22.6 (0.45)	88.0 (1.4)	41.0 (0.58)	nd	nd	nd
SPR (1160)	O	0.860 (0.070)	439 (110)	10.5 (1.8)	7.31 (1.5)	13.0 (0.81)	15.9 (3.5)	nd	nd	nd	nd
	A	1.22 (0.25)	25.5 (5.1)	1.17 (0.063)	38.8 (1.3)	18.9 (2.0)	95.8 (2.1)	60.0 (2.8)	5.3 (1.0)	5.5 (0.13)	5.4 (0.29)
	B	0.612 (0.16)	4.09 (1.2)	0.270 (0.062)	41.3 (1.4)	19.0 (2.2)	103.4 (2)	62.8 (3.3)	13.1 (3.5)	5.3 (0.10)	5.6 (0.30)
	C	0.452 (0.23)	1.10 (1.2)	0.0466 (0.04)	38.1 (3.4)	27.4 (3.5)	94.4 (4.1)	52.7 (0.98)	4.8 (1.6)	5.3 (0.09)	5.5 (0.36)
	Outcrop	0.650 (0.14)	nd	nd	30.2 (2.6)	28.6 (4.8)	87.2 (3.0)	48.6 (0.93)	nd	nd	nd
PR (2020)	O	0.975 (0.11)	477 (24)	16.1 (0.82)	7.95 (2.0)	18.1 (0.53)	16.2 (4.2)	nd	nd	nd	nd
	A	1.25 (0.26)	30.5 (3.9)	1.11 (0.15)	42.6 (4.8)	18.8 (2.2)	93.7 (2.3)	60.0 (3.6)	2.7 (1.4)	4.8 (0.03)	5.5 (0.03)
	B	0.661 (0.19)	9.43 (2.0)	0.370 (0.067)	45.2 (4.8)	16.9 (2.9)	95.2 (4.3)	66.7 (4.8)	5.1 (1.5)	4.5 (0.21)	5.4 (0.14)
	C	0.313 (0.048)	0.699 (1.1)	0.0440 (0.03)	47.9 (3.0)	18.4 (3.4)	101 (4.4)	69.7 (7.12)	6.2 (0.73)	4.3 (0.21)	5.3 (0.18)
	Outcrop	0.886 (0.055)	nd	nd	41.8 (1.8)	37.3 (0.73)	91.9 (0.6)	49.0 (0.65)	nd	nd	nd
SH (2700)	O	0.640 (0.030)	509 (6.4)	14.0 (3.5)	7.24 (0.98)	4.96 (1.3)	28.4 (1.0)	nd	nd	nd	nd
	A	0.308 (0.064)	25.1 (4.2)	1.03 (0.13)	18.1 (2.3)	10.9 (0.63)	74.2 (5.8)	52.4 (0.55)	3.1 (0.29)	4.5 (0.13)	5.3 (0.13)
	B	0.258 (0.061)	8.32 (1.0)	0.445 (0.048)	16.1 (0.33)	10.4 (0.37)	73.5 (2.1)	54.3 (0.98)	4.4 (0.63)	4.7 (0.08)	5.6 (0.07)
	C	0.218 (0.070)	2.42 (0.68)	0.153 (0.057)	18.0 (0.80)	10.5 (0.15)	79.3 (1.1)	56.2 (0.49)	5.2 (0.96)	4.5 (0.11)	5.5 (0.13)
	Outcrop	nd	nd	nd	nd	nd	nd	nd	nd	nd	nd

Table 2-S2. List of all reference compounds used in this study grouped by inorganic and organic species with Ca, Al, Fe, or Na counter-cations. Compounds were either purchased or synthesized by standard laboratory methods. The beamline, energy of the white line, and P to metal ratio are presented. Compounds are noted when acquired from a previous study (O'Day et al. 2020).

Group	Reference Compound	Full Name	Purchased or Synthesized	Beamline	White Line	P/Metal
Apatite	Carbonate Apatite	CAP Carbonate Apatite	Clarkson	CLS SXRMB	2152.26	
	Apatite Sigma	Hydroxyapatite	Sigma Aldrich	SSRL 14-3	2152.35	
	Apatite Mexico	Apatite, Research Grade	Ward Scientific	SSRL 14-3	2152.31	0.663
	Apatite Madagascar	Apatite	Ward Scientific	CLS SXRMB	2152.34	0.377
Other Ca-Pi	CaPO4 Amorphous	Amorphous Calcium Phosphate	Clarkson	CLS SXRMB	2152.39	
	Octacalcium Phosphate	OCP Octacalcium Phosphate	Clarkson	CLS SXRMB	2152.26	
	CaHPO4 Dibasic	Calcium Phosphate Dibasic Dihydrate	Sigma Aldrich	CLS SXRMB	2152.25	
	CaPO4 Precip	Precipitated Calcium Phosphate	Synthesized	CLS SXRMB	2152.3	1.072
Al-Pi	AlPO4 Precip	Precipitate Aluminum Phosphate	Synthesized	CLS SXRMB	2153.12	1.126
	AlPO4	Aluminum Phosphate	Acros Organics	SSRL 14-3	2153.19	
	PO4 on Gibbsite	Phosphate Sorbed on Gibbsite	Synthesized	SSRL 14-3	2153.03	0.010
	PO4 on Gibbsite	Phosphate Sorbed on Gibbsite	Synthesized (O'Day 2020)	SSRL 14-3	2153.03	
Fe-Pi	FePO4 Precip	Precipitated Iron Phosphate	Synthesized	CLS SXRMB	2153.07	2.76
	FePO4 Dihydrate	Iron (III) Phosphate Hydrate	Acros Organics	SSRL 14-3	2153.19	
	PO4 on Ferrihydrite	Phosphate Sorbed on Ferrihydrite	Synthesized	CLS SXRMB	2152.8	1.06
	PO4 on Ferrihydrite	Phosphate Sorbed on Ferrihydrite	Synthesized (O'Day 2020)	SSRL 14-3	2153.01	
	PO4 on Goethite	Phosphate Sorbed on Goethite	Synthesized	SSRL 14-3	2152.92	0.051
	PO4 on Goethite	Phosphate Sorbed on Goethite	Synthesized (O'Day 2020)	CLS SXRMB	2152.75	
Pyrophosphate	NaPyro	Sodium Pyrophsphate Decahydrate	Alfa Aesar	SSRL 14-3	2152.79	
	CaPyro	Amorphous Calcium Pyrophosphate	Aldrich	SSRL 14-3	2152.41	
Fe-Po	IHP on Goethite	Phytic Acid Sorbed on Goethite	Synthesized	CLS SXRMB	2152.6	0.090
	IHP on Ferrihydrite	Phytic Acid Sorbed on Ferrihydrite	Synthesized	CLS SXRMB	2152.67	0.552
	IHP on Ferrihydrite	Phytic Acid on Ferrihydrite	Synthesized (O'Day 2020)	SSRL 14-3	2152.4	
	Fe-IHP	Iron Phytate	Synthesized (O'Day 2020)	CLS SXRMB	2152.86	
	DNA on Ferrihydrite	DNA Sorbed on Ferrihydrite	Synthesized	CLS SXRMB	2152.16	0.053
	DNA on Goethite	DNA Sorbed on Goethite	Synthesized	CLS SXRMB	2152.29	0.010
Al-Po	DNA on Gibbsite	DNA Sorbed on Gibbsite	Synthesized	CLS SXRMB	2152.19	0.003
	DNA on Gibbsite	DNA Sorbed on Gibbsite	Synthesized (O'Day 2020)	CLS SXRMB	2152.18	
	Al-IHP	Precipitated Aluminum Phytate	Synthesized (O'Day 2020)	SSRL 14-3	2152.71	
Ca-Po	Ca-IHP	Calcium Phytate	Synthesized (O'Day 2020)	SSRL 14-3	2152.49	
	Ca-Lecithin	Lecithin (90% Soybean)	Alfa Aesar	CLS SXRMB	2152.2	

Na-Po	Na-IHP	Phytic Acid Sodium Salt Hydrate (Rice)	Sigma Aldrich	CLS SXRMB	2152.3
	Na-DNA	Deoxyribonucleic Acid Sodium Salt (Salmon Testes)	Sigma	CLS SXRMB	2151.97
	Na-AMP	Adenosine 5'-Monophsphate Sodium Salt (Yeast)	Sigma	CLS SXRMB	2152.23
	Na-ATP	Adensosine-5'-Triphosphate Disodium Salt Hydrate	Alfa Aesar	CLS SXRMB	2152.27

Table 2-S3. Percent components of linear combination fits of bulk soil XANES spectra. The R-factor was used as a statistical goodness of fit ($\sum$ (data-fit)^2 / $\sum$ (data)^2). Site descriptions are included in Table 1.

Gradient	Site	Pit	Horizon	Apatite	CaPO4	AlPO4	FePO4	PO4 on Fe	PO4 on Al	Na Pyro	IHP on Fe	Ca-IHP	Na-IHP	Na-DNA	DNA on Fe	DNA on Al	Na-AMP	Ca-Lecithin	Total	R Factor
CZO	SJER	1	A	0	0	12	0	0	55.3	0	0	0	0	0	33.2	0	0	0	100.1	0.0010384
	SJER	2	A	0	0	0	14	24.5	33.3	0	0	0	0	0	30.5	0	0	0	102.1	0.000239
	SJER	3	A	0	53	0	0	0	46.3	0	0	0	0	0	0	0	0	0	99.6	0.0006661
	SJER	3	C	5.8	43	0	0	0	49.4	0	0	0	0	0	0	0	0	0	97.9	0.000683
	SJER	4	A	0	0	0	0	39.2	47.4	0	0	0	0	0	11.9	0	0	0	98.5	0.0004528
	SPR	1	A	0	0	0	15	0	74.7	0	0	0	0	10.1	0	0	0	0	99.5	0.0008949
	SPR	2	A	0	0	0	0	91.4	9.1	0	0	0	0	0	0	0	0	0	100.5	0.004573
	SPR	2	B	0	0	0	21	0	77.9	0	0	0	0	0	0	0	0	0	98.5	0.0019355
	SPR	5	A	0	0	0	0	21.4	58.3	22	0	0	0	0	0	0	0	0	101.3	0.0018375
	PR	2	A	0	0	0	42	0	52.6	0	0	0	0	0	0	6.9	0	0	101.2	0.0010206
	PR	3	A	0	0	0	0	31.5	58.5	0	0	0	9	0	0	0	0	0	98.9	0.0008095
	PR	5	A	0	19.3	0	0	21.6	59.7	0	0	0	0	0	0	0	0	0	100.6	0.0002630
	PR	5	B	0	0	5.5	0	35.2	59.3	0	0	0	0	0	0	0	0	0	100	0.0008558
	PR	5	C	0	0	0	0	21.5	69.2	0	0	0	0	0	0	11.6	0	0	102.3	0.0006985
	SH	1	A	0	0	0	35	0	64.5	0	0	0	0	0	0	0	0	0	99.1	0.0015865
	SH	2	A	0	0	0	0	19.9	62	0	0	0	0	0	0	18.5	0	0	100.4	0.0005511
	SH	4	A	0	0	0	0	0	77.9	0	0	0	0	7.9	11.8	0	0	0	97.6	0.0005449
WM	GR2	1	A	37.3	31	0	0	0	0	0	0	34	0	0	0	0	0	0	101.7	0.0009588
	GR2	2	A	52.8	29	0	0	0	0	0	0	0	18	0	0	0	0	0	99.5	0.0005164
	GR2	4	A	62.1	15	0	0	0	22	0	0	0	0	0	0	0	0	0	99.3	0.0011138
	GR2	4	B	82.4	0	0	0	0	0	0	17.6	0	0	0	0	0	0	0	100	0.001461
	GR2	4	C	31.4	67	0	0	0	0	0	0	0	0	0	0	0	0	0	98.2	0.0031996
	GR3	1	A	41.0	0	0	0	0	21.1	0	0	0	0	0	0	39.6	0	0	101.7	0.0013658
	GR3	2	A	0	51	0	0	0	20.2	0	0	0	0	0	0	30.4	0	0	101.9	0.0107139
	GR3	2	B	51.3	23	28	0	0	0	0	0	0	0	0	0	0	0	0	102.2	0.0068475
	GR3	4	A	72	0	0	0	0	13.5	0	0	0	15	0	0	0	0	0	100.4	0.000625
	GR5	1	A	41	0	0	0	0	21.1	0	0	0	0	0	0	39.6	0	0	101.7	0.0012757
	GR5	3	A	47.6	0	0	0	0	22.8	0	0	0	0	0	0	28.5	0	0	98.9	0.0003533
	GR5	3	C	89.2	0	9.9	0	0	0	0	0	0	0	0	0	0	0	0	99.1	0.0034527
	GR5	4	A	42.1	0	0	0	42.8	0	0	0	0	0	15.7	0	0	0	0	100.6	0.0004621
	BAR	1	A	0	0	0	0	21.8	0	0	32.6	47	0	0	0	0	0	0	101	0.0003275
	BAR	1	B	30.2	0	0	0	44.1	0	0	0	0	0	0	0	24.3	0	0	98.6	0.0004418
	BAR	2	A	51.9	0	0	0	0	33.3	0	0	0	0	0	0	0	0	14	99.2	0.000699
	BAR	2	B	0	42	0	0	0	21.5	0	37.2	0	0	0	0	0	0	0	100.7	0.0004453
	BAR	2	C	102	0	0	0	0	0	0	0	0	0	0	0	0	0	0	102.1	0.0026756
	BAR	3	A	0	28	0	0	0	38.1	0	0	0	34	0	0	0	0	0	100	0.0004306
	BAR	3	B	43.5	0	0	0	0	19.2	0	0	0	0	0	0	0	37	0	100	0.0010941

Table 2-S4. ^{31}P solution NMR summation of area under the peak (relative %) mean and standard error for field replicates (A horizon n = 3, B horizon n=1, C horizon n=1) of orthophosphate (ortho), monoester, diester, pyrophosphate (pyro), phosphonate, and degradation corrected monoester (monoester^{c}) and diester (diester^{c}) at the Southern Sierra Critical Zone Observatory (CZO) and White Mountain (WM) elevational gradients. Site descriptions are included in Table 1. No data is indicated by nd.

Gradient	Horizon	Site	Ortho	Monoester	Diester	Pyro	Phosphonate	Monoester^{C}	Diester^{C}
CZO	A	SJER	70 (11)	26 (10)	3.0 (2)	0.92 (0.4)	0.0 (0.0)	6.6 (2)	22 (10)
		SPR	90 (2)	7.3 (1)	1.6 (0.5)	0.89 (0.2)	0.0 (0.0)	2.2 (0.7)	6.7 (1)
		PR	85 (1)	10 (0.7)	2.6 (0.7)	2.3 (0.8)	0.050 (0.05)	4.4 (1)	8.5 (0.5)
		SH	81 (5)	15 (5)	3.5 (0.2)	0.42 (0.08)	0.020 (0.02)	7.7 (3)	11 (2)
	B	SJER	nd	nd	nd	nd	nd	nd	nd
		SPR	91	6.8	0.6	1.2	0.0	5.2	2.3
		PR	92	4.2	1.3	2.3	0.0	2.1	3.4
		SH	81	14	4.5	0.93	0.0	2.1	12.2
	C	SJER	94	5.8	0.13	0.040	0.0 (0.0)	3.7	2.3
		SPR	96	3.8	0.39	0.31	0.0	2.8	1.4
		PR	89	8.2	1.9	1.3	0.0	6.8	3.2
		SH	95	4.2	0.42	0.040	0.0	2.8	1.9
WM	A	GR2	75 (7)	22 (6)	1.7 (0.7)	0.78 (0.3)	0.0 (0.0)	9.8 (2)	14 (5)
		GR3	74 (3)	24 (2)	1.5 (1)	0.83 (0.07)	0.10 (0.1)	7.8 (5)	17 (5)
		GR5	57 (6)	38 (4)	3.9 (2)	0.88 (0.07)	0.0 (0.0)	7.5 (4)	34 (4)
		BAR	33 (4)	58 (2)	4.7 (2)	1.3 (0.2)	0.12 (0.1)	24 (7)	42 (8)
	B	GR2	64	34	1.7	0.81	0.0	8.0	28
		GR3	82	15	2.8	0.28	0.0	7.6	10
		GR5	74	23	2.6	0.00	0.0	13	13
		BAR	22	72	4.3	0.24	1.0	33	44
	C	GR2	81	17	1.6	0.50	0.0	12	6.5
		GR3	89	10	0.00	1.1	0.0	6.0	3.9
		GR5	78	20	1.5	0.47	0.0	2.8	19
		BAR	92	8.2	0.32	0.00	0.0	5.4	3.1

Table 2-S5. Comparison of mean and standard error of field replicates for total P determined by lithium metaborate fusion on bulk samples and total extractable P by NaOH-EDTA for ^{31}P solution NMR analyses. The extraction efficiency is reported as the proportion (%) of P in NaOH-EDTA to bulk soil in each master soil horizon (A, B, and C) at the Southern Sierra Critical Zone Observatory (CZO) and White Mountain (WM) elevational gradients. An asterisk denotes a significant difference ($p < 0.05$) between elevational gradients within a single master soil horizon using a one-way ANOVA. Values were log transformed when necessary to meet model assumptions. Total and extracted P were not normalized to parent material P concentration.

Parameter	Master Soil Horizon	CZO	WM
Total P	A	968.9 (169); n = 12	1059 (85.0); n = 12
(mg kg^{-1})	B	946.0 (273); n = 3	1147 (194); n = 4
	C*	760.5 (276); n = 4	1796 (274); n = 4
Total NaOH-EDTA	A*	518.6 (127); n = 12	173.0 (32.8); n = 12
extractable P (mg kg^{-1})	B	549.3 (235); n = 3	122.6 (77.2); n = 4
	C*	245.1 (97.1); n = 4	26.63 (6.68); n = 4
NaOH-EDTA P proportion	A*	51.67 (6.56); n = 12	16.23 (2.62); n = 12
of total P (%)	B*	53.15 (8.77); n = 3	10.40 (5.68); n = 4
	C*	36.80 (10.1); n = 4	1.605 (0.491); n = 4

2.10.5 Supplementary Figures

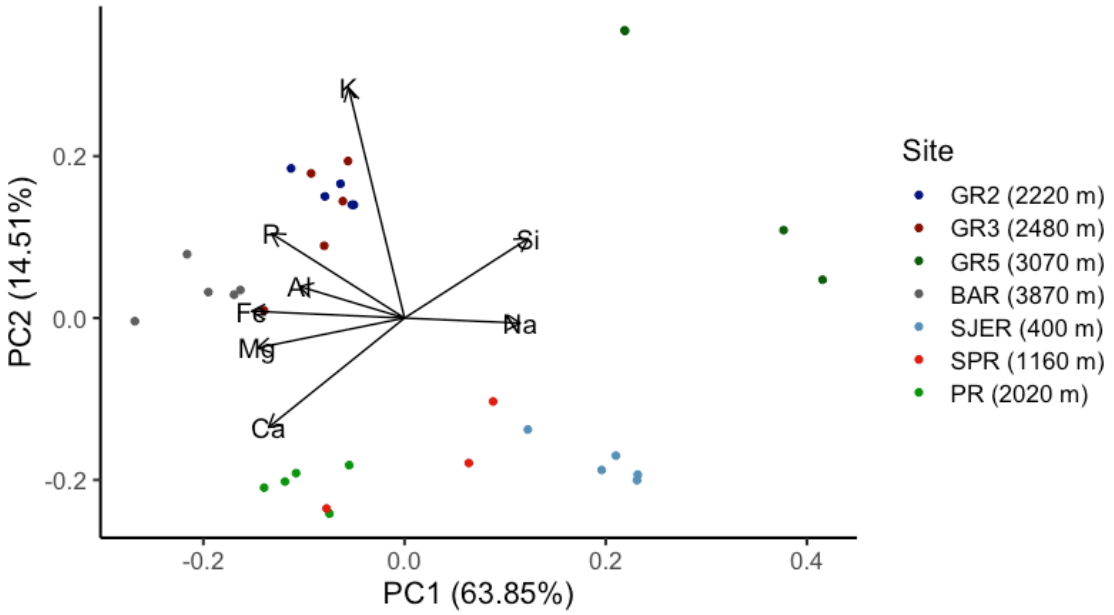

Figure 2-S1. Principle components analysis (PCA) of rock outcrop concentrations of calcium (Ca), magnesium (Mg), iron (Fe), aluminum (Al), phosphorus (P), potassium (K), silica (Si), and sodium (Na) for sites at the Southern Sierra Critical Zone Observatory (San Joaquin Experimental Range: SJER, Soaproot: SPR, and Providence: PR) and White Mountain Elevational Transect (Granite 2: GR2, Granite 3: GR3, Granite 5: GR5, and Barcroft: BAR). Elevation (m) of sites is included in the figure legend.

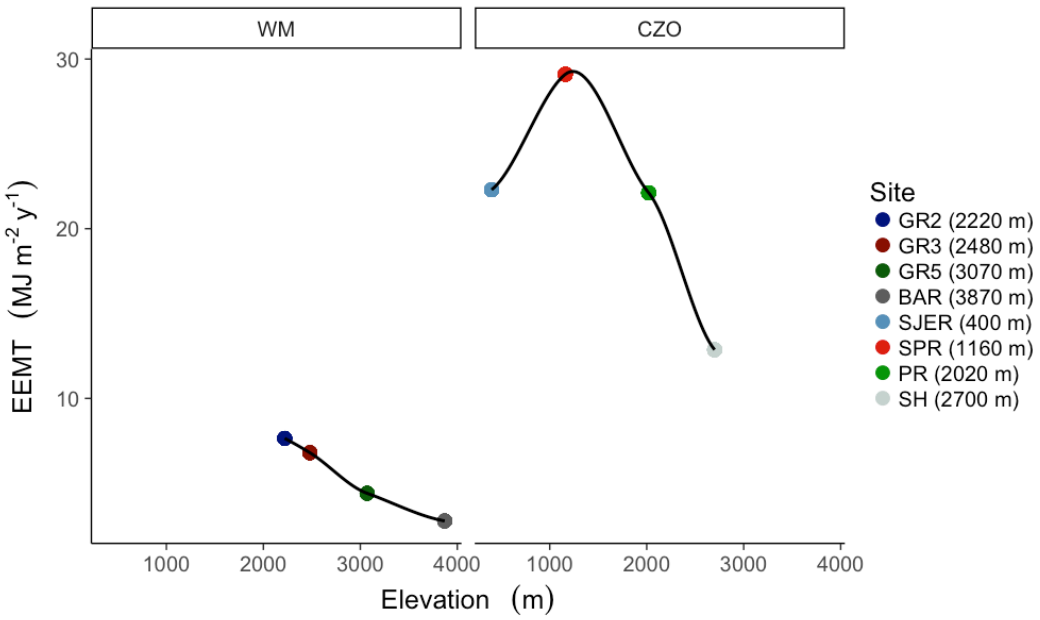

Figure 2-S2. Relationship between effective energy and mass transfer (EEMT) and elevation at the arid White Mountain (WM) and Mediterranean Critical Zone Observatory (CZO). Site details are described in Table 1.

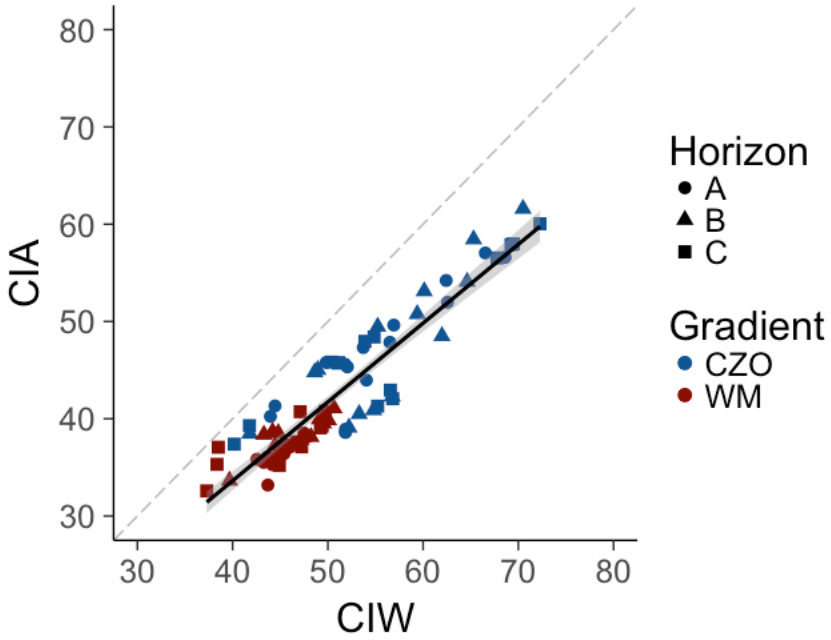

Figure 2-S3. Relationship between the chemical index of weathering (CIW) and chemical index of alteration (CIA) for mineral horizons in the arid White Mountains (WM) and Mediterranean Critical Zone Observatory (CZO). Linear regression found $r^2 = 0.88$ and $p < 0.05$ (n=87).

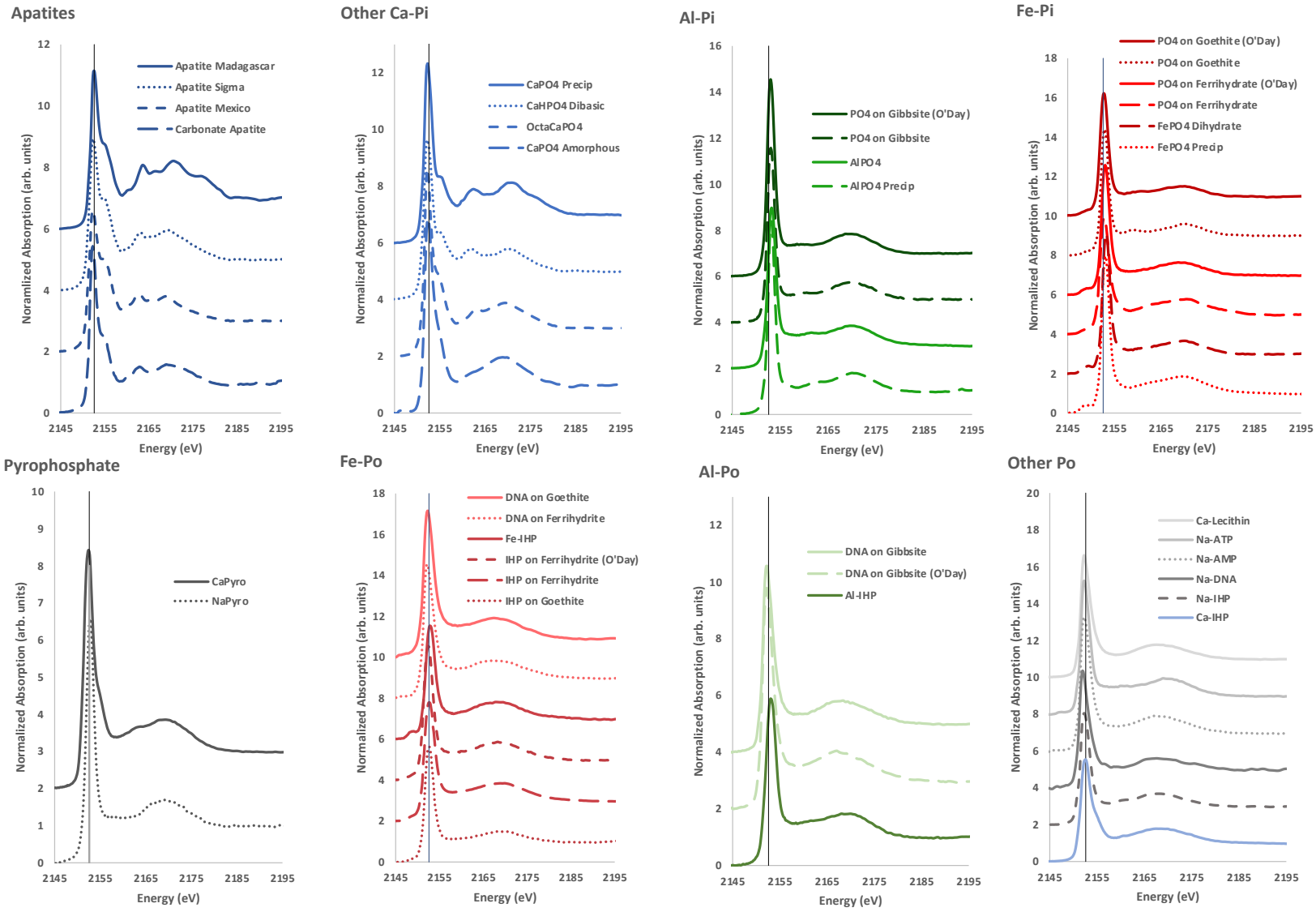
Apatites
Noramlized Absorption (arb. units)
Energy (eV)
Apatite Madagascar
Apatite Sigma
Apatite Mexico
Carbonate Apatite
Other Ca-Pi
Normalized Absorption (arb. units)
Energy (eV)
CaPO4 Precip
CaHPO4 Dibasic
OctaCaPO4
CaPO4 Amorphous
Al-Pi
Normalized Absorption (arb. units)
Energy (eV)
PO4 on Gibbsite (O'Day)
PO4 on Gibbsite
AlPO4
AlPO4 Precip
Fe-Pi
Normalized Absorption (arb. units)
Energy (eV)
PO4 on Goethite (O'Day)
PO4 on Goethite
PO4 on Ferrihydrate (O'Day)
PO4 on Ferrihydrate
FePO4 Dihydrate
FePO4 Precip
Pyrophosphate
Normalized Absorption (arb. units)
Energy (eV)
CaPyro
NaPyro
Fe-Po
Normalized Absorption (arb. units)
Energy (eV)
DNA on Goethite
DNA on Ferrihydrite
Fe-IHP
IHP on Ferrihydrite (O'Day)
IHP on Ferrihydrite
IHP on Goethite
Al-Po
Normalized Absorption (arb. units)
Energy (eV)
DNA on Gibbsite
DNA on Gibbsite (O'Day)
Al-IHP
Other Po
Normalized Absorption (arb. units)
Energy (eV)
Ca-Lecithin
Na-ATP
Na-AMP
Na-DNA
Na-IHP
Ca-IHP

Figure 2-S4. Normalized and background subtracted P K-edge XANES reference spectra for apatites, other Ca bound inorganic P (Ca-Pi), Al bound inorganic P (Al-Pi), Fe bound inorganic P (Fe-Pi), pyrophosphate, Fe bound organic P (Fe-Po), Al bound organic P (Al-Po) and other organic P compounds (Other Po). Energy was calibrated using NaH_2PO_4 standard with peak maximum set to 2152.6, as represented by the vertical black line. Compounds are noted when acquired from a previous study (O'Day et al. 2020).

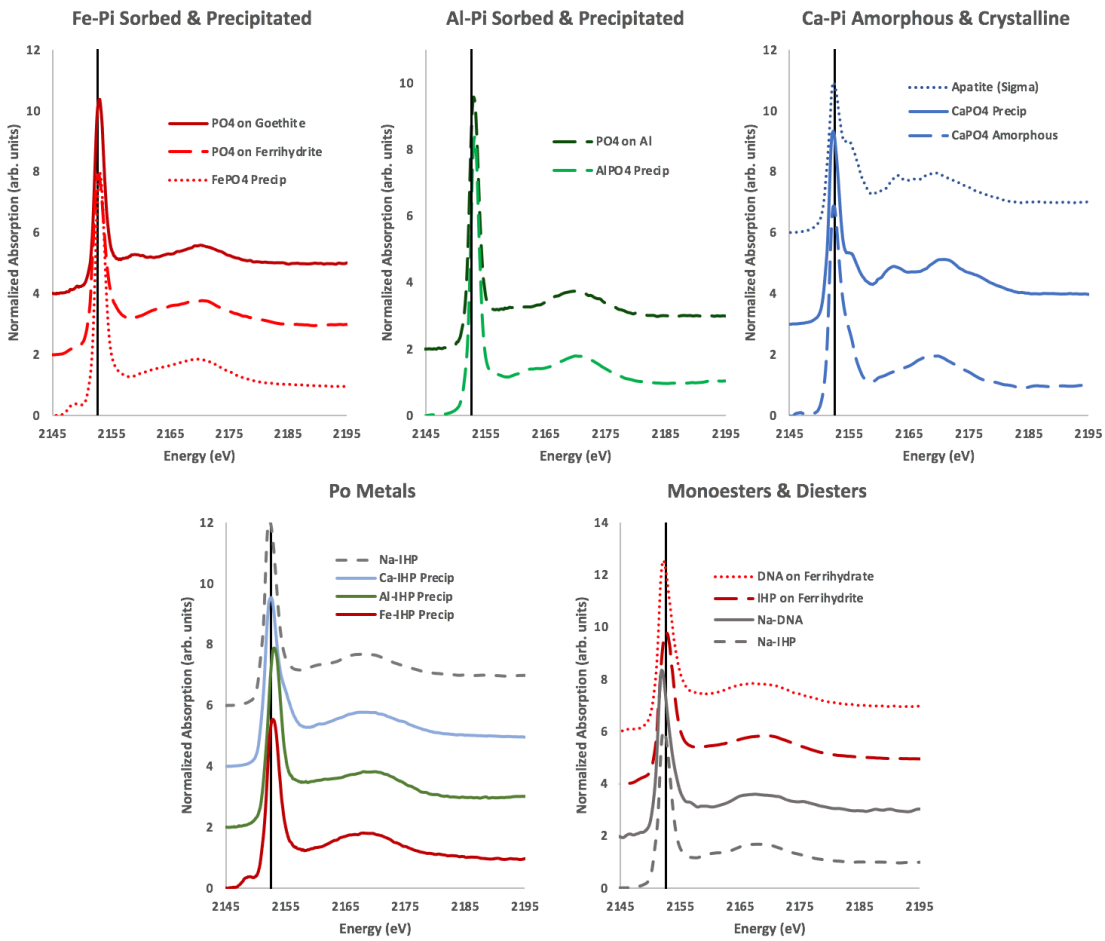

Figure 2-S5. Comparison of a subset of sorbed and precipitated inorganic and organic reference compound spectra used in P K-edge XANES linear combination fits. Distinct pre- and post-edge features are demonstrated by the counter-cation.

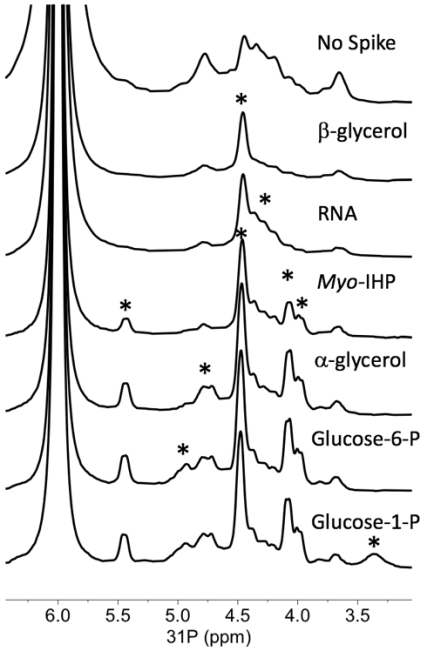

Figure 2-S6. Spiking experiment of the monoester region for a ^{31}P solution NMR spectrum from a CZO SH A horizon sample. The sample was sequentially spiked, and a spectra recorded, with β-glycerophosphate (β-glycerol), ribonucleic acid (RNA), *myo*-insositol phosphate (*myo*-IHP; i.e., phytate), α-glycerophosphate (α-glycerol), glucose-6-phosphate (glucose-6-P), and glucose-1-phosphate (glucose-1-P). The chemical shift(s) associated with the spiked compound for each spectrum is/are indicated by an asterisk.

2.10.6 References

Beauchemin S, Hesterberg D, Chou J, et al. (2003) Speciation of Phosphorus in Phosphorus-Enriched Agricultural Soils Using X-Ray Absorption Near-Edge Structure Spectroscopy and Chemical Fractionation. Journal of Environment Quality 32:1809-1819.

Eynard AD, Del Campillo MC, Barrón V, Torrent J (1992) Use of vivianite ($Fe_3(PO_4)_2 \cdot 8H_2O$) to prevent iron chlorosis in calcareous soils. Fertilizer Research 31:61-67.

He Z, Honeycutt CW, Zhang T, et al. (2007) Distinction of Metal Species of Phytate by Solid-State Spectroscopic Techniques. Soil Science Society of America Journal 71:940-943.

Hesterberg D, McNulty I, Thieme J (2017) Speciation of Soil Phosphorus Assessed by XANES Spectroscopy at Different Spatial Scales. Journal of Environmental Quality 46:1190-1197.

Hsu, PH (1975) Precipitation of phosphate from solution using aluminum salt. Water Research 9:1155-1161.

Ingall ED, et al. (2011) Phosphorus K-edge XANES spectroscopy of mineral standards. Journal of Synchrotron Radiation, 18:189-197.

Kizewski F, Liu Y-T, Morris A, Hesterberg D (2011) Spectroscopic Approaches for Phosphorus Speciation in Soils and Other Environmental Systems. Journal of Environmental Quality 40:751-766.

O'Day PA, Nwosu UG, Barnes ME, et al. (2020) Phosphorus Speciation in Atmospherically Deposited Particulate Matter and Implications for Terrestrial Ecosystem Productivity. Environmental Science & Technology 54:4984-4994.

Prietzel J, Harrington G, Häusler W, Heister K, Werner F, Klysubun W (2016) Reference spectra of important adsorbed organic and inorganic phosphate binding forms for soil P speciation using synchrotron-based K-edge XANES spectroscopy. Journal of Synchrotron Radiation 23:532-544.

Sato S, Solomon D, Hyland C, et al. (2005) Phosphorus Speciation in Manure and Manure-Amended Soils Using XANES Spectroscopy. Environmental Science & Technology 39:7485-7491.

Schwertmann U, Cornell RM (2000) Iron Oxides in the Laboratory: Preparation and Characterization, Second Edition. Wiley-VCH, New York.

3 Precipitation Controls Ecosystem C:N:P Stoichiometry Across Soil Horizons in Temperate Drylands

3.1 Abstract

Carbon:nitrogen:phosphorus (C:N:P) stoichiometric ratios are useful indicators for understanding how nutrient limitation is altered along environmental gradients. Terrestrial ecosystems have the potential to store C within soil, microbial, and plant biomass, however the availability of N and P can constrain net ecosystem production, thereby limiting plant productivity and potential C sequestration. How essential nutrient availability limits terrestrial C sequestration is one of the most uncertain factors in global C cycle and climate model projections, in particular under changing climate scenarios. In order to understand how nutrient biogeochemistry and limitation are altered by climate, we investigated ecosystem C, N, and P concentrations and their ratios along semiarid and Mediterranean elevation gradients. Overall, precipitation was a more important covariate with nutrient stoichiometry compared to temperature in these water-limited ecosystems. We found soil C:N:P increased with precipitation, which led to a shift from microbial N and P limitation in drier sites to C and N limitation in wetter locations. Fine roots followed microbial N:P ratios, but grass, forb, and evergreen aboveground foliage indicated greater P limitation in the wetter Mediterranean sites. Potential extracellular enzyme activity of C, N, and P acquiring enzymes were largely unchanged along the gradient, indicating a complex relationship among enzyme production, stabilization, and efficiency. Microbial, root, and enzyme stoichiometric ratios were unchanged across different master soil horizons within a given soil profile, demonstrating homeostasis of these ecosystem components with depth even though soil total nutrient C:N:P decreased. Although a few stoichiometric relationships of subsoil horizons were significantly different than surficial soil, nutrient ratios tended to be coupled across master horizons. Overall, our study demonstrates how nutrient biogeochemistry is altered by a changing climate across multiple ecosystem components, broadening our understanding of ecosystem resilience and potential C sequestration in a changing world.

3.2 Introduction

Understanding nutrient limitation is critical for predicting how terrestrial ecosystems will respond to a changing climate. Nitrogen (N) and phosphorus (P) are essential nutrients for organism structure and function (Elser et al 1996) and are therefore critical to supporting terrestrial ecosystem development (Vitousek et al. 2010). High nutrient availability increases net ecosystem production and also promotes greater carbon (C) use efficiency, resulting in more C stored in biomass and soil than is lost through respiration (Fernández-Martínez et al. 2014). Although nutrient limitation constrains net primary production by up to 25%, it remains one of the most uncertain factors to global climate model projections (Hungate et al. 2003; Wieder et al. 2015).

Ecosystem functions, such as primary production, respiration, and decomposition, couples C, N, and P due to constraints on the relative proportions of these elements needed for metabolic reactions and synthesis of essential compounds (Sterner and Elser 2002; Finzi et al. 2011). However, P can be independently mineralized because organic P is not bonded directly to C like N, potentially decoupling it from C and N cycling (McGill and Cole 1981). Additionally, available P is derived primarily from mineral weathering in the early stages of ecosystem development and is regulated more by organic matter turnover in more weathered soils (Walker and Syers 1976). Because N and P biogeochemistry are under dissimilar controls (i.e., biological N fixation, P ecosystem retention via sorption; Wood et al. 1984); they may respond differently to increasing atmospheric CO_2 and global change (Vitousek et al. 2008, 2010; Yuan and Chen 2015). In addition, alteration to the biogeochemistry of one element, almost always alters the cycling of another (Finzi et al., 2011). For example, increased P availability can increase biological N_2 fixation (Griffith, 1978; Matzek and Vitousek 2003) and mineralization rates of C and N (Munevar and Wollum 1977; Ross and Bridger 1978). Alternatively, phosphatase enzymes, which mobilize ester-bonded P forms for biological assimilation, require N for synthesis (Olander and Vitousek 2000), so increased N input may enhance phosphatase activity (Marklein and Houlton 2011; Margalef et al. 2017). Therefore, how nutrient concentrations, and their relative proportions, respond under a changing climate will determine organismal responses (Finzi et al. 2011).

Climate exerts a strong influence on soil development and nutrient dynamics (Jenny 1941). Pedogenesis is expected to proceed at a higher rate in wetter locations (where other soil forming factors are held constant), leading to depletion of primary minerals and modification of soil surface chemistry (Walker and Syers 1976). In Hawaiian volcanic soils forming in areas where precipitation exceeds evapotranspiration, soluble base cations (Ca, Mg, Na, and K) are lost from the system and pH and effective cation exchange capacity are lower compared to arid sites (Chadwick et al. 2003). Climate impacts nutrients directly by increasing N and P leaching losses and surficial water erosion (Austin and Vitousek 1998). High leaching and erosion losses of P and the formation of secondary minerals can cause P to be lost from the system or be held in less bioavailable forms (Feng et al. 2016). However, vegetation, which usually co-varies with climate, can help retain nutrients that would otherwise be lost from leaching or erosion (Porder and Chadwick 2009). Climate also has a indirect influence on litter decomposition by affecting vegetation composition, thereby influencing nutrient

chemistry of the litter (Aerts and Chapin 1999). A global synthesis of studies in drylands found aridity negatively affected the concentration of soil organic C and N, but increased the concentration of inorganic P, causing P to become decoupled from C and N (Delgado-Baquerizo et al. 2013). In contrast, a meta-analysis of drought manipulation experiments found extractable N (sum of ammonium and nitrate) increased under drought conditions, but extractable P significantly decreased (He and Dijkstra 2014). Noticeably, C, N, and P may respond to changes in climate in contrasting ways depending on interactions between nutrients, vegetation composition, and soil development.

Although studies usually investigate surficial soil, the distribution of nutrients, roots, microbial biomass, and enzyme activity are impacted by depth, and deeper subsurface horizons likely play a critical role in supporting ecosystem development (Eilers et al. 2012; Yost and Hartemink 2020). Organic matter decreases with depth because of higher inputs of plant detritus near the surface, however 60% of C is stored in soil below 30 cm (Jobbágy and Jackson 2000, 2001). Additionally, P chemical speciation, and therefore bioavailability, is altered by depth (Ippolito et al. 2010; Prietzel et al. 2016). Rooting depths also vary greatly by biome where temperate grasslands have ~80% of roots in the top 30 cm compared to coniferous forests which only have about 50% (Jackson et al. 1996). Rooting depth also impacts microbial biomass distribution (Xu et al. 2012). Microbial biomass have been found to exponentially decrease with depth and the community composition is altered (Eilers et al. 2012; Stone et al. 2014; Dove et al. 2020). This, in turn, causes hydrolytic enzyme activity to decrease (Schnecker et al. 2015). However, deeper microbes have important ecosystem functions by influencing soil formation because they are closer to residual parent material (Buss et al. 2005), impacting long-term C sequestration due to longer turnover times (Rumpel and Kögel-Knabner; Fierer et al. 2005), and scavenging for limiting nutrients that can then be transferred to vegetation (i.e., mycorrhizae; George et al. 2008). Therefore, characterizing nutrient dynamics in only surficial soil may lead to an incomplete assessment of important nutrient dynamics that occur in deeper soil, and these nutrients may serve as a reservoir to help ecosystems adapt to a changing climate.

Stoichiometry, or the relative quantities of chemical elements, is a powerful tool to investigate how the molar C:N:P ratio of living organisms affect and are affect by the surrounding environment (Redfield 1958; Sterner and Elser 2002). Stoichiometric ratios can serve as a proxy for limiting nutrient(s) and as an indicator of ecosystem function (Koerselman and Meuleman 1996; Güsewell et al. 2003; Zechmeister-Boltenstern et al. 2015). Hence, there has been a growing appreciation for applying stoichiometry concepts to terrestrial ecosystems (Elser et al. 2000; Sterner and Elser 2002), particularly in global synthesis papers, to infer nutrient limitation to vegetation (Koerselman and Meuleman 1996; Hedin 2004; Reich and Oleksyn 2004; McGroddy et al. 2004) and microbial biomass (Cleveland and Liptzin 2007). Stochiometric ratios impact numerous ecological processes, including N_2 fixation (Dynarski and Houlton 2018), litter decomposition (Güsewell and Gessner 2009), soil enzyme production (Sinsabaugh et al. 2008) and microbial nutrient immobilization (Manzoni et al. 2010), and microbial and vegetation composition and diversity (Roem and Berendse 2000; Güsewell et al. 2004; Güsewell et al. 2005; Zechmeister-Boltenstern et al. 2015). Ultimately, stoichiometric ratios influence ecosystem functions including C storage and nutrient cycling (Zechmeister-Boltenstern et

al. 2015). Therefore, ecological stoichiometry integrates key processes that regulate nutrient biogeochemistry, providing a conceptual framework for evaluating nutrient dynamics (Sterner and Elser 2002; Spohn 2016).

Recently, the application of stoichiometry has been used to study the potential impacts of climate change on ecosystem compartments. Soil N:P increased along a forest precipitation gradient in China, largely from decreased P, and ratios were not impacted by temperature (Chen et al 2016). This contrasts with soil N:P in arid sites where increasing precipitation resulted in lower N:P from increased P concentration (Delgado-Baquerizo et al. 2013). Although vegetation nutrient concentrations may reflect soil nutrient status (Ordoñez et al. 2009; An et al. 2019), this is not always the case along environmental gradients. For example, P in vegetation have been found to become de-coupled from soil nutrient stocks along a semiarid grassland altitudinal gradient in China (Luo et al. 2015) but not along a temperate grassland elevational gradient in New Zealand (Craine and Lee 2003). A global analysis found foliar C:nutrient ratios increased under experimentally increased CO_2, and ratios may increase further under drought conditions in semiarid regions (Sardans et al. 2012). Along a humid elevational gradient, microbial C:N:P have been found to be homeostatic (Nottingham et al. 2015), whereas in an arid climate elevational gradient, C:P and N:P demonstrated quadratic relationships (He et al. 2016). Across ecosystems globally, soil enzyme C:P decreased with increasing mean annual air temperature (MAT) and mean annual precipitation (MAP), demonstrating declines in P availability in relation to C as weathering intensity increased, but C:N was largely unaffected (Sinsabaugh et al. 2008). Clearly, nutrient stoichiometry can be a valuable tool for exploring how net ecosystem production, and therefore C sequestration, might respond to global change (Elser et al. 2007).

Although climatic impacts on stoichiometry has received considerable attention (Sterner and Elser 2002; McGroddy et al. 2004; Cleveland and Liptzin 2007; Elser et al. 2010), most previous studies focus on only a couple of ecosystem components. For instance, studies have investigated total elemental ratios in soil and aboveground vegetation (Sardans et al. 2006, 2016; Fisher et al. 2013; Gerdol et al. 2019; Zhang et al. 2019; Gong et al. 2020), soil and enzymes (Xu et al. 2017; Xiao et al. 2018), above- and belowground vegetation (Xu et al. 2015; Yu et al. 2017), or soil, microbes, and enzymes (Nottingham et al. 2015; Cui et al. 2018; but see He et al. 2016 and Delgado-Baquerizo et al. 2018). Overall, previous studies typically focus on aboveground vegetation or microbial biomass rather than measuring nutrient stoichiometric ratios in multiple ecosystem compartments, which may omit important feedbacks and interactions that can help elucidate nutrient partitioning and competitive dynamics between above- and below-ground processes (but see Dijkstra et al. 2012; Delgado-Baquerizo et al. 2018). Additionally, nutrient cycling research has traditionally focused on aboveground tissue pools and fluxes over roots (Attiwill and Adams 1993). Foliar and fine root nutrient concentrations are thought to co-vary across a range of biomes including forests (Newman and Hart 2006; Tang et al. 2018), shrublands (Tang et al. 2018) and grasslands (Craine and Lee 2003; Luo et al. 2015; Tang et al. 2018). However, it is largely unknown how nutrient allocation in above- and below-round tissue may be impacted by environmental gradients. Previous research has found microbial biomass and shallow rooted vegetation nutrient stoichiometry are impacted to a greater degree from increasing

aridity than deep rooted tree species (Delgado-Baquerizo et al. 2018). There has recently been a call to include P, with specific inclusion of C:N:P stoichiometric relationships, to Earth System Models because P can constrain C sequestration (Reed et al. 2015), but most stoichiometry-based ecosystem studies include C:N or N:P, with relatively fewer including C:P.

Increasing drought is predicted under climate change scenarios (Dai 2012) and the amount of land area classified as a dryland is expected to increase (Feng and Fu 2013). Arid and Mediterranean systems are an excellent model system to study the impact of precipitation on C, N, and P biogeochemical cycling because they are primarily water limited and therefore are likely sensitive ecosystems to changing precipitation regimes (Austin et al. 2004; Delgado-Baquerizo et al. 2013). Additionally, precipitation has been found to exert a stronger control than temperature over vegetation traits associated with growth and resource conservation (Ordoñez et al. 2009). Evaluating stoichiometry across large gradients can therefore improve our understanding of nutrient cycling and limitation in terrestrial ecosystems (Sterner and Elser 2002).

Therefore, the overall objective of our study is to use a space for time substitution approach along elevational gradients in temperate drylands with low-P containing parent material. We determined: (1) how climate impacts soil, microbial biomass, enzyme activity, fine root, and foliar C:N:P stoichiometry by altering C, N, or P concentrations; (2) if the impact of climate on subsurface soil horizon stoichiometry is decoupled from surficial soil; (3) how stoichiometric ratios are altered with depth into the soil profile; and (4) how ecosystem stoichiometry in these dryland ecosystems compare to global averages. We hypothesize that increases in MAP will cause pH to decrease and a shift in the dominate vegetation will increase plant detrital inputs to soil. These changes will increase soil C:N:P. Previous research at these sites identified notable transitions in P speciation from Ca-P to Fe- and Al-P with increasing MAP, which will likely impact P availability as Al-P is not readily available in the pH range of these soils (Chapter 2). The decrease in the relative proportion of P and reduced bioavailability with increased MAP will be reflected in ecosystem stoichiometry where β-glucosidase (BG):N-acetylglucosaminidase (NAG):acid phosphatase (AP) will decrease as microbial, root, and foliage (across all functional groups) C:N:P increase indicating that P becomes more limiting relative to C and N. We also hypothesize the effects of precipitation on stoichiometry will be consistent across soil genetic horizons because P speciation was largely unchanged with climate-induced weathering across master soil horizons at these sites (Chapter 2).

3.3 Methods

3.3.1 Study Sites

Precipitation, temperature, and vegetation vary along elevational gradients, or bioclimatic sequences, which provides a space-for-time substitution approach to research climate change effects (Tate 1992; Egli et al. 2003). The White Mountain Elevational Transect (WM) is a semiarid climate along the west side of White-Inyo Range. The WM began forming ~163 Ma with an intrusion developing ~70 million years later (Ernst and

Rumble 2003; Ferre et al. 2012). The Southern Sierra Critical Zone Observatory (CZO; Table 1) is a Mediterranean-type climate that traverses the west side of the Sierra Nevada. Sites that comprise the CZO gradient formed 104 to 115 Ma (Bateman and Busacca 1982; Lockwood and Bateman 1976; Bateman and Wones 1972), with the exception of SH (highest elevation site) that was glaciated during the last glacial maximum (Clark and Gillespie 1997). Soils from both elevational gradients are formed from granitic parent. Previous relevant studies conducted in the CZO and WM have established relationships between bedrock mineralogy and vegetation (Hahm et al. 2014) along with climate and soil physio-chemical conditions (Frisbie 2014; Jenny et al. 1949; Dahlgren et al. 1997; Dixon et al. 2009; Moreland 2020), setting a perfect stage for climate change research on nutrient dynamics.

3.3.2 Climate Parameters

Climate data were obtained from PRISM for calendar years 1981 through 2018 based on the latitude and longitude of each site with a resolution of ~4 km (Daly et al. 2000). Monthly total precipitation (mm) and mean temperature (C) was download and aggregated to determine mean annual precipitation (MAP) and mean annual air temperature (MAT) over this period (PRISM Climate Group, Oregon State University, http://prism.oregonstate.edu, created 4 Feb 2004; accessed May 2020).

3.3.3 Sample Collection

The locations of four soil pits at each site were determined to be representative of the major topographic features of the landscape, and therefore were not selected randomly. Soil was collected based on master and subordinate genetic horizons. Sampling tools were sanitized with 10% bleach followed by 70% ethanol prior to collecting samples for microbial biomass and enzyme activity, and these samples were placed on dry ice for transport back to the laboratory. Dominate species of tree and understory vegetation were also sampled (Table 3-S1). For tree species, foliage was collected from the outer sunlit portion of the upper third crowns using pole clippers or by climbing (southern aspect).

3.3.4 Laboratory Analyses

Upon returning to the lab, soil samples were either air dried and sieved (< 2 mm used for all analyses) for pH and total elemental concentrations or were immediately frozen for microbial biomass elemental concentrations and enzyme activity analyses. All results are reported on an oven-dry basis using gravimetric water content conversion (oven dried at 105 °C until constant mass). Soil pH (Accumet Basic, Model AB15, Fisher Scientific with an Ag/AgCl electrode) was measured in a 1:2 soil:solution slurry in deionized water and 0.01M $CaCl_2$ (Sparks et al. 1996). Soil particle size analysis was measured on oven-dried and sieved soil using the hydrometer method (Gee and Bauder 1986).

Fine roots (< 2 mm) were separated from mineral soil using a hydropneumatics elutriator (Scienceware Bel-Art products, Pequannock, NJ, USA) with stacked 2-mm and 500-μm sieves (Hart et al. 2005). Dead roots or mycorrhizae were not separated from live roots and there was no effort to separate roots by vegetation functional groups. Non-root organic material was removed by hand using tweezers after air drying. Aboveground foliage was separated to include only the current year's growth of photosynthetic material from mature and healthy tissue. Foliage and root samples were ground using a Wiley mill (180 μm sieve) or by mortar and pestle when sample size was too small, and then oven dried (65 °C until constant mass) prior to analyses.

3.3.4.1 Soil Total Elemental Concentration

Total soil P concentration of air dried and sieved (<2 mm) soil samples were determined by lithium metaborate fusion (Robertson et al. 1999) and measured by inductively-coupled plasma optical-emission spectrometry (ICP-OES; Perkin-Elmer Optima 5300 DV; University of California, Merced Environmental Analytical Laboratory). Organic C and total N were determined on ground soil samples (CZO were ball milled for 3.5 minutes and WM samples were crushed using an agate mortar and pestle). Carbon and N were obtained for the CZO sites from Moreland (2020). Carbonates were removed prior to analyses using hydrochloric acid fumigation from the WM sites (Harris et al., 2001). Organic C and total N were measured on an elemental analyzer (Costech Analytical ECS 4010 Elemental Analyzer, Costech Analytical Technologies, Inc., Valencia, CA).

3.3.4.2 Microbial Biomass

Carbon, N, and P within the microbial biomass were analyzed by chloroform fumigation-extraction (Brookes et al., 1982; Brookes et al., 1985, Vance et al., 1987, Haubensak et al., 2002) on field moist samples (previously frozen and then thawed) that were sieved <2 mm. Five equal sample sizes were weighed for C and N fumigation, P fumigation, C and N non-fumigated, P non-fumigated, and P non-fumigated plus spike (A horizon: 5 g, B horizon: 5-25 g; C horizon: 10-25 g). The non-fumigated P spike had 250 μg P added to correct for fixation during the extraction. The non-fumigated samples were immediately shaken for 60 minutes with 0.5 M K_2SO_4 for C and N, or 30 minutes with 0.5 M $NaHCO_3$ for P in a 1:3 soil to solution ratio and filtered (Whatman No. 42). Fumigated samples were incubated in a chloroform-filled desiccator for seven days and then also extracted with K_2SO_4 or $NaHCO_3$ after removal of $CHCl_3$ with repeated evacuations. Extracts were analyzed on a total organic C and total N analyzer (Shimadzu TOC-Vcsh with TNM-1 Total Nitrogen Measuring Unit, Kyoto, Japan) and Lachat Quickchem 8500 Flow Injection Analyzer (Method No. 12-115-01-1-Q) for ortho-phosphate. The difference between concentrations in the chloroform fumigated and non-fumigated extracts is considered the chloroform-labile C, N, and P, after correction for P fixation using the spiked replicate. Chloroform-labile pools were converted to microbial C, N, and P with extraction efficiency factors (k_{eC} of 0.45, k_{eN} of 0.54, k_{eP} of 0.4; Beck et al., 1997, Brookes et al., 1982; Brookes et al., 1985). Microbial biomass can be one to

two orders of magnitude lower in deep horizons compared to surficial soil (Fierer et al. 2003; Dove et al. 2020), therefore low microbial biomass contents in some subsurface horizons resulted in more C, N, or P content in the non-fumigated extract. In these cases, the samples were removed prior to statistical analyses.

3.3.4.3 Soil Enzyme Activity

Potential extracellular enzyme activity of β-glucosidase (BG), N-acetylglucosaminidase (NAG), and acid phosphatase (AP) were measured fluorometrically following Bell et al. (2013). Briefly, 2.75 g of field moist samples were mixed with 91 mL of 50 mM sodium acetate buffer (pH = 5.5). The soil slurry (800 μL) was then added to 96-well plates with 200 μL of a 100 μM 4-methylumbelliferone (MUB)-linked substrate (BG: 4-MUB β-D-glucopyranoside; NAG: 4-MUB N-acetyl-β-D-glucosaminide, AP: 4-MUB phosphate), incubated for 3 hours (20 °C), centrifuged (3 min. at 3000 rpm), and the supernatant was transferred to black, flat-well plates. Fluorescence was measured using an excitation wavelength of 365 nm and an emission wavelength of 450 nm on a Tecan M200 Pro (Tecan Group, Männedorf, Switzerland). Potential extracellular enzymes can be used to determine nutrient demand because they mediate nutrient acquisition for soil microorganisms (Olander and Vitousek 2000). Increased BG activity indicates greater C demand, NAG greater N demand, and AP greater P demand. Therefore, BG:NAG, BG:AP, and NAG:AP were used as proxies for C:N, C:P, and N:P relative nutrient demand (i.e., high enzyme N:P indicates N is relatively more limiting), respectively. In addition to presenting extracellular enzyme activities per unit soil oven-dry mass, they were also normalized to microbial biomass C. Expressing potential enzyme activity on a per soil basis represents ecosystem-level properties, while per microbial biomass C reflects a microbial community-level property (Dove et al. 2020). In addition, microbial biomass C normalization allows comparisons of microbial nutrient status across drastically different ecosystems (Boerner et al. 2005).

3.3.4.4 Foliage and Root Total Elemental Concentration

Foliage samples were separated based on funcational groups (grass, forbs, woody shrubs, deciduous trees, and evergreen trees). Total N and P within above- and below-ground tissue were measured by a Kjeldahl digestion (Parkinson and Allen 1975). Briefly, 0.05 g of oven dried samples were mixed with 0.5 g of catalyst (89.7% K_2SO_4 and 10.3% $CuSO_4$) and 3.5 mL H_2SO_4. Samples were heated on a digestion block to 350 C for 5 hours, cooled, and diluted to a final volume of 50 mL. In instances where sample mass was smaller than 0.5 g (root samples were ~8 mg), the relative ratios of sample:catalyst:H_2SO_4 were kept consistent and they were diluted less to keep acid:DI ratio the same. Solutions were allowed to settle overnight, then an aliquot was removed and refrigerated until analyses (up to 1 month). Nitrogen and P concentrations were determined colormetrically using a Lachat AE Flow Injection Auto Analyzer (Methods 13-107-06-2-D and 13-115-01-1-B, Lachat Instruments, Inc., Milwaukee, WI, USA).

3.3.5 Data Analyses

All statistical tests were conducted using R (version 3.4.2; R Development Core Team, 2013), except the path analysis was ran using the Amos package in SPSS software (version 21, Chicago, IL, USA). All concentrations and nutrient ratios were log transformed (soil N concentration was log +1 due to zero values) prior to analyses and the geometric mean with standard errors are presented, as has been recently recommended (Isles 2020).

Carbon:N:P ratios were calculated on a molar basis for all sample types. Changes in concentration or stoichiometry of soil, fine roots, microbial biomass, and enzyme activity with MAP and depth into the mineral soil were analyzed using separate mixed effect models. Models were ran with the lme4 package in R (Bates et al. 2012), and were fit by maximum likelihood with the Laplace Approximation. Marginal (only fixed effects considered) adjusted R^2 values were calculated following Nakagawa et al. (2013) using the MuMIn package (Barton and Barton 2019). Mean annual precipitation, master soil horizon, and their interaction were included as independent variables (fixed effects) and the soil or plant measure as the dependent variable. A random effect was included to account for the dependence of sampling within a single soil pit. Linear mixed effect model regressions, using the slope and intercept of the interaction term from models, are presented only if a statistically significant relationship was identified ($p < 0.05$). When the interaction between B or C horizons with MAP was significantly different than A horizons in the mixed effect model, a linear model post hoc test was performed to investigate if the individual horizon is correlated to MAP. The relationships of concentrations and stoichiometric ratios between master soil horizons (i.e., depth) are presented separately. When B or C horizons were significantly different ($p < 0.05$) from A horizons (0-coded group), a Tukey's post hoc test was performed to evaluate whether means of all master soil horizons were significantly different from each other using the lsmeans function within the emmeans R package (Lenth et al. 2018). The impact of MAP on aboveground foliage nutrient concentrations and ratios were investigated using linear regression models because there was no need to include a random effect since samples were spatially independent. Separate models were conducted for individual functional groups and only significant relationships are included in figures.

Structural equation modeling was performed to analyze hypothesized pathways that may explain how climate (MAP and MAT) influences ecosystem N:P stoichiometry (soil, microbial biomass, enzyme activity, fine roots, and foliage) directly or indirectly through changes in soil conditions (pH, clay, and soil organic carbon; Zechmeister-Boltenstern et al. 2015). Foliage stoichiometry is the site level geometric mean of evergreen, shrub, or forb functional groups (shrub and forb results are reported in Figures 3-S1 and 3-S2) because vegetation was not co-located with the other sample collection. These functional groups were selected because they were each found at most sites. In the model, MAP and MAT can directly impact the stoichiometry of the ecosystem components and can impact stoichiometry by processes such as soil acidification (pH), formation of secondary minerals (clay percent), and enhance or inhibit soil organic matter decomposition (soil organic carbon; SOC). These soil conditions may then alter total nutrients in the soil (soil N:P) which dictates a latent variable of available N:P and the

activity of enzymes (NAG:AP). Available P can be taken up by microbes (microbial N:P), which further influence enzyme stoichiometry, or taken up by roots (root N:P) and allocated to aboveground foliage (foliage N:P). Separate models were conducted for A, B, or all (A + B + C) master soil horizons, along with the three functional groups (9 total models), to assess if the relative contribution of climate changes with depth. The sample size of C horizons was too low to conduct an individual model.

3.4 Results

3.4.1 Ecosystem C, N, and P Concentrations and Stoichiometry with MAP

Ecosystem nutrients and their relative proportions were impacted by increasing MAP, but not always in the same direction (Figures 3-1 and 3-2, Tables 3-2 and 3-S2). Soil N concentration was unchanged by MAP, but C increased in A and B horizons and P decreased in B and C horizons with increasing MAP, resulting in soil to become more P-limited (higher C:P and N:P) across all horizons (Figure 3-1; Table 3-S2). The C:N ratio was unchanged across the entire precipitation gradient. This was because trends within the WM and CZO elevational gradients were contradictory where C:N decreased with MAP for all horizons at the WM but increased at the CZO with increasing MAP (Figure 3-2, Table 3-2).

Decreased C concentration and increased P concentration caused the microbial biomass to become more C-limited relative to N and P with increasing MAP in all horizons (Figures 3-1 and 3-2, Tables 3-2 and 3-S2). The N:P ratio decreased with MAP, indicating increasingly more N-limitation relative to P. B horizons had a significantly different relationship than A horizons with MAP, but both horizons changed in the same direction (i.e., negative).

The activities of BG and NAG per mass of soil were unaffected by MAP in A and B horizons, but both significantly decreased in C horizons (Figure 3-1, Table 3-S2). Acid phosphatase also did not change with MAP in A horizons, but did decrease in B and C horizons. This caused potential extracellular enzyme activity stoichiometries to be largely unchanged in all horizons along the precipitation gradient with the exception of increased BG:AP in B horizons (Figure 3-2; Table 3-2). The increased C acquiring enzyme activity in wetter locations indicates more microbial C limitation.

Fine root C concentration increased in all horizons, whereas N and P decreased with MAP (Figure 3-1, Table 3-S2), resulting in higher C:nutrient ratios (Figure 3-2, Table 3-2). For C:N, B horizons had a greater rate of change (i.e., slope) with precipitation than A horizons. A horizon C:P was unchanged by precipitation, but B and C horizons became more P limited relative to C (higher C:P). Roots became more N limited relative to P with a greater slope in A horizons than B. Although the rate of change (i.e., the slope) with increasing precipitation was different between fine roots in some horizons, the direction of change was consistent across all horizons.

Carbon concentration increased with precipitation in all aboveground vegetation functional groups within a narrow range relative to other nutrients (Figure 3-3, Table 3-S3). Nitrogen concentration also increased in grass, forbs, and deciduous trees, but had a greater rate of change than C with increasing MAP. This resulted in grass, forb, and

deciduous trees becoming more C limited relative N as precipitation increased (Figure 3-3, Table 3-3). In contrast, N concentration decreased in shrubs causing greater N-limitation relative to C (higher C:N) with increasing MAP. Similar to C and N concentration, P concentration also increased in deciduous trees and forbs, however evergreen tree and shrub P concentrations decreased. Ultimately, deciduous trees and forbs were more limited by P than C in drier locations, but evergreen trees and shrubs were more P-limited in wetter locations. The decreased P concentration with MAP in evergreen trees and shrubs also resulted in increased N:P, suggesting that P became more limiting relative to N in these functional groups. Additionally, forbs N:P ratios increased with increasing MAP, but this was driven by the greater increase in N with MAP relative to the increase in P.

3.4.2 Direct and Indirect Effects of MAP and MAT

Precipitation had positive direct effects on foliage and soil enzyme activity N:P and direct negative effects on microbial biomass and root stoichiometry across all horizons (Figures 3-4 and 3-5). Precipitation indirectly influenced ecosystem N:P through a negative effect on pH and positive effect on SOC. This, in turn, influenced soil N:P where the ratio had a negative relationship with pH and positive relationship with SOC. The combined direct and indirect effects of precipitation were positive for soil ($\beta = 0.31$), soil enzyme activity ($\beta = 0.29$), and foliage ($\beta = 0.48$). In contrast, the total effect of MAP was negative for microbial biomass ($\beta = -0.36$) and root ($\beta = -0.48$). In the A horizon model, MAP also had a direct negative effect on soil N:P, the influence on microbial biomass and root N:P became more negative, and soil enzymes were no longer directly impacted. Precipitation no longer directly influenced microbial biomass nutrient stoichiometry in the C horizon model, but the other relationships with measured variables were similar.

In contrast to MAP, temperature had a positive direct effect on root N:P ratios and negatively impacted SOC, which influenced soil N:P. Temperature also had a positive direct effect on foliage N:P, similar to MAP. The combined direct and indirect effects of temperature were positive for foliage ($\beta = 0.72$) and roots ($\beta = 0.14$), but was negative for soil ($\beta = -0.15$), soil enzyme activity ($\beta = -0.02$), and microbial biomass ($\beta = -0.11$). Relationships were similar to the all horizon model after splitting into the individual horizons, but MAT also had a direct negative effect on soil N:P in both A and B only models. Additionally, there was a negative direct effect of MAT on soil enzyme stoichiometry in the B horizon model but not for the A horizon model. Overall, MAP tended to have a more direct and indirect influence on ecosystem N:P compared to MAT, with the exception of foliage. Ecosystem stoichiometry was also directly impacted more by climate than the stoichiometry of other ecosystem components.

3.4.3 C, N, and P Concentrations and Stoichiometry with Depth

Master soil horizon had minimal impact on ecosystem stoichiometry across all sites. Soil C, N, and P concentrations decreased with depth (Figure 3-6, Table 3-S2). However, the P concentration in C horizons was similar to P concentration in the overly

B horizons. Ultimately, C:N was unchanged but C:P and N:P decreased with depth, indicating that C and N became more limiting relative to P (Figure 3-7, Table 3-2). Although microbial biomass C and N also decreased with depth, stoichiometric relationships were unchanged. Potential soil enzyme activity and fine root concentrations and stoichiometries were also not affected by master soil horizon.

3.4.4 Comparison to Terrestrial Global Averages

Compared to terrestrial global averages, soil A horizons indicated more N limitation (Figure 3-8). Carbon:N geometric means were > 19 for sites with woody plant species. Values below the global soil averages were found at grassland dominated sites (SJER and BAR) with C:N < 14.3 (Cleveland and Liptzin 2007). All sites had N:P ratios below the global average of 13.1 in A horizons (Cleveland and Liptzin 2007), also indicating greater N limitation relative to P. Carbon:P demonstrated greater C limitation with the exception of the highest elevation CZO site (SH).

The microbial biomass had distinct differences in stoichiometric ratios between gradients, however the lowest elevation CZO site (SJER) was often more similar to the semiarid WM sites. The semiarid WM sites had higher C:N, C:P, and N:P ratios than the global averages (Figure 3-8). On the other hand, the Mediterranean CZO sites aligned with the global C:N average of 8.6. Except for SJER, CZO sites were below the global averages of C:P at 59.5 and N:P at 6.9 (Cleveland and Liptzin 2007). Therefore microbes were more P-limited in the semiarid sites compared to global averages, but more C- and N-limited in the Mediterranean locations.

Similar to microbial biomass trends, fine roots in the semiarid WM and low-elevation CZO site (SJER) followed different stoichiometric patterns than the forest-dominated Mediterranean CZO sites. Fine root C:N ratios indicated greater C limitation compared to the global average of 49 at WM sites and SJER (Figure 3-8; Jackson et al. 1997). These sites were also higher than the global N:P ratio of 24, suggesting P is more limiting than N (Jackson et al. 1997). On the other hand, the forested CZO sites demonstrated greater N limitation with fine root C:N ratios higher than the global average and N:P ratios below the global average. Aboveground foliage nutrient ratios in evergreen trees were lower than the temperate coniferous average C:N of 59.5, C:P of 1231.8, and N:P of 21.7 (McGroddy et al. 2004). Foliar C:P and N:P ratios tended to be greater in all CZO sites compared to WM sites. At the Mediterranean CZO, fine roots were above the global average, suggesting relatively more N limitation, but aboveground foliage tended to be more limited by P, although the foliar C:N and C:P global averages were higher than all sites in the current study.

3.5 Discussion

Climate plays an important role in nutrient biogeochemistry in these semiarid and Mediterranean drylands. Overall, we found precipitation regulated ecosystem stoichiometry to a greater extent than temperature across all soil depths as indicated by the larger path coefficients (Figure 3-5). This was further supported by relationships in mixed effect models (MAT models not shown because lack of significance). Although

global stoichiometric patterns are often explained better by temperature than precipitation (i.e., Reich and Oleksyn 2004; Li et al. 2014), precipitation likely controls soil weathering, organic matter turnover, and desorption/dissolution reactions in these water-limited ecosystems (Austin et al. 2004; Delgado-Baquerizo et al. 2013). Transitioning from semiarid to Mediterranean sites brought about greater precipitation and a generally higher MAT, higher plant detrital input, and more acidic conditions (Table 3-1; Figure 3-1). Previous research at these sites found the transition from semiarid to Mediterranean ecosystems results in a decrease of Ca-P, increase of Al- and Fe-P, and proportional decrease of organic P compared to inorganic (Chapter 2). Taken together, climate likely impacted ecosystem stoichiometry by increasing soil organic matter mineralization and nitrification (Melillo et al. 2011) and reduced soil P availability (Dijkstra et al. 2012) to influence microbial, enzyme, fine root, and foliar nutrient stoichiometry (Figure 3-9).

As hypothesized, our study is consistent with previous observations where soil C:N:P increases in wetter locations (Figure 3-2). The volume of water moving through soil drives ecosystem development (Walker and Syers 1976), therefore stoichiometry along precipitation gradients and soil chronosequences tend to be consistent with each other with increasing ecosystem C:P and N:P (Williamson et al. 2005; Tian et al. 2009; Turner et al. 2012a; Izquierdo et al. 2013; Chen et al. 2016, but see Di Palo and Fornara 2017). Because soil nutrient availability has been demonstrated to influence microbial and vegetation nutrient status (Ordoñez et al. 2009; Han et al. 2011; Peng et al. 2017; An et al. 2019), we hypothesized that microbial and vegetation nutrient stoichiometries would co-vary with soil stoichiometries. Although aboveground foliage generally co-varied with soil stoichiometry, microbial biomass N:P had a negative relationship with soil.

Microbial biomass stoichiometric patterns were likely driven by water availability (Delgado-Baquerizo et al. 2018). Overall, microbes transitioned from P limitation in dry sites to C- and N-limitation in wetter locations (Figure 3-2). Microbes may be more N- or P-limited rather than C limited at the drier WM sites because mineralization and chemical reactions are water-limited at these semiarid sites (Lajtha and Bloomer, 1988; Austin et al. 2004). In addition, low soil moisture inhibits diffusivity for microbial uptake (Lambers et al. 2006). Increasing precipitation alleviated these constraints at the Mediterranean sites causing increased microbial biomass P per mass of soil, even though total soil P decreased in most horizons (Figures 3-1). Microbial biomass C:N:P ratios were likely a reflection of resource acquisition strategies where wetter locations (Mediterranean CZO) microbes were investing in N and P uptake (high P, low C:P and N:P ratios) and drier locations (semiarid WM) were investing in C-rich structures to prevent desiccation (low P, high C:P and N:P ratios; Delgado-Baquerizo et al. 2018). Changes in microbial biomass function with changing MAP also helps to account for a negative relationship between microbial biomass C and soil C concentrations (Figure 3-1), which is opposite of previous studies (Zechmeister-Boltenstern et al. 2015).

As precipitation increased, and mineralization and chemical reactions were less constrained by water, the influence of vegetation (i.e., litter chemistry, role of mycorrhizae) likely regulated microbial stoichiometric ratios. It is plausible that nutrient resorption is occurring more readily in the dominate vegetation found at the CZO (Aerts and Chapin 1999). This would lead to litterfall with higher C:nutrient ratios and lignin:N,

causing microbial C and N limitation to the microbial biomass at these sites (McGroddy et al. 2004; Santiago et al 2005; Bui and Henderson 2013). Phosphorus is likely being independently mineralized from C and N, as microbial P increased and N:P decreased with precipitation (McGill and Cole 1981). In addition, microbes can modify their surrounding environment to release mineral bound P, which may also be occurring at the CZO sites (Spohn 2016). We found microbial biomass P was higher at low pH and greater MAP, similar to Sun et al. (2013), which may be in part due to production of acids that decrease pH and assist with solubilizing P. Taken together, microbes were able to more readily immobilize P relative to N in locations with more precipitation, acidic pH, and a dominate vegetation of trees that support ectomycorrhizae.

Although microbial biomass nutrient concentrations and stoichiometry were altered by changing precipitation, enzyme activity was homeostatic and therefore did not reflect changes in nutrient availability (unmeasured latent variable in structural equation model; Figures 3-5, 3-S1, and 3-S2). Previous studies have found microbial biomass stoichiometry to be constrained while enzyme ratios varied based on nutrient availability and acquisition strategies (Turner et al. 2012b; Turner and Wright 2014; Nottingham et al. 2015). However, soil enzymes can become stabilized through association with clay minerals or organic matter to persist over long periods of time with reduced activity (Burns et al. 2013; Dove et al. 2020). The percentage of clay decreased with increasing precipitation (Table 3-1; $p < 0.05$; statistics not shown) likely from differences in parent material between the two gradients or impact of atmospheric dust deposition (Table 3-1; Chapter 2). Therefore, measured enzyme activity may reflect stabilized and less active enzymes at the WM, thereby contributing to microbial N and P limitation at these sites. Clay stabilization was likely exacerbated in B and C horizons, that led to significant decreases in enzyme activity with increased precipitation in those horizons (Figure 3-1). Plant phosphatases have been found to be more responsive to changing resource availability than microbial phosphatases (Marklein and Houlton 2011); therefore, vegetation, and their mycorrhizae symbionts, may be producing more enzymes at the Mediterranean sites where they are P-limited and contributed to greater enzyme efficiency (i.e., enzyme activity normalized per unit microbial biomass C) at these sites (Figure 3-S3). Additionally, studies have found mixed results about the response of potential enzyme activity to precipitation changes including a decrease under drought conditions (Sardans and Peñuelas 2005), no response (Yavitt et al. 2004), or increased activity during heavy rain but not influenced under drought (Kreyling et al. 2008). Overall, clay likely stabilized enzymes at the WM, but enzymes were more efficiently produced at the CZO (Figures 3-1 and 3-2). This may indicate that organic P turnover is an important source of bioavailable P at the Mediterranean CZO.

Previous research at these sites identified notable transitions in P speciation from Ca-P in the semiarid WM sites to Fe- and Al-P at the Mediterranean CZO, which likely impacted P availability, as Al-P is not readily available in the pH range of these soils (Chapter 2). The previous study concluded that turnover of organic P pool, rather than mineral P pools, is largely supporting ecosystem development in the Mediterranean sites. As the availability of P declined with increasing precipitation, microbial biomass was likely able to outcompete vegetation, especially for organic species (Bardgett et al. 2003). This ultimately decreased the concentration of nutrients available for plant uptake

(Heijden et al. 2008; Richardson et al. 2009), further enhancing plant P-limitation as evidenced by a lower N:P in microbes and higher N:P in vegetation in wetter locations. This was reflected in the contrasting relationship between microbial and vegetation N:P, where P became progressively more limiting for vegetation at warmer and wetter environments (i.e., followed soil stoichiometry Figures 3-2 and 3-5). However, in comparison to thresholds of foliar nutrient limitation, where a molar N:P ratio >35:1 is considered to be P-limited, <31:1 is N-limited, and between 31-35 is co-limited (Koerselman and Meuleman 1996), the geometric means of individual vegetation functional groups at each site indicated overall N-limitation (except forb species at SJER were co-limited by N and P; Table 3-S4). Taken together, vegetation exhibited overall N-limitation, which is characteristic of temperate ecosystems (McGroddy et al. 2004; Figure 3-8), but increasing precipitation resulted in relatively more P-limited grass, forb, and evergreen functional groups suggesting microbes may be outcompeting vegetation for this resource (Figure 3-5).

The observed low C:nutrient vegetation ratios may be a reflection of water availability controlling ecosystem structure and processes in these drylands (Huxman et al. 2004; Figure 3-8 and Table 3-S4). Foliar and fine root C concentrations increased with MAP, suggesting enhanced photosynthesis as water-limitation was alleviated (Figures 3-1 and 3). We found C:P and C:N ratios are lower than the global average, but they are similar to regional studies also conducted along a climate gradient in China (Zhang et al. 2019) and were typically higher than another study on forbs, shrubs, and trees (Zhao et al. 2014). Foliar C concentrations are typically considered to be well constrained compared to N and P, and tissue is held to be ~50% of the dry mass (Ågren 2008). We found C concentration geometric means across all sites of each functional group ranged from 45.7% (grass) to 51.5% (evergreen), but were higher than a semiarid and arid desertification grassland gradient that found 41.3% (An et al. 2019). Water is commonly considered the primarily limiting resource for net primary production in Mediterranean and semiarid ecosystems because water stress can reduce photosynthetic rates (Yahdjian et al. 2011; Delgado-Baquerizo et al. 2018). Overall, stoichiometric ratios reflected water limitation in these dryland ecosystems.

Although the low C:nutrient ratios compared to global averages in aboveground vegetation could be an indicator that nutrients are in ample supply, this is unlikely. A meta-analysis of arid to semi-humid sites of grass, shrub, forb, or combinations of these functional groups found NPP increased by 50% after N fertilization across all locations (Yahdjian et al. 2011). Another study found drylands are co-limited by N and water using a variety of metrics (Hooper and Johnson 1999). Additionally, fertilization experiments in the Sierra Nevada have found P addition increased concentrations of grass and forb species (Kie and Myler 1987) along with increased growth of Jeffrey pine (*Pinus jeffreyi*) seedlings after general fertilizer (N, P, and other macro- and micronutrients) addition (Walker 2005). Finally, low C:nutrient ratios may also be from luxury consumption, where N and P are taken up in excess of immediate growth requirement but serve as a reserve to support growth later in the year when nutrients may be less available (Chapin 1980). Luxury consumption can even occur in infertile sites (Chapin 1980). In addition, ranges of fine root C:nutrient ratios encompassed global averages (Figure 3-8), and N:P demonstrated a shift from relatively greater P- to N-limitation with increasing

precipitation (i.e., similar to microbial biomass trends, but opposite of aboveground foliage grass, forb, and evergreen functional groups; Figures 3-2 and 3-3). Overall, vegetation at these dryland sites are likely co-limited by both water and N availability.

We also found greater nutrient concentration overall in aboveground biomass compared to fine roots, which has been reported previously (Newman and Hart 2006). Higher foliar nutrient concentrations compared to fine roots supports nutrients being distributed to alleviate the least limiting resource (Liebig 1984; Newman and Hart 2006). However, under changing precipitation, N concentration in aboveground foliage tended to increase across functional groups with increased precipitation, but N concentration decreased in fine roots. Therefore, as foliar N concentrations increased, fine root concentrations proportionally decreased, which is the opposite of the meta-analysis of global forests by Newman and Hart (2006). This suggests vegetation may be allocating more nutrients, especially N, into aboveground tissue than belowground. In our study this may help to maximize photosynthesis through greater investment of N-rich enzymes and P-rich RNA for protein synthesis that also aide in water retention (Wong et al. 1979; Sterner and Elser, 2002). This has important implications for C sequestration because photosynthesis rates are dependent on nutrient concentrations (Herold 1980), and foliar C and N concentrations tended to increase with increased precipitation. As precipitation increased, N was preferentially distributed to aboveground tissue leading above- and below-ground plant tissue to become decoupled (Figures 3-2 and 3-3).

Stoichiometric ratios provide insight to important ecological functions including vegetation growth and reproduction, species interactions, community composition and diversity, and decomposition rates (Güsewell 2004; Ågren 2008; Cernusak et al. 2010; Sistla and Schimel 2012). However, stoichiometric ratios and the ecological functions that underpin them, are sensitive to multiple global change drivers including warming, drought, enhanced CO_2, and increased N deposition. Alterations to plant stoichiometric ratios with global change directly impacts vegetation through physiological responses (i.e., plant growth and metabolism) and indirectly through plant-microbe interactions (Güsewell 2004). Changes in vegetation structure will likely influence microbial community composition and their ecological function (Sistla and Schimel 2012).

Our results suggest foliar and litter C and C:nutrient ratios will likely increase in these dryland ecosystems under warming, drought, and enhanced atmospheric CO_2 from greater investment into water conservation and increased nutrient use efficiency (Sardans et al. 2012; Du et al. 2019). This has important implications for carbon sequestration because warming has been found to increase respiration by 40% and reduce microbial carbon use efficiency (Schindlbacher et al. 2011). On the other hand, increases in N deposition can result in N surplus, leading to increased P-limitation and increasing foliar N:P ratios (Aber et al. 1989; Fenn et al. 1998). Increases in available N via atmospheric deposition may help to alleviate N limitation in these drylands and would shift communities towards species that have higher P uptake affinity and maximal growth with high N:P (Meunier et al. 2017). However, water limitation may constrain increases in NPP in these drylands (Yahdjian et al. 2011) and excess soil C will be respired if stoichiometric ratios are imbalanced with microbial demand (Fernández-Martínez et al. 2014). Overall, global change influences on ecosystem nutrient stoichiometry will

determine how nutrient cycling, primary productivity, and community structure are impacted (Elser et al. 2010; Moe et al. 2005; Zechmeister-Boltenstern et al. 2015).

3.6 Conclusion

Climate exerts strong controls over nutrient cycling, especially in terrestrial drylands (Noy-Meir, 1973; Austin et al. 2004; Delgado-Baquerizo et al. 2013). We found climate exerted direct and indirect effects on ecosystem stoichiometry, but not all ecosystem compartments responded to precipitation changes in the same way. Our current understanding of ecosystem nutrient stoichiometry stands that terrestrial plants have diverse C:N:P ratios and readily respond to environmental gradients (Vitousek 1984; McGroddy et al. 2004; Townsend et al. 2007), whereas microbial biomass (Cleveland and Liptzin 2007) and extracellular enzyme activity (Sinsabaugh et al. 2008, 2009) are more constrained. We demonstrated how measuring multiple ecosystem components provides a better understanding of nutrient dynamics because ecosystem components may not always co-vary. In our case, vegetation and microbial C:N:P had a negative relationship with each other. As others have noted, only measuring the stoichiometry of the microbial biomass may not serve as a good indicator of ecosystem nutrient status because microbes can outcompete vegetation for nutrients (Xu et al. 2012), although others have suggested microbial nutrient ratios may serve as a better index of ecosystem limitation than plant ratios (Cleveland and Liptzin 2007). Overall, these finding help broaden our understanding of how C, N, and P biogeochemical cycling in soil, microbial biomass, and vegetation is altered by precipitation, improving our understanding of how dryland ecosystems may respond to a changing climate.

3.7 References

Aber JD, Nadelhoffer KJ, Steudler P, Melillo JM (1989) Nitrogen saturation in northern forest ecosystems. BioScience 39: 378-286.

Aerts R, Chapin FSC (1999) The Mineral Nutrition of Wild Plants Revisited: A Re-evaluation of Processes and Patterns. Advances in Ecological Research 30:1-67.

Ågren GI (2008) Stoichiometry and nutrition of plant growth in natural communities. Annual Review of Ecology, Evolution, and Systematics 39:153-170.

Attiwill PM, Adams MA (1993) Nutrient cycling in forests. New Phytologist 124:561-582.

Austin AT, Yahdjian L, Stark JM, et al. (2004) Water pulses and biogeochemical cycles in arid and semiarid ecosystems. Oecologia 141:221-235.

Austin AT, Vitousek PM (1998) Nutrient dynamics on a precipitation gradient in Hawai'i. Oecologia 113:519-529.

Bardgett RD, Streeter TC, Bol R (2003) Soil microbes compete effectively with plants for organic nitrogen inputs to temperate grasslands. Ecology 84:1277-1287.

Barton K, Barton MK (2019) Package 'MuMIn'. R package version, 1:6.

Bateman CP, Wones RD (1972) Geologic Map of the Huntington Lake Quadrangle, Central Sierra Nevada, California. United States Geological Survey.

Bateman P and Busacca A (1982) Geologic Map of the Millerton Lake Quadrangle, West-Central Sierra Nevada, California. United States Geological Survey.

Bates D, Maechler M, Bolker B, Walker S (2015) Fitting Linear Mixed-Effects Models Using lme4. Journal of Statistical Software 67:1-48.

Beck TR, Joergensen RG, Kandeler E, Makeschin F, Nuss E, Oberholzer HR, Scheu S (1997) An interlaboratory comparison of ten different ways of measuring soil microbial biomass C. Soil Biology and Biochemistry 29:1023-1032.

Bell CW, Fricks BE, Rocca JD, Steinweg JM, McMahon SK, Wallenstein MD (2013) High-throughput fluorometric measurement of potential soil extracellular enzyme activities. Journal of Visualized Experiments 81:1-16.

Boerner REJ, Brinkman JA, Smith A (2005) Seasonal variations in enzyme activity and organic carbon in soil of a burned and unburned hardwood forest Soil Biology and Biochemistry 37 1419-1426

Brookes PC, Landman A, Pruden G, Jenkinson DS (1985) Chloroform fumigation and the release of soil nitrogen: A rapid direct extraction method to measure microbial biomass nitrogen in soil. Soil Biology and Biochemistry 17:837-842.

Brookes PC, Powlson DS, Jenkinson DS (1982) Measurement of microbial biomass phosphorus in soil. Soil Biology and Biochemistry 14:319–329.

Bui EN, Henderson BL (2013) C:N:P stoichiometry in Australian soils with respect to vegetation and environmental factors. Plant and Soil 373:553-568.

Burns RG, DeForest JL, Marxsen J, et al. (2013) Soil enzymes in a changing environment: Current knowledge and future directions. Soil Biology and Biochemistry 58:216-234.

Buss HL, Bruns MA, Schultz MJ, et al (2005) The coupling of biological iron cycling and mineral weathering during saprolite formation, Luquillo Mountains, Puerto Rico. Geobiology 3:247-260.

Chadwick OA, Gavenda RT, Kelly EF, et al. (2003) The impact of climate on the biogeochemical functioning of volcanic soils. Chemical Geology 202:195-223.

Chapin III, FS (1980) The mineral nutrition of wild plants. Annual review of ecology and systematics 11:233-260.

Chen L, Li P, Yang Y (2016) Dynamic patterns of nitrogen: Phosphorus ratios in forest soils of China under changing environment. Journal of Geophysical Research Biogeosciences 121:2410-2421.

Clark DH, Gillespie AR (1997) Timing and significance of Late-glacial and Holocene cirque glaciation in the Sierra Nevada, California. Quaternary Science 38:21-38.

Cleveland CC, Liptzin D (2007) C:N:P stoichiometry in soil: is there a "Redfield ratio" for the microbial biomass? Biogeochemistry 85:235-252.

Craine J, Lee W (2003) Covariation in leaf and root traits for native and non-native grasses along an altitudinal gradient in New Zealand, Oecologia 134:471-478.

Cregger MA, Schadt CW, McDowell NG, et al. (2012) Response of the Soil Microbial Community to Changes in Precipitation in a Semiarid Ecosystem. Applied and Environmental Microbiology 78:8587-8594.

Cui Y, Fang L, Deng L, et al. (2018) Patterns of soil microbial nutrient limitations and their roles in the variation of soil organic carbon across a precipitation gradient in an arid and semi-arid region. Science of the Total Environment 658:1440-1451.

Dahlgren RA, Boettinger JL, Huntington GL, Amundson RG (1997) Soil development along an elevational transect in the western Sierra Nevada, California. Geoderma 78:207-236.

Dai A (2012) Increasing drought under global warming in observations and models. Nature Climate Change 3:52-58.

Daly C, Taylor G, Gibson W, et al. (2000) High-quality spatial climate data sets for the united states and beyond. American Society of Agricultural Engineers 43:1957-1962

Danger M, Gessner MO, Bärlocher F (2016) Ecological stoichiometry of aquatic fungi: current knowledge and perspectives. Fungal Ecology 19:100-111.

Delgado-Baquerizo M, Eldridge DJ, Maestre FT, et al. (2018) Aridity Decouples C:N:P Stoichiometry Across Multiple Trophic Levels in Terrestrial Ecosystems. Ecosystems 21:459-468.

Delgado-Baquerizo M, Maestre FT, Gallardo A, et al. (2013) Decoupling of soil nutrient cycles as a function of aridity in global drylands. Nature 502:672-676.

Di Palo F, Fornara DA (2017) Plant and soil nutrient stoichiometry along primary ecological successions: Is there any link?. PLOS One 12:1-18.

Dijkstra FA, Pendall E, Morgan JA, et al. (2012) Climate change alters stoichiometry of phosphorus and nitrogen in a semiarid grassland. New Phytologist 196:807-815.

Dixon JL, Heimsath AM, Amundson R (2009) The critical role of climate and saprolite weathering in landscape evolution. Earth Surface Processes 34:1507-1521.

Dove NC, Arogyaswamy K, Billings SA, et al. (2020) Continental-scale patterns of extracellular enzyme activity in the subsoil: an overlooked reservoir of microbial activity. Environ Research Letters 15:1-22.

Du C, Wang X, Zhang M, Jing J, Gao Y (2019) Effects of elevated CO2 on plant CNP stoichiometry in terrestrial ecosystems: A meta-analysis. Science of The Total Environment 650:697-708.

Dynarski KA, Houlton BZ (2018) Nutrient limitation of terrestrial free-living nitrogen fixation. New Phytologist 217:1050-1061.

Egli M, Mirabella A, Sartori G, Fitze P (2003) Weathering rates as a function of climate: results from a climosequence of the Val Genova (Trentino, Italian Alps). Geoderma 111:99-121.

Eilers KG, Debenport S, Anderson S, Fierer N (2012) Digging deeper to find unique microbial communities: The strong effect of depth on the structure of bacterial and archaeal communities in soil. Soil Biology and Biochemistry 50:58-65.

Elser JJ, Bracken MES, Cleland EE, et al. (2007) Global analysis of nitrogen and phosphorus limitation of primary producers in freshwater, marine and terrestrial ecosystems. Ecology Letters 10:1135-1142.

Elser JJ, Fagan WF, Denno RF, et al. (2000) Nutritional constraints in terrestrial and freshwater food webs. Nature 408:578-580.

Elser JJ, Fagan WF, Kerkhoff AJ, et al. (2010) Biological stoichiometry of plant production: metabolism, scaling and ecological response to global change. New Phytologist 186:593-608.

Ernst WG, Rumble D (2003) Oxygen isotopic study of Late Mesozoic cooling of the Mount Barcroft area, central White Mountains, eastern California. Contributions to Mineralogy and Petrology 144:639-651.

Feng J, Turner BL, Lü X, et al. (2016) Phosphorus transformations along a large-scale climosequence in arid and semiarid grasslands of northern China. Global Biogeochemical Cycles 30:1264-1275.

Feng S, Fu Q (2013) Expansion of global drylands under a warming climate. Atmospheric Chemistry and Physics 13:14637-14665.

Fenn ME, Poth MA, Aber JD, et al. (1998) Nitrogen excess in North American ecosystems: predisposing factors, ecosystem responses, and management strategies. Ecological Applications 8:706-733.

Fernández-Martínez M, Vicca S, Janssens IA, et al. (2014) Nutrient availability as the key regulator of global forest carbon balance. Nature Publishing Group 4:471-476.

Ferre EC, Michelsen KJ, Ernst WG, et al. (2012) Vertical zonation of the Barcroft granodiorite, White Mountains, California: Implications for magmatic processes. American Mineralogist 97:1049-1059.

Fierer N, Chadwick OA, Trumbore SE (2005) Production of CO_2 in Soil Profiles of a California Annual Grassland. Ecosystems 8:412-429.

Fierer N, Jackson RB (2006) The diversity and biogeography of soil bacterial communities. Proceedings of the National Academy of Sciences of the United States of America 103:626–631.

Fierer N, Schimel JP, Holden PA (2003) Variations in microbial community composition through two soil depth profiles. Soil Biology and Biochemistry 35:167-176.

Finzi AC, Austin AT, Cleland EE, et al. (2011) Responses and feedbacks of coupled biogeochemical cycles to climate change: examples from terrestrial ecosystems. Frontiers in Ecology and the Environment 9:61-67.

Fisher JB, Malhi Y, Torres IC, et al. (2013) Nutrient limitation in rainforests and cloud forests along a 3,000-m elevation gradient in the Peruvian Andes. Oecologia 172:889-902.

Frisbie JA (2014) Soil organic carbon storage and aggregate stability in an Arid Mountain Range, White Mountains, CA. Dissertation, University of California

Gee, GW and JM Bauder (1986) Particle-size analysis. In: Methods of Soil Analysis, Part 1, Physical and Mineralogical Methods. Agronomy Monograph No. 9 (2nd edition), American Society of Agronomy, Madison, WI pp 383-411.

George E, Marschner H, Jakobsen I (2008) Role of Arbuscular Mycorrhizal Fungi in Uptake of Phosphorus and Nitrogen From Soil. Critical Reviews in Biotechnology 15:257-270.

Gerdol R, Iacumin P, Brancaleoni L (2019) Differential effects of soil chemistry on the foliar resorption of nitrogen and phosphorus across altitudinal gradients. Functional Ecology 33:1351-1361.

Gong H, Li Y, Yu T, et al. (2020) Soil and climate effects on leaf nitrogen and phosphorus stoichiometry along elevational gradients. Global Ecology and Conservation 23:1-7.

Griffith WK (1978). Effects of phosphorus and potassium on nitrogen fixation. In: Phosphorus for Agriculture: A Situation Analysis. Potash/Phosphate Institute, Atlanta pp. 80-94.

Güsewell S (2004) N:P ratios in terrestrial plants: variation and functional significance. New phytologist 164:243-266.

Güsewell S, Bailey KM, Roem WJ, Bedford BL (2005) Nutrient limitation and botanical diversity in wetlands: can fertilisation raise species richness? Oikos 109:71-80.

Güsewell S, Gessner MO (2009) N:P ratios influence litter decomposition and colonization by fungi and bacteria in microcosms. Functional Ecology 23:211-219.

Güsewell S, Koerselman W, Verhoeven JTA (2003) Biomass N:P ratios as indicators of nutrient limitation for plant populations in wetlands. Ecological Applications 13:372-384.

Hahm WJ, Riebe CS, Lukens CE, Araki S (2014) Bedrock composition regulates mountain ecosystems and landscape evolution. Proceedings of the National Academy of Sciences of the United States of America 111:3338–3343.

Han WX, Fang JY, Reich PB, et al. (2011) Biogeography and variability of eleven mineral elements in plant leaves across gradients of climate, soil and plant functional type in China. Ecology Letters 14:788-796.

Harris D, Horwáth WR, Van Kessel C (2001) Acid fumigation of soils to remove carbonates prior to total organic carbon or carbon-13 isotopic analysis. Soil Science Society of America Journal 65:1853-1856.

Hart SC, Classen AT, Wright RJ (2005) Long-term interval burning alters fine root and mycorrhizal dynamics in a ponderosa pine forest. Journal of Applied Ecology 42:752-761.

He M, Dijkstra FA (2014) Drought effect on plant nitrogen and phosphorus: a meta-analysis. New Phytologist 204:924-931.

He X, Hou E, Liu Y, Wen D (2016) Altitudinal patterns and controls of plant and soil nutrient concentrations and stoichiometry in subtropical China. Scientific Reports 6:1-9.

Hedin LO (2004) Global organization of terrestrial plant–nutrient interactions. Proceedings of the National Academy of Sciences of the United States of America 101:10849-10850.

Heijden MGAVD, Bardgett RD, Straalen NMV (2008) The unseen majority: soil microbes as drivers of plant diversity and productivity in terrestrial ecosystems. Ecology Letters 11:296-310.

Herold A (1980) Regulation of photosynthesis by sink activity-the missing link. New Phytologist 86:131-144.

Hooper DU, Johnson L (1999) Nitrogen limitation in dryland ecosystems: Responses to geographical and temporal variation in precipitation. Biogeochemistry 46:247-293.

Hungate BA, Dukes JS, Shaw R, et al. (2003) Nitrogen and climate change. Science 302:1512-1513

Huxman TE, Snyder KA, Tissue D, et al. (2004) Precipitation pulses and carbon fluxes in semiarid and arid ecosystems. Oecologia 141:254-268.

Ippolito JA, Blecker SW, Freeman CL, et al. (2010) Phosphorus biogeochemistry across a precipitation gradient in grasslands of central North America. Journal of Arid Environments 74:954-961.

Isles PD (2020) The misuse of ratios in ecological stoichiometry. Ecology 101:1-7.

Izquierdo JE, Houlton BZ, Huysen TL van (2013) Evidence for progressive phosphorus limitation over long-term ecosystem development: Examination of a biogeochemical paradigm. Plant and Soil 367:135-147.

Jackson RB, Canadell J, Ehleringer JR, et al. (1996) A global analysis of root distributions for terrestrial biomes. Plant Ecology 108:389-411.

Jackson RB, Mooney HA, Schulze E-D (1997) A global budget for fine root biomass, surface area, and nutrient contents. Proceedings of the National Academy of Sciences of the United States of America 94:7362-7366.

Jenny H, Gessel SP, Bingham FT (1949) Comparative study of decomposition rates of organic matter in temperate and tropical regions. Soil Science 68:419-432.

Jobbágy EG, Jackson RB (2000) The vertical distribution of soil organic carbon and its relation to climate and vegetation. Ecological Applications 10:423-436.

Jobbágy EG, Jackson RB (2001) The distribution of soil nutrients with depth: Global patterns and the imprint of plants. Biogeochemistry 53:51-77.

Kie JG, Myler SA (1987) Use of fertilization and grazing exclusion in mitigating lost meadow production in the Sierra Nevada, California, USA. Environ Manage 11:641-648.

Koerselman W, Meuleman AFM (1996) The Vegetation N:P Ratio: a New Tool to Detect the Nature of Nutrient Limitation. The Journal of Applied Ecology 33:1441-1450.

Kreyling J, Beierkuhnlein C, Elmer M, et al. (2008) Soil biotic processes remain remarkably stable after 100-year extreme weather events in experimental grassland and heath. Plant Soil 308:175-188.

Lajtha K, Bloomer SH (1988) Factors affecting phosphate sorption and phosphate retention in a desert ecosystem. Soil Science 146:160-167.

Lambers H, Shane MW, Cramer MD, et al. (2006) Root Structure and Functioning for Efficient Acquisition of Phosphorus: Matching Morphological and Physiological Traits. Annals of Botany 98:693-713.

Lenth R, Singmann H, Love J (2018) Emmeans: Estimated marginal means, aka least-squares means. R package version, 1.1.

Li P, Yang Y, Han W, Fang J (2014) Global patterns of soil microbial nitrogen and phosphorus stoichiometry in forest ecosystems. Global Ecology and Biogeography 23:979-987.

Liebig J (1842) Animal chemistry, or organic chemistry in its application to physiology and pathology. Johnson Reprint Corporation, New York.

Lockwood PJ, Bateman CP (1976) Geologic Map of the Shaver Lake quadrangle, Central Sierra Nevada, California. United States Geological Survey.

Luo W, Elser JJ, Lü XT, et al. (2015) Plant nutrients do not covary with soil nutrients under changing climatic conditions. Global Biogeochemical Cycles 29:1298-1308.

Manzoni S, Trofymow JA, Jackson RB, Porporato A (2010) Stoichiometric controls on carbon, nitrogen, and phosphorus dynamics in decomposing litter. Ecological Monographs 80:89-106.

Margalef O, Sardans J, Fernández-Martínez M, et al. (2017) Global patterns of phosphatase activity in natural soils. Scientific Reports 7:1-13.

Marklein AR, Houlton BZ (2011) Nitrogen inputs accelerate phosphorus cycling rates across a wide variety of terrestrial ecosystems. New Phytologist 193:696-704.

Matzek V, Vitousek P (2003) Nitrogen Fixation in Bryophytes, Lichens, and Decaying Wood along a Soil-age Gradient in Hawaiian Montane Rain Forest. Biotropica 35:12-19.

McGill WB, Cole CV (1981) Comparative aspects of cycling of organic C, N, S, and P through soil organic matter. Geoderma 26:267-286.

McGroddy ME, Daufresne T, Hedin LO (2004) Scaling of C:N:P stoichiometry in forests worldwide: implications of terrestrial Redfield-type ratios. Ecology 85:2390-2401.

Melillo JM, Butler S, Johnson J, et al. (2011) Soil warming, carbon–nitrogen interactions, and forest carbon budgets. Proceedings of the National Academy of Sciences 108:1-5.

Meunier CL, Boersma M, El-Sabaawi R, et al. (2017) From elements to function: toward unifying ecological stoichiometry and trait-based ecology. Frontiers in Environmental Science 5:1-10.

Moe SJ, Stelzer RS, Forman MR, et al. (2005) Recent advances in ecological stoichiometry: insights for population and community ecology. Oikos 109:29-39.

Moreland KM (2020) Climatic controls on deep soil carbon and nitrogen dynamics. Dissertation. University of California, Merced, Merced, CA.

Munevar F, Wollum AG (1977) Effects of the Addition of Phosphorus and Inorganic Nitrogen on Carbon and Nitrogen Mineralization in Andepts From Colombia. Soil Science Society of America Journal 41:540–545.

Nakagama S, Schielzeth H (2013) A general and simple method for obtained R^2 from generalized linear mixed-effects model. Methods in Ecology and Evolution 4:133-142.

Newman GS, Hart SC (2006) Nutrient covariance between forest foliage and fine roots. Forest Ecology and Management 236:136-141.

Nottingham AT, Turner BL, Whitaker J, et al. (2015) Soil microbial nutrient constraints along a tropical forest elevation gradient: a belowground test of a biogeochemical paradigm. Biogeosciences 12:6071-6083.

Noy-Meir I (1973) Desert ecosystems: environment and producers. Annual Review of Ecology and Systematics 4:25-41.

Olander LP, Vitousek PM (2000) Regulation of soil phosphatase and chitinase activity by N and P availability. Biogeochemistry 49:175-191.

Ordoñez JC, Bodegom PMV, Witte JPM, et al. (2009) A global study of relationships between leaf traits, climate and soil measures of nutrient fertility. Global Ecology and Biogeography 18:137-149.

Parkinson JA, Allen SE (1975) A wet oxidation procedure suitable for the determination of nitrogen and mineral nutrients in biological material. Communications in Soil Science and Plant Analysis 6:1-11.

Paul EA (2007) Soil microbiology, ecology, and biochemistry. Academic Press, Massachusetts.

Peng X, Peng Y, Yue K, Deng Y (2017) Different Responses of Terrestrial C, N, and P Pools and C/N/P Ratios to P, NP, and NPK Addition: a Meta-Analysis. Water, Air, & Soil Pollution 228:1-13.

Porder S, Chadwick OA (2009) Climate and soil-age constraints on nutrient uplift and retention by plants. Ecology 90:623-636.

Prietzel J, Klysubun W, Werner F (2016) Speciation of phosphorus in temperate zone forest soils as assessed by combined wet-chemical fractionation and XANES spectroscopy. Journal of Plant Nutrition 179:168-185.

R Core Team. 2013. R: A language and environment for statistical computing. R Foundation for Statistical Computing. Vienna, Austria.

Redfield A (1958) The biological control of chemical factors in the environment. American Scientist 46:205-221.

Reed SC, Yang X, Thornton PE (2015) Incorporating phosphorus cycling into global modeling efforts: a worthwhile, tractable endeavor. New Phytologist 208:324-329.

Reich PB, Oleksyn J (2004) Global patterns of plant leaf N and P in relation to temperature and latitude. Proceedings of the National Academy of Sciences 101:11001–11006.

Richardson AE, Barea JM, McNeill AM, Prigent-Combaret C (2009) Acquisition of phosphorus and nitrogen in the rhizosphere and plant growth promotion by microorganisms. Plant Soil 321:305-339.

Robertson GP, Coleman DC, Sollins P, Bledsoe CS (1999) Standard Soil Methods For Long-term Ecological Research. Oxford University Press, New York.

Roem WJ, Berendse F (2000) Soil acidity and nutrient supply ratio as possible factors determining changes in plant species diversity in grassland and heathland communities. Biological Conservation 92:151-161.

Ross DJ, Bridger BA (1978) Nitrogen availability in some soils from tussock grasslands and introduced pastures. 2. Nitrogen mineralization as influenced by added P, K, and S and by air drying: relationships with ryegrass growth. New Zealand Journal of Science 21:435-442.

Rumpel C, Kögel-Knabner I (2011) Deep soil organic matter—a key but poorly understood component of terrestrial C cycle. Plant and Soil 338:143-158.

Santiago LS, Schuur EA, Silvera K (2005) Nutrient cycling and plant-soil feedbacks along a precipitation gradient in lowland Panama. Journal of Tropical Ecology 21:461-470.

Sardans J, Alonso R, Janssens IA, et al. (2016) Foliar and soil concentrations and stoichiometry of nitrogen and phosphorous across European *Pinus sylvestris* forests: relationships with climate, N deposition and tree growth. Functional Ecology 30:676-689.

Sardans J, Peñuelas J (2005) Drought decreases soil enzyme activity in a Mediterranean *Quercus ilex L.* forest. Soil Biology Biochemistry 37:455-461.

Sardans J, Peñuelas J, Estiarte M (2006) Warming and drought alter soil phosphatase activity and soil P availability in a Mediterranean shrubland. Plant and Soil 289:227-238.

Sardans J, Rivas-Ubach A, Peñuelas J (2012) The C:N:P stoichiometry of organisms and ecosystems in a changing world: A review and perspectives. Perspectives in Plant Ecology, Evolution and Systematics 14:33-47.

Schindlbacher A, Rodler A, Kuffner M, Kitzler B, Sessitsch A, Zechmeister-Boltenstern S (2011) Experimental warming effects on the microbial community of a temperate mountain forest soil. Soil Biology and Biochemistry 43:1417-1425.

Schnecker J, Wild B, Takriti M, et al. (2015) Microbial community composition shapes enzyme patterns in topsoil and subsoil horizons along a latitudinal transect in Western Siberia. Soil Biology Biochemistry 83:106-115.

Sinsabaugh RL, Hill BH, Shah JJF (2009) Ecoenzymatic stoichiometry of microbial organic nutrient acquisition in soil and sediment. Nature 462:795-798.

Sinsabaugh RL, Lauber CL, Weintraub MN, et al. (2008) Stoichiometry of soil enzyme activity at global scale. Ecology Letters 11:1252-1264.

Sistla SA, Schimel JP (2012) Stoichiometric flexibility as a regulator of carbon and nutrient cycling in terrestrial ecosystems under change. New Phytologist 196:68-78.

Spohn M (2016) Element cycling as driven by stoichiometric homeostasis of soil microorganisms. Basic and Applied Ecology 17:471-478.

Spohn M, Widdig M (2017) Turnover of carbon and phosphorus in the microbial biomass depending on phosphorus availability. Soil Biology and Biochemistry 113:53-59.

Sterner RW, Elser JJ (2002) Ecological Stoichiometry: The Biology of Elements from Molecules to the Biosphere. Princeton University Press, New Jersey.

Stone MM, DeForest JL, Plante AF (2014) Changes in extracellular enzyme activity and microbial community structure with soil depth at the Luquillo Critical Zone Observatory. Soil Biology Biochemistry 75:237-247.

Sun H, Wu Y, Yu D, Zhou J (2013) Altitudinal Gradient of Microbial Biomass Phosphorus and Its Relationship with Microbial Biomass Carbon, Nitrogen, and Rhizosphere Soil Phosphorus on the Eastern Slope of Gongga Mountain, SW China. PLOS One 8:1-10.

Tang Z, Xu W, Zhou G, et al. (2018) Patterns of plant carbon, nitrogen, and phosphorus concentration in relation to productivity in China's terrestrial ecosystems. Proceedings of the National Academy of Sciences 115:4033-4038.

Tate KR (1992) Assessment, based on a climosequence of soils in tussock grasslands, of soil carbon storage and release in response to global warming. Journal of Soil Science 43:697-707.

Tian H, Chen G, Zhang C, et al. (2009) Pattern and variation of C:N:P ratios in China's soils: a synthesis of observational data. Biogeochemistry 98:139-151.

Townsend AR, Cleveland CC, Asner GP, Bustamante MMC (2007) Controls over foliar N:P ratios in tropical rain forests. Ecology 88:107-118.

Turner BL, Condron LM, Wells A, Andersen KM (2012a) Soil nutrient dynamics during podzol development under lowland temperate rain forest in New Zealand. Catena 97:50-62.

Turner BL, Lambers H, Condron LM, et al. (2012b) Soil microbial biomass and the fate of phosphorus during long-term ecosystem development. Plant and Soil 367:225-234.

Turner BL, Wright SJ (2014) The response of microbial biomass and hydrolytic enzymes to a decade of nitrogen, phosphorus, and potassium addition in a lowland tropical rain forest. Biogeochemistry 117:115-130.

Vance E, Brookes PC, Jenkinson DS (1987) An extraction method for measuring soil microbial biomass C. Soil Biology and Biochemistry 19:703-77.

Vitousek PM (1984) Litterfall, Nutrient Cycling, and Nutrient Limitation in Tropical Forests. Ecology 65:285-298.

Vitousek PM, Aber JD, Howarth RW, et al. (2008) Human alteration of the global nitrogen cycle: sources and consequences. Ecological Applications 7:737-750.

Vitousek PM, Porder S, Houlton BZ, Chadwick OA (2010) Terrestrial phosphorus limitation: mechanisms, implications, and nitrogen–phosphorus interactions. Ecological Applications 20:5-15.

Walker RF (2005) Growth and Nutritional Responses of Juvenile Jeffrey Pine to Post-Planting Fertilization. Journal of Sustainable Forestry 20:67-83.

Walker TW, Syers JK (1976) The fate of phosphorus during pedogenesis. Geoderma 15:1-19.

Wieder WR, Cleveland CC, Smith WK, Todd-Brown K (2015) Future productivity and carbon storage limited by terrestrial nutrient availability. Nature Geoscience 8:441-444.

Williamson WM, Wardle DA, Yeates GW (2005) Changes in soil microbial and nematode communities during ecosystem decline across a long-term chronosequence. Soil Biology and Biochemistry 37:1289-1301.

Wood T, Bormann FH, Voigt GK (1984) Phosphorus cycling in a northern hardwood forest: biological and chemical control. Science 223:391-393.

Wong SC, Cowan IR, Farquhar GD (1979) Stomatal conductance correlates with photosynthetic capacity. Nature 282:424-426.

Xiao L, Li P, Shi P, Liu Y (2018) Soil nutrient stoichiometries and enzymatic activities along an elevational gradient in the dry-hot valley region of southwestern China. Archives of Agronomy and Soil Science 65:322-333.

Xu SJ, Fan XY, Wang LL, et al. (2015) The patterns of nitrogen and phosphorus stoichiometry across communities along altitudinal gradients in Qilian Mountains, China. Biochemical Systematics and Ecology 62:58-65.

Xu X, Thornton PE, Post WM (2012) A global analysis of soil microbial biomass carbon, nitrogen and phosphorus in terrestrial ecosystems. Global Ecology and Biogeography 22:737-749.

Xu Z, Yu G, Zhang X, et al. (2017) Soil enzyme activity and stoichiometry in forest ecosystems along the North-South Transect in eastern China (NSTEC). Soil Biology and Biochemistry 104:152–163.

Yahdjian L, Gherardi L, Sala OE (2011) Nitrogen limitation in arid-subhumid ecosystems: A meta-analysis of fertilization studies. Journal of Arid Environments 75:675-680.

Yavitt JB, Wright SJ, Wieder RK (2004) Seasonal drought and dry-season irrigation influence leaf-litter nutrients and soil enzymes in a moist, lowland forest in Panama. Austral Ecology 29:177-188.

Yost JL, Hartemink AE (2020) How deep is the soil studied – an analysis of four soil science journals. Plant Soil 1-14.

Yu H, Fan J, Harris W, Li Y (2017) Relationships between below-ground biomass and foliar N:P stoichiometry along climatic and altitudinal gradients of the Chinese grassland transect. Plant Ecology 218:661-671.

Yuan ZY, Chen HYH (2015) Decoupling of nitrogen and phosphorus in terrestrial plants associated with global changes. Nature Publishing Group 5:465-469.

Zechmeister-Boltenstern S, Keiblinger KM, Mooshammer M, et al. (2015) The application of ecological stoichiometry to plant–microbial–soil organic matter transformations. Ecological Monographs 85:133-155.

Zhang J, Elser JJ (2017) Carbon:Nitrogen:Phosphorus Stoichiometry in Fungi: A Meta-Analysis. Frontiers in Microbioly 8:1-9.

Zhang Y, Li C, Wang M (2019) Linkages of C: N: P stoichiometry between soil and leaf and their response to climatic factors along altitudinal gradients. Journal of Soils and Sediments 19:1820-1829.

Zhao N, He N, Wang Q, et al. (2014) The Altitudinal Patterns of Leaf C:N:P Stoichiometry Are Regulated by Plant Growth Form, Climate and Soil on Changbai Mountain, China. PLOS One 9:1-9.

3.8 Tables

Table 3-1. Site characteristics at the semiarid White Mountain (WM) and Southern Sierra Critical Zone Observatory (CZO) elevational transects with the corresponding elevation, mean annual precipitation (MAP; mm y^{-1}), mean annual temperature (MAT; °C), soil moisture regime (SMR), soil temperature regime (STR), dominate vegetation, clay percentage and pH in $CaCl_2$. Mean and standard errors are reported across all mineral soil horizons. Site abbreviations represent Granite 2 (GR2), Granite 3 (GR3), Granite 5 (GR5), Barcroft (BAR), San Joaquin Experimental Range (SJER), Soaproot (SPR), Providence (PR) and Short Hair (SH).

Gradient	Site	Elevation (m)	MAP (mm y^{-1})	MAT (°C)	SMR	STR	Vegetation	Clay (%)	pH	Sample Size (Clay and pH)
WM	GR2	2220	247	8.5	Aridic	Mesic	Pine/Shrub	9.7 ± 0.9	6.7 ± 0.04	16
WM	GR3	2480	277	7.3	Aridic	Frigid	Pine/Shrub	21 ± 2	6.6 ± 0.04	23
WM	GR5	3070	421	3.3	Aridic	Cryic	Pine/Shrub	9.0 ± 0.9	6.1 ± 0.02	15
WM	BAR	3870	538	0.1	Aridic	Cryic	Grass	6.1 ± 0.2	5.3 ± 0.07	27
CZO	SJER	400	502	16.7	Xeric	Thermic	Oak/Pine/Grass	6.3 ± 0.9	5.2 ± 0.06	23
CZO	SPR	1160	860	13.6	Xeric	Mesic	Pine/Oak	9.4 ± 1	5.4 ± 0.09	28
CZO	PR	2020	994	9.2	Xeric	Frigid	Conifer	5.2 ± 0.6	4.4 ± 0.08	26
CZO	SH	2700	1066	4.8	Xeric	Cryic	Conifer	4.1 ± 0.3	4.6 ± 0.04	26

Table 3-2. Results of mixed effect models to investigate the relationships between soil, microbial biomass, enzyme activity, and fine root molar carbon:nitrogen (C:N), C:phosphorus (C:P), and N:P stoichiometry with mean annual precipitation (MAP), master soil horizon (A, B, and C; A = 0-coded), and their interaction (MAP x B and MAP x C). Coefficients (bolded when $\alpha = 0.05$), marginal R^2 (only fixed effects), and sample size (n) are reported. Stoichiometric ratios were log transformed to meet model assumptions.

Sample	Ratio	Intercept	MAP	B	C	MAP x B	MAP x C	R^2	n
Soil	C:N	1.1	**0.00034**	-0.075	-0.035	-0.000045	-0.000089	0.29	178
	C:P	1.3	**0.00072**	**-0.59**	**-0.99**	0.00013	0.00016	0.51	185
	N:P	0.21	**0.00037**	**-0.46**	**-0.86**	0.00014	0.00021	0.47	178
Enzyme	C:N	0.68	-0.00036	-0.29	-0.19	0.00028	0.00022	0.06	112
	C:P	-0.23	-0.00015	**-0.36**	0.21	**0.00051**	-0.00032	0.06	139
	N:P	-0.96	0.00036	-0.075	0.33	0.00015	-0.00054	0.11	113
Microbe	C:N	1.5	-0.00047	-0.64	-0.22	-0.000058	0.00016	0.13	78
	C:P	3.1	-0.0019	-0.22	0.75	0.00054	Not Included	0.29	45
	N:P	2.0	-0.0019	-0.83	0.78	**0.0014**	Not Included	0.23	51
Root	C:N	1.5	**0.00034**	-0.048	0.038	**0.00019**	0.00012	0.52	155
	C:P	3.1	0.000044	-0.13	-0.0019	**0.00031**	**0.00023**	0.22	155
	N:P	1.6	**-0.00030**	-0.069	-0.057	**0.00011**	0.00011	0.25	158

Table 3-3. Linear regression model coefficients and R^2 for the relationship of aboveground vegetation molar carbon:nitrogen (C:N), C:phosphorus (C:P), and N:P stoichiometries with mean annual precipitation (MAP). Separate models were ran for different functional groups (grass, forb, shrub, deciduous, and evergreen) and ratios were log transformed.

Functional Group	Ratio	MAP	R^2	n
Grass	C:N	**-0.00036**	0.11	106
	C:P	**-0.00013**	0.01	106
	N:P	**0.00023**	0.03	107
Forb	C:N	**-0.00034**	0.27	107
	C:P	**-0.00015**	0.06	107
	N:P	**0.00024**	0.14	109
Shrub	C:N	**0.00022**	0.13	128
	C:P	**0.00020**	0.04	128
	N:P	-0.000026	<0.01	128
Deciduous	C:N	**-0.00029**	0.54	22
	C:P	**-0.00051**	0.40	22
	N:P	-0.00021	0.12	23
Evergreen	C:N	0.000039	0.02	86
	C:P	**0.00032**	0.34	86
	N:P	**0.00026**	0.30	90

3.9 Figures

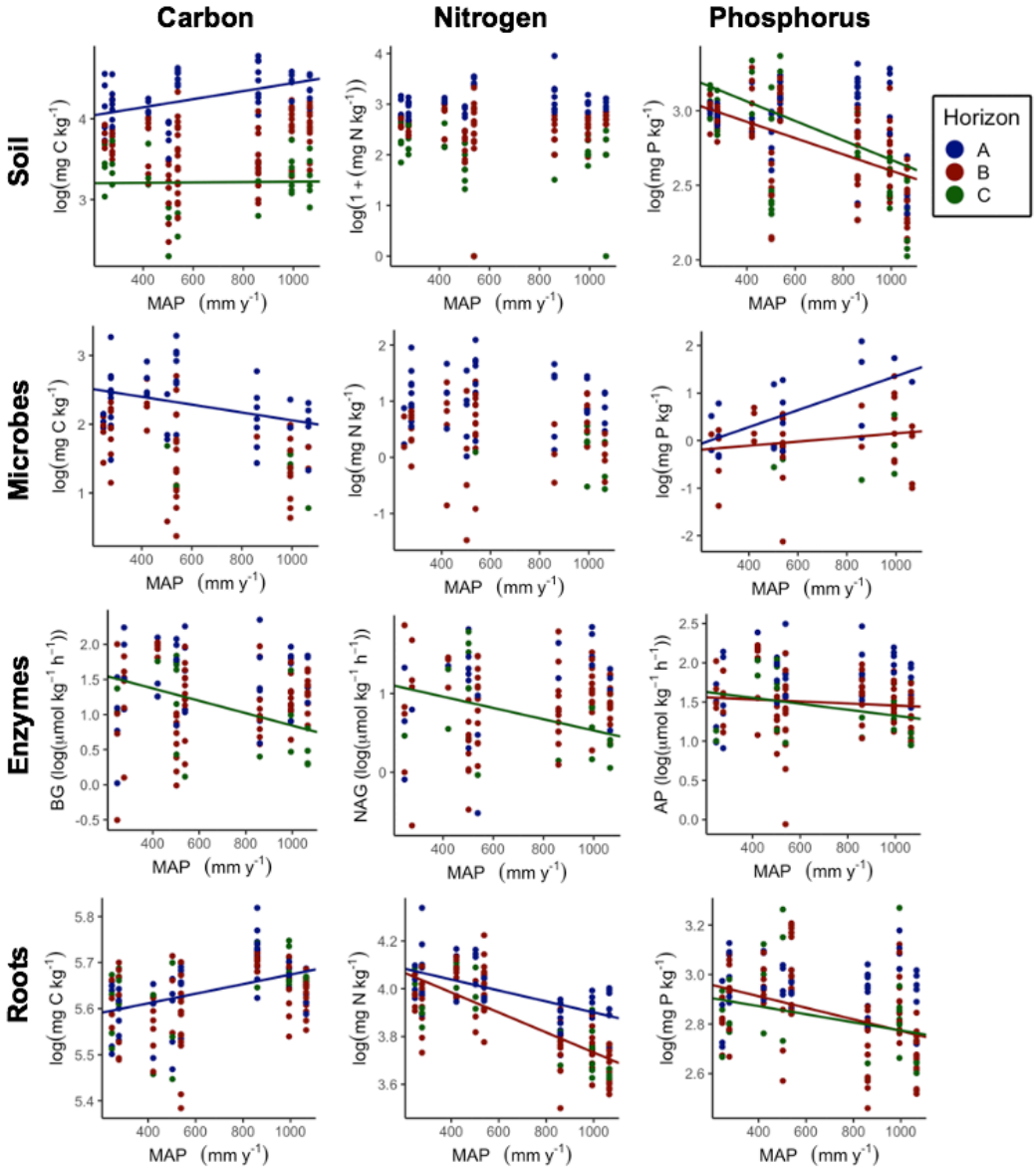

Figure 3-1. Relationships between mean annual precipitation (MAP) and carbon (C), nitrogen (N), and phosphorus (P) in soil, microbial biomass, potential enzyme activity, and fine roots for each master soil horizon. Mixed effect model regression lines are only plotted when significant ($\alpha = 0.05$). B and C horizons, when included, indicate the relationship of the B or C horizon is significantly different than A horizons (0-coded group) with MAP. Nutrient concentrations (mg nutrient kg^{-1}) and enzyme activities (μmol kg^{-1} h^{-1}) were log transformed to meet model assumptions (N concentration was value + 1 due to zeros). Sample sizes are included in Table S2.

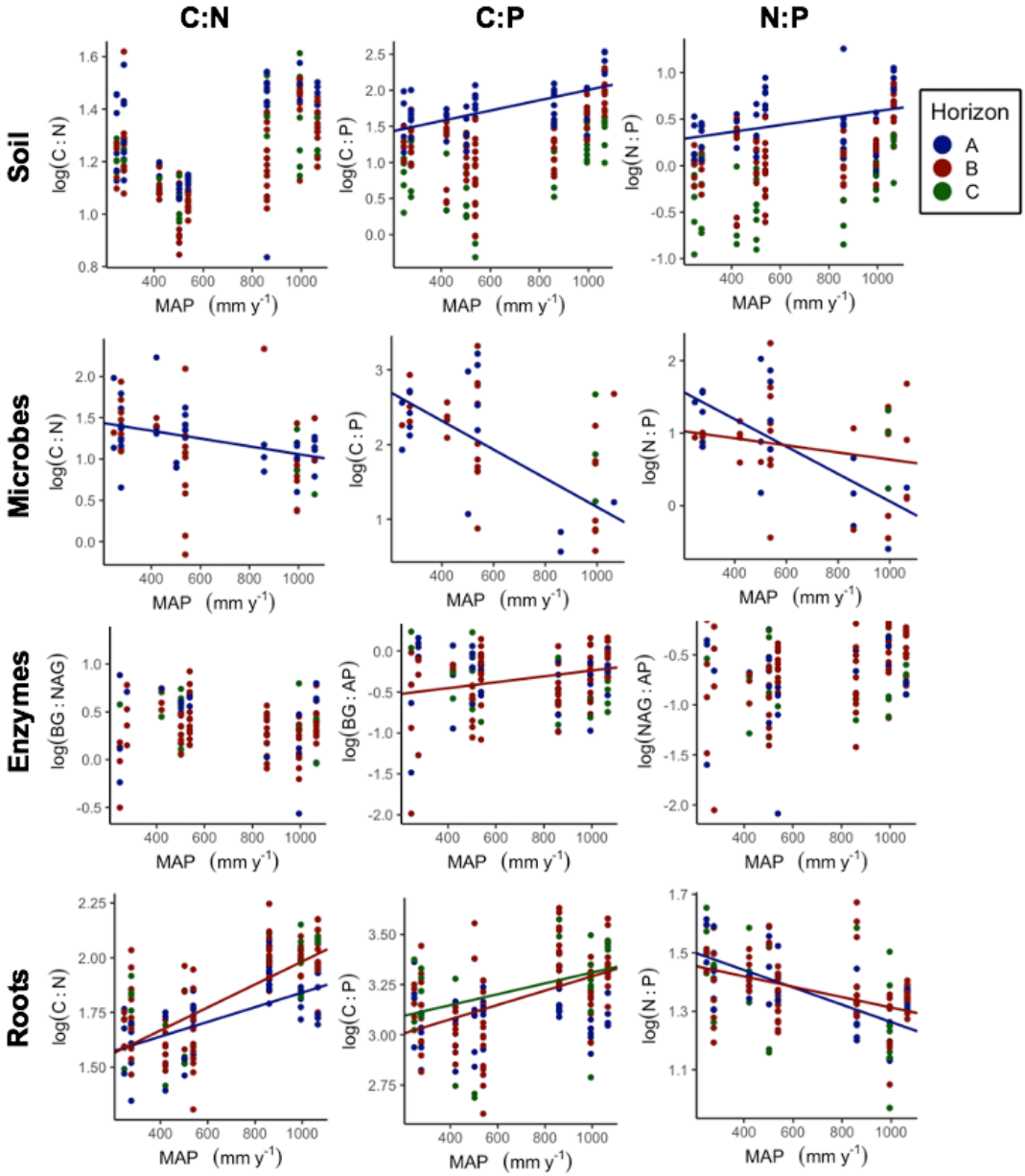

Figure 3-2. Relationships between mean annual precipitation (MAP) and molar carbon:nitrogen (C:N), C:phosphorus (C:P), and N:P in soil, microbial biomass, potential enzyme activity, and fine roots for each master soil horizon. Mixed effect model regression lines are only plotted when significant ($\alpha = 0.05$). B and C horizons, when included, indicate the relationship of the B or C horizon is significantly different than A horizons (0-coded group) with MAP. C horizons were not included for microbial biomass C:P or N:P models due to the low sample size. Sample sizes are included in Table 2.

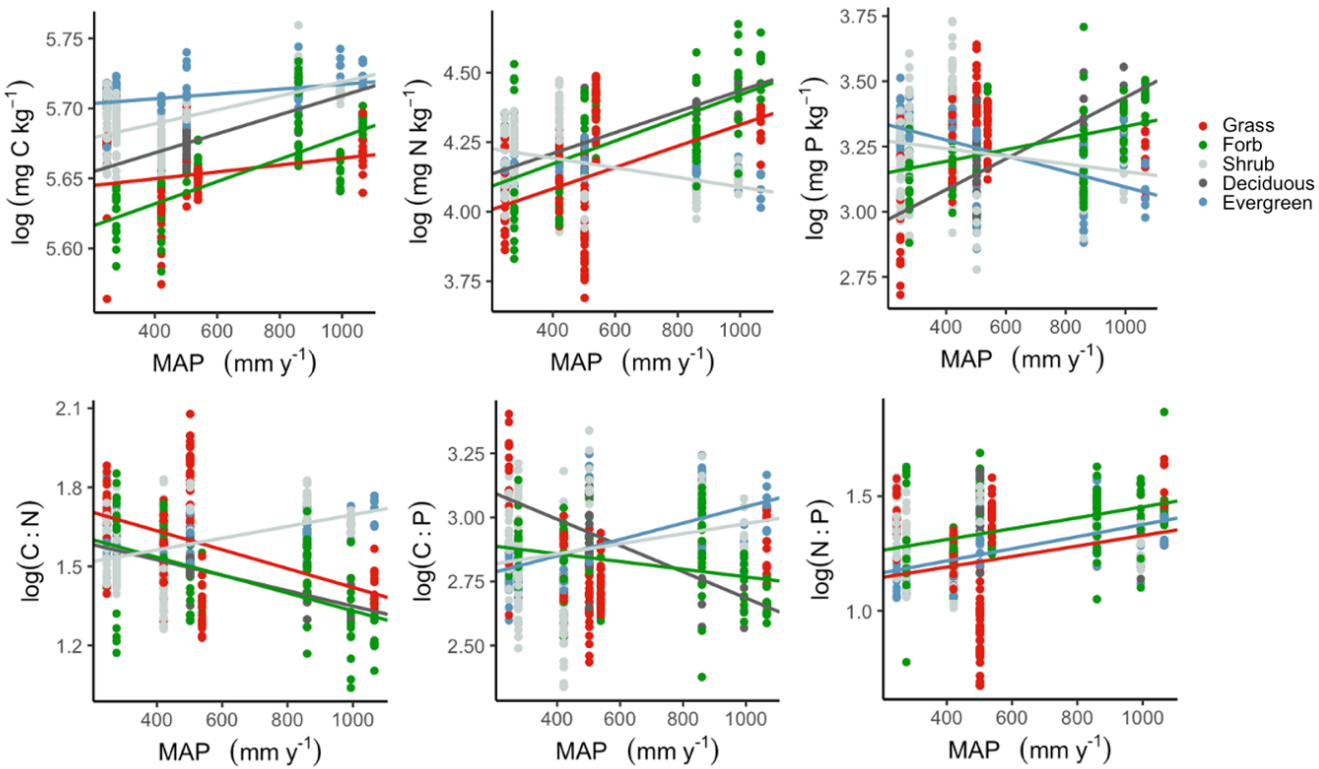

Figure 3-3. Relationships between carbon (C), nitrogen (N), and phosphorus (P) concentrations and molar C:N, N:P, and N:P stoichiometry for grass, forb, shrub, deciduous, and evergreen vegetation functional groups using photosynthetic material. Linear model regression lines are only included when the relationship was significant ($\alpha = 0.05$). Sample sizes are included in Tables 3 and S3.

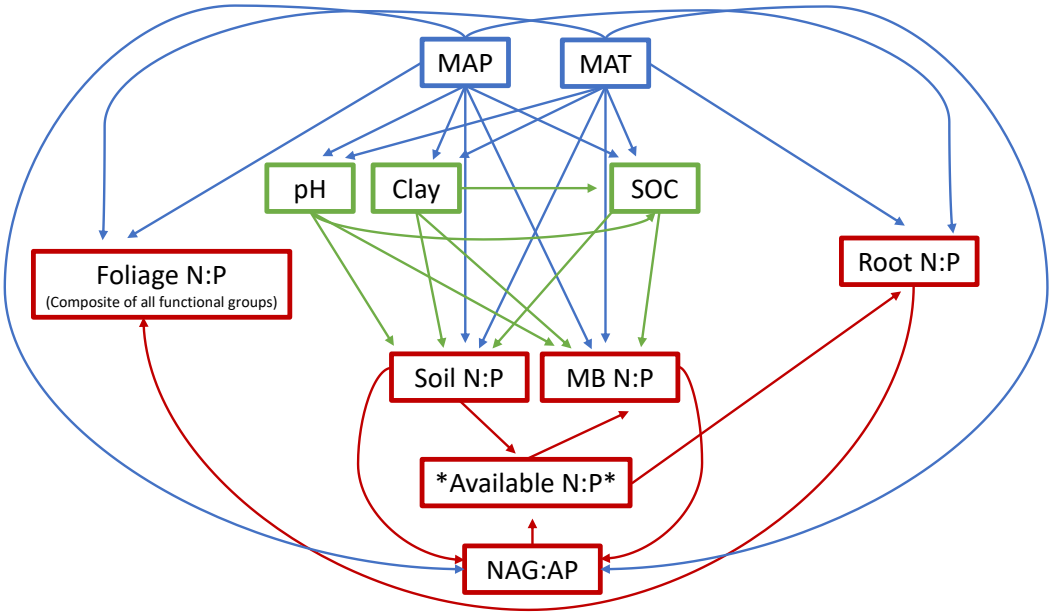

Figure 3-4. Initial conceptual model designed to represent hypothesized relationships between climate, soil properties, and ecosystem stoichiometry. All boxes are measured variables where a latent variable of available nitrogen:phosphorus (N:P) is denoted by asterisks. Foliage N:P was as separate models for evergreen trees, woody shrubs, and forbs. Variables or paths from this hypothesized model were modified over multiple iterations to report the most robust and succinct structural equation models based on AIC criterion.

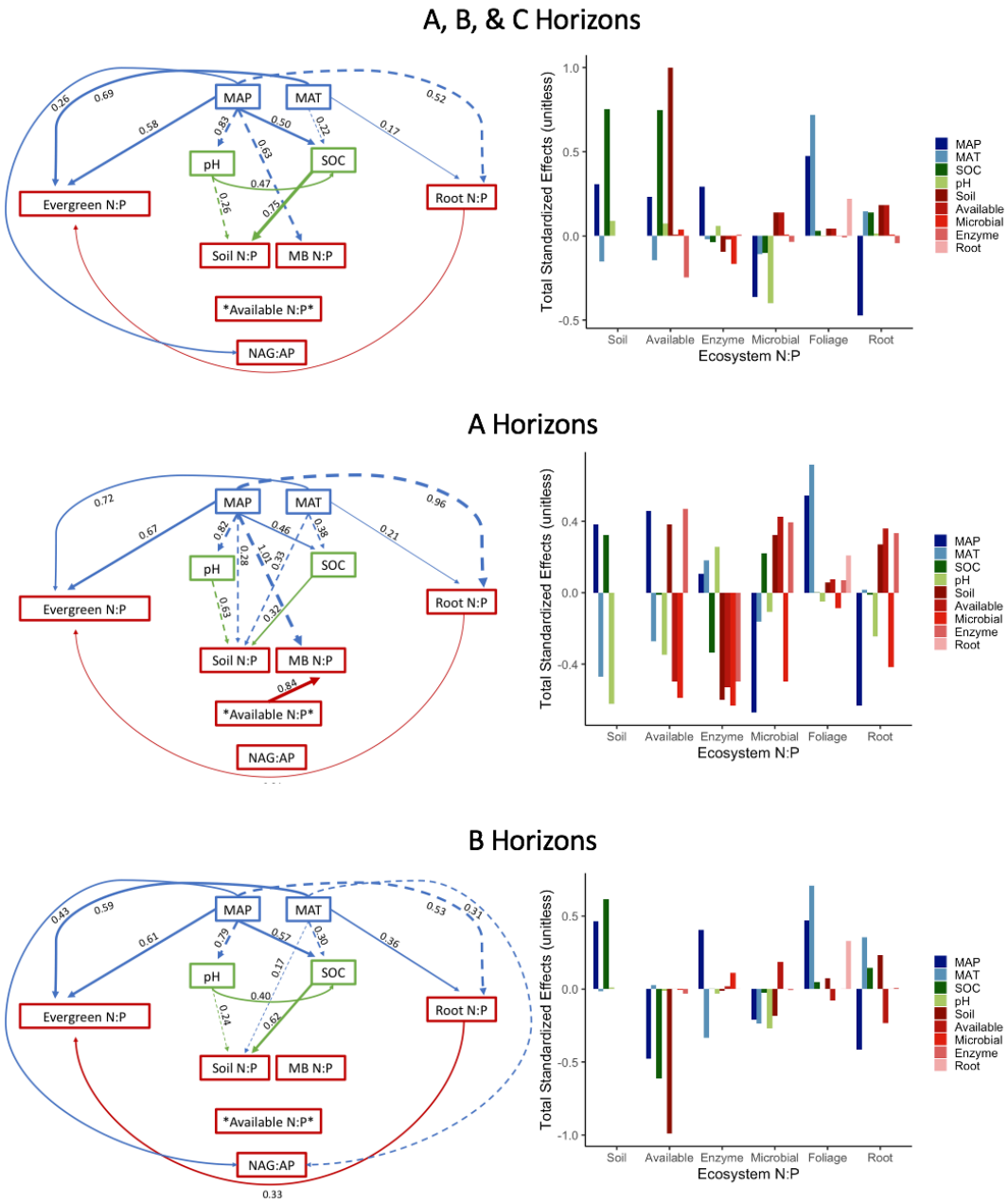

Figure 3-5. Final structural equation models in all (A + B + C), A, or B horizons representing direct climate (MAP and MAT) impacts on soil, microbial biomass, potential enzyme activity, fine root, and aboveground evergreen foliage nitrogen:phosphorus (N:P) and the indirect climatic effects on ecosystem stoichiometry due to changes in soil properties (pH, soil organic carbon). Only significant relationships are reported ($\alpha = 0.05$). Standardized correlation coefficients, analogous to relative regression weights, are included next to the paths. Path line thickness is positively related to the coefficient, and are solid when the relationship is positive or dashed when negative. Statistics for all horizon model: $\chi^2 = 65.5$, $p < 0.05$, df = 11, $\chi^2/df = 6.0$, RMSEA = 0.16,

AIC = 151; A horizon model: $\chi^2 = 35.0$, $p < 0.05$, df = 11, $\chi^2/df = 3.2$, RMSEA = 0.2, AIC = 121; B horizon model: $\chi^2 = 54.7$, $p < 0.05$, df = 11, $\chi^2/df = 5.0$, RMSEA = 0.2, AIC = 141.

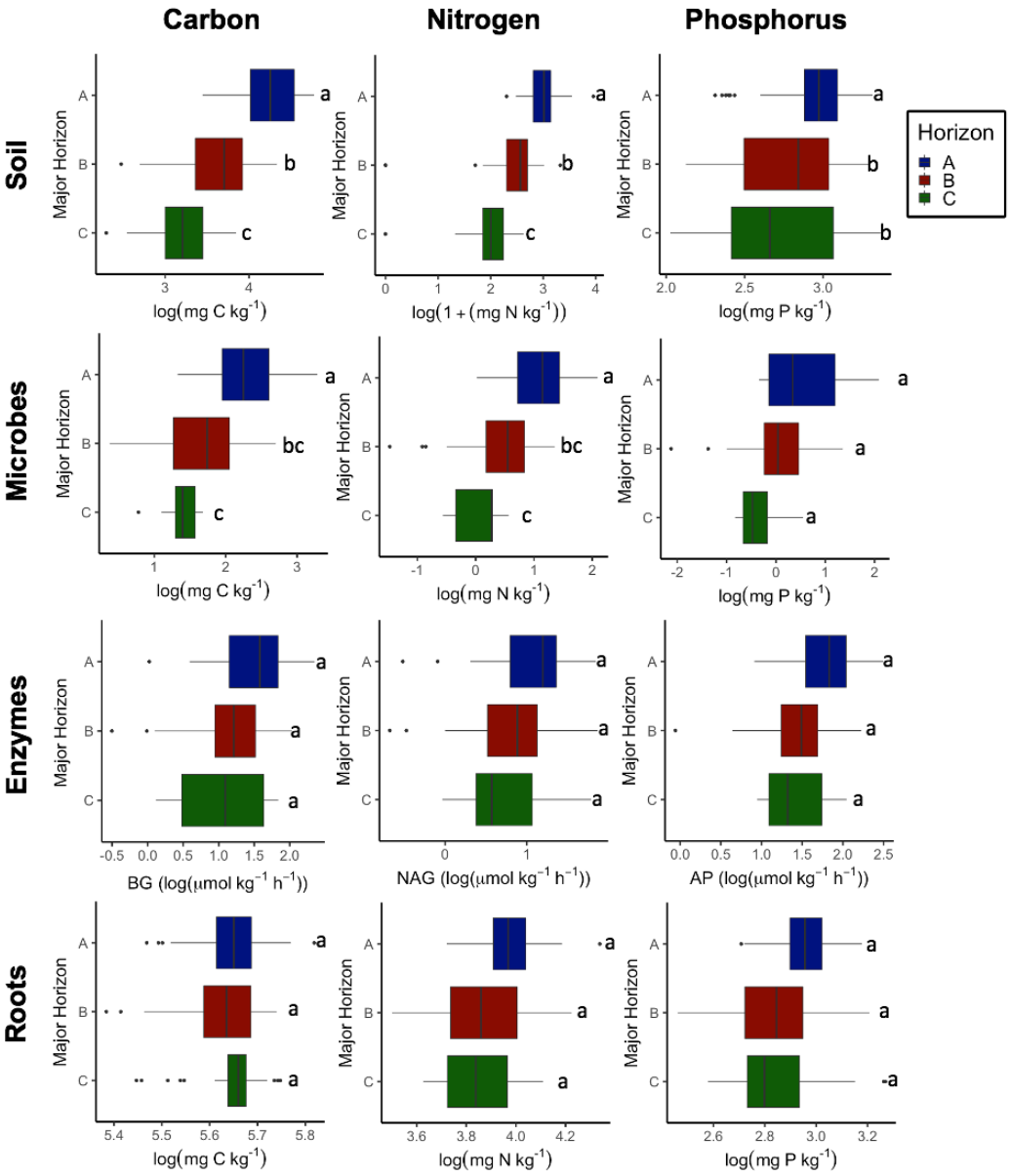

Figure 3-6. Median and distribution of log transformed carbon (C), nitrogen (N), and phosphorus (P) in soil (mg nutrient kg^{-1}), microbial biomass (mg nutrient kg^{-1}), potential enzyme activity (μmol kg^{-1} h^{-1}), and fine roots (mg nutrient kg^{-1}) of master soil horizons across all sites. The box represents the 25th and 75th percentiles, whiskers are the highest and lowest values within 1.5 x the inter-quartile range (i.e., distance between 25th and 75th percentiles), and points outside the box are outliers. Lowercase letters represent significantly different master soil horizons from the mixed effects model (Table S2). Tukey's post-hoc tests were conducted when B or C horizons were significantly different than A (0-coded group) to determine significance between B and C horizons. Horizons are considered significantly different when $\alpha = 0.05$. Sample sizes are included in Table S2.

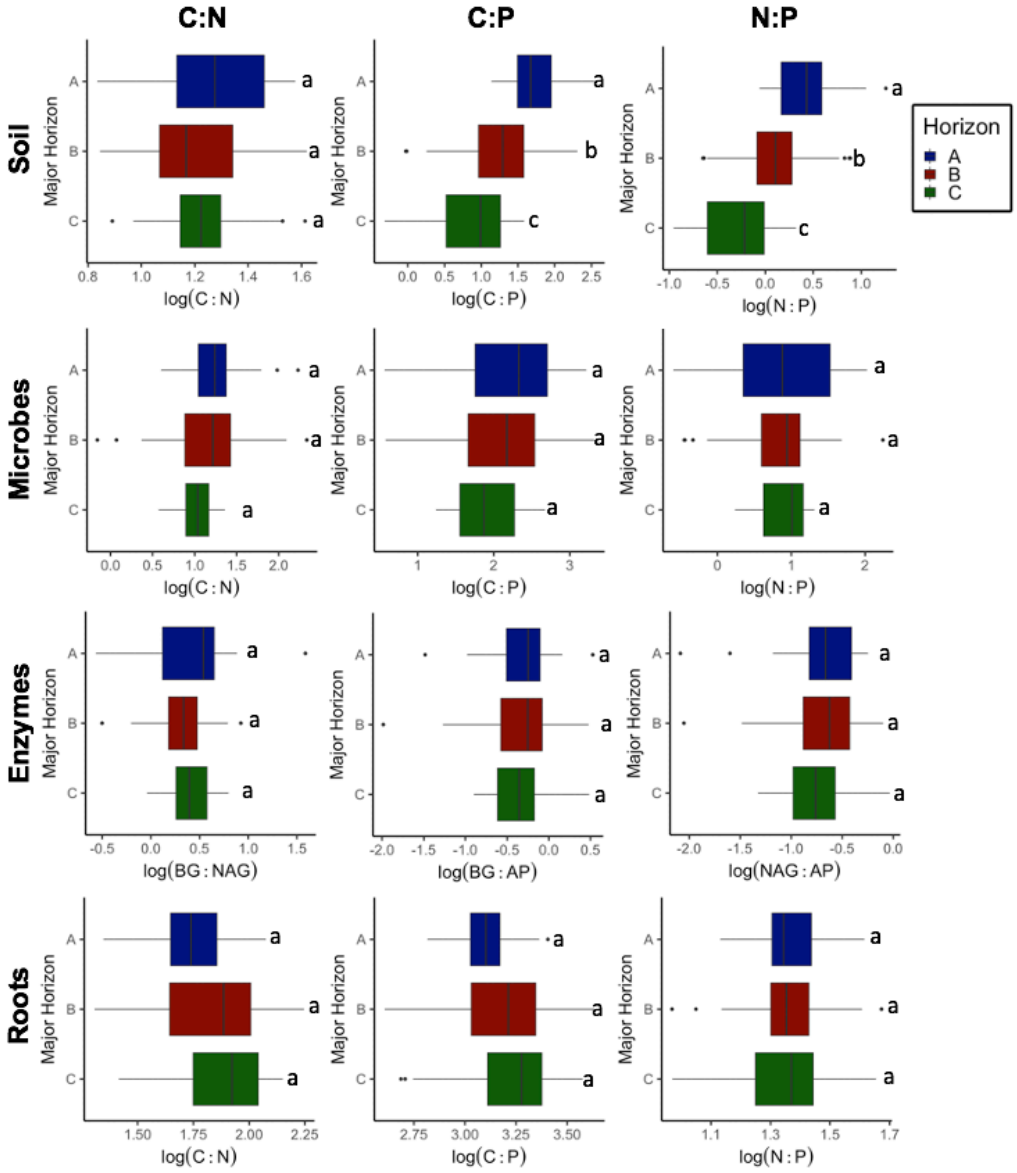

Figure 3-7. Median and distribution of molar carbon:nitrogen (C:N), C:phosphorus (C:P), and N:P in soil, microbial biomass, potential enzyme activity, and fine roots of master soil horizons across all sites. The box represents the 25th and 75th percentiles, whiskers are the highest and lowest values within 1.5 x the inter-quartile range (i.e., distance between 25th and 75th percentiles), and points outside the box are outliers. Lowercase letters represent significantly different master soil horizons from the mixed effects model (Table 2). Tukey's post-hoc tests were conducted when B or C horizons were significantly different than A (0-coded group) to determine significance between B and C horizons. Horizons are considered significantly different when $\alpha = 0.05$. Sample sizes are included in Table 2.

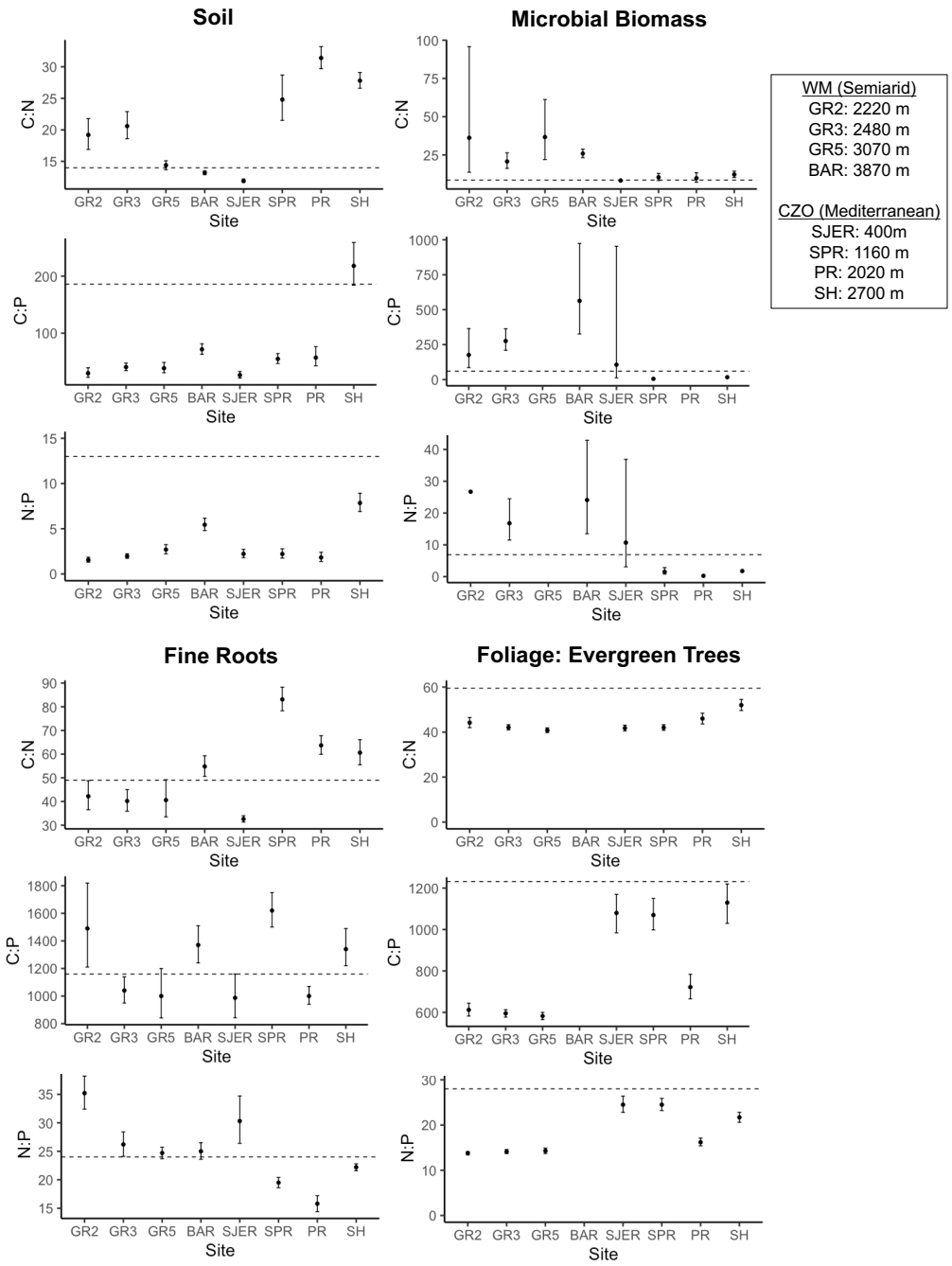

Figure 3-8. Geometric mean and standard error of A horizon soil, microbial biomass, fine root, and aboveground foliage carbon:nitrogen (C:N), C:phosphorus (C:P), and N:P. The dotted line indicates global averages of stoichiometric ratios from Cleveland and Lipzin (2007) for soil and microbial biomass, Jackson et al. (1997) for fine roots, and McGroddy et al. (2004) for temperate evergreen foliage. Sites are in order of increasing elevation for the semiarid White Mountain Elevational Transect (GR2, GR3, GR5, and BAR) and the Southern Sierra Critical Zone Observatory (SJER, SPR, PR, SH), and additional site characteristics are described in Table 1.

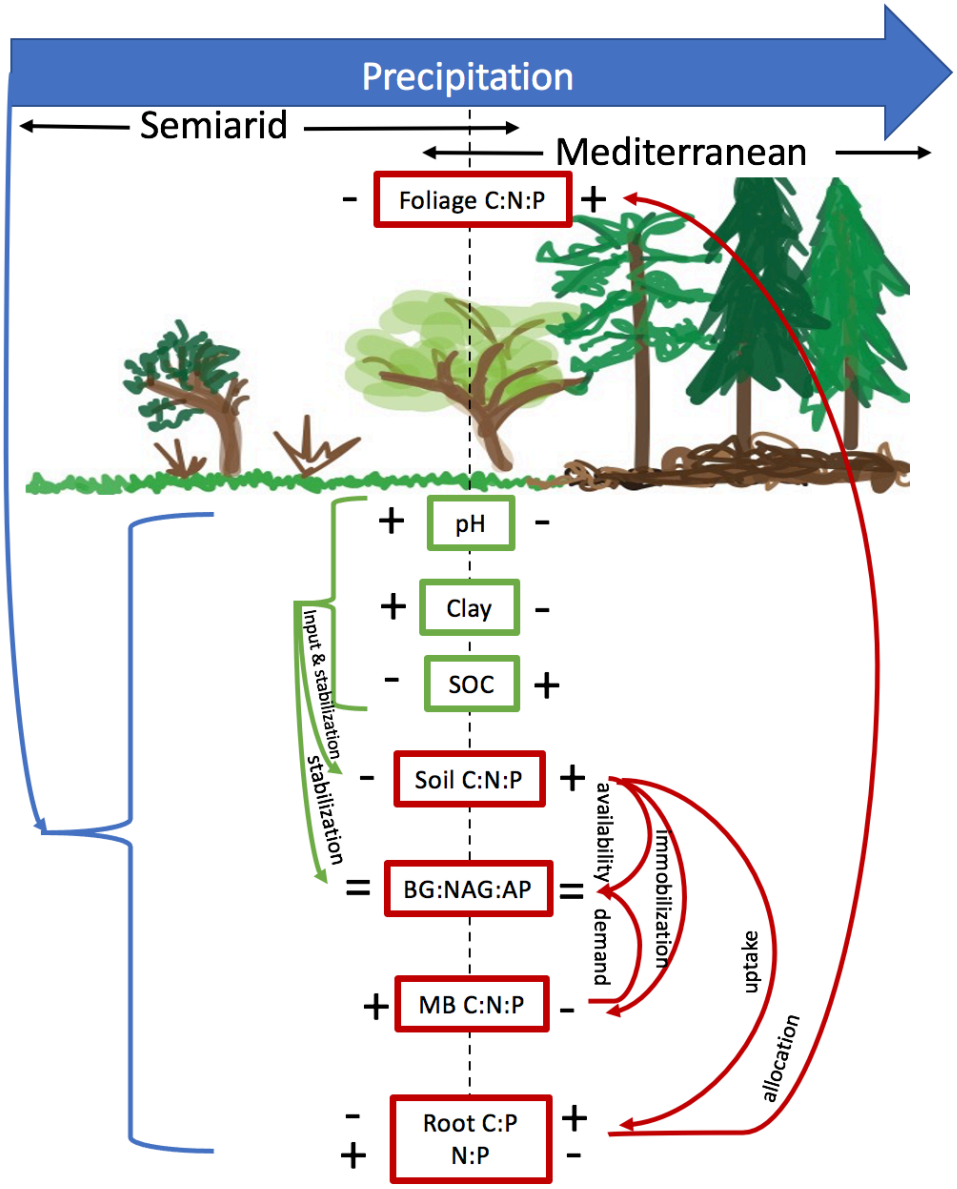

Figure 3-9. Conceptual model demonstrating how increases in precipitation moving from semiarid to Mediterranean climates impacts pH, clay, and soil organic carbon (SOC). These soil properties can stabilize soil nutrients and extracellular enzymes. Soil nutrients impact the carbon:nitrogen:phosphorus (C:N:P) stoichiometry of the microbial biomass and roots through immobilization and uptake, respectively. Availability of soil nutrients and microbial biomass demand dictates enzyme activity. Nutrients are then allocated from roots to aboveground foliage.

3.10 Supplementary Tables

Table 3-S1. List of species collected for foliage carbon (C), nitrogen (N), and phosphorus (P) analyses at each site at the semiarid White Mountain (WM) and Mediterranean Critical Zone Observatory (CZO) elevational gradients based on functional group. No data (nd) indicates the functional group was not collected at a site. Site characteristics are described in Table 1.

Gradient	Site	Elevation (m)	Evergreen	Deciduous	Shrub	Forb	Grass
WM	GR2	2220	*Pinus edulis*	nd	*Artemisia tridentate, Chrysothamus viscidiflorus, Ephedra nevadensis*	*Eriogonum ovalifolium*	*Hesperostipa comate, Achanterum speciosus*
WM	GR3	2480	*Pinus edulis*	nd	*Artemisia tridentate, Chrysothamus viscidiflorus, Ephedra nevadensis*	*Eriogonum ovalifolium, Linanthus pungens*	nd
WM	GR5	3070	*Pinus edulis*	nd	*Artemisia tridentate, Chrysothamus viscidiflorus, Ephedra nevadensis*	*Eriogonum ovalifolium, Linanthus pungens*	*Achanterum speciosus, Elymus elymoides*
WM	BAR	3870	nd	nd	nd	*Eriogonum ovalifolium*	*Achanterum speciosus, Elymus elymoides*
CZO	SJER	400	*Pinus sabiniana*	*Quercus douglasii, Quercus wislizenii*	*Ceanothus leucodermis*	*Croton setiger*	*Aveca barbata, Bromus diandrus, Bromus hordeaceus*
CZO	SPR	1160	*Pinus ponderosa*	*Quecus chrysolepis, Quecus kelloggii*	*Arctostaphylos biscida*	*Chamaebatia foliolosa, Ribes montigenum*	nd
CZO	PR	2020	*Pinus jeffreyi*	*Quecus kelloggii*	*Arctostaphylos patula, Ceanothus velutinus*	*Ribes montigenum*	nd
CZO	SH	2700	*Pinus contorta spp. murrayana*	nd	nd	*Eriogonum ovalifolium*	nd

Table 3-S2. Results of mixed effect models to investigate the relationships between soil, microbial biomass, enzyme activity, and fine root molar carbon (C), nitrogen (N), and phosphorus (P) with mean annual precipitation (MAP), master soil horizon (A, B, and C; A = 0-coded), and their interaction (MAP x B and MAP x C). Coefficients (bolded when $\alpha = 0.05$), marginal R^2 (only fixed effects), and sample size (n) are reported. Nutrient concentrations (mg nutrient kg^{-1}) and enzyme activities (μmol kg^{-1} h^{-1}) were log transformed to meet model assumptions (soil N concentration was value + 1 transformed due to zeros).

Sample	Nutrient	Intercept	MAP	B	C	MAP x B	MAP x C	R^2	n
Soil	C	3.9	**0.00050**	**-0.51**	**-0.74**	-0.00021	**-0.00048**	0.52	185
	N	2.9	0.00016	**-0.56**	**-0.84**	-0.000062	-0.00040	0.35	185
	P	3.1	-0.00022	0.082	**0.26**	**-0.00033**	**-0.00065**	0.34	186
Enzyme	C	1.4	0.00012	-0.31	0.30	-0.00017	**-0.0010**	0.13	139
	N	0.65	0.00061	0.018	0.60	-0.00038	**-0.0013**	0.10	113
	P	1.5	0.00041	0.069	0.19	**-0.00054**	**-0.00079**	0.15	149
Microbe	C	2.6	**-0.00057**	**-0.60**	-0.98	-0.000092	0.00026	0.38	98
	N	1.1	-0.000089	**-0.61**	-0.91	-0.000052	-0.00011	0.31	100
	P	-0.43	**0.0018**	0.15	-0.43	**-0.0014**	-0.0012	0.29	63
Root	C	5.6	**0.00011**	-0.022	0.0048	-0.0000016	-0.0000050	0.19	167
	N	4.1	**-0.00023**	0.022	-0.029	**-0.00019**	-0.00013	0.58	158
	P	2.9	0.000065	0.089	0.021	**-0.00030**	**-0.00023**	0.21	158

Table 3-S3. Linear regression model coefficients and R^2 for the relationship of aboveground vegetation photosynthetic material carbon (C), nitrogen (N), and phosphorus (P) concentrations (mg kg^{-1}) with mean annual precipitation (MAP). Separate models were ran for different functional groups (grass, forb, shrub, deciduous, and evergreen) and concentrations were log transformed to meet model assumptions.

Functional Group	Ratio	MAP	R^2	n
Grass	C	**0.000024**	0.03	106
	N	**0.00038**	0.14	107
	P	0.00015	0.02	107
Forb	C	**0.000080**	0.46	107
	N	**0.00041**	0.36	109
	P	**0.00022**	0.14	109
Shrub	C	**0.000050**	0.32	128
	N	**-0.00017**	0.08	128
	P	**-0.00015**	0.02	128
Deciduous	C	**0.000068**	0.43	22
	N	**0.00038**	0.62	23
	P	**0.00059**	0.50	23
Evergreen	C	**0.000017**	0.13	86
	N	-0.000023	<0.01	90
	P	**-0.00030**	0.31	90

Table 3-S4. Site foliar carbon:nitrogen (C:N), C:phosphorus (C:P), and N:P geometric mean, lower and upper standard error, and sample size for evergreen, deciduous, shrub, forb, and grass functional groups. Site characteristics are described in Table 1. Not all functional groups were present at each site and when n=1, standard error is indicated by no data (nd).

			----------Foliage C:N----------				**----------Foliage C:P----------**				**----------Foliage N:P----------**			
Gradient	Site	Functional Group	Mean	Lower SE	Upper SE	Sample Size	Mean	Lower SE	Upper SE	Sample Size	Mean	Lower SE	Upper SE	Sample Size
WM	GR2	Evergreen	44.2	42.0	54.2	16	612	582	751	16	13.8	13.4	15.4	17
		Shrub	36.8	35.2	46.5	27	910	858	1240	27	24.8	23.5	32.5	27
		Forb	26.1	nd	nd	1	591	nd	nd	1	22.6	nd	nd	1
		Grass	50.8	46.1	72.1	13	1410	1220	2340	13	27.7	26.0	34.8	13
	GR3	Evergreen	42.1	41.0	47.1	18	595	577	677	18	14.1	13.7	16.1	18
		Shrub	35.5	33.9	47.3	35	667	617	1060	35	18.8	17.9	24.9	35
		Forb	37.6	32.7	65.5	16	827	781	1040	16	20.4	17.8	35.2	16
	GR5	Evergreen	40.8	39.8	44.1	9	582	565	637	9	14.3	13.7	16.1	9
		Shrub	30.0	28.0	45.2	35	479	443	758	35	16.0	15.3	20.1	35
		Forb	38.0	36.3	47.4	23	622	580	876	23	16.4	15.8	19.6	23
		Grass	35.5	33.5	47.0	22	617	578	844	22	17.4	16.8	20.4	22
	BAR	Forb	24.5	23.2	28.6	9	475	448	562	9	19.4	19.0	20.5	9
		Grass	21.4	20.6	26.1	24	559	537	687	24	26.1	25.3	30.4	24
CZO	SJER	Evergreen	41.8	40.5	47.0	14	1080	984	1500	14	24.5	22.8	32.7	16
		Deciduous	31.4	30.2	36.0	12	880	796	1240	12	28.0	25.8	37.2	12
		Shrub	54.0	51.2	62.0	7	1480	1360	1870	7	27.4	25.0	35.0	7
		Forb	25.9	24.3	32.4	12	893	832	1140	12	34.5	32.6	42.1	12
		Grass	64.0	60.5	89.8	35	529	501	722	35	8.2	7.8	11.1	36
	SPR	Evergreen	42.0	40.8	47.7	18	1070	998	1460	18	24.5	23.2	31.1	18
		Deciduous	23.6	22.5	26.1	5	532	471	701	5	22.5	20.5	28.0	5
		Shrub	56.5	54.9	62.4	12	1210	1150	1430	12	21.4	20.4	25.0	12
		Forb	30.8	28.9	41.4	22	804	733	1240	22	26.1	24.5	35.5	24
	PR	Evergreen	46.0	43.6	51.7	5	722	665	869	5	16.2	15.4	18.4	6
		Deciduous	23.0	21.3	27.3	5	514	460	660	5	22.4	20.0	29.5	6
		Shrub	45.0	44.1	48.5	12	855	808	1040	12	19.0	18.0	22.7	12

	Forb	19.3	17.4	27.8	12	541	510	663	12	28.0	25.4	39.7	12
SH	Evergreen	52.0	49.6	58.4	6	1130	1030	1380	6	21.7	20.6	24.6	6
	Forb	17.2	16.4	20.1	12	459	445	511	12	29.5	27.1	39.7	12
	Grass	26.1	24.9	30.5	12	774	720	996	12	29.7	27.3	39.6	12

3.11 Supplementary Figures

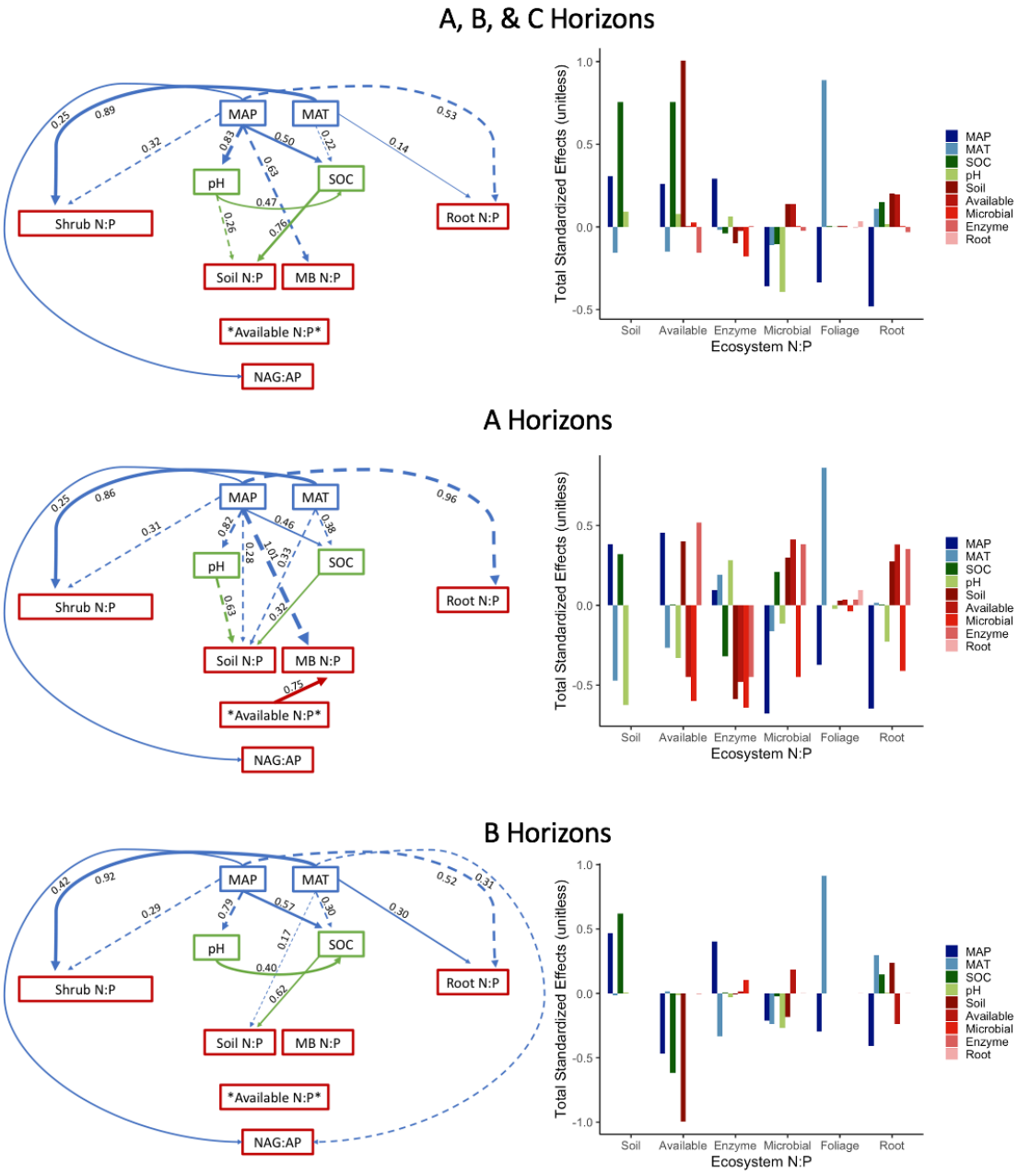

Figure 3-S1. Final structural equation models in all (A + B + C), A, or B horizons representing direct climate (MAP and MAT) impacts on soil, microbial biomass, potential enzyme activity, fine root, and aboveground shrub foliage nitrogen:phosphorus (N:P) and the indirect climatic effects on ecosystem stoichiometry due to changes in soil properties (pH, soil organic carbon). Only significant relationships are reported (α = 0.05). Standardized correlation coefficients, analogous to relative regression weights, are included next to the paths. Path line thickness is positively related to the coefficient, and are solid when the relationship is positive or dashed when negative. Statistics for all

horizon model: $\chi^2 = 33.9, p < 0.05$, df = 11, χ^2/df = 3.1, RMSEA = 0.11, AIC = 120; A
horizon model: $\chi^2 = 17, p = 0.11$, df = 11, χ^2/df = 1.5, RMSEA = 0.1, AIC = 103; B
horizon model: $\chi^2 = 28.4, p < 0.05$, df = 11, χ^2/df = 2.6, RMSEA = 0.13, AIC = 114.

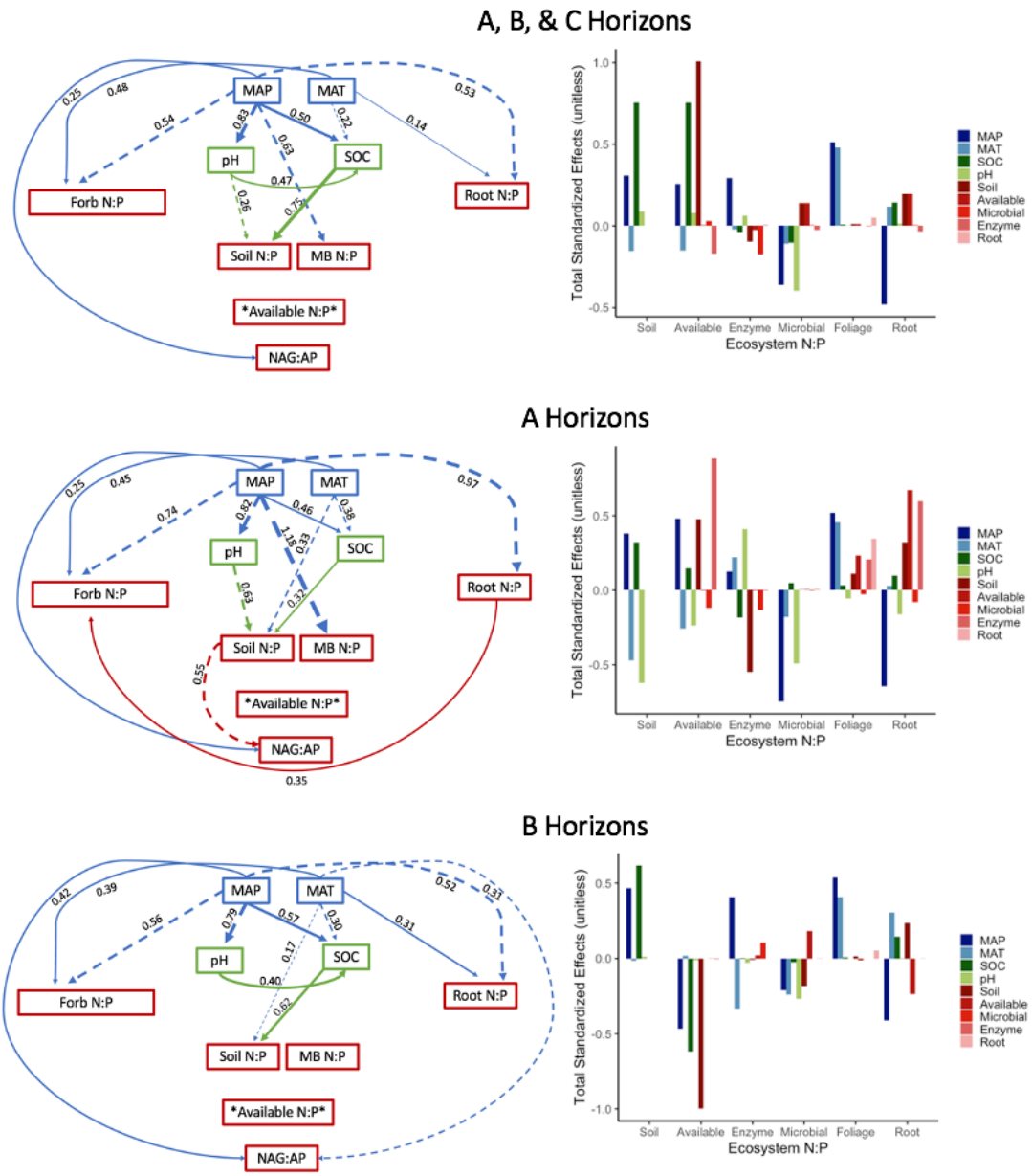

Figure 3-S2. Final structural equation models in all (A + B + C), A, or B horizons representing direct climate (MAP and MAT) impacts on soil, microbial biomass, potential enzyme activity, fine root, and aboveground forb foliage nitrogen:phosphorus (N:P) and the indirect climatic effects on ecosystem stoichiometry due to changes in soil properties (pH, soil organic carbon). Only significant relationships are reported (α = 0.05). Standardized correlation coefficients, analogous to relative regression weights, are included next to the paths. Path line thickness is positively related to the coefficient, and are solid when the relationship is positive or dashed when negative. Statistics for all horizon model: $\chi^2 = 116$, $p < 0.05$, df = 11, χ^2/df = 10.5, RMSEA = 0.23, AIC = 202; A horizon model: $\chi^2 = 48$, $p < 0.05$, df = 11, χ^2/df = 4.4, RMSEA = 0.25, AIC = 134; B horizon model: $\chi^2 = 65$, $p < 0.05$, df = 11, χ^2/df = 5.9, RMSEA = 0.25, AIC = 151.

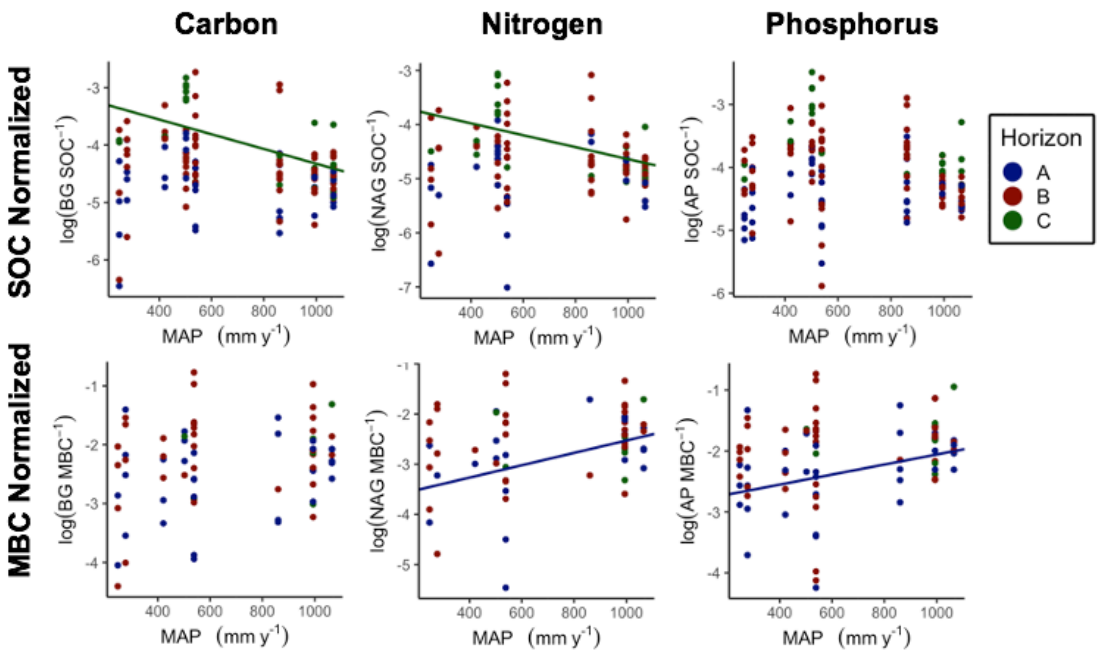

Figure 3-S3. Relationships between mean annual precipitation (MAP) and β-glucosidase (BG), N-acetylglucosaminidase (NAG), and acid phosphatase (AP) potential enzyme activity normalized to soil organic carbon (SOC) and microbial biomass carbon (MBC) for each master soil horizon. Mixed effect model regression lines are only plotted when significant ($\alpha = 0.05$). B and C horizons, when included, indicate the relationship of the B or C horizon is significantly different than A horizons (0-coded group) with MAP.

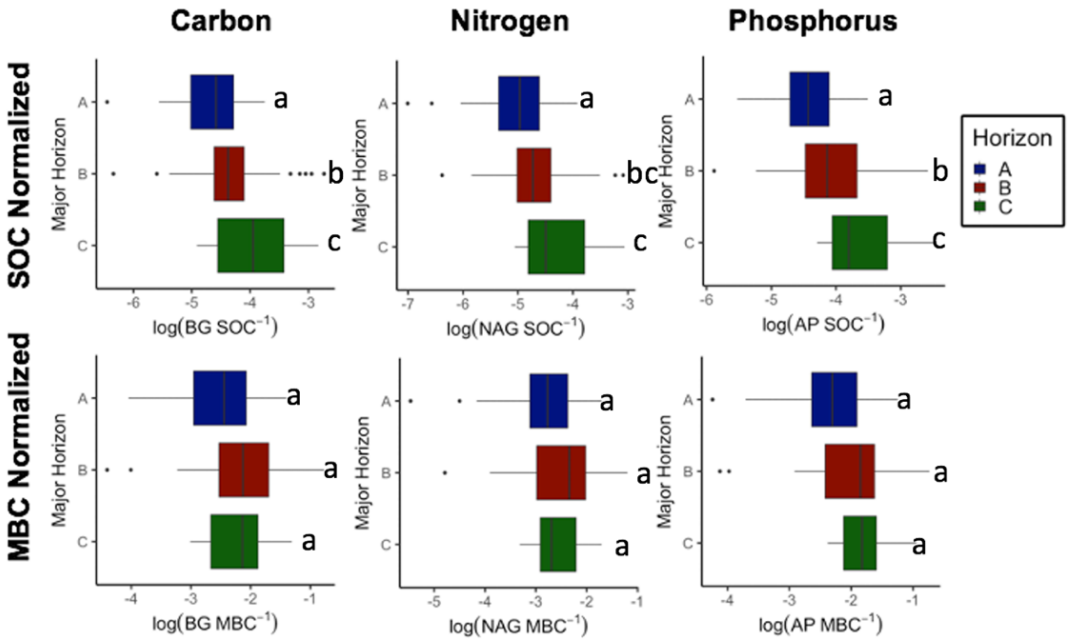

Figure 3-S4. Median and distribution of β-glucosidase (BG), N-acetylglucosaminidase (NAG), and acid phosphatase (AP) potential enzyme activity normalized to soil organic carbon (SOC) and microbial biomass carbon (MBC) in master soil horizons across all sites. The box represents the 25th and 75th percentiles, whiskers are the highest and lowest values within 1.5 x the inter-quartile range (i.e., distance between 25th and 75th percentiles), and points outside the box are outliers. Lowercase letters represent significantly different master soil horizons from the mixed effects model. Tukey's post-hoc tests were conducted when B or C horizons were significantly different than A (0-coded group) to determine significance between B and C horizons. Horizons are considered significantly different when $\alpha = 0.05$.

4 The Median Isn't the Message: Elucidating Nutrient Hot Spots and Hot Moments in a Sierra Nevada Forest Soil

4.1 Abstract

Hot spots (HS) and hot moments (HM) of nutrients under contrasting biogeochemical cycles were investigated by assessing long-term spatial and temporal patterns at two plots in coarse-textured Sierra Nevada forest soils derived from granite (Humic Dystroxerepts). Nutrient fluxes were measured in a 6- x 6-m grid with resin capsules installed at 0-, 20-, 40-, and 60-cm that were collected during the fall and spring over a 4-year period (fall 2011 through spring 2016; no collection in WY2015). Hot spots, or areas where elevated nutrient flux persisted throughout time, formed more readily for nutrients under biological control (PO_4^{3-}, NH_4^+, NO_3^-) than those under geochemical control (Ca^{2+}, Mg^{2+}, and Na^+). More HS-HM were identified in the upper soil profile for all nutrients. Geochemically controlled nutrients produced a greater number of HM, or areas where elevated flux was transient, and they tended to persist deeper into the soil profile than nutrients under biological control. Multiple nutrient HS-HM commonly co-occurred together in space. The formation of nutrient flux outliers underpins the identification of both HS and HM. To better understand the underlying patterns in outlier formation, mixed effect models were used to identify trends in time (i.e., water year and season) and space (i.e., depth). A multi-year drought occurred from WY2012-2015 which dampened the occurrence of outliers, particularly for geochemically controlled nutrients. Outliers were more prevalent in the fall, after the first major precipitation event, for biologically-controlled nutrients along with Na^+, whereas Ca^{2+} outliers formed more readily after snowmelt in the spring. Overall, the persistent formation of biologically controlled outliers, even over contrasting water years and different seasons, designated them as HS. Biologically controlled HS-HM likely play a major role in ecosystem development as these macronutrients are persisting over time in some locations as HS, found at higher concentrations relative to the surrounding soil matrix, and are co-occurring in discrete spatial locations where belowground biomass can detect, proliferate, and exploit these resources.

4.2 Introduction

Understanding the ecological significance, spatial and temporal patterns, and biotic and abiotic controls of soil nutrient heterogeneity remains a frontier in terrestrial ecosystem science (Lovett et al. 2005; Turner and Gardner 2015). Plants can exhibit a morphological response to soil nutrient patchiness by actively foraging, or a physiological response by increasing specific root nutrient uptake rates, in spatial locations with elevated nutrients (Robinson 1994). These responses can provide an interspecific competitive advantage to species that have the capacity to exploit these nutrient-rich patches (Hodge et al. 1999; Robinson et al. 1999; Wang et al. 2018), lead to increased shoot biomass in populations (Day et al. 2003), and impact biodiversity and structure at the community level (Wijesinghe et al. 2005; Maestre et al. 2005; Maestre and Reynolds 2007; García Palacios et al. 2011). Plants that utilize nutrient rich patches can also outcompete microorganisms for these resources over the long-term (Kaye and Hart 1997; Schimel and Bennet 2004; Hodge et al. 2000).

The existence of areas of elevated biogeochemical activity in soil have been recognized by the terrestrial ecological community for a long-time as so-called "hot spots" (HS; Parkin 1987; Hill et al. 2000; McClain et al. 2003; Vidon et al. 2010). Biogeochemical activity can also be "hot" in the temporal dimension; these so-called "hot moments" (HM; McClain et al. 2003; Vidon et al. 2010) are defined by a high rate of biogeochemical activity occurring at a specific location for a short period of time relative to the rate observed in the bulk soil over longer time periods. Hot spots have been identified quantitatively by their positive skew (Kurunc et al. 2011) and as a statistical outliers in nutrient pool sizes, transformation rates, or fluxes (e.g., Johnson et al. 2010; Darrouzet-Nardi and Bowman 2011). To date, there has been no comparable approach to identify and define HM, frequently causing researchers to not conceptually differentiate between these two phenomena. Many investigations of HS-HM exam the dynamics of only one or two nutrients (Bernhardt et al. 2017) over a relatively short timeframe (i.e., within one year; Gibson 1986; Kleb and Wilson 1997; Johnson et al. 2014; Barcellos et al. 2018), and often use destructive sampling techniques when conducted in the field (i.e., Charley and West 1977; Kleb and Wilson 1997; Bruckner et al. 1999; Farley and Fitter 2001; Washburn and Arthur 2003; Harms and Grimm 2008; Mueller et al. 2008). Taken together, this makes repeated sampling of the same location impossible, and therefore an inability to quantitatively differentiate HS from HM when they are at the same spatial scale, and commonly leads to classifying single spatial points as a HS when it may actually be HM.

It is important to differentiate HS from HM because the factors that control their occurrence are often quite different. For example, HS may occur in localized areas where vegetation centralizes substrate availability due to preferential (wet and dry) atmospheric deposition, throughfall, litterfall, and decreased erosion (Halvorson et al. 1994; Schlesinger et al. 1996; Weathers et al. 2001; Darrouzet-Nardi and Bowman, 2011;). Additionally, depressional topographical positions may form HS relative to upland landscape positions due to the accumulation of material and distinct hydrological characteristics (Harms and Grimm 2008; Barcellos et al. 2018). On a smaller scale, surface microtopography, such as rocks and preferential flowpaths, can funnel soluble

nutrients into the mineral soil to form nutrient and microbial HS (Bundt et al. 2001; Johnson et al. 2011; Frei et al. 2012; Göransson et al. 2014). In contrast, HM are regulated by abiotic or biotic controls that only occur in the short-term to elevate nutrient processing rates or fluxes. For example, pulses of nutrients or microbial activity may only be activated during re-wetting events of dry soil (McClain et al. 2003; Harms and Grimm 2008; Barcellos et al. 2018) or after catastrophic disturbances, such as wildfire (Van Stan et al. 2017). Dead and decaying roots or macrofauna can create biopores that accrue nutrients and serve as microbial HM (Kazyakov and Blagodatskaya 2015; Hoang et al. 2016). Lastly, interactions among soil texture, moisture, and the microbial community can form HM of denitrification after precipitation events in urban soils (Palta et al. 2014). These contrasting controls regulate how long the area is "hot" and dictate the respective impact HS-HM have on the biogeochemical behavior of the ecosystem.

The ability of vegetation to acquire nutrients is likely driven by how species respond to spatially and temporally heterogeneously distributed nutrients. A plant's response to nutrient heterogeneity is impacted by the arrangement of "hot" verse "cold" spatial locations and the timing and frequency of nutrient pulses, the "spot" verse "moment" in relation to plant demand (Jingguo and Bakken 1997; Jackson & Caldwell, 1989; Bilbrough and Caldwell 1997; Fransen et al. 1999; Wijesinghe et al. 2001). For example, a morphological response (root growth) may take longer than a physiological response (increased nutrient uptake rate). Increased nutrient uptake rates have been found to occur between hours to a few days (Drew and Saker 1975; Jackson and Caldwell 1991; Cui and Caldwell 1997), whereas root proliferation ensues between 1 day to a few weeks (Jackson and Caldwell 1989; Caldwell et al., 1991; Cui and Caldwell 1997; Hodge 2004). Therefore, plants that have low morphological plasticity, but a large rooting system that encompass a high volume of soil and can exhibit physiological plasticity, would likely benefit most from HM (Crick and Grime 1987; Cui and Caldwell 1997; Wang et al. 2018), however plants have been found to elicit a morphological response to temporally available nutrients (i.e., HM; Wang et al. 2018).

Forests that experience Mediterranean-type climates like those in the Sierra Nevada are excellent model systems to explore HS-HM phenomena. Nutrient fluxes in Sierran forests are driven largely by activated hydrologic flowpaths that occur primarily following rains in the fall after a prolonged summer dry-period, and following relatively rapid snowmelt in the spring (Williams et al. 1995 Homyak et al. 2014; Hunsaker and Johnson 2017). The frequent and extreme dry-wet cycle results in HS-HM formation (Johnson et al. 2011; Woodward et al. 2013; Johnson et al. 2014). Major findings of a one-year study recognized magnesium (Mg^{2+}) persisted over fall and spring collections to designate some areas as HS, whereas other nutrients (ammonium: NH_4^+, nitrate: NO_3^-, ortho-phosphate: PO_4^{3-}, and calcium: Ca^{2+}) expressed HM because they varied spatially with time (Johnson et al. 2014). Although these studies improved our understanding of HS-HM controls in Mediterranean forests, nutrient flux collections were only done in the fall and spring of a single year and therefore may not represent long-term nutrient dynamics, especially in a changing climate.

Using the same plots and sampling design and building upon the data collected over a one-year period by Johnson et al. (2014), we investigated long-term spatial and temporal patterns in nutrient fluxes in a Sierran mixed-conifer forest using ion exchange

resin capsules. Specifically, we characterized the magnitude and spatial distribution of nutrient fluxes (PO_4^{3-}, NH_4^+, NO_3^-, Na^+, Ca^{2+}, and Mg^{2+}) after the first significant fall rains following the dry summer growing season and after snowmelt in the spring over a four year period. By sampling the soil solution at the same spatial locations (horizontally and vertically) repeatedly over time using ion exchange capsules, we were able to separate operationally the occurrence of nutrient HS from HM. We hypothesized that nutrients whose fluxes through the soil are primarily under biological (i.e., microbial) control would occur more frequently as HM rather than HS because of the need for the co-occurrence of high substrate availability and high microbial activity with activated hydrological flowpaths for high fluxes to occur (McClain et al. 2003). In contrast, we hypothesized that nutrients whose fluxes through the soil are primarily under geochemical control (i.e., chemical weathering, ion exchange reactions) would occur more frequently as HS rather than HM because they are less dependent on high rates of microbial activity which occurs only infrequently in soil (Blagodatskaya and Kuzyakov 2013). We also hypothesized that both HS and HM would occur more frequently in surficial than in deeper soil horizons because microbial activity, nutrient substrate availability, and water fluxes should be highest in the upper soil profile.

4.3 Methods

4.3.1 Site Descriptions

The study area is located on the western slope of the southern Sierra Nevada. This region experiences a Mediterranean-type climate where maximum mean annual air temperature is 14.8 °C, minimum mean annual air temperature is 2.7 °C, and mean annual precipitation is 1015 mm y^{-1}, with ~35-60% falling as winter snow (Hunsaker et al. 2012). The vegetation is a mixed-conifer forest with dominate tree species of sugar pine (*Pinus lambertiana* Douglas), white fir (*Abies concolor* (Gordon & Glend.) Lindl. Ex Hildebr.), ponderosa pine (*Pinus ponderosa* P. Lawson & C. Lawson), and incense cedar (*Calocedrus deucrrens* (Torr.) Florin). Soils are derived from granitic parent material and classified in the Shaver soil series, a coarse-loamy, mixed, superactive, mesic Humic Dystroxerept (Johnson et al. 2014).

4.3.2 Sampling Design

Johnson et al. (2014) established a 6- x 6-m grid of resin capsules (UNIBEST PST-1, https://www.unibestinc.com/technology; UNIBEST Corporation, Washington, USA; Yang and Skogley 1992; Dobermann et al. 1994) at two representative plots within a Sierran mixed-conifer forest. These locations were near the plots where previous field investigations on HS-HM nutrient phenomena took place (Johnson et al. 2011; Woodward et al. 2013). Plot 1 (Lat. 37.061, Long. -119.183) is at an elevation of 1,980 m, eastern aspect, and on a 20% slope, and Plot 2 (Lat. 37.065, Long. -119.203) is at an elevation of 1,910 m, eastern aspect and on a 5% slope. Plot 1 has less dense vegetation than Plot 2, with 85% and 95% average overstory canopy cover and 45 and 75 m^2 ha^{-1} tree basal area, respectively (Woodward et al. 2013). At each plot, 16 resin capsules were

placed carefully at 2-m intervals horizontally within this grid immediately below the O horizon (i.e., 0-cm mineral depth) using a hand trowel to minimize disturbance. Adjacent to these resin capsules, WECSA® Access System units (WECSA® LLC; Montana, USA) were installed at 20-, 40-, and 60-cm at an angle that varied according to the microtopography, such that the deeper capsules would be vertically coincident with their respective 0-cm capsule. The WECSA® system consisted of a thinned-walled PVC casing with a removable cap on one end and a removable resin capsule carrier that fits inside the casing; this allows the delivery and retrieval of a resin capsule so that the same soil location can be sampled repeatedly over time. The WECSA® systems were not installed in mineral soil locations when large roots or rocks prevented vertical placement below the 0-cm resin. This sampling design resulted in a horizontal and vertical matrix consisting of 60 resin capsules in Plot 1 and 63 in Plot 2 that allowed repeated sampling of the same locations with minimal soil disturbance (i.e., only the replacement of the 0-cm capsules required any subsequent soil disturbance). When deployed, these resin capsules capture bioavailable element flux (i.e., inorganic nutrient ions) in the soil solution via ion exchange reactions (Binkley 1984; Hart and Binkley 1984; Doberman et al. 1994).

Resin capsules were installed at both plots in August 2011 and retrieved in October 2011 after the first major precipitation event in the fall. Then, new resin capsules were installed and left in situ until the completion of snowmelt in June 2012 (hereafter referred to as the Water Year 2012 collection; Johnson et al. 2014). This procedure was repeated in Plot 1 for water years (WY) 2013 and 2014 and for Plot 2 for WY 2013, 2014, and 2016 (resin capsules were not installed during WY 2015 in either plot; Table 4-S1). The major precipitation events in the fall were identified as ≥ 50 mm of precipitation falling in a single event (WY2012) or two separate events (all other WY).

Precipitation and soil moisture data were acquired over the entire study period to evaluate the hydrologic environment experienced by the resin capsule during incubation. Volumetric water content ($cm^3\ cm^{-3}$) was collected from the north aspect Upper Providence Creek station (Long. 37.075, Lat. -119.182; 1920 m) located ~2 km from the resin plots (Critical Zone Observatory; https://doi.org/10.6071/Z7WC73). Values were recorded hourly using Decagon Devices ECHO-TM at 10-, 30-, 60-, and 90-cm depths and then averaged by day using the dplyr package in R (R Core Team 2013; Hadley et al. 2018). Precipitation ($mm\ d^{-1}$) was also collected at the Upper Providence station using a Belfort-TM 50780 shielded weighing rain gauge (Kings River Experimental Watershed; Hunsaker and Safeeq 2018). Soil penetration resistance (kPa) was measured at each plot using a Field Scout SC900 Soil Compaction Meter (Spectrum Technologies, Inc., Aurora, IL, USA) with a 1.27-cm cone size to identify compaction differences between the plots that may impact water fluxes. Compaction measurements were made after the last set of resin was collected and taken throughout both plots in undisturbed soil between the locations where WECSA® access systems were installed. Measurements were recorded for a total of 106 points at Plot 1 and 87 in Plot 2. Penetration resistance was logged at each point from 0- to 45-cm (maximum instrument depth) and averaged at every 2.5-cm increment.

4.3.3 Laboratory Analyses

After the capsules were collected and upon returning to the laboratory at University of California, Merced, the adhering soil was removed with deionized water. The resin capsules were processed following the procedure described in Johnson et al. (2014). Briefly, the resin capsules were extracted with three sequential 20-mL solutions of 2 M KCl in 100-mL Erlenmeyer flasks on a platform shaker at low speed for 20 min. each. The three extracts were then combined (60 mL). For the WY 2012 samples (data reported in Johnson et al. 2014), extracts were sent to the Oklahoma State University Soil, Water and Forage Laboratory (SWAFL) and analyzed for NH_4^+-N, NO_3^--N, and PO_4^{3-}-P on a Lachat 8000 Flow-Injection Analyzer (Hach Co., Loveland, CO, USA), and Ca^{2+}, Mg^{2+}, and Na^+ were analyzed using a Jarrell Ash Inductively Coupled Plasma Optical Emission Spectrometer (ICP-OES; Thermo Scientific, Waltham, MA, USA). For extracts generated from resin capsules collected after the first water year (i.e., WY 2013 through 2014 and 2016), extracts were analyzed for NH_4^+-N, NO_3^--N, and PO_4^{3-}-P on a Lachat 8000 flow-injection analyzer, and Ca^{2+}, Mg^{2+}, and Na^+ on an Perkin-Elmer Optima 5300 DV ICP-OES (Waltham, MA, USA) at the Environmental Analytical Laboratory, University of California, Merced. Nutrient fluxes were calculated by converting nutrient concentrations in the extracts to a μmol cm^{-2} d^{-1} basis; this was achieved by transforming mass to moles for that particular nutrient, multiplying the concentrations by the total extractant volume (60 mL), and then dividing those values by the cross-sectional area of the capsule exposed to the soil (5.7 cm^2 for WECSA® deployed capsules and 11.4 cm^2 for 0-cm depth capsules; Johnson et al. 2014) and the incubation period (Table 4-S1). Although the number of days the resin was deployed varied by year (Table 4-S1), high nutrient fluxes generally occur in these ecosystems only during brief periods immediately following the first significant rainfall in the fall after the summer dry period, and in the spring during snowmelt (Williams et al. 1995; Holloway and Dahlgren 2001; Homyak et al. 2014; Hunsaker and Johnson 2017).

4.3.4 Calculations

4.3.4.1 HS-HM Identification

Hot spots and HM were identified as positive moderate outliers (PMO) or positive extreme outlier (PEO), or data points that are statistically separate from the rest of the dataset, using the following equations (Johnson et al. 2014):

$$Moderate: Q3 + 1.5(IQR) < X < Q3 + 3(IQR) \quad \text{[Equation 1]}$$

and

$$Extreme: X > Q3 + 3(IQR), \quad \text{[Equation 2]}$$

where X is the outlier value, Q3 is the third quartile value (75th percentile) and IQR is the interquartile range (25th-75th percentiles). Details of nutrient flux descriptive

information is included in Table 4-S2. The 25th percentile, 75th percentile, and IQR for a given nutrient flux were determined using all grid locations, depths, seasons, and years, but data from each plot were analyzed separately. Plots were not treated as analytical replicates due to physical and chemical differences that may masks individual plot outlier, and therefore HS-HM, patterns. After a spatial location was identified as a positive moderate or extreme outlier, we classified it operationally as either a HS or a HM to incorporate the temporal dimension to both HS and HM classifications. Positive moderate outliers and PEO were not separated for HS-HM classifications, however separation of PEO and PMO allows for the underlying "hotness" of outliers to be evaluated. A location was recognized as a HS when it was an outlier for 50% or more of the sampling periods (total of six for Plot 1 and eight for Plot 2). If the location was an outlier for less than 50% of the sampling periods, it was designated as a HM. All nutrient distributions had a positive skew, therefore negative outliers were not quantified (Johnson et al. 2014).

4.3.4.2 HS-HM Magnitude

The contribution of HS or HM to the total nutrient flux was also evaluated by calculating the percentage of the sum of all nutrient fluxes for a given sampling period that were HS, HM, or bulk matrix soil (i.e., not a HS or HM) for each incubation period. The nutrient averages and standard errors across all sampling periods is reported. We also calculated the percent of the sampled area that occurred as either a HS-HM or bulk matrix soil.

4.3.5 Statistical Analyses

All statistical analyses were carried out for each plot using CRAN-R (version 3.4; R Development Core Team 2013). After HS-HM identification, using equations 1 and 2 and classifying resin locations as a HS or HM based on the percentage of time outliers formed, the total number of HS and HM for each nutrient was calculated. A non-parametric Kruskal-Wallis test by ranks was used to determine if nutrients under biological- versus geochemical-control created more HS or HM. Tests were performed on the total number of HS or HM for all nutrients in their respective grouping (i.e., biological or geochemical) with plots, HS, and HM analyzed separately.

Generalized linear models were run for grouped nutrients within biologically and geochemically control categories to determine the effect of depth (continuous) on the presence of HS and HM. A Poisson error distribution was used to model the total number of HS or HM at each depth interval (discrete counts). Separate models were run for the different control groups, HS, HM, and plots. The geochemically controlled nutrient HS models could not be conducted due to the low number of response variables (i.e., few HS).

Spearman Rank correlation coefficients were calculated to identify if multiple nutrient HS, HM, or HS-HM commonly occurred together in space using the rcorr function within the R corrplot package (Wei and Simko 2017). Hot spot or HM presence

was coded as a binary response variable (no HS or HM was coded with 0 and HS or HM as 1) and data from each plot was again analyzed separately.

Mixed-effect models were conducted to understand the relationship between outlier presence (binary response) with water year, season, and depth, with models ran separately for each plot. Water year (categorical; WY 2012 coded as 0), depth (continuous), season (categorical; fall coded as 0), and the interaction between depth and season were used as fixed effects. Random intercepts were used to account for repeated measures on the grid locations (n = 60 at Plot 1 and 63 at Plot 2) and for the spatial dependency of the vertically associated grid points (n = 16). Models were performed with the lme4 package in R(Bates et al. 2012) and were fit by maximum likelihood with the Laplace Approximation. Simplified models were used for Ca^{2+} in Plots 1 and 2 and Mg^{2+} in Plot 2 because the full models would not converge due to the lack of response variables (i.e. no outliers) for WY 2013. In the simplified models, WY 2013 was removed from the dataset but all other model characteristics remained the same. Multicollinearity of the fixed variables was inspected by calculating the Variance Inflation Factor (VIF) using the VIF function in the car R package (Fox and Weisberg 2019). All VIF values were less than 4 (with the exception of the simplified outlier presence models, which were less than 9) for all independent variables (including the interaction term). Marginal (only fixed effects considered) and conditional (both fixed and random effects considered) R^2 values were calculated following Nakagawa et al. (2013) using the R MuMIn package (Barton and Barton 2019). When explanatory variables (WY, depth) were statistically significant ($\alpha < 0.05$), Tukey's Post Hoc tests were performed to evaluate whether means were significantly different from each other using the lsmeans function within the emmeans R package (Lenth et al. 2018).

4.4 Results

4.4.1 HS-HM Patterns

Hot moments were more common than HS, but when HS did occur they tended to be for biologically controlled nutrients (i.e., NH_4^+, NO_3^-, PO_4^{3-}) rather than those under geochemical control (i.e., Na^+, Ca^{2+}, Mg^{2+}; Figure 4-1). In Plot 1, biologically controlled HS (5 for PO_4^{3-}, 5 for NH_4^+, 8 for NO_3^-) were significantly greater in total count than geologically controlled nutrient HS (0 for Ca^{2+} or Mg^{2+}, 1 for Na^+; $p < 0.05$; Figure 4-1). Plot 2 showed a similar pattern as Plot 1 for biologically and geochemically controlled nutrient HS (3 PO_4^{3-}, 4 NH_4^+, 14 NO_3^-, 0 Ca^{2+}, 3 Mg^{2+}, and 4 Na^+), although this was not significant ($p = 0.261$). Geochemically controlled nutrients occurred as a greater number of HM than biologically controlled nutrients (Plot 1: $p < 0.05$, Plot 2: $p < 0.05$; Figure 4-1), with Na^+ having the greatest total number of HM (43 in Plot 1 and 49 in Plot 2).

Hot spot and HM counts under both biological- and geochemical- control declined with soil depth in mineral horizons ($p < 0.05$; Table 4-1; Figure 4-1). Phosphate, NH_4^+, and all geochemically controlled nutrient HS were only identified at the 0-cm mineral soil sampling depth, but NO_3^- HS occurred down to 40 cm. Although HM for both control groups also decreased with depth ($p < 0.05$), geochemically controlled

nutrient HM tended to persist with depth. For example, Na^+ in Plot 1 had 9 HM at 60 cm and 11 in Plot 2 . In contrast, biologically controlled nutrient HM counts were never greater than 3 (NO_3^- in Plot 1) in either plot at 60 cm.

4.4.2 HS-HM Nutrient Covariance

Hot spots formed more readily for multiple nutrients in the same location within their respective control group (i.e., biological or geochemical) at Plot 1 (Figure 4-2), but Plot 2 HS correlations occurred across both controls. In Plot 1, PO_4^{3+} and NH_4^+ had the highest Spearman Rank correlation ($\rho = 0.78$, $p < 0.05$, n = 120) for HS, but had a relatively lower correlation in Plot 2 ($\rho = 0.25$, $p < 0.05$, n = 126). The other biologically controlled nutrient HS were positively correlated in both plots (NH_4^+ and NO_3^-, PO_4^{3+} and NO_3^- ; Figure 4-2). There were not any observed HS for Ca^{2+} or Mg^{2+} at Plot 1, but Na^+ was positively correlated with biologically controlled nutrients (Figure 4-2). At Plot 2, Na^+ had the highest correlation with Mg^{2+} ($\rho = 0.55$, $p < 0.05$, n = 126). Magnesium HS were also highly correlated with NH_4^+ at Plot 2 ($\rho = 0.55$, $p < 0.05$, n = 126).

Similarly to HS correlation patterns at Plot 1, HM were more positively correlated within the respective control groups at both plots (Figure 4-2). All biologically controlled HM at Plot 1 were significantly correlated ($\rho = \sim 0.50$, $p < 0.05$, n = 180) and Ca^{2+} was positively related to Mg^{2+} ($\rho = \sim 0.62$, $p < 0.05$, n = 120). In Plot 2, HM under biological and geochemical control demonstrated some significant positive relationships between groups.

Most spatial locations exhibited a HS or HM for more than one nutrient. There were 9 locations in Plot 1 and 21 in Plot 2 that were a HS or HM for all six nutrients. All three biologically controlled nutrients frequently occurred as a HS or HM at the same location (15 spots in Plot 1 and 24 in Plot 2). There were a greater number of significant correlations between nutrients when HS-HM were analyzed together, especially between biologically controlled nutrients at Plot 2 ($\rho > 0.74$, $p < 0.05$, n = 126; Figure 4-2). As HS are less common than HM, only 3 locations in Plot 1 and 1 spot in Plot 2 were HS for all biologically controlled nutrients. Calcium never expressed a HS, therefore there were not any co-located HS for all three geochemically controlled nutrients, but considering HS and HM together, there were 17 spots in Plot 1 and 26 in Plot 2. Out of the 60 potential locations in Plot 1 and 63 in Plot 2 (not all 64 locations could have access tubes installed due to hitting a root or rock), there were only 8 spots in Plot 1 and 3 in Plot 2 that were never a HS or HM for any nutrient.

4.4.3 Magnitude of Total Nutrient Flux Attributed to HS-HM Phenomena

Hot spots or HM accounted for more of the nutrient fluxes than the bulk matrix soil (Figure 4-3). Nitrate HS (Plot 1: 50 ± 8%, Plot 2: 72 ± 6%) also contributed to a greater portion of the flux than HM. Phosphate and NH_4^+ HS and HM contribute relatively equally, especially at Plot 1. On the other hand, geochemically controlled nutrient fluxes were largely due to HM ranging from 58 ± 4% for Mg^{2+} at Plot 2 to 85 ± 3% for Ca^{2+} at Plot 2.

Biologically controlled HS tended to represent less of the total sampling area (Plot 1: PO_4^{3-} 10%, NH_4^+ 10%, NO_3^- 15%; Plot 2: PO_4^{3-} 6%, NH_4^+ 7%, NO_3^- 25%) than HM (Plot 1: PO_4^{3-} 33%, NH_4^+ 29%, NO_3^- 35%; Plot 2: PO_4^{3-} 40%, NH_4^+ 46%, NO_3^- 33%). Geochemically controlled nutrients showed the opposite pattern with a larger area of HM (Plot 1: Ca^{2+} 65%, Mg^{2+} 48%, Na^+ 83%; Plot 2: Ca^{2+} 75%, Mg^{2+} 49%, Na^+ 89%) than HS (Plot 1: Ca^{2+} 0%, Mg^{2+} 0%, Na^+ 2%; Plot 2: Ca^{2+} 0%, Mg^{2+} 6%, Na^+ 7%). Although biologically controlled HS occurred in less of the sampled area, they accounted for a similar or greater amount of the total nutrient fluxes compared to HM.

4.4.4 Underlying Controls on HS-HM Formation

The expression of a resin capsule location as a statistical outlier underpins that area being classified as a HS or HM. The regular formation of outliers over repeated sampling events for biologically controlled nutrients designated some of these locations as HS, whereas outlier formation was more transient in geochemically controlled nutrients, designating them mostly as HM. Effects of water year, season, and depth were investigated to determine how these spatiotemporal variables control outlier formation and therefore dictate that respective location as either a HS or HM.

Water year was a significant predictor of nutrient outlier likelihood, particularly for geochemically controlled nutrients (Tables 4-2 and 4-3). For biologically controlled nutrients, the likelihood of outliers were not significantly different in WY 2012, 2013, or 2014 but were significantly higher in WY 2016 from the other years (Table 4-3). For geochemically controlled nutrients, outliers were likely in WY 2012 and WY 2016 than WY 2013 and WY 2014 at both plots (WY 2013 was not included in the model for Ca^{2+} and Mg^{2+} at Plot 1 or Ca^{2+} at Plot 2 due to singularity; no outliers for these nutrients in WY 2013; Table 4-3). Overall, geochemically controlled nutrients demonstrated a greater dependence on WY than biologically controlled nutrients for the formation of outliers.

Outliers for biologically controlled nutrients tended to be greater in the fall and those under geochemical control demonstrated inconsistent patterns with season among nutrients (Table 4-2). Biologically controlled nutrients at Plot 1 and NH_4^+ at Plot 2 outliers were more likely after the first major precipitation event in the fall than after spring snowmelt, but NO_3^- outliers were more common in the spring at Plot 2 (Table 4-2). Geochemically controlled nutrients did not follow similar patterns with season among nutrients at the two plots (Table 4-2). For example, the likelihood of Ca^{2+} outliers was higher in the spring, Mg^{2+} was not significantly different between seasons, and Na^+ followed trends of biologically controlled nutrients with more outliers in the fall, although this was only significant in Plot 1. Overall, biologically controlled nutrient outliers and Na^+ were greater in the fall and Ca^{2+} was the only nutrient that had a higher number of outliers in the spring at both plots.

The likelihood of outliers decreased with depth into the soil profile for all nutrients under biological and geochemical control at both plots (Table 4-2). The interaction of season and depth was significant for predicting outlier likelihood of Ca^{2+} in both plots and Na^+ in Plot 2 (Tables 4-2 and 4-3). Calcium outliers were found deeper in the soil profile after snowmelt in the spring (Table 4-3). Alternatively, Na^+ outliers persisted deeper into the mineral soil after the first major precipitation event in the fall

(Table 4-3). This indicates that Ca^{2+} and Na^{+} outlier occurrence with depth responds differently after fall rains and spring snowmelt.

4.4.5 Positive Extreme Outlier Count

The majority of outliers were identified as PEO rather than PMO in both plots (Figure 4-4). At the plot level, PEO averaged from 55-94% of the total outliers when considering all nutrients and plots separately. In Plot 1, biologically controlled nutrients had a fairly consistent number of PEO during all years sampled (2012, 2013, and 2014) and the year with the highest value varied by nutrient, with NO_3^- highest in 2015, NH_4^+ in 2012, and PO_4^{3-} in 2014. Geochemically controlled nutrients all followed a similar pattern in Plot 1 with 2012 having the highest number of PEO. Plot 2 had the highest number of PEO for all nutrients during the 2016 sampling year. Extreme outliers occurred more readily in the fall compared to the spring for biologically controlled nutrients (PO_4^{3-}: 76% Plot 1, 64% Plot 2; NH_4^+: 88% Plot 1, 79% Plot 2; NO_3^-: 78% Plot 1, 52% Plot 2) and Na^+ (88% Plot 1, 73% Plot 2). On the other hand, Ca^{2+} extreme outliers were more common in the spring (70% in Plot 1 and 53% in Plot 2) and Mg^{2+} was more consistent between seasons (55% were PEO in the fall at Plot 1 and 45% at Plot 2) than the other geochemically controlled nutrients. Positive extreme outliers occurred primarily in the 0-cm depth for all nutrients. Nitrate was the only biologically controlled nutrient to exhibit a PEO at 60-cm. All geochemically controlled nutrients had PEO at all depths measured, with Na^+ having the greatest number with depth.

4.5 Discussion

It is well known that soil nutrient distribution is heterogeneous in space and time. Hot spots have commonly been used to describe areas of elevated biogeochemical activity, in contrast, HM have received less attention. Although researchers agree HM are spatial locations where enhanced biogeochemical cycling occurs for brief periods, to our knowledge there has been no quantitative approach used to define HM that allows for their separation from HS. This is partially due to study designs where many investigations are collected over a relatively short timeframe (i.e., less than one year; Gibson 1986; Kleb and Wilson 1997; Johnson et al. 2014; Barcellos et al. 2018) and often use destructive sampling techniques (i.e., Charley and West 1977; Kleb and Wilson 1997; Bruckner et al., 1999; Farley and Fitter 2001; Washburn and Arthur 2003; Harms and Grimm 2008; Mueller et al. 2008). This leads to acknowledgment of nutrient spatial heterogeneity in these systems, but lacks explicit qualitative and quantitative characterization of the patches. Hot spots and HM may be formed via dissimilar mechanisms and they likely play different roles in supporting short- verse long-term biota nutrient acquisition, therefore separating this terminology is critical for the advancement of ecology. The objective of the current study was to investigate long-term spatial and temporal patterns by repeatedly sampling the soil solution at the same spatial locations (horizontally and vertically) using ion exchange resins to operationally separate the occurrence of PO_4^{3-}, NH_4^+, NO_3^-, Na^+, Ca^{2+}, and Mg^{2+} HS from HM.

4.5.1 HS-HM Occurrence

Our findings partially supported our hypothesis that biologically controlled nutrients would more frequently occur as HM than HS. We found HM were more common than HS for all nutrients, but biologically controlled nutrients produced both HS and HM (Figure 4-1). We also hypothesized that nutrients under geochemical control would readily create HS, which was not supported by our results (Figure 4-1). Although geochemically controlled nutrients only require substrate abundance and water flow, they more frequently occurred as HM and did not persist over time. As the consistent formation of outliers underpins the classification of an area as a HS, biologically controlled nutrient outliers were sometimes able to persist over multiple seasons and collection years, designating them as HS or HM, whereas geochemically controlled nutrients outliers were transient and therefore almost exclusively HM (Tables 4-2 and 4-3; Figures 4-1 and 4-4).

4.5.2 Water as a Control on HS-HM Formation

Inter-annual precipitation exhibited considerable variability over the four year study period that greatly impacted geochemically controlled nutrient outlier formation, and therefore the designation of spatial locations as either HS or HM (Figures 4-4 and 4-5). Our study occurred during a multi-year drought (Bales et al. 2018), which played a major role in solute transport of geochemically controlled nutrients and largely contributed to their designation as HM (Figures 4-4 and 4-S1). Over the sampling years, total precipitation was higher in WY 2012 (1030 mm yr^{-1}) and 2016 (1246 mm yr^{-1}) compared to 2013 (822 mm yr^{-1}) and 2014 (640 mm yr^{-1}; Figure 4-5). Calcium, Mg^{2+}, and Na^{+} fluxes and outlier formation were greatest during WY 2012 and 2016 and substantially lower in the extreme drought years (Figures 4-4 and 4-S1, Tables 4-S3 and S4). Therefore, although these nutrients do not rely on microbial processing and are found in generally high concentrations, we found their formation of HS-HM is heavily dependent on water flux. There was a notable increase of outliers that occurred in WY2016, which followed the extreme drought years. Geochemically controlled nutrients likely accumulated during the extreme drought years, and where subsequently lost during the wet year, similar to findings of geochemical nutrients fluxes in a dry tropical forest (Campo et al. 2000). Overall, geochemically controlled nutrient fluxes were dampened by drought, leading to fewer nutrient rich patches to persist and designating these nutrients more readily as HM rather than HS. It is possible these nutrients would have persisted as HS, as we hypothesized, if all sampling was conducted under normal water years.

In contrast, outliers under biological control tended to form over all water years, including during extreme drought, contributing to their designation as HS-HM (Figure 4-4; Tables 4-2 and 4-3). Additionally, there was no observable decrease in the relative percentage of total outliers as PEO (Figure 4-4). This indicated that labile C, water, or other limiting resources were accessible to the microbial biomass to promote mineralization and nitrification, and soil moisture during all sampling years was high enough to transport these ions to the resin capsules (Parker and Schimel 2011). A nearby study, with similar vegetation and elevation to our resin plots, found soil solution

collected by lysimeters also found comparable dissolved inorganic and organic N in drought and normal water years (Yang et al. 2020) providing additional support that biologically controlled nutrients are resilient to drought in this study system.

Nutrient fluxes related to seasonality also impacted the formation of outliers, where fall rains largely contributed to the transport of biologically controlled and Na^+ fluxes (Figures 4-4 and 4-S1, Tables 4-2 and 4-S3). Nutrients are known to accumulate during the hot, dry summers that characterize Mediterranean climates. It has been proposed that nutrient-rich O horizon lateral flow, or interflow, during the first fall rains may create HS-HM in the mineral soil when percolating through preferential flow paths (Miller et al. 2005; Burcar et al., 1994; Johnson et al. 2011; Woodward 2012). Previous research in the Sierra Nevada found O horizon interflow had higher biological and geochemical nutrient concentrations compared to mineral soil solution and stream water, although it is highly variable (Miller et al. 2005; Johnson et al. 2011; Woodward 2012). Our findings demonstrate that although biologically controlled nutrient outliers were not very sensitive to yearly drought conditions, they were responsive to fall rains following seasonal drought. When the first major precipitation event in the fall occurred, even in drier years, O horizon interflow became nutrient-rich (Miller et al. 2005, 2006; Johnson et al. 2011) and likely infiltrated mineral soil via preferential flow paths (Bundt et al. 2001) to form outliers. It is possible that we would have observed more "cold spots" of biologically controlled nutrients if we collected samples between these major water fluxes, making more spatial locations be designated as HM in the current study.

On the other hand, the large flux of water during spring snowmelt only significantly promoted the formation of Ca^{2+} outliers. Snowmelt has been found to have a greater concentration of Ca^{2+} than O horizon interflow (Woodward 2012), which may have driven the formation of more outliers in the spring. Calcium and Mg^{2+} patterns were overall consistent with results from the previous one-year study (Johnson et al. 2014). However, Mg^{2+} outliers did not show any significant pattern with season which does contradict the Woodward et al. (2013) study and may be due to the suppression of Mg^{2+} fluxes during drought years. It is also possible that the observed differences are caused by differences in resin deployment. In Woodward et al. (2013), the spring collection resins were deployed in parallel with the prior fall rain, making portioning these events apart nearly impossible. In order to account for this, the current study deployed resin at separate times during the year and also normalized flux values to the number of days resin was deployed prior to calculating outliers to allow for direct seasonal comparison.

Although microbially mediated reactions for N and P have important abiotic drivers including temperature, moisture, and pH, our findings show drought and seasonal precipitation did not have a noticeably negative impact on biologically controlled HS-HM formation. This suggests the soil HS-HM identified may be particularly important for plant uptake because total N and P uptake can be reduced during drought (Schlesinger et al. 2016).

4.5.3 Depth as a Control on HS-HM Formation

As hypothesized, the number of HS-HM for all nutrients significantly decreased with depth into the soil (Figure 4-1; Table 4-1). This likely occurred because microbial

activity, nutrient substrate availability, and water fluxes were highest in the upper soil profile. Biologically controlled HS-HM were rarely found at the 60 cm depth, but geochemically controlled nutrients had HM that persisted with depth. For Ca^{2+}, this is driven mostly by outliers that formed deeper in the mineral soil after snowmelt in the spring, likely controlled by mass flow. Ion exchange resins adsorb ions largely from soil solution that pass by the capsules from mass flow with little contribution of diffusion, allowing resin to capture nutrients that are available for vegetation and microbial uptake (Binkley 1984). Considering biologically controlled nutrients, NO_3^- has a high diffusion coefficient relative to PO_4^{3-}, making it more mobile in the soil solution (Tinker and Nye 2000), which may explain why HS for NO_3^- persisted deeper than the other biologically controlled nutrients. Sodium differs from the other nutrients studied because it is not an essential elements for vegetation and microbial biomass productivity, therefore it does not accumulate within their biomass to a significant degree and may act like a semi-conservative tracer. Sodium had the greatest number of HM below 0-cm depths out of all nutrients (Figure 4-1). In the previous one year study at this site using the same sampling devices and locations, biologically controlled HS-HM were also concentrated in the upper sampling depths and geochemically controlled HS-HM were identified at greater depths (Johnson et al. 2014). However, all nutrient HS-HM tended to persist more with depth in Johnson et al. (2014) likely because outliers were calculated with the 0-cm population separate from the deeper depths. Globally, nutrients required by plants in larger amounts are generally found in the upper profile, while others such as Na^+ persist deeper in the profile (Jobbágy and Jackson 2001). Therefore, it is not surprising that nutrient HS and HM follow these larger depth patterns of overall nutrient cycling.

4.5.4 Formation of Co-varied HS-HM

We found notable differences in HS, HM, or HS-HM formation between the two plots, which may have been caused from compaction differences. Plot 2 demonstrated more soil compaction around 5-cm, allowing for higher pore connectivity in these sandy soils, and also had a shallower slope (Plot 1: 20%, Plot 2: 5%). This may have resulted in greater surface infiltration in both preferential flow paths and the surrounding matrix soil to create more co-occurring HS-HM across all nutrients (Figures 4-2 and 4-S2). Alternatively, the steeper slope at Plot 1 likely contributed to greater surface runoff allowing O horizons interflow to become more rich in nutrients, particularly those under biological control. When water infiltrated the soil through preferential flow paths at Plot 1, this may have more readily created co-occurring biologically controlled nutrient HS, HM or HS-HM that were rarely associated with nutrients under geochemical control (Figure 4-2).

4.5.5. HS-HM Terminology

Recently, Bernhardt et al. (2017) have proposed replacing the HS-HM terminology because it: 1) separates spatial from temporal phenomena, and that both are fundamental traits of any biogeochemical occurrence; and 2) creates unnecessarily a false “hot” versus “not” dichotomy, and fails to recognize the full distribution of

biogeochemical process rates that are of greater interest than the maximum rates. They argue the more "nuanced" term ''ecosystem control points'' should be used instead of HS-HM as "ecosystem control" connotes the rate must be of sufficient magnitude or frequency to significantly affect ecosystem dynamics, and "points" incorporates both spatial and temporal characteristics. They suggest that changing the HSHM terminology will help advance our understanding of the importance of biogeochemical heterogeneity in ecosystems. Here, we are continuing to use HS-HM terms, but have applied a spatial and temporal component to both where HS are "hot" in space relative to the surrounding matrix *and* "hot" in time relative to HM. This accounts for locations that are "hot or not" and also considers spaces that are infrequently verses commonly "hot" to account for varying degrees of biogeochemical process rates and fluxes. Previous soil biogeochemical HS-HM studies have commonly characterized all statistical outliers (or disproportionately large using another mathematical metric) as HS and further designated some of these same locations as HM when there was temporal variation (i.e., Robson et al. 2007; Darrouzet-Nardi and Bowman 2011; Woodward et al. 2013; Johnson et al. 2014). Our modified application of HS-HM terminology builds upon how previous studies have used these terms when describing biogeochemical reaction rates or fluxes at the same spatial scale to help clarify the widely known "hot" terms.

4.5.6 HS-HM Ecological Significance

By definition, HS-HM are found in select spatial compartments, therefore they may occupy a relatively small percentage of the total soil volume. We found that although biologically controlled HS accounted for less than 26% of the sampling area on average, they were responsible for an average of 25-72% of N and P fluxes across all sampling periods. Biologically controlled HM comprised another 29-46% and were largely responsible for the remaining fluxes. This finding is similar to an alpine ecosystem where HS only accounted for 14% of the study area, but provided more than 50% of the bioavailable inorganic N as measured by resin bags deployed at 3-cm depth (Darrouzet-Nardi and Bowman 2011). Additionally, rhizosphere HS have been found to account for up to 33% of C and N mineralization while only occupying 8-26% of the soil volume in a meta-analysis (Finzi et al. 2015) and a review paper found HS-HM effect sizes were up to ~250% higher compared to background conditions (Bernhardt et al. 2017). Therefore, HS-HM may play a disproportionately large role in regulating ecosystem processes and function compared to the amount of space they occupy.

Our findings demonstrate that HS-HM of nutrients required in large amounts for vegetation and microorganisms may be key players in supporting ecosystem development in this Mediterranean mixed conifer forest. We found HS-HM primarily occurred in the topsoil of this Mediterranean forest soil (Table 4-1 and Figure 4-1) and vegetation nutrient uptake is usually associated with fine roots and mycorrhizae, which are concentrated in the upper 20 cm of forest soils (Hendrick and Pregitzer 1996). This suggests HS-HM may be easily assessable to vegetation to actively forage by increasing the allocation of resources belowground and proliferating fine roots within nutrient rich patches (Drew and Saker 1975; Hutchings and De Kroon 1994; Hodge 2004; Hodge 2006). However, HS-HM can be areas of intense competition for available nutrients

between vegetation and microorganisms (Jingguo and Bakken 1997), especially N (Kaye and Hart 1997), and the extremely dry summers in Mediterranean-type climates limits root development in the surficial O horizon (Hart and Firestone 1991). Because the majority of HS-HM were found at the interface of organic and mineral soil (i.e., the 0-cm depth), microbes likely obtain nutrients from the organic layer with minimal plant competition until leaching occurs into the mineral soil (Johnson et al., 2011). Although microorganisms may outcompete vegetation in the short-term for HM, plants that access HS with their roots and mycorrhizal symbionts can acquire more nutrients in the long-term (Hodge et al. 2000; Schimel and Bennett, 2004; Cui and Caldwell 1997).

In addition to the arrangement of spots, a plants response to nutrient heterogeneity is impacted by the chemical composition and concentration(s) of the spot, the duration of the nutrient pulse, and the frequency it occurs (Jingguo and Bakken 1997; Jackson & Caldwell, 1989; Bilbrough and Caldwell 1997; Fransen et al. 1999; Wijesinghe et al. 2001). We found biologically controlled nutrients tended to form areas where multiple HS-HM occurred, which were likely spatially correlated due to vegetation redistribution (Schlesinger et al. 1996) and subsequent mineralization (Hill et al. 2019; Figure 4-2). Multiple nutrients from these co-varying patches are likely exploited in tandem (Tibbett and Sanders 2002), and are therefore more beneficial than patches of singular nutrients. These HS-HM are also primarily composed of PEO, which are highly elevated relative to the surrounding soil matrix, making them more likely to be detected (Figure 4-4). We identified nutrients under biological- control are elevated for extended periods of time in some locations (i.e., are HS; Figure 4-1), which may stimulate a morphological response of the belowground biomass (Robinson 1994; Hutchings et al. 2003; Wang et al. 2018), whereas the majority of nutrients exhibited HM and are more likely elicit a physiological response (Fransen et al. 1999), although some plants have been found to elicit a morphological response to temporally available nutrients (i.e., Wang et al. 2018). Additionally, HS can provide a refugia that plants can "count on" over time to provide the necessary resources for root proliferation into the shorter HM (Robinson 1994). Therefore, we hypothesize that plants with low morphological plasticity, but a large rooting system that encompasses a high volume of soil and can exhibit physiological plasticity, would likely benefit most from HM (Crick and Grime 1987; Cui and Caldwell 1997; Wang et al. 2018), while HS would benefit species with high morphological plasticity to exploit the patch (Jackson and Caldwell 1989; Hutchings and de Kroon 1994). Because these HS-HM of co-varying macronutrients are found at soil depths relevant to roots, have extremely high fluxes compared to the soil matrix, are persisting over time in some locations, and are responsible for a large portion of the total nutrient flux, they likely play a disproportionate role in supporting ecosystem development.

Understanding the temporal and spatial controls that produce areas of elevated nutrients is critical to advance our ability to characterize HS-HM in predictive ecological models. However, incorporating HS-HM into terrestrial models is challenging (Groffman et al. 2009) and understanding spatial variation scaling (especially for nutrients other than N) requires more attention (Landsberg et al. 1991). Most ecological models use nutrient averages for scaling (i.e. kg ha^{-1}; Strayer et al. 2003), discounting outliers found in soil microsites (Schimel and Bennet 2004), and are often not spatially explicit (Landsberg 2003) or do not consider multiple HS with varying concentrations (i.e., Ryel and

Caldwell 1998). Before we can incorporate HS and HM into terrestrial modeling, we need to better quantify their presence and relationship with other soil and environmental factors. A detailed review by Bernhardt et al. (2017) found that only 7% of studies using the term HS-HM pose hypotheses driven research questions about HS-HM dynamics, which has resulted in little empirical and theoretical advancement. However, in order to make advances on mechanistic understanding of HS-HM formation we need to conceptually separate these concepts and use sampling designs that allow for their distinct characterization. In addition to operationally defining and separating HS from HM, our study design is a unique way to capture HS-HM dynamics by using resin capsules for repeated sampling of the same spatial location (with minimal disturbance once access tubes are initially installed), analyzing multiple nutrients that are under contrasting biological and geochemical controls, separating periods of time that are known to regulate biogeochemical fluxes (with normalization by the number of incubation days to allow for direct comparison), capturing inter-annual variability by sampling over multiple years, using more advanced statistical analyses to account for repeated measures and spatial dependence, and conducting random sampling to understand overall dynamics of HS, HM, and the surrounding soil matrix. Here, we have made explicit hypotheses that could be coupled in future studies that are more targeted to understand the mechanisms creating HS-HM by sampling within rooting zones, preferential flow paths, etc. to systematically investigate locations where these elevated patches are expected to occur and further elucidate systematic long-term controls and ecological implications.

4.6 References

Bales RC, Goulden ML, Hunsaker CT, Conklin MH, Hartsough PC, O'Geen AT, Hopmans JW, Safeeq M (2018) Mechanisms controlling the impact of multi-year drought on mountain hydrology. Scientific Reports 8:1-8.

Barcellos D, O'Connell C, Silver W, Meile C, Thompson A (2018) Hot Spots and Hot Moments of Soil Moisture Explain Fluctuations in Iron and Carbon Cycling in a Humid Tropical Forest Soil. Soil Systems 2:1-22.

Barton K, Barton MK (2019) Package 'MuMIn'. R package version, 1:6.

Bates D, Maechler M, Bolker B, Walker S (2015) Fitting Linear Mixed-Effects Models Using lme4. Journal of Statistical Software 67:1-48.

Bernhardt ES, Blaszczak JR, Ficken CD, Fork ML, Kaiser KE, Seybold EC (2017) Control Points in Ecosystems: Moving Beyond the Hot Spot Hot Moment Concept. Ecosystems 20:665–682.

Bilbrough CJ, Caldwell MM (1997) Exploitation of springtime ephemeral N pulses by six Great Basin plant species. Ecology 78:231-243.

Binkley, D (1984) Ion exchange resin bags: factors affecting estimates of nitrogen availability. Soil Science Society of America Journal 48:1181-1184.

Blagodatskaya E, Kuzyakov, Y (2013) Active microorganisms in soil: critical review of estimation criteria and approaches. Soil Biology and Biochemistry 67:192-211.

Bruckner A, Kandeler E, Kampichler C (1999) Plot-scale spatial patterns of soil water content, pH, substrate-induced respiration and N mineralization in a temperate coniferous forest. Geoderma 93:207-223.

Burcar S, Miller WW, Tyler SW, Johnson DW (1994) Seasonal preferential flow in two Sierra Nevada soils under forested and meadow cover. Soil Science Society of America Journal 58:1555-1561.

Bundt M, Widmer F, Pesaro M, Zeyer J, Blaser P (2001) Preferential flow paths: biological 'hot spots' in soils. Soil Biology and Biochemistry 33:729-38.

Caldwell, MM, Manwaring JH, Jackson RB (1991) Exploitation of phosphate from fertile soil microsites by three Great Basin perennials when in competition. Functional Ecology 5:757-764.

Campo J, Maass JM, Jaramillo VJ, Yrízar AM (2000) Calcium, potassium, and magnesium cycling in a Mexican tropical dry forest ecosystem Biogeochemistry 49:21-36.

Charley JL, West NE (1977) Micro-patterns of nitrogen mineralization activity in soils of some shrub-dominated semi-desert ecosystems of Utah. Soil Biology and Biochemistry 9:357-65.

Crick, JC, Grime, JP (1987) Morphological plasticity and mineral nutrient capture in two herbaceous species of contrasted ecology. New Phytologist 107:403-414.

Cui M, Caldwell MM (1997) A large ephemeral release of nitrogen upon wetting of dry soil and corresponding root responses in the field. Plant and Soil 191:291-9.

Darrouzet-Nardi A, Bowman, WD (2011) Hot spots of inorganic nitrogen availability in an alpine-subalpine ecosystem, Colorado Front Range. Ecosystems 14:848-863.

Day KJ, Hutchings MJ, John EA (2003) The effects of spatial pattern of nutrient supply on yield, structure and mortality in plant populations. Journal of Ecology 91:541-53.

Dobermann, A, Langner, H, Mutscher, H, Yang, JE, Skogley, EO, Adviento, MA, & Pampolino, MF (1994) Nutrient adsorption kinetics of ion exchange resin capsules: A study with soils of international origin. Communications in Soil Science and Plant Analysis 25:1329-1353.

Drew MC, Saker LR (1975) Nutrient Supply and the Growth of the Seminal Root System in Barley: II. Localized, compensatory increases in lateral root growth and rates op nitrate uptake when nitrate supply is restricted to only part of the root system. Journal of Experimental Botany 26:79-90.

Farley RA, Fitter AH (2001) Temporal and spatial variation in soil resources in a deciduous woodland. Journal of Ecology 87:688-96.

Finzi AC, Abramoff RZ, Spiller KS, Brzostek ER, Darby BA, Kramer MA, Phillips RP (2015) Rhizosphere processes are quantitatively important components of terrestrial carbon and nutrient cycles. Global Change Biology 21:2082-2094.

Fox J, Weisberg S. (2019) An R Companion to Applied Regression. Sage, California.

Fransen B, Blijjenberg J, de Kroon H (1999) Root morphological and physiological plasticity of perennial grass species and the exploitation of spatial and temporal heterogeneous nutrient patches. Plant and Soil 211:179-89.

Frei S, Knorr KH, Peiffer S, Fleckenstein JH (2012) Surface micro-topography causes hot spots of biogeochemical activity in wetland systems: A virtual modeling experiment. Journal of Geophysical Research: Biogeosciences 117:1-18.

García Palacios P, Maestre FT, Gallardo A (2011) Soil nutrient heterogeneity modulates ecosystem responses to changes in the identity and richness of plant functional groups. The Journal of Ecology 99:551-562.

Gibson DJ (1986) Spatial and temporal heterogeneity in soil nutrient supply measured using in situ ion-exchange resin bags. Plant and Soil 96:445-50.

Göransson H, Edwards PJ, Perreijn K, Smittenberg RH, Venterink HO (2014) Rocks create nitrogen hotspots and N:P heterogeneity by funnelling rain. Biogeochemistry 121:329-338.

Groffman PM, Butterbach-Bahl K, Fulweiler RW, Gold AJ, Morse JL, Stander EK, Tague C, Tonitto C, Vidon P (2009) Challenges to incorporating spatially and temporally explicit phenomena (hotspots and hot moments) in denitrification models. Biogeochemistry 93:49-77.

Halvorson JJ, Bolton H, Smith JL, Rossi RE (1994) Geostatistical analysis of resource islands under *Artemisia tridentata* in the shrub-steppe. The Great Basin Naturalist 54:313-328.

Harms TK, Grimm NB (2008) Hot spots and hot moments of carbon and nitrogen dynamics in a semiarid riparian zone. Journal of Geophysical Research: Biogeosciences 113:1-14.

Hart SC, Binkley D (1984) Colorimetric interference and recovery of adsorbed ions from ion exchange resins. Communications in Soil Science and Plant Analysis 15:893-902.

Hart SC, Firestone, MK (1991) Forest floor-mineral soil interactions in the internal nitrogen cycle of an old-growth forest. Biogeochemistry 12:103-127.

Hendrick RL, Pregitzer KS (1996) Temporal and depth-related patterns of fine root dynamics in northern hardwood forests. Journal of Ecology 84:167-176.

Hill AR, Devito KJ, Campagnolo S, Sanmugadas K (2000) Sub- surface denitrification in a forest riparian zone. Biogeochemistry 51:193-223.

Hill EJ, Jones DL, Paterson E, Hill PW (2019) Hotspots and hot moments of amino acid N in soil: Real-time insights using continuous microdialysis sampling. Soil Biology and Biochemistry 131:40-43.

Hoang DTT, Pausch J, Razavi BS, Kuzyakova I, Banfield CC, Kuzyakov Y (2016) Hotspots of microbial activity induced by earthworm burrows, old root channels, and their combination in subsoil. Biology and Fertility of Soils 52:1105–1119.

Hodge A, Robinson D, Griffiths BS, Fitter AH (1999) Why plants bother: root proliferation results in increased nitrogen capture from an organic patch when two grasses compete. Plant, Cell & Environment 22:811–820.

Hodge A, Stewart J, Robinson D, Griffiths BS, Fitter AH (2000) Competition between roots and soil micro-organisms for nutrients from nitrogen-rich patches of varying complexity. Journal of Ecology 88:150-64.

Hodge A (2004) The plastic plant: root responses to heterogeneous supplies of nutrients. New Phytologist 162:9-24.

Hodge A (2006) Plastic plants and patchy soils. Journal of Experimental Botany 57: 401-411.

Holloway JM, Dahlgren RA (2001) Seasonal and event-scale variations in solute chemistry for four Sierra Nevada catchments. Journal of Hydrology 250:106-21.

Homyak PM, Sickman JO, Melack JM (2014) Pools, transformations, and sources of P in high-elevation soils: Implications for nutrient transfer to Sierra Nevada lakes. Geoderma 217:65-73.

Hunsaker CT, Whitaker TW, Bales RC (2012) Snowmelt Runoff and Water Yield Along Elevation and Temperature Gradients in California's Southern Sierra Nevada. Journal of the American Water Resources Association 48:667-678.

Hunsaker CT, Johnson DW (2017) Concentration-discharge relationships in headwater streams of the Sierra Nevada, California. Water Resources Research 53:7869–7884.

Hunsaker CT, Safeeq M (2018) Kings River Experimental Watersheds meteorology data. Fort Collins, CO: Forest Service Research Data Archive.

Hutchings MJ, De Kroon H (1994) Foraging in Plants: the Role of Morphological Plasticity in Resource Acquisition. Advances in Ecological Research 25:159-238.

Hutchings MJ, John EA, Wijesinghe DK (2003) Toward understanding the consequences of soil heterogeneity for plant populations and communities. Ecology 84:2322–2334.

Jackson RB, Caldwell MM (1989) The timing and degree of root proliferation in fertile-soil microsites for three cold-desert perennials. Oecologia 81:149-153.

Jackson RB, Caldwell MM (1991) Kinetic responses of *Pseudoroegneria* roots to localized soil enrichment. Plant and Soil 138:231-238.

Jingguo W, Bakken LR (1997) Competition for nitrogen during decomposition of plant residues in soil: Effect of spatial placement of N-rich and N-poor plant residues. Soil Biology and Biochemistry 29:153–162.

Jobbágy EG, Jackson RB (2001) The distribution of soil nutrients with depth: Global patterns and the imprint of plants. Biogeochemistry 53:51–77.

Johnson DW, Glass DW, Murphy JD, Stein CM, Miller WW (2010) Nutrient hot spots in some Sierra Nevada forest soils. Biogeochemistry 101:93-103.

Johnson DW, Miller WW, Rau BM, Meadows MW (2011) The Nature and Potential Causes of Nutrient Hotspots in a Sierra Nevada Forest Soil. Soil Science 176:596–610.

Johnson DW, Woodward C, Meadows MW (2014) A Three-Dimensional View of Nutrient Hotspots in a Sierra Nevada Forest Soil. Soil Science Society of America Journal 78:225–236.

Kaye JP, Hart SC (1997) Competition for nitrogen between plants and soil microorganisms. Trends in Ecology & Evolution 12:139-143.

Kleb HR, Wilson SD (1997) Vegetation Effects on Soil Resource Heterogeneity in Prairie And Forest. The American Naturalist 150:283–298.

Kurunc A, Ersahin S, Uz BY, Sonmez NK, Uz I, Kaman H, Bacalan GE, Emekli Y (2011) Identification of nitrate leaching hot spots in a large area with contrasting soil texture and management. Agricultural Water Management 98:1013–1019.

Kuzyakov Y, Blagodatskaya E (2015) Microbial hotspots and hot moments in soil: Concept & review. Soil Biology and Biochemistry 83:184–199.

Landsberg J (2003) Modelling forest ecosystems: state of the art, challenges, and future directions. Canadian Journal of Forest Research 33:385–397.

Landsberg JJ, Kaufmann MR, Binkley D, Isebrands J, Jarvis PG (1991) Evaluating progress toward closed forest models based on fluxes of carbon, water and nutrients. Tree Physiology 9:1–15.

Lenth R, Singmann H, Love J (2018) Emmeans: Estimated marginal means, aka least-squares means. R package version, 1.1.

Loupe TM, Miller WW, Johnson DW, Sedinger JS, Carroll EM, Walker RF, Stein CM (2009) Effects of mechanical harvest plus chipping and prescribed fire on Sierran runoff water quality. Journal of Environmental Quality 38:537-547.

Lovett GM, Jones CG, Turner MG, Weathers KC (2005) Ecosystem Function in Heterogeneous Landscapes. Springer, New York.

Maestre FT, Bradford MA, Reynolds JF (2005) Soil nutrient heterogeneity interacts with elevated CO_2 and nutrient availability to determine species and assemblage responses in a model grassland community. New Phytologist 168:637–650.

Maestre FT, Reynolds JF (2007) Amount or pattern? Grassland responses to the heterogeneity and availability of two key resources. Ecology 88:501–511.

McClain ME, Boyer EW, Dent CL, Gergel SE, Grimm NB, Groffman PM, Hart SC, Harvey JW, Johnston CA, Mayorga E, McDowell WH, Pinay G (2003) Biogeochemical Hot Spots and Hot Moments at the Interface of Terrestrial and Aquatic Ecosystems. Ecosystems 6:301–312.

Miller WW, Johnson DW, Denton C, Verburg PSJ, Dana GL, and Walker RF (2005) Inconspicuous nutrient laden surface runoff from mature forest Sierran watersheds. Water Air Soil Pollution 163:3-17.

Miller WW, Johnson DW, Loupe TM, Sedinger JS, Carroll EM, Murphy JD, Walker RF, and Glass DW (2006) Nutrients flow from runoff at burned forest site in Lake Tahoe Basin. California Agriculture 60:65-71.

Mueller EN, Wainwright J, Parsons AJ (2008) Spatial variability of soil and nutrient characteristics of semi-arid grasslands and shrublands, Jornada Basin, New Mexico. Ecohydrology 1:3–12.

Nakagawa S, Schielzeth H (2013) A general and simple method for obtaining R^2 from generalized linear mixed-effects models. Methods in Ecology and Evolution 4:133-142.

Palta MM, Ehrenfeld JG, Groffman PM (2014) "Hotspots" and "Hot Moments" of denitrification in urban brownfield wetlands. Ecosystems 17:1121-1137.

Parker SS, Schimel JP (2011) Soil nitrogen availability and transformations differ between the summer and the growing season in a California grassland. Applied Soil Ecology 48:185-192.

Parkin TB (1987) Soil Microsites as a Source of Denitrification Variability. Soil Science Society of America Journal 51:1194-1199.

R Core Team (2013) R: A language and environment for statistical computing. R Foundation for Statistical Computing. Vienna, Austria.

Robinson D (1994) The responses of plants to non-uniform supplies of nutrients. New Phytologist 127:635–674.

Robinson D, Hodge A, Griffiths BS, Fitter AH (1999) Plant root proliferation in nitrogen rich patches confers competitive advantage. Proceedings of the Royal Society of London Series B: Biological Sciences 266:431–435.

Robson TM, Lavorel S, Clement JC, Le Roux X (2007) Neglect of mowing and manuring leads to slower nitrogen cycling in subalpine grasslands. Soil Biology and Biochemistry 39:930-941.

Ryel RJ, Caldwell MM (1998) Nutrient acquisition from soils with patchy nutrient distributions as assessed with simulation models. Ecology 79:2735–2744.

Schimel JP, Bennett J (2004) Nitrogen mineralization: challenges of a changing paradigm. Ecology 85: 591-602.

Schlesinger WH, Raikes JA, Hartley AE, Cross AF (1996) On the spatial pattern of soil nutrients in desert ecosystems. Ecology 77:364–74.

Schlesinger WH, Dietze MC, Jackson RB, Phillips RP, Rhoades CC, Rustad LE, Vose JM (2016) Forest biogeochemistry in response to drought. Global change biology 22: 2318-2328.

Strayer DL, Ewing HA, Bigelow S (2003) What kind of spatial and temporal details are required in models of heterogeneous systems? Oikos 102:654–662.

Tibbett M, Sanders, FE (2002) Ectomycorrhizal Symbiosis can Enhance Plant Nutrition through Improved Access to Discrete Organic Nutrient Patches of High Resource Quality. Annals of Botany 89:783-789

Tinker PB, Nye PH (2000) Solute movement in the rhizosphere. Oxford University Press, New York.

Turner MG, Gardner RH (2015) Landscape ecology in theory and practice. Springer, New York.

Vidon P, Allan C, Burns D, Duval TP, Gurwick N, Inamdar S, Lowrance R, Okay J, Scott D, Sebestyen S (2010) Hot spots and hot moments in riparian zones: potential for improved water quality management. Journal of the American Water Resources Association 46:278–298.

Wang P, Shu M, Mou P, Weiner J (2018) Fine root responses to temporal nutrient heterogeneity and competition in seedlings of two tree species with different rooting strategies. Ecology and Evolution 8:3367–3375.

Washburn CS, Arthur MA (2003) Spatial variability in soil nutrient availability in an oak-pine forest: potential effects of tree species. Canadian Journal of Forest Research 33:2321-2330.

Weathers KC, Cadenasso ML, Pickett STA (2001) Forest edges as nutrient and pollutant concentrators: potential synergisms between fragmentation, forest canopies, and the atmosphere. Conservation Biology 15:1506–1514.

Wei T, Simko V (2017) R package "corrplot": Visualization of a Correlation Matrix. R package version, 0.84.

Wijesinghe DK, John EA, Beurskens S, Hutchings MJ (2001) Root system size and precision in nutrient foraging: responses to spatial pattern of nutrient supply in six herbaceous species. Journal of Ecology 89:972–983.

Wijesinghe DK, John EA, Hutchings MJ (2005) Does pattern of soil resource heterogeneity determine plant community structure? An experimental investigation. Journal of Ecology 93:99–112.

Williams MW, Bales RC, Brown AD, Melack JM (1995) Fluxes and transformations of nitrogen in a high-elevation catchment, Sierra Nevada. Biogeochemistry 28:1-31.

Woodward C (2012) Nutrient Hot Spots in a Sierra Nevada Soil: Physical Assessments and Contributing Factors. University of California, Riverside, Riverside, CA.

Woodward C, Johnson DW, Meadows MW, Miller WW, Hynes MM, Robertson CM (2013) Nutrient hot spots in a Sierra Nevada forest soil: temporal characteristics and relations to microbial communities. Soil Science 178:585–595.

Yang JE, Skogley EO (1992) Diffusion kinetics of multinutrient accumulation by mixed-bed ion-exchange resin. Soil Science Society of America Journal 56: 408-414.

Yang Y, Hart S, McCorkle E, Stacy E, Barnes M, Hunsaker C, Johnson D, Asefaw Berhe A (2020) Stream water chemistry in mixed-conifer headwater basins: role of water sources, seasonality, watershed characteristics, and disturbances. Ecosystems, in review.

4.7 Tables

Table 4-1. Generalized linear model results with Poisson error distributions to determine the effect of depth (continuous) on the number of hot spots (HS) and hot moments (HM) for nutrients under putative biological- (Bio; PO_4^{3-}, NH_4^+, NO_3^-) and geological-control (Geo; Ca^{2+}, Mg^{2+}, Na^+). Separate models were ran for HS and HM at Plot 1 and Plot 2. Model fit Chi-squared values of 0 were produced in geological-controlled nutrient HS models due to a lack of response variables (i.e., few observed HS). Astericks denote $p <$ 0.05.

HS-HM	Control	Depth	Chi-Squared
Plot 1			
HS	Bio	-0.08 (0.02)*	0.76
HS	Geo	Not Included	
HM	Bio	-0.04 (0.1)*	0.57
HM	Geo	-0.01 (<0.01)*	0.42
Plot 2			
HS	Bio	-0.12 (0.03)*	0.71
HS	Geo	Not Included	
HM	Bio	-0.03 (0.01)*	0.82
HM	Geo	-0.01 (<0.01)*	0.92

Table 4-2. Results of mixed effect models for Plot 1 and Plot 2 on outlier likelihood (binary response) of PO_4^{3-}, NH_4^+, NO_3^-, Ca^{2+}, Mg^{2+}, and Na^+ as effected by the fixed effects of water year (categorical, 2012 coded as 0), season (categorical, fall coded as 0), depth (continuous), and season by depth interaction. Model coefficients were determined for each fixed effect using maximum likelihood (Laplace approximation), with standard errors in parentheses. Significant ($p < 0.05$) results are shown in bold. Individual (repeated sampling from same location; n = 60 for Plot 1, n = 63 for Plot 2) and Vertical (spatial dependency of 0-, 20-, 40-, and 60-cm; n = 16) were included as random effects. The variance is reported for each random effect with standard deviation in parentheses. Data for Water Year 2016 was not collected for Plot 1; therefore, this factor was not included in the model and is denoted within the table as no data (ND). Water Year 2013 was not included in models for Ca^{2+} and Mg^{2+} in Plot 1 and Ca^{2+} in Plot 2 due to singularity and large eigenvalue ratios created by the lack of response variables (i.e., no outliers) and are marked as "Not Included." Model R^2 values are reported for the fixed effects only (i.e., marginal) and for the fixed and random effects together (i.e., conditional).

	Fixed Effects						Random Effects		R-Squared	
Nutrient	**2013**	**2014**	**2016**	**Season**	**Depth**	**Season x Depth**	**Individual**	**Vertical**	**Fixed**	**Fixed + Random**
Plot 1										
PO_4^{3-}	**-1.4 (0.63)**	0.77 (0.51)	ND	**-1.4 (0.55)**	**-0.12 (0.03)**	-0.04 (0.06)	0.87 (0.93)	0.44 (0.66)	0.73	0.81
NH_4^+	-0.35 (0.56)	0.12 (0.54)	ND	**-2.9 (0.70)**	**-0.11 (0.03)**	0.03 (0.04)	2.5 (1.57)	0.11 (0.33)	0.20	0.40
NO_3^-	-0.17 (0.46)	-0.06 (0.45)	ND	**-1.4 (0.51)**	**-0.06 (0.02)**	-0.03 (0.03)	2.2 (1.47)	0.11 (0.34)	0.42	0.66
Ca^{2+}	Not included	**-5.5 (1.1)**	ND	-0.12 (0.77)	**-0.07 (0.02)**	**0.08 (0.03)**	<0.01 (<0.01)	3.0 (1.7)	0.62	0.80
Mg^{2+}	Not included	**-4.1 (0.86)**	ND	-1.0 (0.76)	**-0.05 (0.02)**	0.05 (0.2)	<0.01 (<0.01)	1.14 (1.1)	0.43	0.72
Na^+	-5.7 (0.98)	**-4.9 (0.82)**	ND	**-3.1 (0.90)**	**-0.03 (0.01)**	-0.07 (0.04)	<0.01 (<0.01)	2.7 (1.7)	0.73	0.85
Plot 2										
PO_4^{3-}	1.1 (0.55)	0.67 (0.57)	**2.2 (0.54)**	-0.34 (0.41)	**-0.08 (0.02)**	-0.04 (0.03)	0.10 (0.32)	<0.01 (<0.01)	0.63	0.64
NH_4^+	**1.8 (0.57)**	0.40 (0.62)	**2.9 (0.59)**	**-1.9 (0.45)**	**-0.09 (0.02)**	0.01 (0.02)	0.47 (0.69)	0.30 (0.54)	0.55	0.64
NO_3^-	**0.99 (0.45)**	0.65 (0.46)	**2.5 (0.49)**	0.45 (0.39)	**-0.09 (0.02)**	-0.04 (0.02)	0.37 (0.60)	<0.01 (<0.01)	0.66	0.69
Ca^{2+}	Not included	**-3.9 (1.0)**	0.05 (0.33)	0.29 (0.46)	**-0.08 (0.02)**	**0.06 (0.2)**	<0.01 (<0.01)	<0.01 (<0.01)	0.65	0.65
Mg^{2+}	**-2.2 (0.71)**	**-3.3 (1.1)**	**2.1 (0.49)**	0.47 (0.51)	**-0.10 (0.02)**	0.02 (0.02)	0.63 (0.79)	0.33 (0.57)	0.66	0.74
Na^+	**-5.1 (1.0)**	**-3.4 (0.52)**	**-1.2 (0.33)**	-0.30 (0.45)	**-0.02 (0.01)**	**-0.07 (0.02)**	<0.01 (<0.01)	<0.01 (<0.01)	0.70	0.70

Table 4-3. Post-hoc findings of mixed effect models for outlier likelihood of PO_4^{3-}, NH_4^+, NO_3^-, Ca^{2+}, Mg^{2+}, and Na^+ for water years and season by depth interaction (fixed effects). Water years are averaged over the level of season. The season by depth interaction compares the respective depth (0-, 20-, 40-, and 60-cm) in the fall compared to the spring. Model coefficients are displayed with the standard error in parenthesis. P values are adjusted with Tukey's method and are in bold when significant at $p < 0.05$. Water Year 2016 was not collected for Plot 1 (ND = no data). Water Year 2013 was not included in models for Ca^{2+} and Mg^{2+} in Plot 1 and Ca^{2+} in Plot 2 due to singularity and large eigenvalue ratios created by the lack of response variables (i.e., no outliers) and are marked as "Not Included." Results are only presented for significant independent variables from the original mixed model presented in Table 2 (blank cells $p > 0.05$).

	Water Year						Season x Depth			
Nutrient	**2012 to 2013**	**2012 to 2014**	**2012 to 2016**	**2013 to 2014**	**2013 to 2016**	**2014 to 2016**	**0**	**20**	**40**	**60**
Plot 1										
PO_4^{3-}	1.4 (0.63)	-0.77 (0.51)	ND	**-2.2 (0.63)**	ND	ND				
NH_4^+	0.35 (0.54)	-0.12 (0.54)	ND	-0.48 (0.56)	ND	ND				
NO_3^-	0.17 (0.46)	0.06 (0.45)	ND	-0.11 (0.45)	ND	ND				
Ca^{2+}	Not included	**5.5 (1.1)**	ND	Not included	ND	ND	0.12 (0.77)	**-1.47 (0.55)**	**-3.1 (0.78)**	**-4.7 (1.2)**
Mg^{2+}	Not included	**4.1 (0.86)**	ND	Not included	ND	ND				
Na^+	**5.7 (0.98)**	**4.9 (0.82)**	ND	-0.80 (0.92)	ND	ND				
Plot 2										
PO_4^{3-}	-1.1 (0.55)	-0.67 (0.57)	**-2.2 (0.54)**	0.39 (0.48)	**-1.2 (0.43)**	**-0.15 (0.47)**				
NH_4^+	**-1.8 (0.57)**	-0.40 (0.62)	**-2.9 (0.59)**	**1.4 (0.53)**	**-1.1 (0.42)**	**-2.5 (0.54)**				
NO_3^-	-0.99 (0.45)	-0.65 (0.46)	**-2.5 (0.49)**	0.34 (0.43)	**-1.5 (0.43)**	**-1.8 (0.45)**				
Ca^{2+}	Not included	**3.9 (1.0)**	-0.05 (0.33)	Not included	Not included	**-4.0 (1.0)**	-0.29 (0.46)	**1.5 (0.40)**	**-2.6 (0.70)**	**-3.8 (1.1)**
Mg^{2+}	**2.2 (0.71)**	**3.3 (1.1)**	**-2.1 (0.49)**	1.1 (1.2)	**-4.3 (0.77)**	**-5.4 (1.1)**				
Na^+	**5.1 (1.0)**	**3.4 (0.52)**	**1.2 (0.33)**	-1.7 (1.1)	**-3.9 (1.0)**	**-2.2 (0.52)**	0.30 (0.45)	**1.7 (0.38)**	**3.0 (0.67)**	**4.4 (1.1)**

4.8 Figures

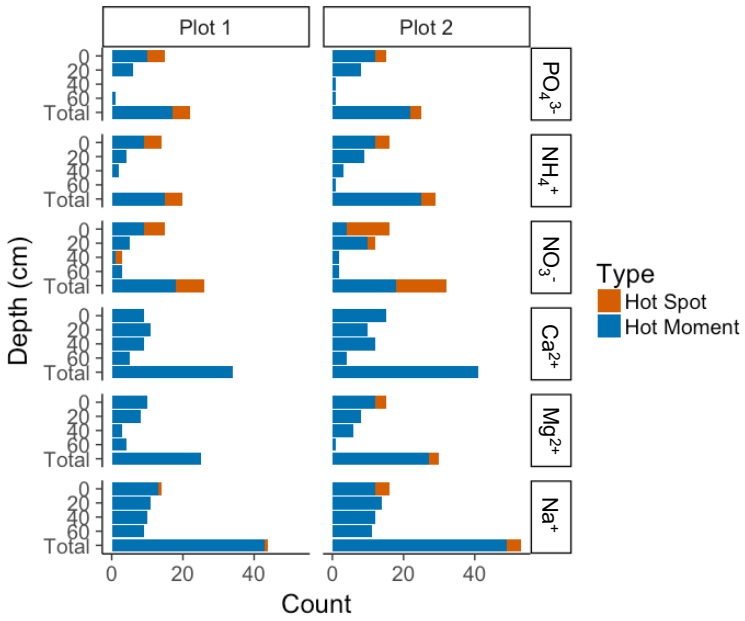

Figure 4-1. The total number of hot spots (HS; orange) and hot moments (HM; blue) for each nutrient by depth based on Plot 1 and Plot 2 seperately.

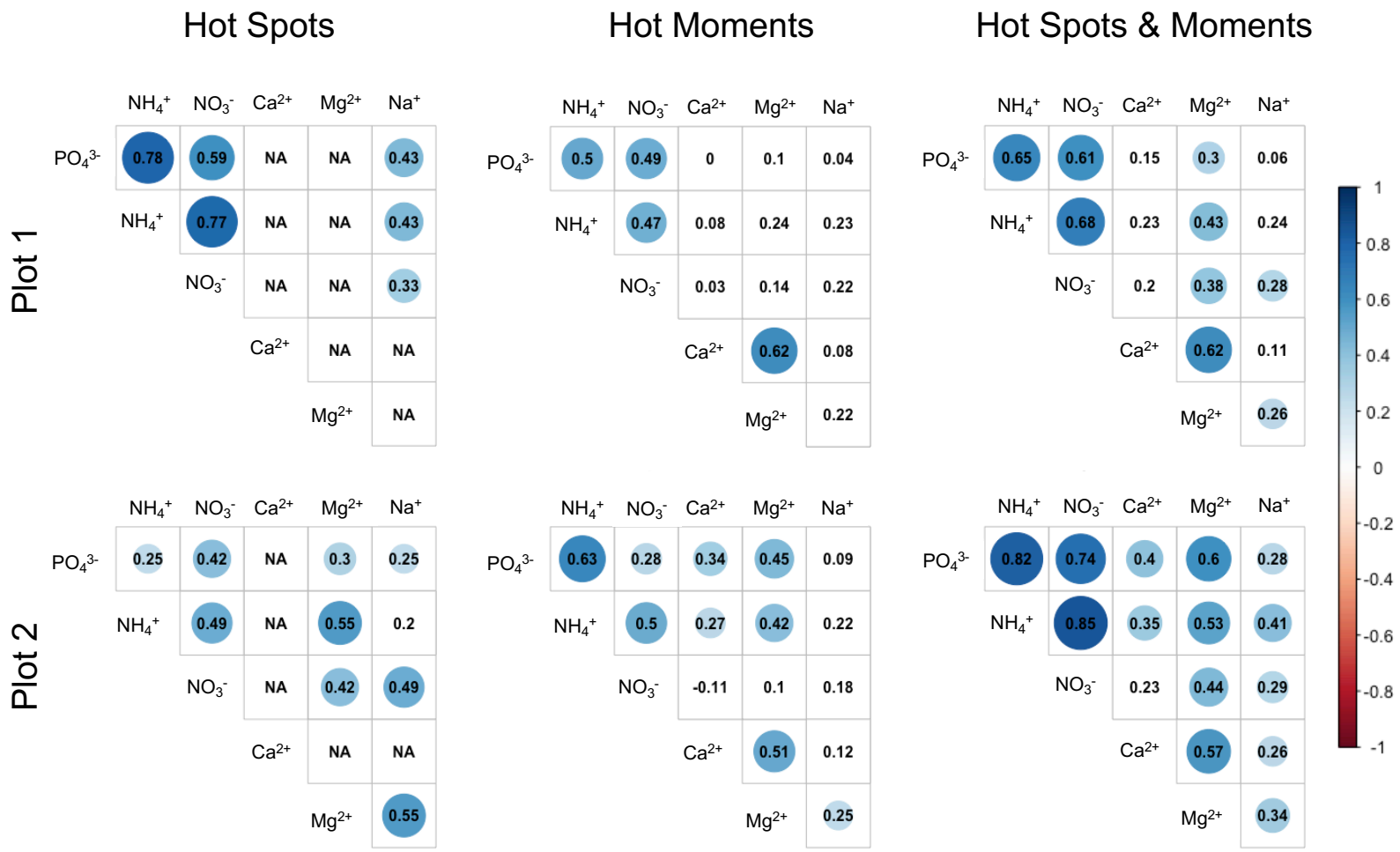

Figure 4-2. Spearman rank correlation coefficients for hot spot (HS), hot moment (HM), or HS and HM presence in each plot separately. Circle size is larger when the correlation coefficient is farther from 0. Positive correlations are in blue and negative in red. NA indicates a lack of response variable to determine the coefficient (i.e., there were no HS or HM) and blank squares indicant the relationship is not significant at $\alpha = 0.05$.

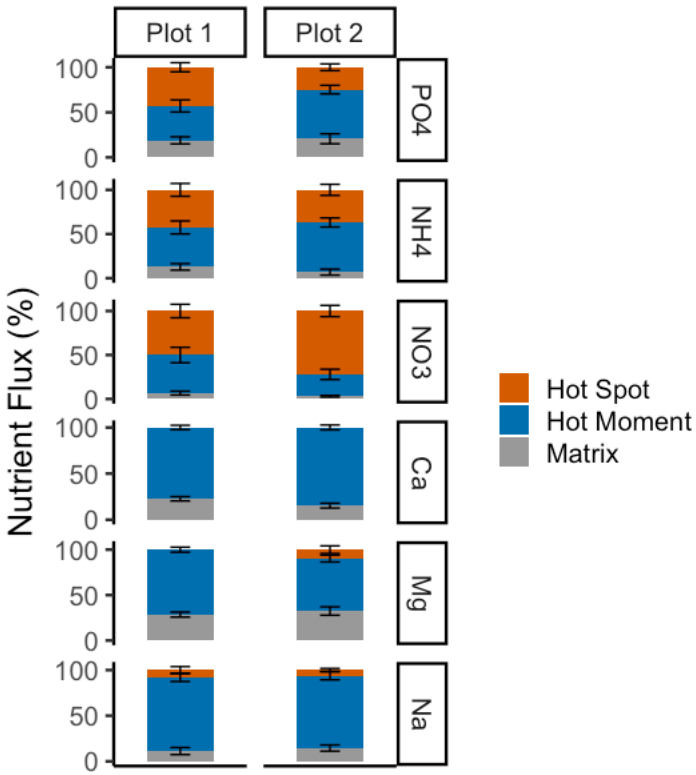

Figure 4-3. Percent and standard error of the total nutrient flux observed in hot spots (HS; orange), hot moments (HM; blue), and the soil matrix (non-HS and -HM; gray) in Plot 1 and Plot 2.

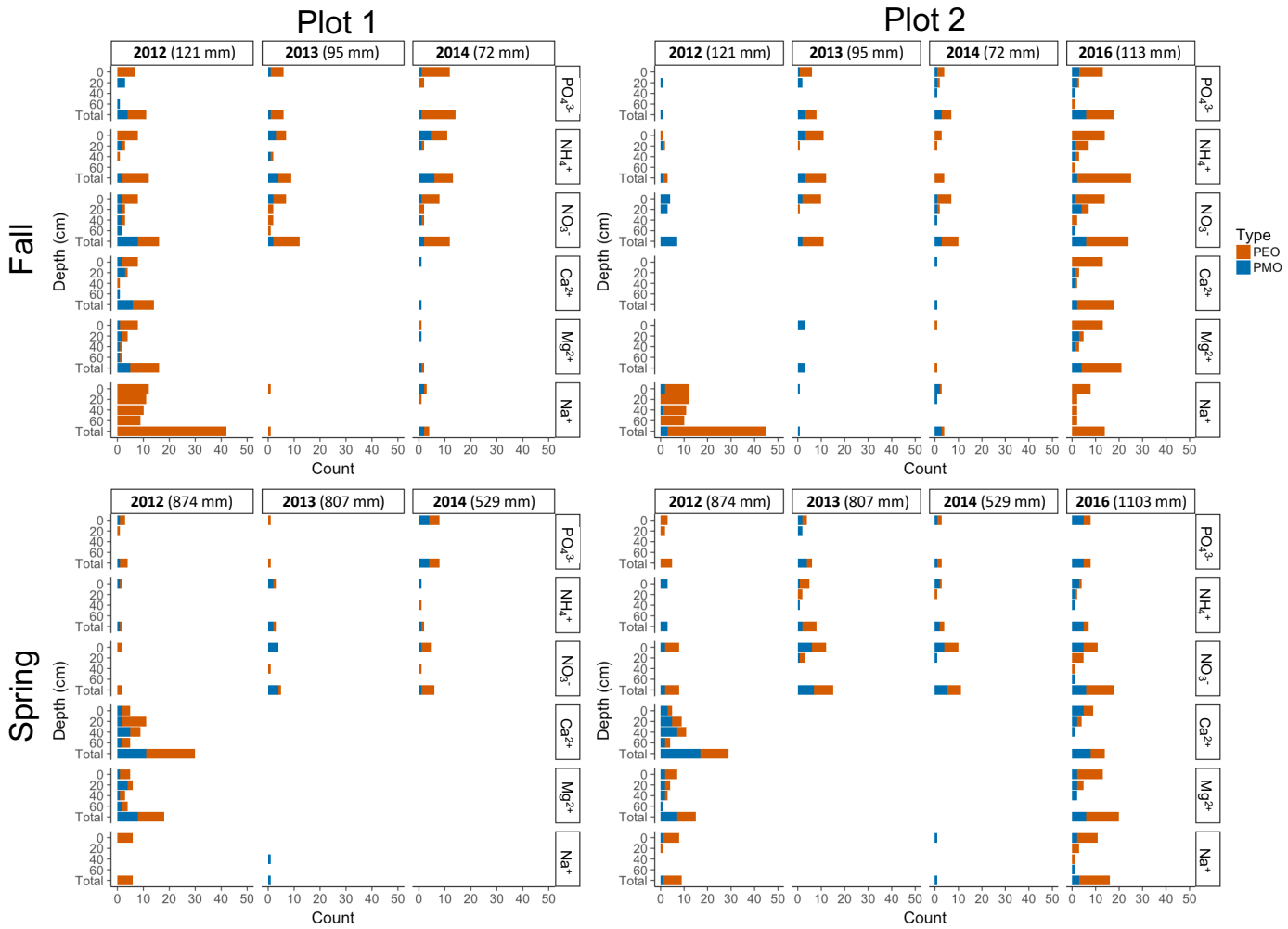

Figure 4-4. Distribution of positive moderate outliers (PMO; orange) and positive extreme outliers (PEO; blue) with water year, season, and depth for each nutrient and plot. No data were collected in Plot 1 for 2016 (blank cells). Total precipitation (mm) during each sampling event is included.

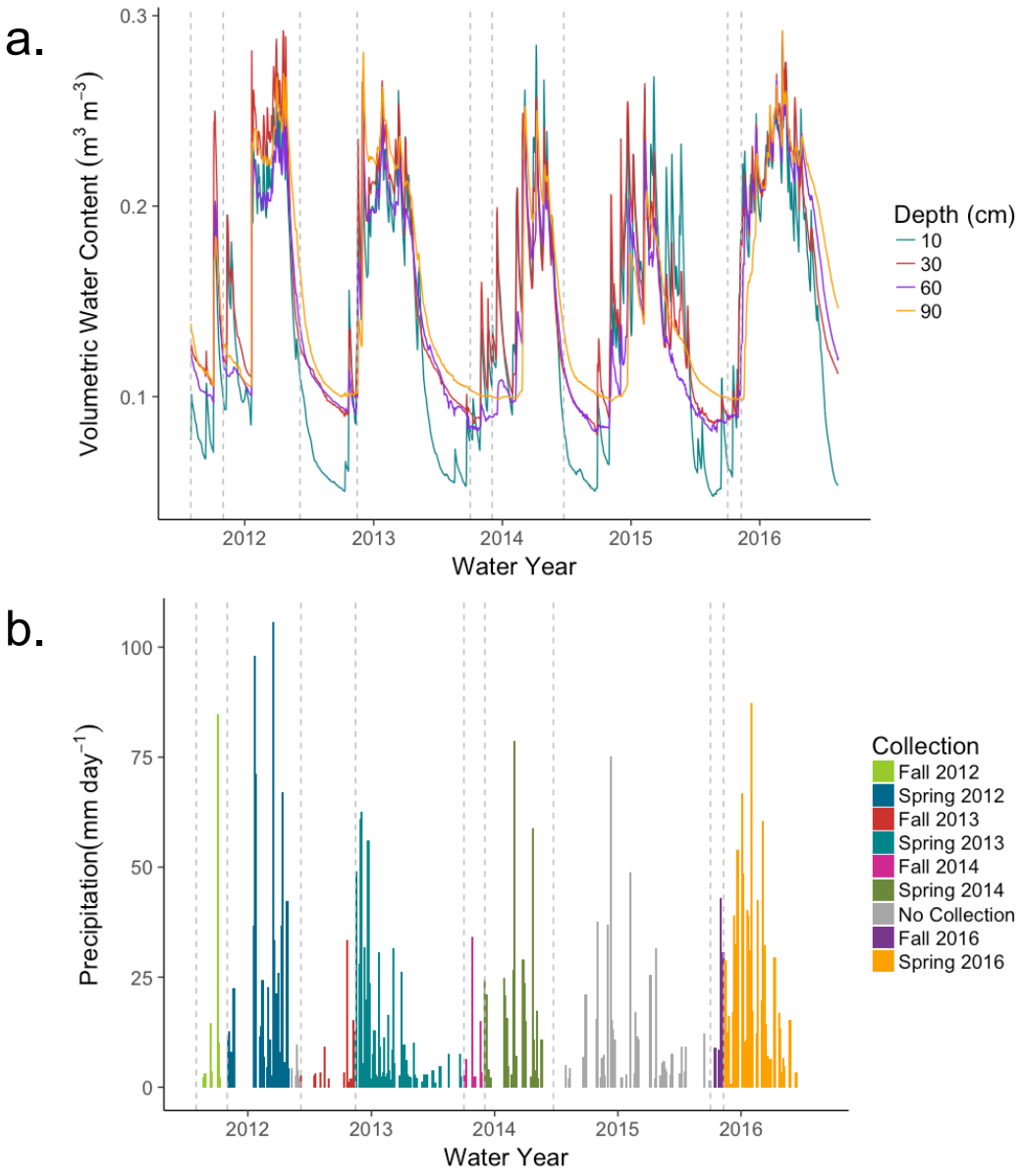

Figure 4-5. Volumetric water content (m^3 m^{-3}) at 10-, 30-, 60-, and 90-cm soil depths (a.) and precipitation (mm d^{-1}; b.) over the sampling periods. Resin capsule deployment and/or collection is denoted by dashed lines. No data were collected for WY2014 in fall or spring.

4.9 Supplementary Tables

Table 4-S1. Resin deployment information with installation date (M/D/Y), removal date (M/D/Y), and the total number of days for each sampling period.

Water Year	Plot	Season	Install Date	Remove Date	# Days
2012	1 & 2	Fall	08/01/11	11/01/11	92
		Spring	11/01/11	05/02/12	183
2013	1 & 2	Fall	06/06/12	11/15/12	162
		Spring	11/15/12	10/02/13	321
2014	1 & 2	Fall	10/02/13	12/03/13	62
		Spring	12/03/13	06/24/14	203
2016	2	Fall	10/02/15	11/10/15	39
		Spring	11/10/15	08/11/16	275

Table 4-S2. Nutrient flux (μmol cm^{-2} day^{-1}) descriptive information including mean (standard deviation), median, minimum, maximum, interquartile range (25^{th}-75^{th} quartiles), and skew for PO_4^{3-}, NH_4^+, NO_3^-, Ca^{2+}, Mg^{2+}, and Na^+ at Plot 1 and Plot 2.

Nutrient	Mean (SD)	Median	Minimum	Maximum	IQR	Skew
		nmol cm^{-2} d^{-1}				
Plot 1						
NH_4^+	1.27 (3.22)	0.150	0	29.7	1.12	5.13
NO_3^-	3.76 (16.2)	0.135	0	186	1.53	8.47
PO_4^+	2.25 (6.17)	0.456	0	60.1	1.27	5.38
Ca^{2+}	16.0 (28.0)	4.69	0	188	13.6	3.18
Mg^{2+}	2.74 (5.26)	0.926	0	46.8	2.43	4.39
Na^+	1.92 (6.92)	0.0572	0	56.3	0.197	5.81
Plot 2						
NH_4^+	4.37 (0.0303)	0.184	0	614	1.17	17.6
NO_3^-	7.51 (25.1)	0.138	0	280	3.38	6.40
PO_4^+	0.860 (2.51)	0.231	0	24.5	0.566	6.28
Ca^{2+}	18.7 (56.8)	3.48	0	649	13.5	7.43
Mg^{2+}	4.08 (16.5)	0.650	0	203	1.88	8.52
Na^+	1.38 (4.65)	0.0792	0	51.6	0.276	6.43

Table 4-S3. Results of mixed effect models for Plot 1 and Plot 2 for cubed root transformed PO_4^{3-}, NH_4^+, NO_3^-, Ca^{2+}, Mg^{2+}, and Na^+ fluxes (normalized to the number of resin deployment days; μmol/cm^2/day) as effected by the fixed effects of water year (categorical, 2012 coded as 0), season (categorical, fall coded as 0), depth (continuous), and season by depth interaction. Model coefficients were determined by restricted maximum likelihood (REML) and standard errors are reported in parentheses. Coefficients in bold indicates significant at $p < 0.05$. Individual (repeated sampling from same location; n = 60 for Plot 1, n = 63 for Plot 2) and Vertical (spatial dependency of 0-, 20-, 40-, and 60-cm; n = 16) were included as random effects. The variance is reported for each random effect with standard deviation in parentheses. Water Year 2016 was not collected for Plot 1, therefore the effect is not included in the model and is denoted within the table as no data (ND). Model R^2 values are reported for the fixed effects only (i.e., marginal) and for the fixed and random effects together (i.e., conditional).

	Fixed Effects						Random Effects		R-Squared	
Nutrient	**2013**	**2014**	**2016**	**Season**	**Depth**	**Season x Depth**	**Individual**	**Vertical**	**Fixed**	**Fixed + Random**
Plot 1										
PO_4^{3-}	-0.010	0.002	ND	**-0.039**	**0.002**	**0.0005**	0.0006	<0.0001	0.30	0.44
	(0.006)	(0.006)		**(0.008)**	**(0.0002)**	**(0.0002)**	(0.024)	(<0.0001)		
NH_4^+	**-0.021**	**-0.034**	ND	**-0.041**	-0.002	**0.0008**	0.0007	<0.0001	0.40	0.58
	(0.005)	**(0.005)**		**(0.007)**	(0.0002)	**(0.0002)**	(0.027)	(<0.0001)		
NO_3^-	**-0.029**	**-0.018**	ND	**-0.048**	**-0.002**	**0.0008**	0.0009	0.0005	0.24	0.42
	(0.009)	**(0.009)**		**(0.012)**	**(0.0002)**	**(0.0003)**	(0.030)	(0.023)		
Ca^{2+}	**-0.161**	**-0.159**	ND	0.017	**-0.001**	**0.0009**	0.0005	0.0007	0.57	0.67
	(0.008)	**(0.008)**		(0.011)	**(0.0002)**	**(0.0003)**	(0.022)	(0.026)		
Mg^{2+}	**-0.074**	**-0.077**	ND	-0.002	**-0.001**	**0.0005**	0.0002	0.0005	0.40	0.58
	(0.005)	**(0.005)**		(0.007)	**(0.0002)**	**(0.0002)**	(0.015)	(0.022)		
Na^+	**-0.069**	**-0.0574**	ND	**-0.03**	-0.0002	-0.0001	<0.0001	0.0003	0.25	0.3
	(0.008)	**(0.008)**		**(0.010)**	(0.0002)	(0.0003)	(<0.0001)	(0.016)		
Plot 2										
PO_4^{3-}	**0.0146**	**0.013**	0.003	**-0.018**	**-0.001**	-0.0001	0.0002	<0.0001	0.27	0.34
	(0.005)	**(0.005)**	(0.005)	**(0.006)**	**(0.0001)**	(0.0002)	(0.002)	(<0.0001)		
NH_4^+	0.014	**-0.024**	0.049	**-0.055**	**-0.002**	**0.0007**	0.0006	<0.0001	0.37	0.44
	(0.009)	**(0.009)**	(0.009)	**(0.011)**	**(0.0002)**	**(0.0003)**	(0.024)	(<0.0001)		
NO_3^-	0.013	0.002	0.073	-0.021	**-0.003**	0.0003	0.001	<0.0001	0.44	0.51
	(0.011)	(0.011)	(0.011)	(0.013)	**(0.0003)**	(0.0003)	(0.032)	(<0.0001)		
Ca^{2+}	**-0.011**	**-0.133**	-0.021	-0.004	**-0.002**	**0.001**	0.0002	<0.0001	0.35	0.36
	(0.013)	**(0.013)**	(0.013)	(0.015)	**(0.0003)**	**(0.0004)**	(0.012)	(<0.0001)		
Mg^{2+}	**-0.03**	**0-0.049**	0.008	-0.006	**-0.001**	0.0002	0.0001	<0.0001	0.23	0.25
	(0.009)	**(0.009)**	(0.009)	(0.010)	**(0.002)**	(0.0003)	(0.011)	(0.006)		
Na^+	**-0.053**	**-0.044**	-0.049	**-0.026**	**-0.0006**	-0.0002	<0.0001	0.00001	0.23	0.24
	(0.007)	**(0.007)**	(0.007)	**(0.008)**	**(0.0002)**	(0.0002)	(<0.0001)	(0.004)		

Table 4-S4. Post-hoc findings of mixed effect models nutrient flux (μmol/cm^2/day) of PO_4^{3-}, NH_4^+, NO_3^-, Ca^{2+}, Mg^{2+}, and Na^+ for water years and the season by depth interaction (fixed effects). Water years are averaged over the levels of season. The season by depth interaction compares the respective depth (0-, 20-, 40-, and 60-cm) in the fall compared to the spring. Model coefficients are displayed with the standard error in parentheses. P values are adjusted with Tukey's method and are in bold when significant at $\alpha < 0.05$. Water Year 2016 was not collected for plot 1 (no data; ND). Cells are blank when independent variable was not significant ($p > 0.05$) in the original mixed effect model (Table S3).

	Water Year						**Season x Depth**			
Nutrient	**2012 to 2013**	**2012 to 2014**	**2012 to 2016**	**2013 to 2014**	**2013 to 2016**	**2014 to 2016**	**0**	**20**	**40**	**60**
Plot 1										
PO_4^{3-}	0.01 (0.006)	-0.002 (0.006)	ND	-0.013 (0.006)	ND	ND	**0.039 (0.008)**	**0.03 (0.005)**	**0.02 (0.006)**	0.01 (0.008)
NH_4^+	**0.021 (0.005)**	**0.034 (0.005)**	ND	**0.013 (0.005)**	ND	ND	**0.041 (0.007)**	**0.026 (0.005)**	**0.011 (0.005)**	-0.004 (0.007)
NO_3^-	**0.029 (0.009)**	0.018 (0.009)	ND	-0.011 (0.009)	ND	ND	**0.048 (0.012)**	**0.033 (0.008)**	**0.017 (0.008)**	0.001 (0.012)
Ca^{2+}	**0.161 (0.008)**	**0.016 (0.008)**	ND	-0.002)	ND	ND	-0.017 (0.011)	**-0.035 (0.007)**	**-0.054 (0.007)**	**-0.072 (0.011)**
Mg^{2+}	**0.074 (0.005)**	**0.077 (0.005)**	ND	0.003 (0.005)	ND	ND	0.002 (0.007)	-0.008 (0.005)	**-0.017 (0.005)**	**-0.027 (0.007)**
Na^+	**0.069 (0.007)**	**0.057 (0.008)**	ND	-0.012 (0.008)	ND	ND				
Plot 2										
PO_4^{3-}	**-0.015 (0.005)**	-0.013 (0.005)	-0.003 (0.005)	0.002 (0.005)	0.011 (0.005)	0.001 (0.005)	**0.018 (0.006)**	**0.02 (0.003)**	**0.022 (0.004)**	**0.024 (0.006)**
NH_4^+	-0.014 (0.009)	**0.024 (0.009)**	**-0.049 (0.009)**	**0.038 (0.009)**	**-0.036 (0.009)**	**-0.073 (0.009)**	**0.055 (0.011)**	**0.041 (0.007)**	**0.027 (0.007)**	0.012 (0.011)
NO_3^-	-0.013 (0.011)	-0.002 (0.011)	**-0.073 (0.011)**	0.011 (0.107)	**-0.060 (0.011)**	**-0.071 (0.011)**	0.0211 (0.013)	0.015 (0.008)	0.01 (0.009)	0.004 (0.013)
Ca^{2+}	**0.107 (0.013)**	**0.133 (0.013)**	0.021 (0.013)	0.026 (0.013)	**-0.086 (0.013)**	**-0.112 (0.013)**	0.004 (0.015)	**-0.021 (0.01)**	**-0.045 (0.01)**	**-0.07 (0.016)**
Mg^{2+}	**0.03 (0.009)**	**0.049 (0.009)**	-0.008 (0.009)	0.02 (0.009)	**-0.038 (0.009)**	**-0.058 (0.009)**	0.006 (0.011)	0.02 (0.007)	-0.002 (0.007)	-0.006 (0.011)
Na^+	**0.053 (0.007)**	**0.044 (0.007)**	**0.049 (0.007)**	-0.009 (0.007)	-0.005 (0.007)	0.005 (0.007)				

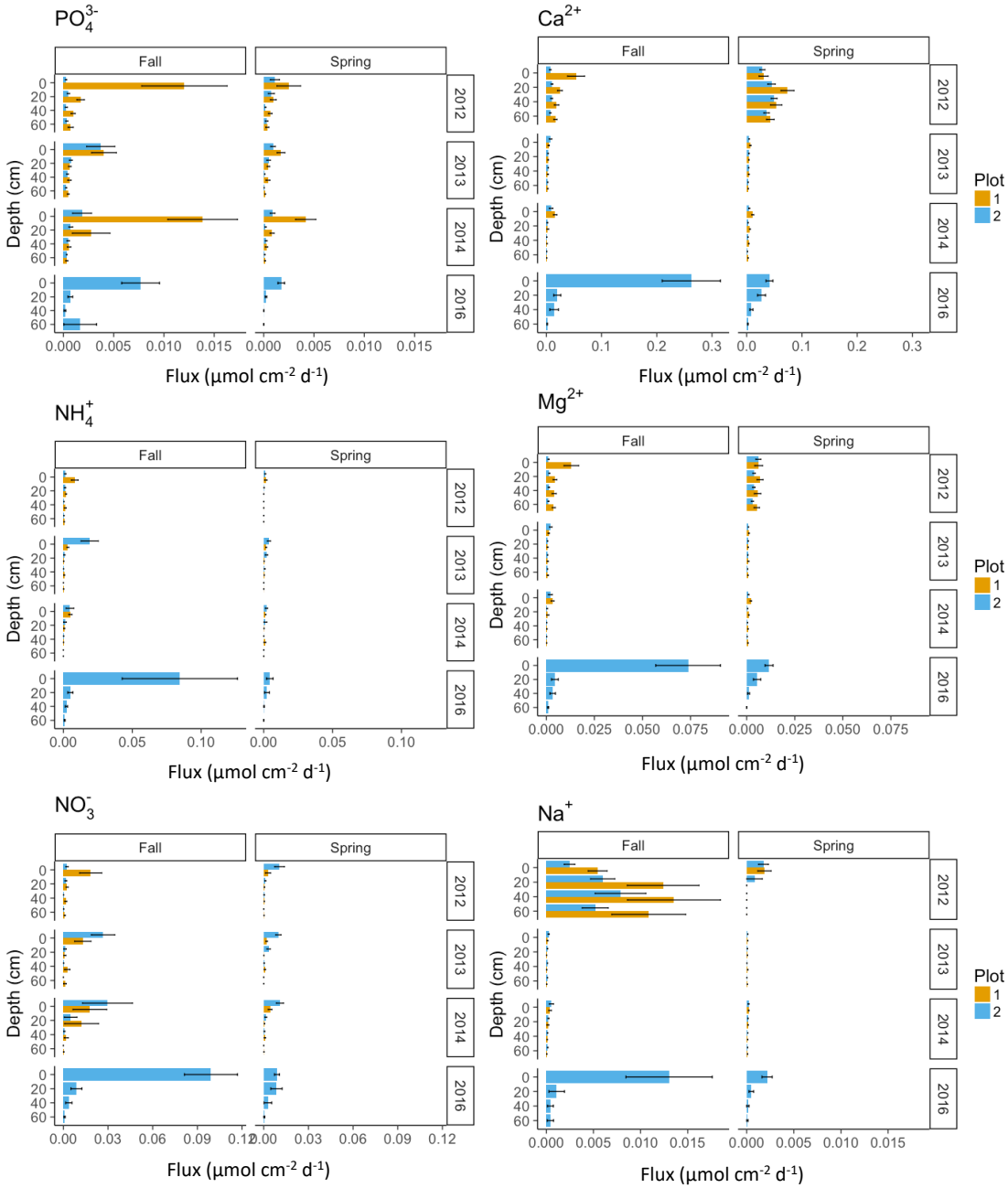

Figure 4-S1. Nutrient fluxes (µmol cm^{-2} d^{-1}) with the mean and standard error for a) biologically controlled and b) geochemically controlled nutrients based on water year, season (fall and spring), and depth. Each nutrient flux was normalized by number of days resin was deployed (see Table S1). No data were collected for Plot 1 during water year 2016.

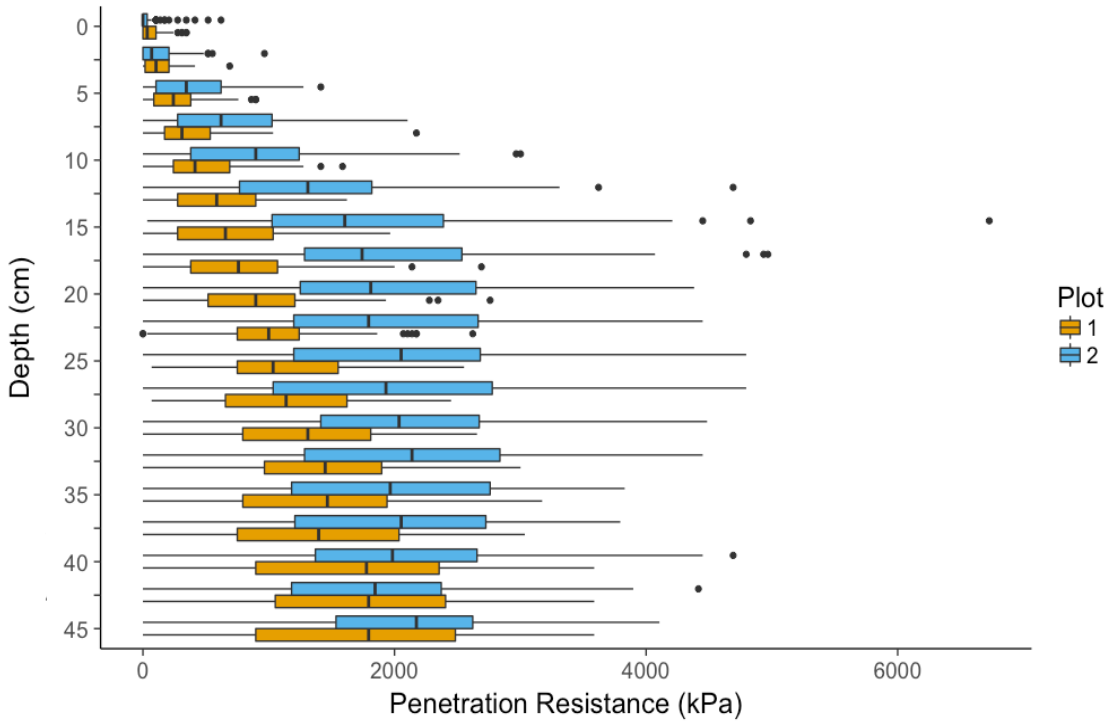

Figure 4-S2. Plot 1 (orange) and Plot 2 (blue) results from the penetrometer where penetration resistance (kPa) increases with depth into the soil. Measurements were collected from non-disturbed locations adjacent to the resin capsule locations and averaged at 2.5-cm increments from 0- to 45-cm. The box represents the first and third quartiles (the 25th and 75th percentiles), whiskers are the highest and lowest values within 1.5 times the inter-quartile range, and points outside the box are outliers.

5 Conclusion

Understanding how dryland ecosystems are impacted by changing climatic conditions is critical to better predict how terrestrial systems will respond to global climate change. My dissertation addresses several current knowledge gaps encompassing biogeochemistry of nutrients under different biological and geochemical controls, including carbon (C), nitrogen (N), phosphorus (P), calcium (Ca), magnesium (Mg), and sodium (Na). Specifically, I investigated how climate controls soil P stock, concentration, and chemical speciation in Chapter 2, C:N:P ratios within soil, microbial biomass, enzyme stoichiometry, fine root, and aboveground foliage in Chapter 3, and how nutrient hot spots (HS) and hot moments (HM) form over a long-term study that encompassed a period of drought. My dissertation includes nutrients with coupled and contrasting biogeochemical cycles and uses two separate gradients from semiarid to Mediterranean ecosystems (Chapters 2 and 3) along with an exemplar location to study multi-year nutrient fluxes (Chapter 4). Taken together, these chapters provide a better overall understanding of climatic impacts on nutrient biogeochemistry in terrestrial drylands. I found that nutrients under biological and geochemical controls are altered by changes in climate which has important implications for ecosystem function and development in semiarid and Mediterranean ecosystems.

Increases in overall temperature and precipitation induced greater chemical weathering and more acidic soil conditions at Mediterranean sites compared to semiarid. This resulted in greater P stock, likely due to sorption with secondary Fe and Al minerals along with vegetation mining Ca-P from deep C horizons and recycling P on the soil surface as organic P species (Chapter 2). Organic P species may be mineralized independently from C because there is a proportional decrease of the organic P pool while C increased with climate-induced weathering intensity. However, inorganic P species found in the more weathered locations may not be available at the soil pH range (Penn and Camberato 2019). Therefore ecosystem development may be relying on the turnover of the organic pool which is composed of primarily diester species that are more bioavailable than monoester species (Condron et al 2005). Overall, bioavailable P in the semiarid ecosystems is likely regulated by geochemical control whereas P bioavailability are likely influenced more by biological control at the Mediterranean sites (Delgado-Baquerizo et al. 2013; Feng et al. 2016).

Nutrient bioavailability is the key to supporting ecosystem development. Stoichiometric ratios can serve as a proxy for relative nutrient limitation (Koerselman and Meuleman 1996; Güsewell et al. 2003). Changes in precipitation explained more of the variability in ecosystem stoichiometry than temperature in these water-limited ecosystems (Chapter 3). This is likely because water constrains response of ecosystem processes to temperature. The microbial biomass transitioned from P limitation in dry sites, where mineralization and chemical reactions are likely water-limited, to C- and N-limitation in wetter locations where P is being independently mineralized from soil organic matter and P-acquiring enzymes are more efficiently being produced. In contrast to microbial biomass N:P, vegetation became more P-limited in wetter Mediterranean sites, following total elemental soil stoichiometry. Because these more weathered sites

are likely relying on turnover of the organic pool, microbes may be able to outcompete vegetation for this source of bioavailable P.

Nutrient hot spots (HS) and hot moments (HM) can be a source of bioavailable nutrients to help plants outcompete microbes (Kaye and Hart 1997). Nutrient fluxes under primarily biological-control (N and P) were more resilient to drought than those under geochemical-control (Ca, Mg, Na) in one of the more weathered Mediterranean sites (Chapter 4). This led biologically controlled nutrients to form HS and HM, whereas geochemically controlled nutrients formed HM. Biologically controlled nutrients are commonly the most limiting nutrients to ecosystem development (Elser et al. 2007); therefore these HS-HM are likely particularly important for bioavailable nutrients because they were responsible for 25-72% of N and P fluxes even though they occupied less than 26% of the sampling area. Although microorganisms may outcompete vegetation in the short-term for HM, plants that access HS with their roots and mycorrhizal symbionts can acquire more nutrients in the long-term (Hodge et al. 2000; Schimel and Bennett, 2004; Cui and Caldwell 1997). Because HS-HM of co-varying macronutrients are found at soil depths relevant to roots, have extremely high fluxes compared to the soil matrix, are persisting over time in some locations, and are responsible for a large portion of the total nutrient flux, they likely play a disproportionate role in supporting ecosystem development in a changing climate.

Globally, the amount of land area classified as drylands is expected to increase (Feng and Fu 2013), along with an increasing frequency of droughts (Dai 2012). Decreasing soil moisture slows important biogeochemical processes including soil weathering, organic matter turnover, and desorption and dissolution reactions (Austin et al. 2004; Delgado-Baquerizo et al. 2013). In semiarid locations, this may decrease bioavailable P, which is currently largely being supported by weathering of primary mineral apatite along with dissolution and desorption of secondary Ca-P. Bioavailable P may also decrease in ecosystems experiencing a Mediterranean-type climate where organic P mineralization is likely the primary source of P. Therefore, nutrient HS and HM will likely play a disproportionate role in supporting ecosystem development in these temperate drylands under a changing climate.

5. 1 References

Austin AT, Yahdjian L, Stark JM, et al. (2004) Water pulses and biogeochemical cycles in arid and semiarid ecosystems. Oecologia 141:221-235.

Condron LM, Turner BL, Cade-Menun BJ (2005) Chemistry and dynamics of soil organic phosphorus. In: Sims JT, Sharpley AN (eds) Phosphorus: Agriculture and the Environment. American Society of Agronomy, Crop Science Society of America, Soil Science Society of America, Inc., Madison, WI pp. 87-121

Cui M, Caldwell MM (1997) A large ephemeral release of nitrogen upon wetting of dry soil and corresponding root responses in the field. Plant and Soil 191:291-9.

Dai A (2012) Increasing drought under global warming in observations and models. Nature Climate Change 3:52–58.

Delgado-Baquerizo M, Maestre FT, Gallardo A, et al. (2013) Decoupling of soil nutrient cycles as a function of aridity in global drylands. Nature 502:672-676.

Elser JJ, Bracken MES, Cleland EE, et al. (2007) Global analysis of nitrogen and phosphorus limitation of primary producers in freshwater, marine and terrestrial ecosystems. Ecology Letters 10:1135-1142.

Feng J, Turner BL, Lü X, et al. (2016) Phosphorus transformations along a large-scale climosequence in arid and semiarid grasslands of northern China. Global Biogeochemical Cycles 30:1264-1275.

Hodge A, Stewart J, Robinson D, Griffiths BS, Fitter AH (2000) Competition between roots and soil micro-organisms for nutrients from nitrogen-rich patches of varying complexity. Journal of Ecology 88:150-64.

Kaye JP, Hart SC (1997) Competition for nitrogen between plants and soil microorganisms. Trends in Ecology & Evolution 12:139-43.

Koerselman W, Meuleman AFM (1996) The Vegetation N:P Ratio: a New Tool to Detect the Nature of Nutrient Limitation. The Journal of Applied Ecology 33:1441-1450.

Penn CJ, Camberato JJ (2019) A Critical Review on Soil Chemical Processes that Control How Soil pH Affects Phosphorus Availability to Plants. Agriculture 9:1-18.

Schimel JP, Bennett J (2004) Nitrogen mineralization: challenges of a changing paradigm. Ecology 85:591-602.